The University Of Sheffield.

PolyHIPE Microspheres for Injectable Bone Tissue Engineering Applications

By:

Thomas Paterson

A thesis submitted in partial fulfilment of the requirements for the degree of

Doctor of Philosophy

University of Sheffield

Faculty of Engineering

Department of Materials Science and Engineering

Submitted: March 2017

Abstract

Injectable microsphere-based delivery systems have great potential in tissue engineering, since they remove the need for open surgery. Current bone filler systems for non-load bearing applications do not fully resorb and only allow regrowth of bone at the implant interface. Within this thesis, a tissue engineered injectable bone filler was developed and optimised. This was in the form of polymeric microspheres that support human embryonic stem cell-derived mesenchymal progenitor (hES-MP) cells for implantation. A polymer high internal phase emulsion (polyHIPE) microsphere fabrication system was selected over a range of other fabrication techniques including 2-photon direct write, projection based stereolithography and microfluidic particle manufacture. A combination of the microfluidic technique and the double emulsion method were selected for further study due to their rapid production rate and inclusion of customisable internal microfeatures (porosity). Using a EHA/IBOA copolymer system the manufacturing conditions were explored to allow independent control over the microspheres external diameter (70 - 1000 μm) and interconnected internal pore size (2 – 60 μm). Static culture of hES-MP cells over 30 and 60 days on EHA/IBOA microspheres were conducted and increased cell activity was observed. Cell enabled microsphere aggregate formation was observed and the steady ingrowth of cells was observed up to day 30. The detection of calcium and collagen deposits confirmed the presence of osteoblasts within the pores of the microspheres. Osteocyte like cell morphology was observed within the pores of the microspheres after 60 days in culture. A biodegradable PCL polyHIPE system was used to repeat the key experiments performed with the non-degradable EHA/IBOA system and similar results were observed. Injection studies found superior cell survival on porous PCL microsphere compare to non-porous microspheres. A Chorioallantoic membrane assay was used to determine angiogenic potential of both seeded and unseeded microspheres. An increased angiogenic response was observed for pre-seeded microspheres. This research began with initial selection of micro-particles for a tissue engineering injectable scaffold and successfully progressed to the pre-in-vivo stage, having investigated manufacturing conditions, biocompatibility, degradability, injectability and angiogenic potential.

Contents

Abstract 1

Contents 2

PhD by pictures 9

Acknowledgments 10

Outputs 11

Presentations 11

Posters 11

List of abbreviations 12

Chapter 1: Literature review and Introduction 15

1.1 Tissue engineering 15

1.1.1 Basic principles of tissue engineering 15

1.1.2 Bone tissue engineering 16

1.1.3 Materials for bone tissue engineering 17

1.1.4 Top down and bottom up tissue engineering 19

1.2 Applications for particles in tissue engineering 22

1.2.1 Injectable scaffolds 22

1.2.3 Microcarriers for cells/stem cells 22

1.2.4 Microparticle aggregates 23

1.2.5 Bioactive agent releasing scaffolds 24

1.2.6 Incorporation of polymer microparticles into tissue engineering scaffolds 24

1.3 Porosity in scaffolds for tissue engineering 25

1.3.1 Porosity in bone tissue engineering 25

1.3.2 The effect of porosity In-vitro vs In-vivo 25

1.3.3 Interconnecting porosity and cell migration 26

1.3.4 The effect of porosity on mechanical and degradation properties 28

1.3.5 Porous particles 28

1.4 Manufacturing methods for particles used in tissue engineering 28

1.4.1 Established particle manufacturing techniques 30

1.4.2 Additive manufacturing 31

1.4.3 Microfluidic enabled rapid lithography particle manufacture 31

1.4.4 Micromoulding techniques 33

1.4.5 Emulsion 33

1.5 Emulsion templating 35

1.5.1 Photocurable polyHIPE: what is it made of? 36
1.5.2 Biodegradable polymers 38
1.5.3 Porosity in polyHIPEs 38
1.5.4 Interconnectivity in polyHIPEs 38
1.5.5 Destabilising mechanisms 39
1.5.6 Pickering HIPEs 40
1.5.7 PolyHIPE microspheres 41
1.6 Applications of polyHIPEs, polymer particles and porous microspheres in tissue engineering 43
1.7 Mesenchymal stem cells and their differentiation 44
1.7.1 The differentiation process 44
1.7.2 The role of cells in natural bone 45
1.7.3 The role of cells in tissue engineering and in-vitro testing of scaffolds 46
1.7.4 Supplements used in culture of bone cells 46
1.7.5 The effect of hypoxia on cells 47
1.7.6 Cell co-culture impact on differentiation 47
1.8 Vascularisation of tissue engineered constructs 48
1.8.1 Necessity for vasculature in tissue engineering 48
1.8.2 Current strategies in vascularisation 49
1.8.3 Methods for testing vascularisation 51
1.9 Findings from literature review 54
1.10 Main aim: 55
Specific aims: 55
Chapter 2: Materials and methods 57
2.1 Light based photocuring of monomers: Stereolithography 57
2.1.1 Laser based photocuring of monomers using a digital micromirror device 57
2.1.2 Preparing a monomer solution of polyethylene glycol for photocuring 57
2.1.3 Image design and production for software controlling digital micro mirrors 58
2.1.4 Direct laser write of a photocurable monomer using single photon curing 58
2.1.5 Photo-polymerisation of computer designed objects using 2-photon manufacture 58
2.2 Microfluidic device manufacture and microsphere manufacture using said microfluidic device 59
2.2.1 Manufacture of a microfluidic device for fluid encapsulation 59
2.2.2 Encapsulation of oil in water using the microfluidic device 60
2.2.3 Iterations of microfluidic device to produce high yield continuous production with minimal user input during operation 60
2.3 Polymerising photocurable emulsions into microspheres and thin films 62

2.3.1 Water in oil (EHA/IBOA copolymer) mixing to form a high internal phase emulsion.. 62
2.3.2 Reaction for polycaprolactone methacrylation to form a photocurable monomer 62
2.3.3 Water in oil (polycaprolactone) mixing to form a high internal phase emulsion 63
2.3.4 Water in oil (Thiol-ene) mixing to form a high internal phase emulsion 63
2.3.5 Photocuring HIPE into porous microspheres using the closed tank stir reactor method 63
2.3.6 Photocuring HIPE into porous microspheres using T-junction microfluidics..... 64
2.3.7 Photocuring HIPE into thin films over glass coverslips 65
2.4 Imaging of microspheres and analysis of both microsphere and pore diameter 66
2.4.1 Imaging of porous microspheres using optical microscopy..... 66
2.4.2 Imaging of porous microspheres using scanning electron microscopy 66
2.4.3 Methods used to measure microsphere diameters..... 66
2.4.4 Methods used to measure microsphere internal pore size 66
2.4.5 Degradation study of polycaprolactone microspheres with standard and accelerated degradation..... 67
2.4.6 Manufacturing of solid polycaprolactone microspheres 67
2.5 Surface modification through plasma coating..... 68
2.5.1 Plasma coating of polyacrylic acid 68
2.6 General cell culture techniques 69
2.6.1 Freezing cells for storage in liquid nitrogen 69
2.6.2 Defrosting cells from liquid nitrogen for use in cell culture 69
2.6.3 Supplement inclusion into media for the culture hES-MP cells..... 69
2.6.4 hES-MP culture and standard maintenance between passages 70
2.6.5 Passage technique for hES-MP cell expansion 70
2.7 Culture of hES-MP cells on microspheres..... 71
2.7.1 Microsphere sterilisation in alcohol before cell culture 71
2.7.2 The culture of hES-MP cells on a thin film 71
2.7.3 Technique used to seed hES-MP cells onto microsphere 71
2.7.4 hES-MP culture on microspheres for a time course study of ingrowth..... 71
2.7.5 Survival study: injection of hES-MP cells bound to microspheres from a syringe..... 72
2.8 Quantitative analysis of cell growth and differentiation on microspheres 73
2.8.1 Cell activity measurements using the Resazurin salt assay 73
2.8.2 Total sample DNA and Alkaline phosphatase production measurements..... 73
2.9 Cell cultured microsphere sample preparation and sectioning..... 74
2.9.1 Fixing cells..... 74
2.9.2 Cryostat microtome 74

2.9.3 Hexamethyldisilazane treatment of samples for imaging of cells using scanning electron microscopy 74
2.10 Fluorescent microscopy of cell cultured microsphere samples 75
2.10.1 Cell wall permeabilization using detergent 75
2.10.2 Staining of f-actin filaments using a phalloidin-fluorescein isothiocyanate stain 75
2.10.3 Staining of cell nuclei filaments using a 4',6-diamidino-2-phenylindole stain 75
2.10.4 Confocal/fluorescent microscope set-up for imaging 75
2.10.5 Imaging of Live & dead cells on a microsphere through staining 75
2.10.6 Imaging of mature collagen through Second Harmonic Generation imaging 76
2.11 Staining of cell cultured microsphere samples for optical microscopy 77
2.11.1 Haematoxylin and Eosin staining 77
2.11.2 Calcium staining using Alizarin red 77
2.11.3 Collagen staining using Sirius red 77
2.11.4 Polysaccharide staining using Toluidine Blue 77
2.11.5 Antibody staining for sclerostin using 3,3'-Diaminobenzidine staining for optical microscopy imaging 78
2.12 In-vivo study of vascularisation response using a Chorioallantoic membrane assay 79
2.12.1 Preparing the Chorioallantoic membrane model for implantation of scaffolds 79
2.12.2 Implantation of EHA/IBOA microspheres into a Chorioallantoic membrane model for angiogenic potential assessment 79
2.12.3 Implantation of polycaprolactone microspheres into a Chorioallantoic membrane model for angiogenic potential assessment 79
2.12.4 Scaffold Retrieval from the Chorioallantoic membrane assay and in-situ imaging 79
2.12.5 Staining techniques used on the tissue samples removed from the Chorioallantoic membrane 80
2.13 Digital techniques used on images 81
2.13.1 Computer generated trace of cells within microsphere sections 81
2.13.2 False coloured scanning electron microscopy images 81
2.13.3 Manipulation of image stacks from confocal microscopy: Z-stack 81
2.13.4 Manipulation of image stacks from confocal microscopy: Stereoscopic image 81
2.13.5 Manipulation of image stacks from confocal microscopy: Z-project 81
2.14 Statistical analysis 82
2.14.1 Unpaired students T-test 82
2.14.2 ANOVA multiple comparison test 82
2.14.3 Microsphere data analysis and method of displaying data on Tukey boxplot 82
2.14.4 Analysis of the SHG data from images captured using the confocal microscope 83
2.14.5 Method used to assemble data on the cell infiltration into microspheres over time 83

2.14.6 Measurement of cell nuclei alignment on polycaprolactone microsphere agglomerations 84
2.14.7 Techniques use to analyse the vascularisation response to the implants 84
Chapter 3: Fabrication methods for particle manufacture 85
3.1 Chapter aims 85
3.2 Introduction 85
3.2.1 Photocuring monomers: Lithography techniques 85
3.2.2 Microparticles: their manufacture and applications in tissue engineering 86
3.2.3 Polymers and materials used within chapter 4 87
3.3 Results 88
3.3.1 Photocuring of shaped objects using controlled laser based radiation 88
3.3.2 Two photon laser photocuring (manufacturing) of CAD designed microparticles particle 89
3.3.3 Producing microspheres through encapsulation of oil phase in water phase using a microfluidic device 91
3.3.4 EHA/IBOA polyHIPE microspheres manufactured using the microfluidic device, via encapsulation and photocuring 94
3.4 Discussion 96
3.5 Conclusion 100
Chapter 4: PolyHIPE microsphere production 101
4.1 Chapter aims 101
4.2 Introduction 101
4.2.1 Microspheres and their application in tissue engineering 101
4.2.2 Photocured emulsions: The polyHIPE 101
4.2.3 Turning the emulsion into microspheres: manufacturing techniques 102
4.3 Results 103
4.3.1 The effect of manufacturing parameters on the internal porosity of the polyHIPE 103
4.3.2 Porous microspheres manufactured via double emulsion and the effect of processing parameters on resulting microsphere size 107
4.3.3 Porous microsphere manufactured via microfluidics and the effect of processing parameters on resulting microsphere size 113
4.3.4 Direct comparison of both manufacturing techniques on microsphere pore size, diameter distribution and structure 117
4.4 Discussion 120
4.5 Conclusion 125
Chapter 5: Cell culture on EHA/IBOA polyHIPE microspheres 126
5.1 Chapter aims: 126

5.2 Introduction....126
5.2.1 Chapter introduction....126
5.2.2 Human embryonic stem cell-derived mesenchymal progenitor cells....126
5.2.3 Mesenchymal stem cells and their osteogenic differentiation....126
5.2.4 Media supplements used in the culture of bone cells....127
5.3 Results....128
5.3.1 Culture and proliferation of hES-MP cells on EHA/IBOA copolymer....128
5.3.2 Agglomeration of EHA/IBOA microspheres and hES-MP cells which form over time132
5.3.3 Cell growth and migration into EHA/IBOA microspheres from long term culture....138
5.3.4 The effects of media additives on ingrowth of hES-MP cells into microspheres within an agglomeration....140
5.3.5 The effects of media supplements on the extracellular matrix production of hES-MP cell cultured with microspheres....143
5.3.6 Investigation into the identity of cells within pores of the polyHIPE microspheres ...146
5.4 Discussion....151
5.5 Conclusion....156
Chapter 6: Degradable polyHIPE microspheres....157
6.1 Chapter aims....157
6.2 Introduction....157
6.2.1 Degradable materials and their use within the body....157
6.2.2 Thiol-ene polymer as a polyHIPE....157
6.2.3 Polycaprolactone polymer as a polyHIPEs....158
6.3 Results....159
6.3.1 The manufacture of Thiol polyHIPE microspheres and hES-MP cell growth on both microspheres and flat sheets....159
6.3.2 Manufacturing polycaprolactone based polyHIPE microspheres....163
6.3.3 Accelerated degradation of polycaprolactone polyHIPE microspheres over a 60 day time period....166
6.3.4 Culture of hES-MP cells on polycaprolactone microspheres and the formation of cell enabled agglomerations....167
6.3.5 Cell ingrowth into polycaprolactone polyHIPE microspheres over time....172
6.3.6 Measure of extracellular matrix within agglomerations of microspheres and cells cultured in media with different additives....176
6.4 Discussion....180
6.5 Conclusion....186
Chapter 7: Assessment of PolyHIPE microsphere's vascularisation potential using chick chorioallantoic membrane assays....187

7.1 Chapter aims 187
7.2 Introduction 187
7.2.1 Vascularisation of tissue engineered scaffolds 187
7.2.2 Injectable microspheres and vascularisation 188
7.2.3 Chorioallantoic membrane assays as a measure of vascularisation 188
7.2.4 Major contributors to the chapter 188
7.3 Results 190
7.3.1 Vascularisation potential of EHA/IBOA polyHIPE microspheres assessed using a CAM assay 190
7.3.2 Survival of cells when injected from a syringe using porous and non-porous carriers 195
7.3.3 Analysis of CAM assay after the injection of both porous and non-porous polycaprolactone polymer microspheres with short and long term pre-culture. 196
7.3.4 Statistical analysis of blood vessels as a method of comparing angiogenic potential of both EHA/IBOA and polycaprolactone microspheres in a CAM model 201
7.4 Discussion 202
7.5 Conclusion 206
Chapter 8: Final discussion on an injectable system for bone tissue engineering 207
8.1 Chapter aims 207
8.2 Requirements of an injectable scaffold 207
8.3 Manufacturing efficiency 207
8.4 Biocompatibility 208
8.4.1 Cell toxicity 208
8.4.2 Osteoconductivity/Osteogenesis 208
8.4.3 Support mineralisation 210
8.5 Mechanical properties 210
8.6 Pore size 210
8.6.1 Control over construction parameters 211
8.7 Bioresorbability 211
8.7.1 Degradation 211
8.8 Vascularisation response 212
8.8.1 Vascularisation comparison 212
8.9 Scaffold deployment 213
8.9.1 Injectability 213
8.10 Final Conclusions 214
8.11 Future work 215
Bibliography 216

PhD by pictures

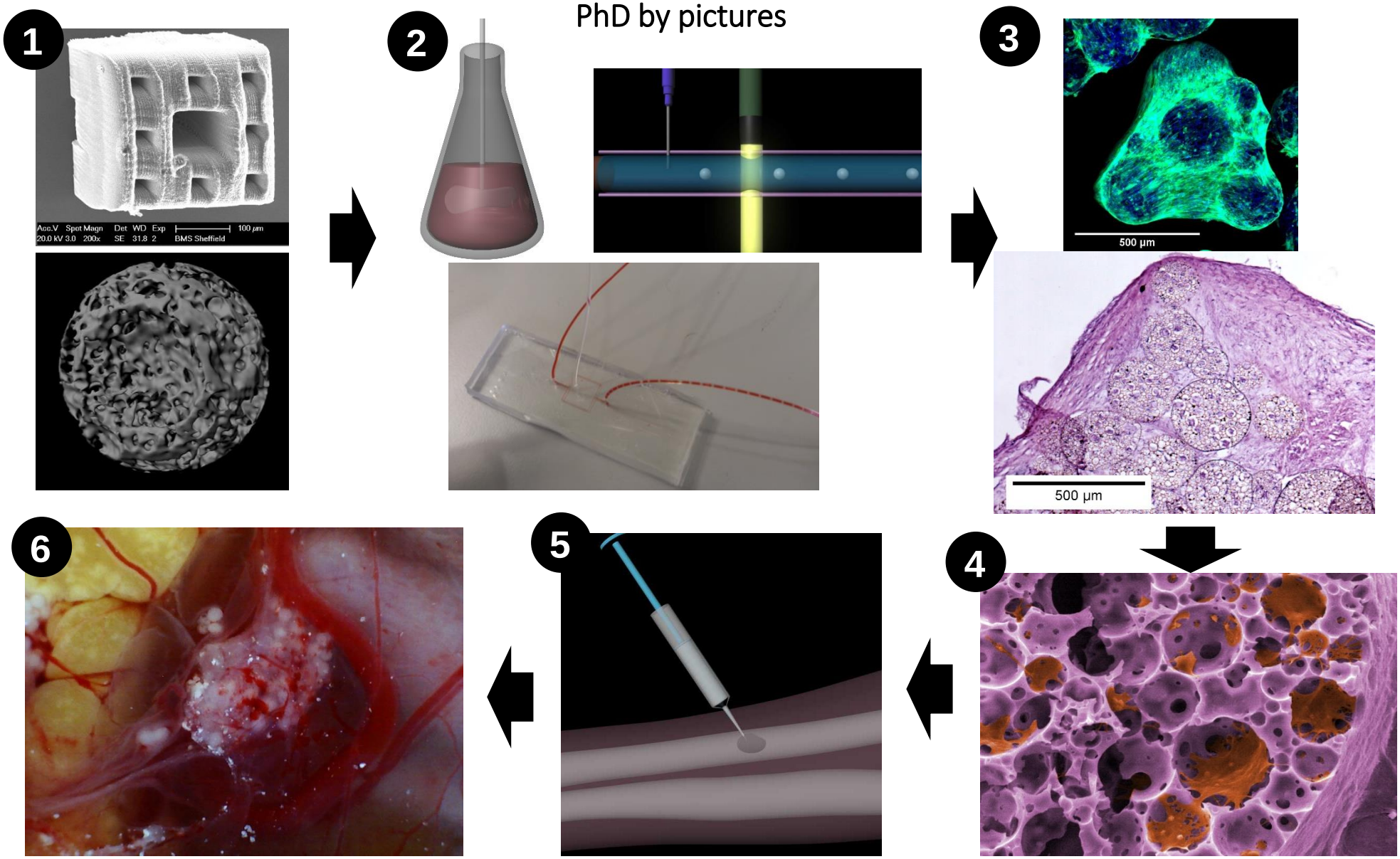

1: Different microparticle manufacturing methods trialled (chapter 3). 2: Manufacturing method investigated and optimised (chapter 4). 3) Culture with hES-MP cells and cell-microsphere agglomeration (chapter 5 & 6). 4: Measured cell ingrowth and identified cell types present (chapter 5 & 6). 5: Investigated cell survival while bound to microspheres during injection (chapter 7). 6: Angiogenic potential assessed using a CAM assay (chapter 7).

Acknowledgments

I would like to thank the following people for their help, support and advice during my PhD. With special thanks to my supervisor Dr Frederik Claeyssens for being a fantastic supervisor, always open and supportive whichever way I wanted to go with my research. For supporting me as an independent researcher and for always having new ideas. To my supervisor Dr Gwendolen Reilly for your patience with Fred and myself while we attempted to do cell work, your knowledge has been invaluable. Colin Sherborne for being a mentor and a friend over the 5 years of working together and teaching me everything I know about lasers, photocuring and polyHIPEs. Jim Dugan for teaching me the correct scientific method, providing excellent and honest advice to improve my work where others would have simply said that the research was good enough. Also for being an excellent example of how a postdoc should behave, I hope I can be as good as you were. To Dr Nicola Green for training me on the confocal microscope and helping me with the SHG images. Hossein for making all those PCL microspheres for me when I didn't have time. To Giulia Gigliobianco for all the work you did on with the CAM assay, you have a stronger stomach than I do. Thanks to Emma (王爱娟) for the year of work together in Sheffield and for inviting me to China for the Chinese Biomaterials Congress in 2015.

I would like to thank the University of Sheffield and the EPSRC for funding my PhD. To all the lab technicians who have helped me and made the lab run smoothly; Mark, Robert, Claire and Vanessa. A special mention goes to the Kroto research institute and its multidisciplinary research which made me aware of a much broader swath of research than I would otherwise have been exposed to and for fostering a forward-thinking research environment.

Special thanks to my family (Anne, Dan, Grandma, Dave, Eva and Maddy), for putting up with years of sparse contact during my research period and always supporting me. Everlasting thanks to my mum, I don't think I would have been able to complete this PhD without your support. To Ilida Ortega a great deal of thanks, firstly for publishing my first paper and making me feel like a scientist and for the inspiration gained by observing your successful rise through academia, showing that it is possible. Sarah, for keeping me strong in those final days of thesis writing, I am not sure when this thesis would have been finished without our late-night thesis dates. Thomas Chen, for spending so many hours working with me during your master's project, helping me establish the initial microfluidic production setup. It seems so simple in hindsight but I remember how much hard work you put in. To Darren for all the conferences we went to together. To Sarina, so you don't hold it against me that you were not mentioned by name. To Miki Tillett for your support over the majority of the years I spent working on my PhD. Finally, special thanks to all my colleagues who have helped me and worked with me over the years.

Outputs

Presentations

"Porous microsphere production with tuneable internal porosity for 3d cell culture" Thomas Paterson, James Dugan, Colin Sherborne, Gwendolen Reilly, Frederik Claeyssens. **Talk**, ESB 2016, Lyon, France

"Highly porous particles for cell delivery vehicles in bone tissue engineering" Thomas Paterson, James Dugan, Colin Sherborne, Nicola Green, Gwendolen Reilly, Frederik Claeyssens. **Talk**, Chinese Biomaterials Congress 2015, Haikou, China

"Porous particles as cell delivery vehicles for bone tissue engineering" Thomas Paterson, James Dugan, Colin Sherborne, Chia-Cheng Chen, Nicola Green, Gwendolen Reilly, Frederik Claeyssens. **Talk and poster presentation**, ESB 2015, Krakow, Poland

"Manufacturing of PolyHIPE-based porous microparticles for bone tissue engineering" T. Paterson, C. Sherborne, G. Reilly, F. Claeyssens. **Talk**, USES 2014, United Kingdom

Posters

"Manufacturing porous microspheres which successfully support bone formation and stimulate an increased vascularisation response" Thomas Paterson, James Dugan, Colin Sherborne, Nicola Green, Gwendolen Reilly, Frederik Claeyssens. **Poster presentation**, TERMIS 2017, Davos, Switzerland

"Highly Porous Particles for Cell Recruitment and Delivery in Bone Tissue Engineering" Thomas Paterson, James Dugan, Colin Sherborne, Nicola Green, Gwendolen Reilly, Frederik Claeyssens. **Poster presentation**, TERMIS world congress 2015, Boston, USA

"PolyHIPE-based porous microparticles for tissue engineering" T. E. Paterson, C. Sherborne and F. Claeyssens**. Poster presentation**, TERMIS 2014, Italy

"PolyHIPE-based porous microparticles for bone tissue engineering" T. Paterson, C. Sherborne, R. Owen, S. Puwunun, G. Reilly, F. Claeyssens. Poster presentation, **ESB 2014**, United Kingdom

List of abbreviations

1PP	One photon polymerisation
2.5D	2.5 dimensions
2PP	Two photon polymerisation
3D	3 dimensions
A2P	Ascorbate-2-phosphate
ALP	Alkaline phosphatase
AMEM	Alpha Modification of Eagle's Medium
BMP	Bone morphogenetic protein
BMP-2	Bone morphogenetic protein 2
CAD	Computer-aided design
CAM assay	Chorioallantoic membrane assay
CO_2	Carbon dioxide
CTCF	Corrected total cell fluorescence
DAPI	4',6-diamidino-2-phenylindole
DEX	Dexamethasone
dH_2O	Distilled water
DMD	Digital micromirror device
DMSO	Dimethyl sulfoxide
DNA	Deoxyribonucleic acid
ECM	Extracellular matrix
EDTA	Ethylenediaminetetraacetic acid
EHA	2-ethyl hexyl acrylate
FCS	Foetal Calf serum
FGF	Fibroblast growth factor

FITC	Fluorescein Isothiocyanate
GAG	Gycosaminoglycan
HMDS	Hexamethyldisiloxane
HES	Human embryonic stem (cells)
hES-MP	Human embryonic stem cell-derived mesenchymal progenitors
HIPE	High internal phase emulsion
H&E	Haematoxylin and eosin stain
IBOA	Isobornyl acrylate
IGF	Insulin-like growth factor
IMS	Industrial methylated spirits
IQR	Interquartile range
MSC	Mesenchymal stem cell
NaOH	Sodium hydroxide
OCT	Optimal cutting temperature compound
o/w	Oil in water (emulsion)
pAA	Poly acrylic acid
pAAc	Poly acrylic acid coated
PBS	Phosphate buffered solution
PCL	Polycaprolactone
PDMS	Polydimethylsiloxane
PEG	Polyethylene glycol
PGA	Polyglycolide
PGL	Polyglycolic acid
PLA	Polylactic acid
PLGA	Poly-lactic-co-glycolic acid
PMMA	Poly(methyl methacrylate)

PolyHIPE	Polymer high internal phase emulsion
UV	Ultraviolet radiation
Rpm	Rotations per minute
SEM	Scanning electron microscope
TGF-β	Transforming growth factor beta
THF	Tetrahydrofuran
TMPTA	Trimethylolpropane triacrylate
VEGF	Vascular endothelial growth factor
w/o	Water in oil emulsion
w/o/w	Water in oil in water emulsion
βGP	Beta-glycerol phosphate

Chapter 1: Literature review and Introduction

1.1 Tissue engineering

1.1.1 Basic principles of tissue engineering

The combination of a scaffold and cells in an engineered solution to restore, replace or imitate a tissue within the body for a regenerative application (figure 1.1). Tissue engineered constructs are being engineered to provide a solution for a diverse ranging of regenerative applications from skin patches for burns patients [1] to whole organ replacement [2, 3]. In this thesis, the application considered is one of bone tissue engineering.

The common source of cells used for tissue engineering are stem cells [4-6]. Stem cells range from true omnipotent stem cells to progenitors of a single cell line. For applications stem cells are usually chosen which have their differentiation potential limited to a few different cell types, as this adds additional control over the resulting cell type. These cells can be obtained from many sources, although autologous stem cells are usually used if the cells are going to be used in a patient. Cells can be taken at birth from the placenta and stored [7] or stem cells can be harvested from the adult body [8]. Stem cells have been found in almost all tissues in the body, popular sources for future tissue engineering are those from the blood [8], fat [9, 10] or bone marrow [11] as these are easier to access and remove from the body within minimal surgery.

The scaffold's role is to help cells attach to the scaffold, and then proliferate and differentiate in-vivo to help restore or replace the surrounding biological tissue. For this they must have suitable mechanical stability, biocompatibility, biodegradability, porosity, surface chemistry and surface roughness to create an object a surgeon can implant and provide a suitable microenvironment for cells. The scaffold must direct cell differentiation to a desired cell type (or to maintain areas of stem cells in artificial stem cell niches [12, 13]). This can be done chemically (biologically) or through the use of topology and ideally through both. The differentiation of a stem cell is influenced by a wide variety of additional factors such as cell to cell and cell to extracellular matrix (ECM) interactions, surface chemistry, protein absorption, intracellular and extracellular signalling along with integrin and ligand connections [14].

An ideal scaffold should be able to influence or control these factors to direct the differentiation of cells into the desired phenotype. By mimicking the natural structure of the ECM where a cell is found within the body it has been shown that this has an effect on the differentiation of cells to that phenotype [15, 16]. Controlling the morphology of a cell also has an impact on its phenotype [17], forcing a cell to morphologically resemble another cell has been found to exhibit those cells phenotypes [18, 19]. The mechanical properties of the scaffold are also linked to cell differentiation

[15, 16, 20]. Different young's modulus of a substrate have been shown to alter the differentiation of cells on the surface of the material [21, 22].

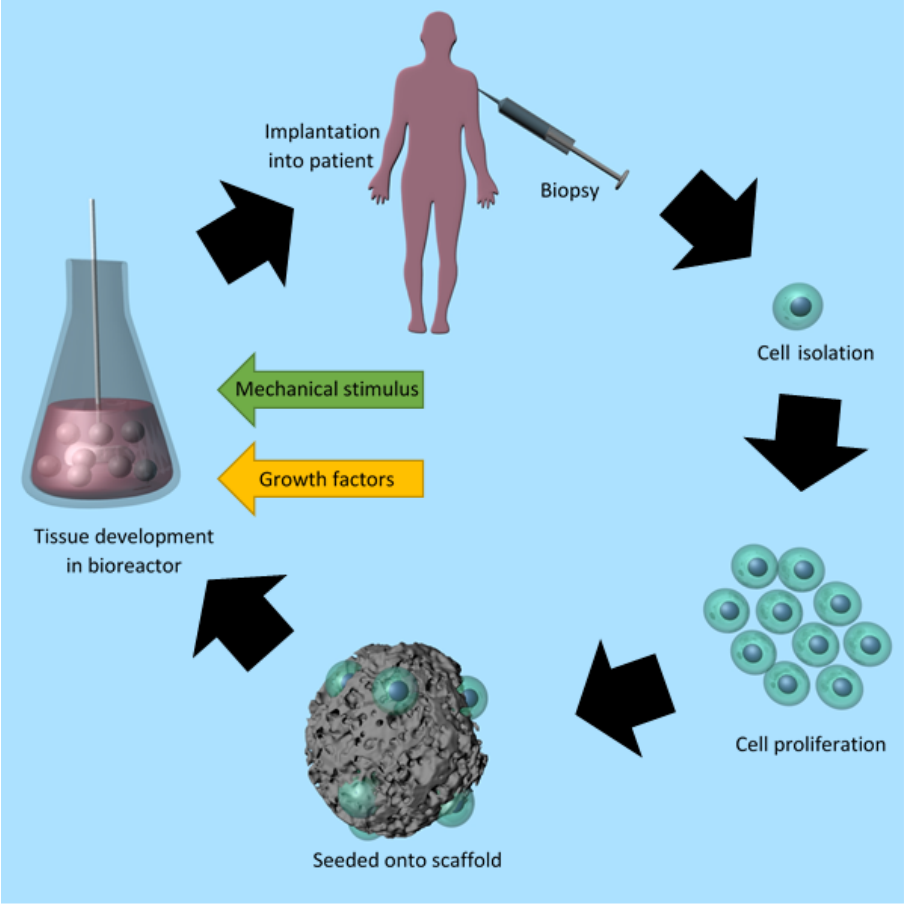

Figure 1.1. Diagram for the process of tissue engineering. Cells are extracted from the patient and isolated to the target cell type. Cells are then *expanded up to the number of cells required. Cells are combined with the scaffolds and cultured in a bioreactor along with mechanical stimuli and growth factors. The scaffolds are then implanted into the patients.*

1.1.2 Bone tissue engineering

Despite appearances bone is a living tissue like any other in the body. Bone is a composite of collagen and the mineral component hydroxyapatite. Bone is under a constant state of remodelling and can react to stimulus and heal damage from trauma. Many cell types and unique architecture form bones, along with a complete vasculature system. The skeletal system is not only for locomotion, support and protection but also as a reservoir for calcium. This vital tissue can become damaged beyond the ability of the bones to heal themselves to their original structure. Complex fractures and cancer can cause damage too severe to heal without surgical intervention. Advanced surgical procedures have been developed using ceramic fillers [23], titanium pins [24] or entire joint replacements [25] to name but a few. These surgical interventions usually remain within the body permanently and can cause biological problems such as the generation of non-degradable/removable wear particles, infection or mechanical issues such as shear loading.

Tissue engineering for bone aims to repair or replace the bone with functioning living tissue, which will become part of the patient over time. As bone is constantly remodelling, a biodegradable implant, if timed correctly will disintegrate as the natural tissue remodels and takes its place. Combining a scaffold with the patient's own cells allows for the remodelling to begin not only at the interface of the implant, but throughout the implant. Many challenges currently exist in this field, many are common to all tissue engineering, such as issues of sufficient vascularisation and the need for multi-cell cultures, but others are more specific to bone, such as coping with the load bearing nature of bone and the comparatively slow remodelling.

Disease states such as non-union fractures, voids and osteoporosis that require packing with a material to treat. The current options range from ceramic fillers, bioactive glasses and autologous bone fillers (see table 1). A significant drawback of these techniques is that while there may be fusion and ingrowth around the edge of implant there is little to no growth in the centre of the material. A tissue engineered solution may allow for complete healing of these wounds by enabling complete regrowth. Complex fractures can take months to heal completely, often requiring open surgery and the implantation of metal devices to enable full recovery. Tissue engineering is highly unlikely to replace metal implants but it could be used to prepare a site within the bone for metal implants where little bone remains, as may be found with revision surgery. Voids left within the bone after a cancer is removed could be filled with a viable construct to allow full remodelling without needing secondary surgery to harvest additional bone tissue [26]. Dental sockets within the jaw also require packing after a surgery to remove teeth [27].

1.1.3 Materials for bone tissue engineering

A wide range of materials are currently used for bone tissue engineering. Arguably the most prominent is metal which is used in joint replacement and pins. This prominence is due to the high stiffness of the material (compared to most other materials), along with its fracture toughness and biocompatibility for some metals, such as titanium. The development of resorbable bioglass has led to many different compositions of glass used for bone applications. Glass is a very strong material, especially under compression. The addition of Strontium into bioglass has had many successful applications as strontium has been found to cause a high level of bone growth when compared to scaffolds without strontium [28, 29].

The ability to control the precise chemistry of polymers allows high levels of control and tailoring to the properties of the scaffold. Many synthetic polymers have been tested for tissue engineering such as polystyrene, poly-lactic-co-glycolic acid (PLGA), polylactic acid (PLA), polyglycolic acid (PGL) and silicone among many others and are reviewed extensively elsewhere [30]. Other polymers such as 2-ethyl hexyl acrylate (EHA) and isobornyl acrylate (IBOA) contain a non-degradable carbon backbone

which limits their use in-vivo [31]. Thiol-ene polymers are formed by click chemistry of a reaction between a thiol and alkene to form an alkyl sulphide.

Table 1.1. Table of current bone fillers in the literature

Class	Material	Degradable	Manufacture method	Advantages/ disadvantages	Refs
Bioglass	Lime phosphosilicate glass	No	Melted at high temperatures	+ Biocompatible + Osteoconductive + strong interface binding with bone - Brittle	[32]
	Strontium bioglass	No	Melted at high temperatures	+ additional Osteogenic effect + Mild antibacterial effect	[33]
Bioglass/ cement	Resin modified glass ionomer	No		+ Ease of handling - Unpolymerised polymers leach from material	[34, 35]
Cement	Calcium phosphate cements	Yes (some)	Sintering at high temperatures with the exclusion of water	+ Osteoconductive - Exothermic setting mechanisms	[36, 37]
	Hydroxyapatite	Very slow (years)	Various	- Slow degradation + Osteoconductive	[38, 39]
	Poly(methyl methacrylate) (PMMA) cement	No	Sintering at high temperatures	- Exothermic setting reaction - Non-stable interface +combined with other components have improved some issues	[40, 41]
	Zinc phosphate cement		Sintering at high temperatures	- Zinc causes encapsulation response - Brittle cement	[42]
	Zinc polycarbonate cement		Sintering at high temperatures	+ Sets via non-exothermic reaction - Leaches unreacted metal particles	[43]
Natural polymer	Soybean-Based	Yes	Thermosetting of defatted soybean curd	+ Low immunogenicity - Very rapid degradation	[44]
	Demineralized bone matrix	Yes	Acid extraction of mineral content of bone	- Variability in product + Contains relevant bio molecules	[45]
	Autografts	Yes	Surgery from patient	- Secondary wound site + No immune rejection	[46]
	Platelet Gel	Yes	Platelets collected from	+ No immune rejection	

			patient before surgery	+ no secondary surgery site - Clinical efficacy not established	
Synthetic polymer	Polylactic acid & hydroxyapatite	Yes	Polymer melted and mixed with hydroxyapatite	+Hydroxyapatite component - Acidic build up on degradation	[23]
	PLA/PGA/PCL	Yes	Polycondensation	+ Biodegradable - Undergoes bulk erosion	[47, 48]
	Polyhydroxy-alkanoates	Yes (generally)	Produced by microorganisms	+ Minimal inflammation - Time consuming extraction method	[49]
	Polypropylene fumarate	Yes	two-step reaction of two polymers	+ Readily removable degradation products + Variable mechanical properties - Not as widely researched	[50]

1.1.4 Top down and bottom up tissue engineering

Top down tissue engineering is the traditional approach of creating a bulk scaffold as a single entity (figure 1.2). The scaffold will often require tailoring to fit into the implant location as this will be patient and wound site specific. Bulk scaffolds allow for long range design features such as channels to induce vascularisation and importantly for bone tissue engineering usually have more robust mechanical properties than modular scaffolds.

Bottom up tissue engineering is where a scaffold is built up out of smaller units in a modular fashion [51]. The smaller units are designed and manufactured independently and are then assembled at some point in time, up to the implantation of the scaffold. This can be weeks before the implantation or it can be during the implantation, depending on how the scaffold is designed. When producing a scaffold using the bottom-up approach by combining smaller building blocks, there are several general methodologies and more specific techniques which have been reported in the literature [52, 53].

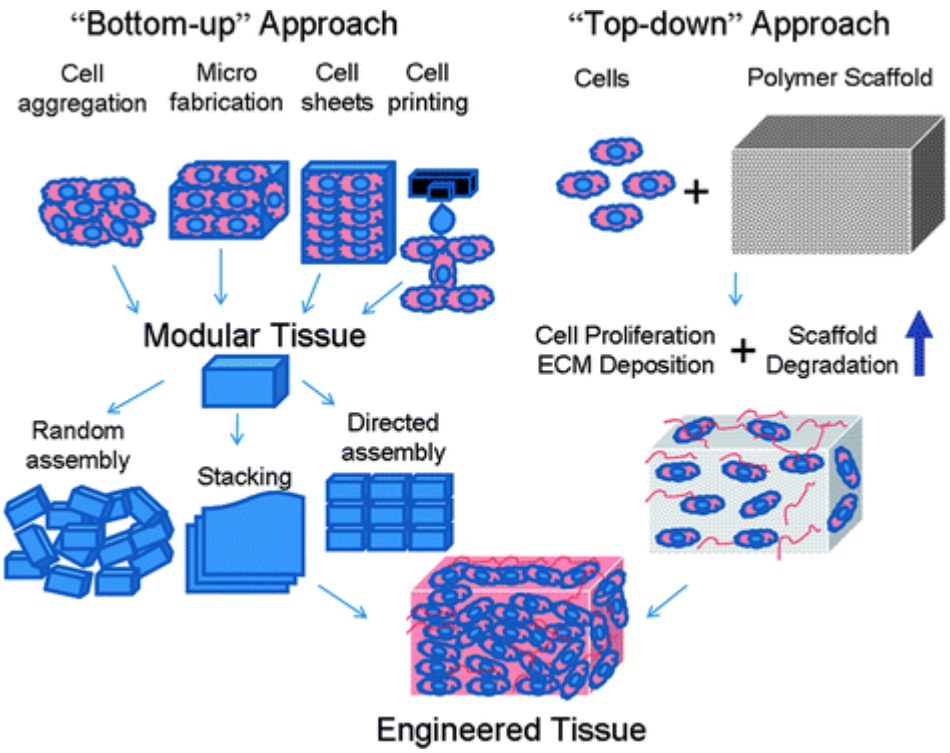

Figure 1.2. Two methods of tissue engineering: the top down approach and the bottom-up approach. For the top down approach cells are combined with a monolithic scaffold and often encouraged to grow throughout the scaffold using a bioreactor. There are multiple methods for producing tissue engineered scaffolds by the modular route. These techniques often initially lack the more robust mechanical properties that can be engineered into precise and custom scaffolds but can be delivered via minimal invasive surgery. Reprinted with permission from Royal Society of Chemistry, journal: Soft matter. [51]. Copyright 2009.

Random packing

Random packing is where the building blocks are randomly combined without any long-range order. The structure can be formed either by packing of the modular units into a confined space, or by capillary action. A scaffold formed in this way has very limited mechanical properties as there is an absence of any initial interaction between the modular units. This can change over time, especially where cells are involved and can produce ECM or remodel the scaffold. Initially the random packing arrangement will not recover after shear, and will dissociate easily [54]. This provides a poor structure for use as a scaffold under load bearing applications unless further steps are taken. Some groups use gels in combination with the modular units to improve mechanical properties and bring rigidity to the scaffolds [55-57].

Self-assembly

Directed assembly (self-assembly) uses particles which attract and bind to one another, providing the structure with some mechanical properties. This allows the scaffold to recover from shear, and it will not disperse with agitation. Layer-by-layer techniques which allow for electrostatic interactions are examples of this methodology [58]. Microparticles designed to physically fit/slot together are another

example [59]. Scaffolds formed this way generally do not have any long-range order but do possess some (usually weak) mechanical properties.

Additive manufacturing/directed assembly

Additive manufacturing allows modular units to be placed precisely where desired, to build up a scaffold [60]. Particles are often linked or bound together in some fashion, such as heating, to provide permanent bonding [61]. This gives this manufacturing style the most robust mechanical properties under tension and shear when compared to the other methods of modular scaffold assemble. It is possible to form long range order in these scaffolds and to design complex 3D architecture. This allows for more control over the scaffold, but fabrication requires long time periods. In this it is unlike self-assembly, which forms quickly irrespective of its scale (i.e. small quantities take as long to form as bigger quantities). Rapid manufacturing of scaffolds need to be redesigned for each application/patient.

For the first two techniques either a mould is created or the modular units assemble in-situ, which allows then to directly take the shape of the implant site. Rapid prototyping requires imaging technologies to determine the dimensions of the target implant site [62]. For most applications, the rapid prototyping offer advantages in manufacturing and scaffold design that cannot be matched by random packing or directed assemble. For some specific applications, such as voids within the bone or even the brain after a stroke [63] (where open surgery is best avoided) it is beneficial to be able to deliver the scaffold through a needle which is not possible with additive manufacturing formed bulk scaffolds.

1.2 Applications for particles in tissue engineering

1.2.1 Injectable scaffolds

The main advantages of using particles for tissue engineering is that they can be injected into the body, obviating the need for open surgery. This style of key hole surgery is a far less invasive technique than open surgery. Once injected, the particles would fill a void of any shape within the body. In contrast a traditional scaffold would need to be redesigned based on scans of the patient, during the operation or having the patient's wound altered to fit the shape of the implant. For tissue engineering, particles can be utilised in areas that are either difficult to access surgically or in an area where the act of open surgery would cause more harm than the scaffold would bring. Injectable scaffolds are however often unable to support load immediately once implanted and can therefore only be realistically used in non-load critical areas.

This practice is based on the previous methodologies of direct cell transplantation to the damaged areas within the body but where it is difficult to track these transplanted cells. Those studies that have tracked the cells have found that the majority of the cells do not remain at the site of implantation but are often found within the liver [64]. The advantage of utilising particles is the anchoring effect they have on cells. When these cells are bound to a substrate they are prevented from dispersing throughout the body and remain bound to the microcarrier [65]. Current bone fillers are usually formed from fragmented ceramic power or bone cement, designed to set in-situ [66]. A tissue engineered approach of cell loaded scaffolds would allow uniform bone formation throughout the implant [67]. For injectable gels, problems occur in structuring the scaffold, with it being very difficult to engineer any kind of porosity [68]. As self-assembling scaffolds are formed from solid particles, these can be made to incorporate pores, channels, cells, biological chemicals, and other functional features.

1.2.3 Microcarriers for cells/stem cells

Microparticles have been used to provide enhanced surface area for the expansion of cells in in vitro culture [69]. When cells are taken from a patient to expand up to a greater number for re-implanting, the standard method is to culture these on flat plastic. A large surface area is required to allow the production of the high number of cells required for tissue engineering. Particles are used in a suspension system to greatly increase the area available for the cells to grow. This is especially true for porous microspheres which have an extremely high surface area. This idea was first developed in 1967 by van Wezel and was used to mass produce vaccines for viral infections using mammalian cells [70]. The additional surface area for growing depends on the size of the particles, the number of particles in the system and the level of porosity in the particles. The materials used for these particles have to be denser than the medium the cells are grown in as this allows the particles to remain in suspension and not float on the surface.

A drawback to this process are that the particles while being stirred are exposed to shear stress. This can damage the cells, impede their growth or causes them to change in phenotype into mechano-induced cells [71]. Collisions between the particles or with the exterior of the flask walls can damage or dislodge cells. Also, the retrieval of the cells from the culture is more difficult than flat surfaces, and depends on the porosity of the particles. However, for implantation as a delivery system it is not necessary to detach the cells from the scaffold. [72]. These cell carriers are consequently used as an implantation vehicle to directly implant the cells back into the patient. Porous particles can prevent cells being damaged or scrapped off during implantation via injection [73]. Within the body these particles can act as artificial (stem) cell niches, which could provide a constant production of differentiated cells to populate the wound/organ/tissue [12].

1.2.4 Microparticle aggregates

There are two techniques which are used to aggregate particles into a larger structure. The traditional technique is particle sintering where particles are produced and then sintered together either thermally or chemically [74]. The newer technique is to allow cells which have been cultured on the surface of particles to aggregate together through cell division and ECM production.

For particle sintering the particles are randomly arranged and are joined to one-another. This produces a very highly interconnected structure although with limited total pore volume [61]. Controlling pore size is achieved by controlling the size of the particles and thereby engineering the size of the gaps between particles. There are however many disadvantages to this technique. The first is that the sintering process usually requires an external treatment of heat or chemicals which is highly toxic to cells. This results in the cells only being able to colonise the structure after the sintering has taken place. It is then difficult to get cells to penetrate deeply with the structure unless elaborate perfusion techniques are used. The scaffolds also lose their ability to be directly injected into the body as they are now a large solid object unable to flow. If the particles where to be sintered inside the body to get around this disadvantage the sintering method would need to be non-toxic to host tissue ruling out most chemical treatments [75]. Salem et al. demonstrated biotinylated polymer particle self-assemble when avadin was added to the particles in solution, forming an agglomeration of the particles [76].

Aggregation through cells relies on cell proliferation and the production of ECM which gradually brings adjacent particles together to form a structure. This then allows for the direct injection of cell laden particles into wound sites. This avoids the need of open surgery which bulk scaffolds or externally sintered particles would require for implantation. This technique is reliant on the number and proliferation of the cells on the exterior of the particles. Therefore, the various culture conditions the particles and cells are exposed to could vastly alter the success of a cell binding scaffold. Parameters

such as duration of culture, particle size, particle porosity, mixing intensity, initial cell number are important considerations.

1.2.5 Bioactive agent releasing scaffolds

Biomolecules incorporated in the scaffold to be delivered upon implantation are a powerful way to enhance a scaffolds bioactivity. Drugs and biomolecules are included to enhance bone growth and to control and increase vascularisation. The compounds can be added to the scaffold material to be released on degradation; packed into the porosity of a scaffold to leach out over time; or bound to the surface of the scaffold. Commonly used biomolecules for bone scaffolds include bone morphogenetic protein (BMP) [77], Insulin-like growth factor (IGF) [78, 79], FGF [80], vascular endothelial growth factor (VEGF) [79, 81], heparin and transforming growth factor beta (TGF-β). BMP has been shown to increase bone formation, endochondral ossification and in low quantities to attract stem cells via chemotaxis [82, 83]. VEGF can recruit cells and initiate the formation of blood vessel rapidly but if expressed for too long can form 'leaky' vessels [84].

Drugs that have been previously used in studies include gentamicin, vancomycin, alendronate, ibuprofen and methotrexate [85]. Additionally, gene therapy is used to modulate transcription factors [86], mesenchymal stem cell (MSC) growth and differentiation [87] or to increase bone formation using plasmid encoded VEGF [88].

1.2.6 Incorporation of polymer microparticles into tissue engineering scaffolds

The incorporation of polymer microparticles have been included in gels or soft biomaterials to improve the mechanical properties of the gel. Even within a solid scaffold, micro-particle additions have the same effect as composite systems used widely in material science. Introducing particles within another matrix retards the progress of crack propagation through the material. This increases the materials toughness and increases the amount of energy required to deform the material. The polymer particles also provide a solid structure for cells to grow on. Cells within a high water content material such as a hydrogel are not observed forming the morphology typical of cells grown on a solid structure, which can affect the differentiation of the cells [69] or prevent cells which require surface binding from proliferating. The addition of microparticles is also a mechanism for adding growth factors and bioactive agents into a scaffold.

1.3 Porosity in scaffolds for tissue engineering

Here we are considering porosity in general and not specifically in relation to porosity of particles. When considering the porosity of a material Bružauskaitė et.al. classified the pores into various classes based on scale. Macro-roughness (>100 μm), micro-pore size (100 nm – 100 μm) and nano-roughness (<100 nm) [89]. Different sized pores have different effects on cell migration, proliferation and differentiation along with more fundamental differences in the ability for nutrients to diffuse through the structure. Macropores are important for the formation of vasculature and nanopores can be beneficial for cell adhesion and the formation of ECM fibres [90-92]. When considering porosity; the extent (percentage) of the porosity within the material, whether it is interconnected, the size of the pores, the distribution of pore sizes and pore shape may all have an impact on the cell cultured on the material.

1.3.1 Porosity in bone tissue engineering

The widely reported ideal pore size for bone tissue engineering is one greater than 100 μm, sometimes reported to be 300 μm for in-vivo applications [93]. There is a vast amount of conflicting data to define a definitive ideal pore range and factors such as cell line used, age of cells or animals and location of implantation may all have different reactions to porosity. Smaller pores are acknowledged as increasing the surface roughness allowing the scaffold to perform better. Lee et al. found that when cultured on a porous polycarbonate membrane that when pore size was increased from 200 nm to 8 μm the proliferation of MG63 cells increased and the osteogenic differentiation reduced [94]. The increase of expansion room made available by the larger pores may have allowed the MG63 cells to continue proliferating which would have prevented differentiation from occurring. When scaffolds with larger pores are compared to scaffolds with both large and small pores the ones with both pore types induced a superior response [95]. It is hypothesised that the combination of pore sizes combines the impact of two length scales and hence more closely mimicking natural ECM. Some groups have reported that ordered and disordered pore geometry has an effect on bone regeneration with ordered geometry producing compact laminar bone and disordered pores producing anisotropic bone growth [96]. Mechanical roughness of a scaffold has the beneficial effect of allowing increased binding integration along the boundary of the scaffold and the bone.

1.3.2 The effect of porosity *In-vitro* vs *In-vivo*

One unified statement from the literature is that the ideal pore size for bone tissue engineering is different for in-vitro systems and in-vivo systems. Results observed in in-vitro the lab are often not replicated when using an in-vivo animal model and vice-versa. Bone ingrowth into pores is superior in larger pores in-vivo and better in smaller pores in-vitro. In in-vivo studies pores around 100 μm tend to cause cells to become chondrocyte like before osteogenesis, potentially due to the hypoxic

environment [93]. Pores less than 50 μm in in-vivo studies tend to form fibrous tissue [97]. This is potentially due to the lower availability of oxygen within the body. Within in-vitro cultures abnormally high levels of oxygen are present which increases the diffusion rate into smaller porosity. Within the body this would not occur. It is perhaps by this limitation that creates such differences between in-vivo and in-vitro experiments on pore size.

1.3.3 Interconnecting porosity and cell migration

Cells have been observed to migrate through pore sizes far smaller than the cell diameter and to extend processes through even smaller gaps. Differences are found between different cell types and some cells can pass through smaller gaps when co-cultured with another cell type. The size of the interconnections also play an important role in nutrient and O_2 diffusion and therefore have an influence on hypoxia and diffusion range [98]. Saunders et al. found smooth muscle cells were able to pass through pores of 2 μm in diameter [99]. Kim et al. found that feeder cells (MEF and STO fibroblasts) were able to migrate through membranes 3 μm in diameter (1.6% cell migration) and far more easily through 8 μm pores (9.3% cell migration) but the cells did not pass through 1 μm pores [100]. For all the pores sizes trialled, cell body extrusions such as lamella were found to be able to cross the membrane and although these were more prominent in 3 μm or above they were still present in 1 μm pores allowing interaction between the feeder layer and the human embryonic stem cells the other side of the membrane [100].

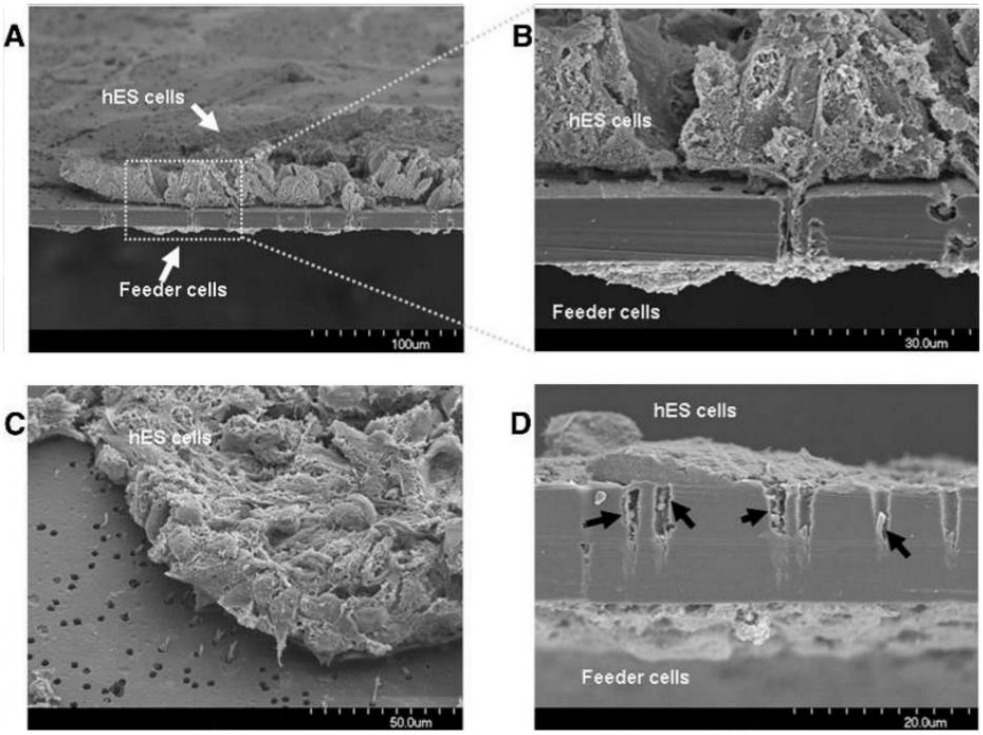

Figure 1.3. SEM image of hES cells separated from feeder cells by a porous membrane. (a – c) pore size is 3 µm with cell processes from the hES cells observed interacting with the feeder layer by extending through the membrane. (d) The pores in the membrane for this image are 1 µm in diameter and cell processes are observed within the channels. Reprinted with permission from John Wiley and Sons, journal: Stem cells [100] . Copyright 2007.

In research more related to bone, Li et al. found that human umbilical cord derived MSC could pass through a 3 µm gap in a membrane but could not pass through a 400 nm gap [101]. When comparing different pore sizes with MSC migration Peyton et al. found that more cells traverse through the smaller 12 µm membrane gap than the larger 17 µm gap [102] suggesting that a larger pore size does not always allow for better cell passage. This is also interesting as the group pointed out that 17 µm is the same diameter as the cell whereas 12 µm was smaller than the cell meaning that cells passed through pores preferentially where they had to restructure themselves to fit through.

In a recent study Akino et. al found that MSC cells were influenced by co-culture with another specific cell type (keloid-derived fibroblasts) which enabled the MSC to migrate more efficiently through 8 µm pores than with normal dermal fibroblasts [103]. Here they also found that MSC cells were able to pass through 3 µm sized pores when cultured with the keloid derived fibroblasts [103]. Other groups have found similar results on cell migration with epithelial cells [104] and neutrophils [105]. This suggests that excretory mechanisms, potentially injury related mechanisms, can change the behaviour of cells to allow them to respond in ways not possible under normal circumstances.

1.3.4 The effect of porosity on mechanical and degradation properties

Porosity in a material reduces the mechanical strength of the bulk material; but not the mechanical properties of which the cells are exposed to when in contact with the material. As porosity is increased a reduction in mechanical properties is observed [77]. This often places a limit to the extent that a material can include porosity before it becomes too weak to use in the desired application. Metal foams tend to be the material most able to include high levels of porosity while still maintaining suitable mechanical properties for load bearing application.

Increasing the porosity of a material, especially if that pore structure is interconnected, vastly increased the surface area on which surface degradation can occur. This may limit a materials use or may be designed in to speed up the degradation of polymers with longer degradation times. The higher amount of degradation may also result in the production of a greater quantity of degradation products. For polymers, such as polycaprolactone (PCL) this results in a highly acidic by-product which can be very damaging to bone and bone cells. This acidic by-product is released over a much longer time scale with PCL than with polymers such as polyglycolide (PGA) and PLA for which the acidic build up occurs more rapidly, with less time to dissipate, resulting in a more acid local environment.

1.3.5 Porous particles

As described in section 1.2 particles are an excellent way to locally deliver cell therapies however the porosity needs, discussed above, are equally necessary for microparticles. Porous particles are able to allow cells to bind to both the interior and exterior of the particle[67, 106]. Cells on the inside or in surface depressions are better able to resist shear forces [107]. Porous cells also provide a higher surface area for cells to grow on, and allow for increased perfusion through particles if the porosity is interconnected.

1.4 Manufacturing methods for particles used in tissue engineering

Non-porous and porous particles in the order of 10 to 1000 μm, have been manufactured via numerous methods reported in the literature. Non-porous particles are generally easier to manufacture than their porous counterparts, as a secondary system are often required to produce the porosity within the particles. Any method of forming particles should ideally allow control over the size, shape, surface characterisation and porosity (if any). Having precise control over particle shape and properties is essential in maximising its functionality in various tissue engineering applications. There are many methods by which particles can be formed such as emulsion polymerisation [108], precipitation polymerisation, spray drying [109-111], hot melt encapsulation [112-115], gelation [116-119], grinding/milling [120-122] and electrospraying [123, 124]. Porous particles can formed via supercritical CO_2 [125-127], thermally induced phase separation [128], freeze thaw cycles [129], solvent evaporation [130], particle leaching [131] and polymer high internal phase emulsion (HIPE)/double

emulsion formulations [132]. A selection of the techniques frequently used to manufacture particles is described in table 1.2 and the more relevant techniques for the thesis are described in more detail below.

1.4.1 Established particle manufacturing techniques

Table 1.2. Table of the more common manufacturing methods for producing particles.

Technique	Description	Refs
Grinding/milling	Potential the simplest method of producing particles of a polymer is to grind the material. Increased grinding will decrease the size of the particles produced although a polydisperse size distribution will always be present.	[120-122]
Supercritical CO_2	The polymer is dissolved in supercritical CO_2 at high pressure and then the solution is rapidly decompressed allowing nucleation of the polymer, forming microparticles.	[125-127]
Solvent evaporation	A polymer is dissolved in a solvent and then this mixture is added to a solution in which the solvent in insoluble. Within this solution, the polymer forms into spherical droplets. The solvent is left to evaporate which leaves behind solid particles of the polymer. This technique tends to form a distribution of particles sizes but the parameters can be tuned to create a reasonably narrow distribution of sizes.	[130]
Gelation	A standard example of gelation is gelatine being exposed to calcium ions and solidifying into a solid structure from a viscous liquid. This system is often used to encapsulate cells within hydrogels. These encapsulated cells can then be used for bio-printing or for hiding cells from a body's immune system.	[116-118]
Spray drying	Polymer is extruded across a heat source, such as heated extrusion tip, into a fast flow of hot air and the particle is formed as the polymer cools. The high temperatures involved can damage any bioactive molecules included in the polymer. 86- 88	[110, 111, 132]
Electrospraying	Electrospraying is very similar to electrospinning but produces particles instead of fibres. Particle size can be altered by altering the solvent system used, voltage charge, extrusion rate, polymer concentration or environmental parameters such as temperature and humidity. 100 -101	[123, 124, 129]
Hot melt	Hot melt is often used to coat another substance, such as drugs, with a polymer coating. The size of the particles formed can be easily altered from 1 to 1000 μm in diameter by altering processing parameters.	[112-115]
Additive manufacturing	A popular technology in recent years that allows the construction of objects from computer generated structures. This is discussed in greater detail below.	[133-135]
Flow lithography	Fluidic channels can be used to turn particle production, which is usually a batch process, into a continuous process. Liquid pre-polymer passes through the channel whilst a light source cures the polymer as it passes. This is discussed later in the chapter.	[136-139]
Micromoulding techniques	This is a batch manufacturing process where a polydimethylsiloxane (PDMS) mould is created which contains shaped holes. Pre-polymer solution is poured into this mould and then cured. Particles are then ejected from the mould which can be used again.	[139]
Emulsion	Emulsions are a combination of two immiscible solutions, with one of the phases forming particles within the other phase. Water in oil (w/o) or oil in water (o/w) emulsions can be utilised to form solid particles. A polymer high internal phase emulsion is an excellent example of an advanced emulsion system and this is discussed in detail later in the chapter.	[108, 132]

1.4.2 Additive manufacturing

Additive manufacturing has great potential in tissue engineering due to its unprecedented ability to construct 3D scaffolds with almost absolute freedom and control over microfeatures. One of the additive manufacturing techniques used to produce particles is projection based stereolithography, this technique incorporates a dynamic mask. A digital micro-mirror device (DMD) is an array of mirrors which can be programmed to reflect a specific image, with each mirror acting as a pixel of that image (figure 1.4). The DMD allows the projection of a pattern of light onto a surface [133]. This can be focused down to produce micron-scale features [134]. A DMD is often used to build 3D structures, with a new layer being added after the previous layer has been cured [135]. A DMD can easily make any 2D shape, but requires time to produce 3D objects. The DMD is significant in that it can mass produce particles of any shape and is even able to produce different shapes on the fly during manufacture, which can ensure a high degree of mixing between different particle types.

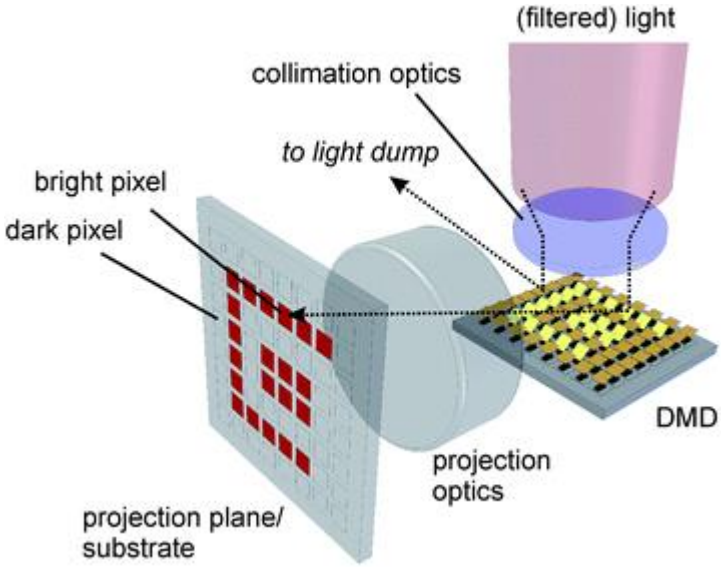

Figure 1.4. DMD set-up showing micro-mirror array projecting light towards either the substrate or the light dump depending on the angle of the mirrors on the DMD. Reprinted with permission from Royal Society of Chemistry, journal: Analytical Methods [140] . Copyright 2007.

1.4.3 Microfluidic enabled rapid lithography particle manufacture

Fluidic channels can be used to turn particle production, which is usually a batch process, into a continuous process. Liquid pre-polymer passes through the channel whilst a light source cures the polymer as it passes [136-139]. These channels are often formed from polydimethylsiloxane (PDMS), a silicone-based organic polymer, and the standard for microfluidics. This material has an advantage for photocurable chemistry because it forms a competitive oxygen layer a few microns thick from its surface, which prevents free radical polymerisation [136], thus preventing polymer from curing onto it. There are many variations of this technique reported in the literature [141]. Such as a single channel, which is patterned with selective curing from a Digital Micromirror Device (DMD) [141-144].

The main microfluidic technique used in the literature, to produce particles via a laser based system, is a process called continuous flow lithography. A similar but more advanced technique is called stop flow lithography (figure 1.5). In continuous flow lithography, the monomer is constantly flowing through a channel in a microfluidic and photocuring takes place within the monomer flow. In stop flow lithography, the velocity of the monomer is controlled, allowing the monomer flow to be halted so that photocuring can be applied to a non-flowing area. After photocuring the monomer flow is then resumed, allowing formed particles to be carried away from the curing site by the flow. Stop flow lithography requires an advanced level of control of the systems pressure, either via a pump or by microfluidic switches. The disadvantage to this microfluidic method is that new layers cannot be easily added to existing particles, rendering all particles produced 2.5D [137, 142]. The only control over particle height is by varying the height of the microfluidic channel [136]. There have been several clever solutions to this problem [138, 145], but none which offer complete control over the 3D shape.

Both 1PP (photon polymerisation) and Two photon polymerisation (2PP) can be adapted for a fast throughput by stop flow lithography [136, 146]. This involves the continuous stop and start flow of a photocurable medium, controlled around the polymerisation process to create a suspension with 100's of small structures. Recent developments include trapping cells within the photocured resin. PDMS is used as the throughput chamber due to its polymerisation inhibition properties at its surface [136, 146].The same limitations apply as with the majority of 2PP processes. Limited patterning distance to the focal volume, slow patterning speeds and long-time scales for producing macro objects [146].

A common research question directed towards stereolithography applications is their suitability for mass production. Stop flow lithography is a viable method for this problem, producing large quantities of particles with micro resolution. System outputs of 100 particles/second have been reported [136]. There is also an ever increasing requirement to produce micro particles with increasing resolution and chemical properties [136]. Increased resolution allows greater customisability of the scaffold and allows the control of cells from smaller length scales (such as nano features).

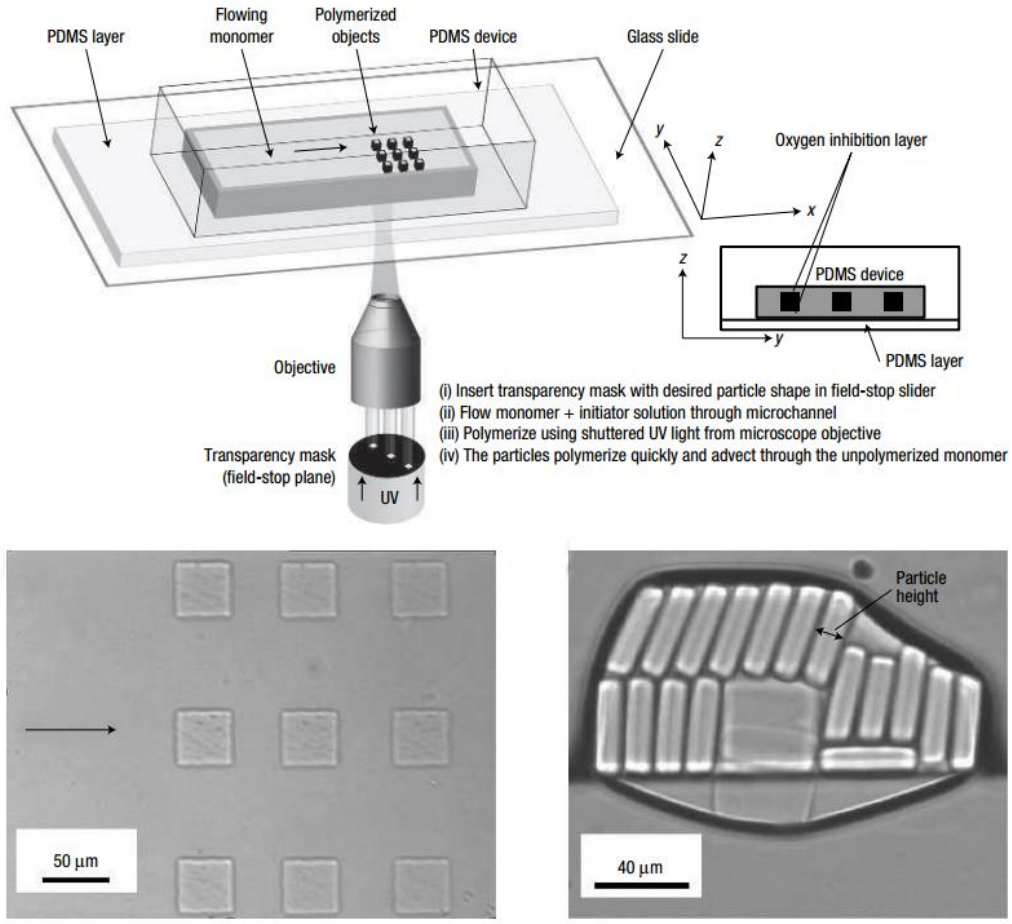

Figure 1.5. Shaped microparticles formed using a UV radiation source and a photomask in a PDMS channel containing flowing monomer. Reprinted with permission from Macmillan Publishers Ltd: Nature Materials [136]. Copyright 2006.

1.4.4 Micromoulding techniques

This is a batch manufacturing process where a PDMS mould is created which contains shaped holes. Pre-polymer solution is poured into this mould and then cured. Particles are then ejected from the mould which can be used again [139]. PDMS can reproduce nanometre sized features so this method can reproduce fine details. This can be combined with a flow technique as when monomer is flowed in; the channel expands allowing monomer through, once the flow stops the channel contracts forcing the mould down into the channel (figure 1.5).

1.4.5 Emulsion

Emulsions are a combination of two immiscible solutions, with one of the phases forming particles within the other phase (figure 1.6). This can be done in a stirred tank, which is described below, but also as a microfluidic device. These microfluidic systems can be fabricated to allow the pre-polymer to be encapsulated in an insoluble phase [137, 147-149]. Water in oil (w/o) or oil in water (o/w) emulsions

can be utilised to form solid particles. A polymer high internal phase emulsion is an excellent example of an advanced emulsion system and this is discussed in detail later in the next section.

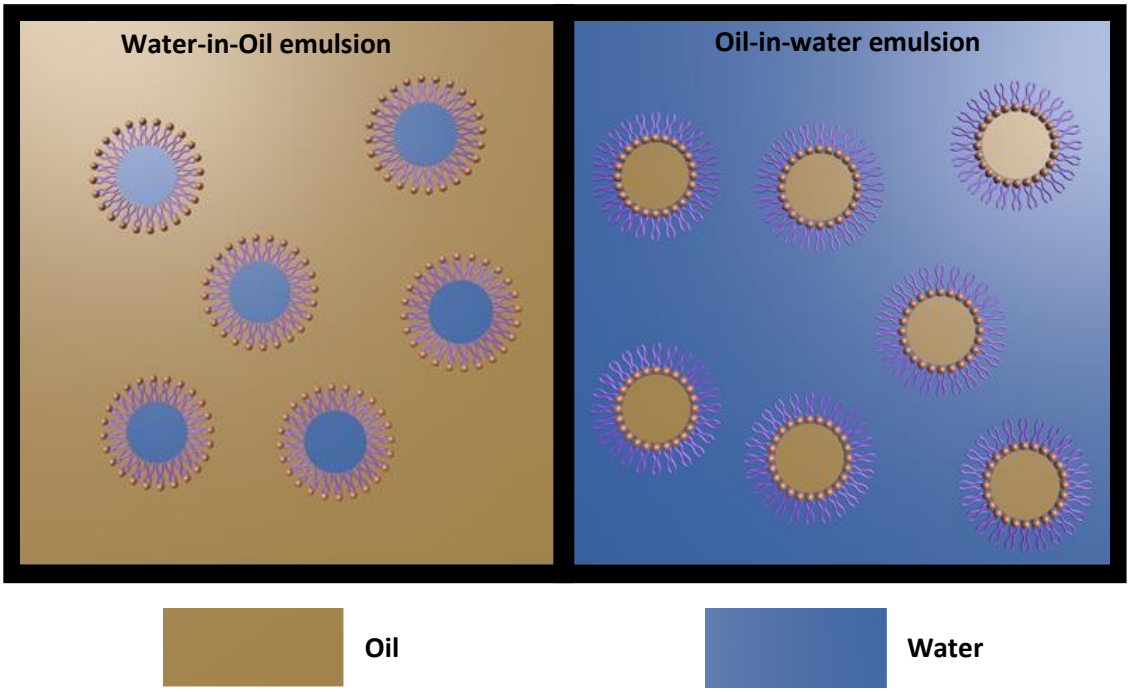

Figure 1.6. Diagram of both a water-in-oil emulsion and an oil-in-water emulsion. Discrete droplets of one phase are present in another continuous phase, with surfactant molecules surrounding the droplets. These molecules have a hydrophilic and hydrophobic section and allow the formation on an emulsion.

1.5 Emulsion templating

The process of emulsion templating preserves the internal structure of an emulsion when converted to a solid material. An emulsion is a solution of two immiscible liquids, such as an oil and a water phase, where one phase encapsulates (continuous) the other as droplets (dispersed phase). As an emulsion, a HIPE is in a semi-stable state, with some reverting to distinct and separate phases rapidly and others, such as mayonnaise, remain in the emulsion state for prolonged periods of time. The stability of an emulsion is dictated by the interfacial energy of the system. A system attempts to minimise the interfacial energy by reducing the surface area between the two phases. The ultimate reduction in surface area is a complete separation of the emulsion into two distinct phases. This is the end state for all emulsions, unless they are fixed by emulsion templating, with the only difference being the time required to return to that state. A reduction in surface area is also achieved by having larger droplets and therefore the formation of smaller droplets requires energy to be put into the system. The greater the energy placed into the system the small the droplets can become as the total surface area between the phases increases. The emulsions stability is therefore dependent on the time it can resist the destabilisation of the emulsion.

The solid portion of a polyHIPE is formed from the monomer phase surrounding the droplet, which can be polymerised to leave behind a solid shell from which the water phase can be drained. A high internal phase emulsion (HIPE) is an emulsion of water and oil which can be formed with up to 99% porosity [150] but must contain at least 74% water. When the water content is greater than 74%, water droplets start deforming to allow higher porosity [151] (figure 1.7). The droplets are all distinct from each other at this stage with a thin layer of the continuous phase surrounding each droplet. Emulsion templating involves retaining the internal structure of an emulsion during the solidification process to form a solid structure. This is done by substituting a monomer as one of the phases and then curing the monomer. When combined with an initiator, the polyHIPE can be used as a curable material, forming structures which may include a high level of interconnected porosity. During the curing stage, some combinations of polymers and initiators allow the formation on interconnecting voids between the larger pores. This allows the easy drainage of the droplet phase from the material in post processing.

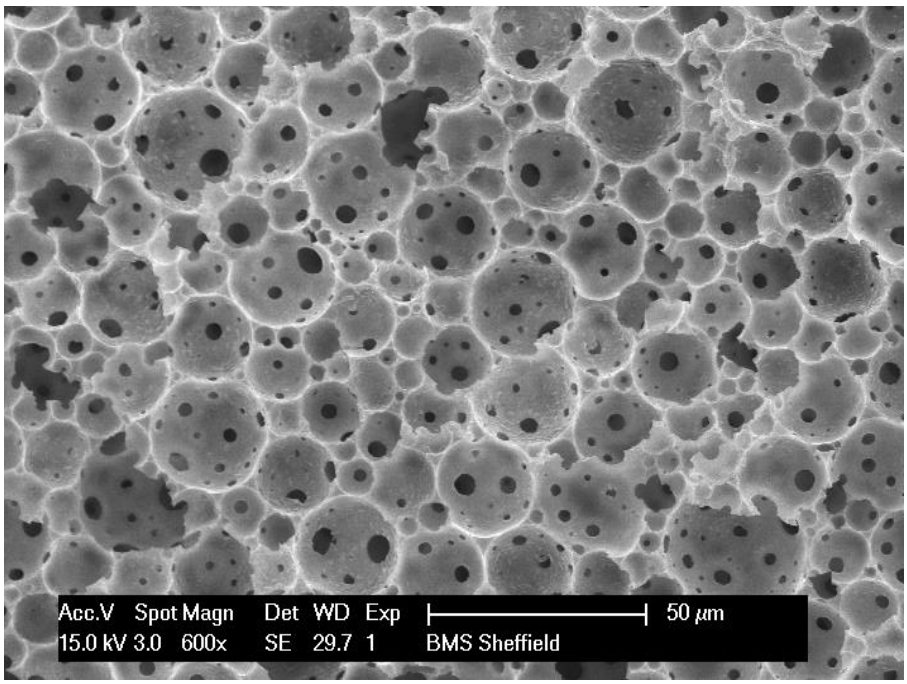

Figure 1.7. Emulsion template of the co-polymer system 2-Ethyl Hexyl Acrylate/Isobornyl acrylate formed from an emulsion via photocuring with 80% water content. As the polymer is formed from a HIPE emulsion the pores are interconnected with the neighbouring pores.

1.5.1 Photocurable polyHIPE: what is it made of?

Several different initiators exist for curing a polymer, such as a thermal initiator and a photoinitiator. polyHIPEs formed from these two classes are very similar in structure and in components used to manufacture them with a few noticeable exceptions, such as level of interconnectivity. Photoinitiators were used in the thesis so will be highlighted in the literature review. The following components are commonly used to formulate a polyHIPE. There are exceptions to those listed below but most polyHIPE material contain the following.

Surfactant

A surfactant is formed from two regions, one hydrophobic and one hydrophilic and their main function is to stabilise an emulsion. The surfactant is dissolved into the continuous phase [152] and resides on the interface between the two phases and allows the formation of a boundary between the two phases. A well-known example of this is household soap, which allows the emulsification of fat droplets inside water. When surfactant is added to the monomer it lowers the interfacial tension of the droplets [153] and also increases the likelihood of the formation of interconnected porosity [150]. While generally the more surfactant added to a system the more stable it becomes, it is possible to add too much surfactant which causes the self-assemble of micelles. Micelles are where the surfactant self-assembles into a sphere with all the hydrophilic or hydrophobic tails arranged inwards to minimise surface energy and thus effectively removing surfactant from the system. The most common surfactant is Span 80 [154] although many others exist along with natural surface active materials such

as gelatine and starch. The addition of a surfactant decreases the surface tension and viscosity of the monomer solution. This causes thinner wall formation between the pores within the scaffold which increases the interconnecting pore size of the polyHIPE. The surfactant does not undergo any changes during the curing stage and can thusly be removed from the polyHIPE to remove any toxic effect this may have on cells. It can be difficult to ensure all surfactant has been removed from the polyHIPE during the post processing step although techniques like Soxhlet extraction are widely used [155].

Crosslinker

The degree of crosslinking affects both the mechanical properties and therefore the cell response to the material. The crosslinker increases the number of branched connections within the polymer. Increasing the stiffness of a material is possible by increasing the crosslinker concentration within the monomer solution. Stiffness is well known to have a significant effect on cell differentiation [21, 156] and high stiffness materials may cause stress shielding in bone, reducing bone mass and density in surrounding areas [157, 158]. Being able to alter the stiffness of a material is highly desirable. It is worth noting that the stiffness of a material can be different at scales of magnitude. The materials stiffness on the microscopic scale to which cells experience can be different to bulk stiffness which is influenced by other factors such as porosity [159].

Polymerisation

PolyHIPE materials can be formed by free radical polymerisation (thermal and photo-initiators), click chemistry [160], atom transfer radical polymerisation [161], ring-opening metathesis polymerisation [162, 163] and poly-condensation [164]. An interesting rout for producing polyHIPEs is photocuring due to the flexible method of deployment possible by optical instruments along with a very rapid curing speed. The rapid nature of the photocuring process allows for a greater variety of emulsions to be used that would have been unstable over the time required for thermal curing to occur. However, the thickness of an entity formed by photocuring is limited by the ability of the light to penetrate a material. This places a limit on the curing of large bulk structures that would be possible with thermal curing. A workaround exists in additive manufacturing where a larger object is built with the gradual addition of material. This approach would allow an entity of any practical size to be formed that would not be possible if curing a large volume of material at one.

The initiator can be situated in either the continuous phase or the droplet phase and this has a significant effect on the resulting interconnecting porosity. With the initiator in the continuous phase the polyHIPE has an increased likelihood of containing open pores as the curing of the material is uniform, allowing shrinkage to occur which produces the interconnections. When the initiator is in the droplets the curing of the polymer occurs initially at the boundaries of the discontinuous phase and then cures inwards. This inhibits the formation of open porosity as the material is unable to contract uniformly to produce the interconnections between pores.

Monomer

A monomer or a combination of monomers is used to form the bulk material of the polyHIPE. To form a continuous polymer phase within an oil-in-water emulsion the polymer must by hydrophobic. The stronger the hydrophobicity the more stable the emulsion will be. This can be a problem for biocompatible polymers as cell attachment is superior on hydrophilic surfaces. Oil-in-water emulsions can be formed with hydrophilic polymers but the droplet phase then has to be an oil. This greatly increases the post processing time and expense of forming a scaffold. Hydrophobic surfaces can be treated with coatings such as plasma deposited acrylic acid or collagen to increase the cell absorption efficiency although this again adds time and expense to the scaffold forming process. A co-polymer system allows for the combination of material properties to overcome a shortfall of a particular material. The popular materials styrene is often used and produce very effective polyHIPEs although they are not biodegradable and are not desirable materials for tissue engineering scaffolds.

1.5.2 Biodegradable polymers

Popular biodegradable polymers are difficult to form into polyHIPEs because of the lower level of hydrophobicity of the polymers. PCL polyHIPEs have been formed by combining the PCL material with a secondary material with very hydrophobic properties. These polyHIPEs are successful however, the second polymer is often not degradable so the polymers cannot fully degrade when implanted. Polymer such as PCL and PLGA produce acidic by-products when these materials degrade which can adversely affect the surrounding biology.

1.5.3 Porosity in polyHIPEs

Increasing the volume of porosity in the polyHIPE can be controlled by changing the volume of water (discontinuous phase) added to the continuous phase. Increasing the porosity of the material increases the mass diffusion of nutrients and oxygen but reduces the bulk stiffness of the scaffold.

1.5.4 Interconnectivity in polyHIPEs

There is some debate on the cause of the formation of interconnections between the pores. In a study by Cameron et.al. where the transition of pores from the liquid to solid state were imaged, they stated that the contraction of the monomer transitioning to a polymer caused the interconnectivity [165]. Other groups argue that it is mechanical action, most likely in post-processing, which opens the thin polymer walls between the pores having observed the opening of pores during Soxhlet washing [166]. It is unlikely to singularly be due to this second method as polyHIPE has been imaged before any post-processing has occurred still contains interconnected pores but it may be that both techniques can contribute to the interconnectivity.

1.5.5 Destabilising mechanisms

Many methods of destabilisation mechanisms exist which cause different effects on the emulsion over time (table 1.3 & figure 1.8). They are not mutually exclusive and many can occur in parallel. The main effect by which many emulsions eventually collapse is coalescence. This is where the films between droplets become so thin that the adjacent droplets merge together into a larger droplet. Increasing the concentration of the surfactant in the system can increase the time scale over which this occurs.

Table 1.3. Table of the different destabilisation mechanisms which can affect emulsions over time.

Technique	Description	Refs
Ostwald ripening	Ostwald ripening results in the increase of the droplet size distribution with smaller droplets losing volume to larger droplets. This results in a droplet population of many large and many very small droplets. Over sufficient time this process will lead to the complete collapse of the emulsion. The minimisation of interfacial tension is the driver for this phenomenon as surface area is reduced as an outcome of the larger droplet formation.	[167-169]
Flocculation	Droplets may converge and clump together in an emulsion, leaving an uneven distribution of droplets throughout the emulsion in a process known as flocculation. This is caused by van der Waals attraction between the droplets and can be reversed by adding shear force the solution, although this will not prevent flocculation from reoccurring.	[167, 170]
Creaming/ Sedimentation	A density difference between the two phases of an emulsion will lead to either creaming or sedimentation. The greater the difference in densities the faster this will occur and the higher the viscosity of a solution the slower this will occur. If the droplets are denser than the surrounding continuous phase sedimentation occurs and the droplets will sink and congregate near the bottom of the emulsion. If the droplets are less dense they rise to the surface, in this occurrence the effect is called creaming.	[171, 172]
Phase inversion	A dramatic destabilisation event can occur whereby the droplet and the continuous phase invert and swap roles within the emulsion. A source of great frustration when developing new emulsions, this is called phase inversion. During the phase inversion, a period of time exists where both emulsions exist simultaneously. The process occurs by the drive towards minimal surface energy. This effect can be capitalised on and induced as an easy method to encapsulate air or water and has many applications in the food, cosmetics and pharmaceutical industries	[173]

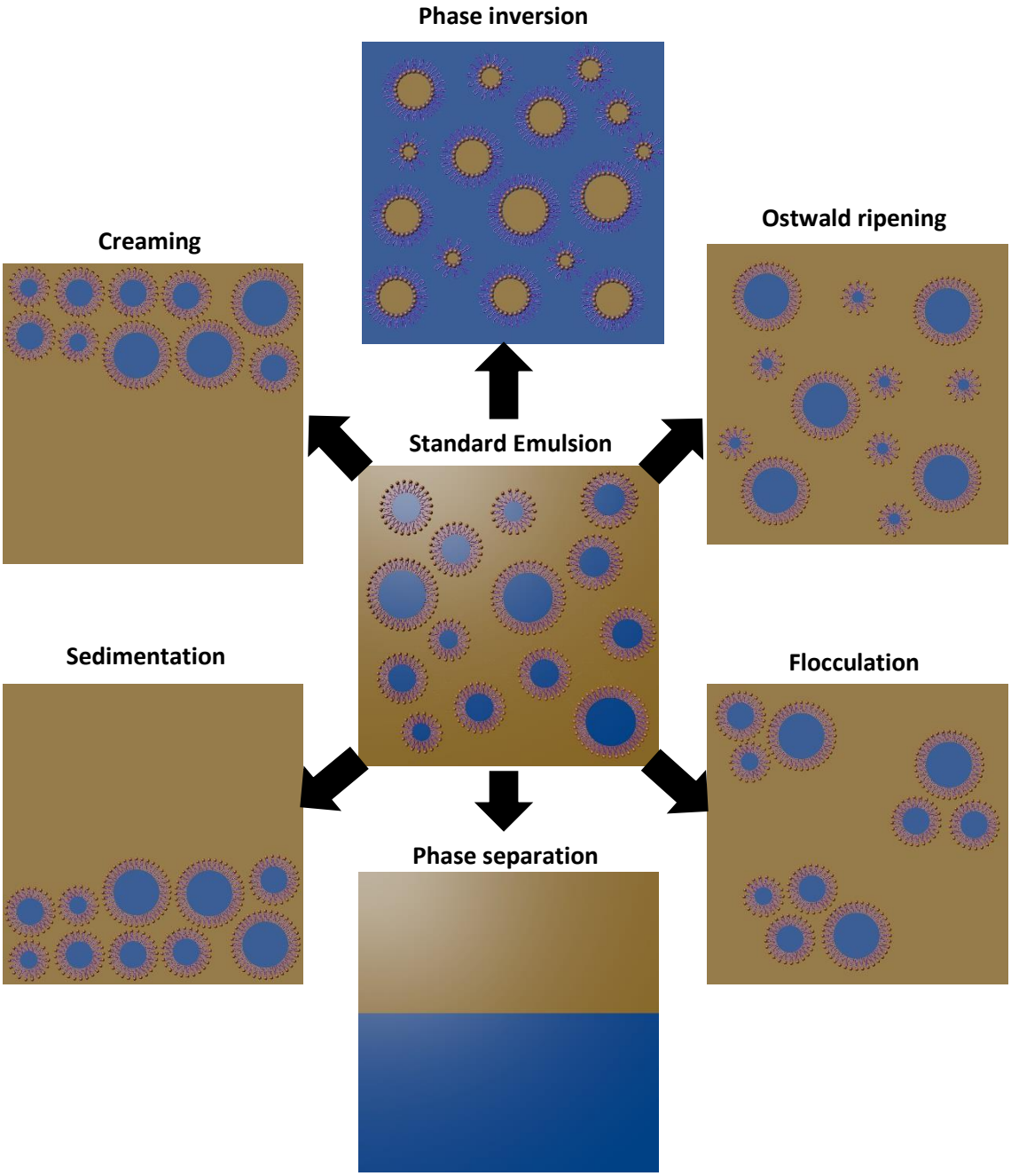

Figure 1.8. Diagram showing the different destabilisation mechanisms described in the table 1.3.

1.5.6 Pickering HIPEs

Concerns exist about the inclusion of certain surfactants into a polymer designated for *in-vivo* use. Toxicity may arise from the surface when it leaches out of the polymer or when it is released by the degradation of the scaffold. Processing techniques exist to remove these but add additional cost and time to the material preparation. Biocompatible surfactants do exist and methods to produce HIPEs without surfactants have been developed [174]. Of great interest for surfactant-less emulsions are Pickering HIPEs. These Pickering HIPEs are stabilised by (nano-) particles which become situated at the interface between the two phases, acting as a surfactant [175]. This often results in a thicker wall diameter between the porosity and produces polyHIPEs without interconnected porosity [176, 177].

More recently some groups have overcome this disadvantage and have produced larger interconnecting pores [159]. The addition of a nano-particles to stabilise the emulsion offers the potential to include bioactive materials such as nano-hydroxyapatite which can have osteoconductive effects once implanted [178, 179].

1.5.7 PolyHIPE microspheres

PolyHIPE microspheres can be formed through the formation of a double emulsion (figure 1.9). This is a multiphasic emulsion system whereby droplets of one phase, containing droplets of another phase, are dispersed in a continuous phase [180]. Alternatively posed, a double emulsion is hierarchical, it is an emulsion of an emulsion resulting in one emulsion being surrounded the same phase as the encapsulated initial phase. It is commonly referred to as a water in oil in water emulsion (w/o/w) and a counterpart oil in water in oil emulsion (o/w/o) can also be formed. Most techniques are currently two step processes, first creating the emulsion and then producing the double emulsion.

A few routes are devised to produce mono-disperse microparticles, membrane emulsification and microfluidics. Membrane emulsification allows improved control of microsphere production to decrease the spread of microsphere diameter, allowing a more monodisperse population (10 – 17 % size variation) [181]. A membrane is formed with uniform holes and the HIPE solution is passed through this membrane and then solidified [182]. Gokmen et al. used microfluidics to produce particles of polyHIPE [183]. This technique encapsulated the primary emulsion in a continuous stream of water and then photo-cured the particles. Using this method, they also produced cylindrically shaped particles by curing lines of the material in the tubing [183]. Direct write or curing into a stream of flowing HIPE is also possible as Dendukuri *et.al.* demonstrated with their microfluidic for making plugs and disks out of a 'UV sensitive polymer' [137].

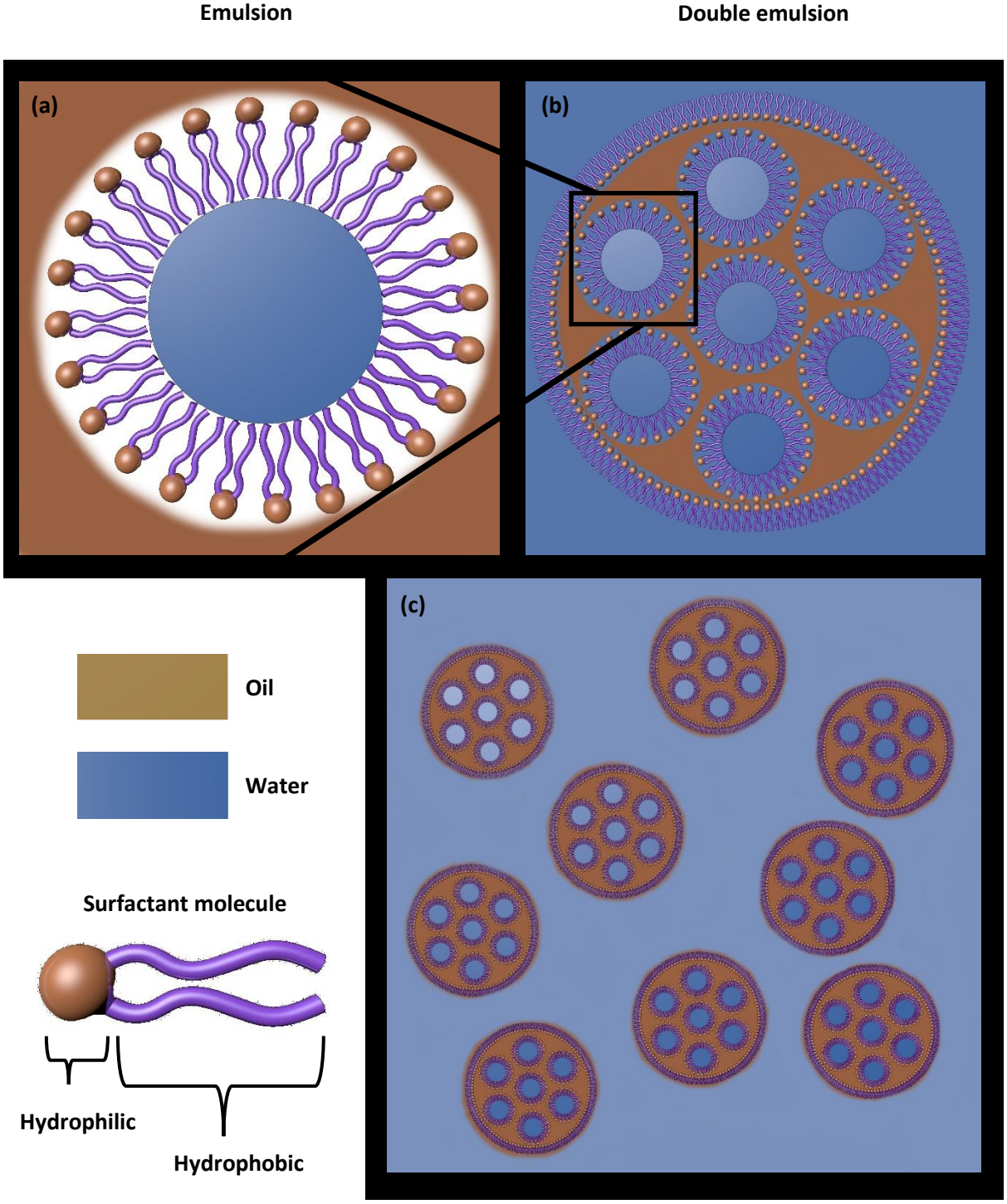

Figure 1.9. (a) Standard emulsion with a water phase surrounded by oil with surfactant molecules along the interface. (b) Double emulsion with the emulsion from (a) surrounded by a second phase with surfactant molecules along the interface. This forms a droplet of an emulsion. (c) Many of the droplets of emulsion within a continuous phase resulting in a double emulsion.

1.6 Applications of polyHIPEs, polymer particles and porous microspheres in tissue engineering

Cosgriff et.al. have developed an injectable polyHIPE system which cures in-situ within the body [184]. This offers a major structural benefit over using microspheres as immediately after curing the material has long range mechanical properties and stability. Akay et. al found that polyHIPE scaffolds containing 100 μm pores resulted in faster osteoblast migration than when compared to scaffolds with pores of 40 or 60 μm [185]. The pore size of the scaffold did not affect the total migration distance of the osteoblasts into the scaffolds (1.4 mm) which must be limited by another independent process such as hypoxia. Busby et al. used formed polyHIPE structures containing PCL, which they had to combine with another material (styrene, methacrylate or toluene) to allow the reduction in viscosity necessary for the PCL to be formed into an emulsion [186]. The group showed that the polyHIPE allowed the attachment of human fibroblasts but acknowledged their own lack of data on whether any of the cells had penetrated into the porosity. Non-degradable polyHIPEs formed from styrene and coated with laminin were shown to support neuronal cells up to 7 days and were superior to the plastic control [187]. In other reports it is found that elongated pores proved superior to spherical pores for neuronal cell culture [89].

Moglia *et al.* produced porous polyHIPE microspheres through a microfluidic method made from ethylene glycol dimethacrylate into which they added Bone morphogenetic protein 2 (BMP-2) into the continuous phase [188]. After testing for BMP-2 they found a loading efficiency of 73%. BMP-2 is a biomolecule which stimulates bone growth. There was no work with cells included in the paper to show the effect of the BMP-2 from their microspheres, however the effect of BMP-2 is well studied. Non-porous but highly roughened PCL/THF (tetrahydrofuran) microspheres were formed by Want et al. and were assembled into large aggregate structures via the crystallisation of the PCL [189].

Bone marrow MSC cells were shown to be supported and to show superior osteogenic effects when compared to a salt leached scaffold alternative. PLGA microspheres formed by a single water in oil emulsion, with pores of 3.4 to 5.1 μm formed by the evaporation of the solvent, were reported on by Zhang et. al [130]. The group adapted the microspheres with a further surface coating of type 1 collagen and could support Ovarian cancer cells in culture over 7 days. Several successful polyHIPEs have been formed from various thiol materials which are degradable [160, 190, 191], but the degradation products are not necessarily bioresorbable.

1.7 Mesenchymal stem cells and their differentiation

1.7.1 The differentiation process

Huang et al. divided the process of osteogenic differentiation into 3 stages in terms of the growth factors and ECM depositions involved [192]. During the first stage (days 1 – 4) there is increased proliferation of the MSC cells. The second stage (days 5 – 14) is one of early differentiation, marked by elevated Alkaline phosphatase (ALP) activity and the early deposition of type 1 collagen. VEGF and IGF-1 are also upregulated during these early stages. The third stage (days 14 – 28) is marked by a fall in the ALP activity and a high expression of osteopontin and osteocalcin. The beginning of the bone mineral deposition also begins at this stage with calcium, collagen and phosphates being secreted.

1.7.2 The role of cells in natural bone

The role of bone cells within bone (table 1.4) and tissue engineering (table 1.5) are discussed.

Table 1.4. Table for the role of the major cells found in bone tissue.

Cell	Role in bone
MSC	MSC cells are self-perpetuating multipotent stem cells which can differentiate into several different cell types. Direct differentiation into osteoblasts, chondrocytes, adipocytes and adipocytes is possible and have been widely documented in the literature [193, 194]. The morphology of a MSC cell is a small cell body with a few long and thin cell processes extending from the cell body.
Osteoblast	Osteoblasts are part of the cycle of remodelling bone. These cells produce ECM and enable the mineralisation and growth of bone. Active in groups of cells they produced crosslinked collagen and hydroxyapatite. Osteoblasts produce bone in response to damage through trauma, osteoclast activity and can increase bone mass when the bone is under load by producing more bone than the osteoclasts resorb. Osteoblast activity can be inhibited to allow for osteoclasts to remove more bone than is produced. This can be in response to lack of loading on the bone or if the bone is being reduced to increase the amount of calcium available to the body.
Osteocyte	Osteocytes are the most common cell type within bone and are responsible for maintaining the bone and responding to damage or stress. Bone without osteocytes has been shown to be weaker than normal bone [195]. Osteocytes are terminally differentiated osteoblasts which become embedded in the bone matrix, after which they exhibit a morphological change and alter their genetic expression [196]. The formation of an osteocytes has long been considered a passive process of being covered by bone matrix [197]. More recent advances have begun to show that this is an active process whereby the osteoblast is triggered to burry itself inside the bone matrix. Osteocyte morphology is similar to a star like pattern (stellate) with many dendritic processes extending from the cell body and connecting to other osteocytes. The force applied to bone is thought to be sensed by the cell dendrites which stretch from canaliculi from osteocyte to osteocyte in a process known as mechanotransduction [195, 197]. There is some debate on whether osteocytes resorb bone in a similar fashion to osteoclasts for dynamic calcium release and measuring this is reportedly very difficult [198]. Osteoblasts have been shown to be able to migrate through porous networks [185]. A more detailed description is highlighted in an excellent review of osteocytes by L. Bonewald called ‘the amazing osteocyte’ [197].
Osteoclast	Osteoclast cells resorb bone and are differentiated from the haematopoietic lineage. They secrete specialised lytic enzymes and acid to degrade bone matrix [199].
Lining cells	Lining cells are osteoblast cells which have flattened onto the surface of non-remodelling bone. They are connected to one another by gap junctions and send cell processes into the bones canaliculi. They are thought to be either dormant osteoblasts which will be re-activated with the right chemical signals or dormant precursor osteoblasts and a source of osteoblast proliferation [200].
Chondrocytes	Chondrocytes can be found within cartilage and produce mainly collagen and proteoglycan ECM. Chondrocytes can survive in highly avascular cartilage and are slow in proliferating in response to trauma when under these conditions. Chondrocytes are formed by MSC cells encasing themselves in collagen ECM which in time becomes the lacunae where the cell resides. Chondrocytes can be found in cartilage growth plates in adolescent bones. During human growth they undergo a process of endochondral ossification to help transform the surrounding tissue into bone [201].

1.7.3 The role of cells in tissue engineering and in-vitro testing of scaffolds

Table 1.5. Table of the cells used in tissue engineering and cell lines used for testing scaffolds.

Cell type	Role in Tissue engineering and testing in-vitro
MSC	Particular attention has been paid to MSCs from adults for regenerative technologies, due to their pluripotency [194]. MSC cells can be obtained from many sources such as bone marrow, adipose tissue, dental pulp, placenta and blood [202]. Problems exist with using MSC cells as it is difficult to observe where they migrate to once implanted and it is acknowledged that a large percentage die immediately on implantation. However, MSCs are one of the sole cell sources, which can be extracted from a patient, that can be used to produce large numbers of osteoblast or osteoclast cells.
Osteoblast	Osteoblasts cells are naturally non-proliferative once differentiated from a precursor cell line. Cancerous osteoblast cell lines such as MG63s are used to test scaffolds in-vitro and lay down matrix but these cannot be used for in-vivo cell loading [203].
Osteocyte	Osteocytes are by nature non-proliferative and adapted to survive mildly hypoxic conditions. Proliferative osteocyte cell lines exist for testing scaffolds but these are not a cell line that it is possible to easily extract from a patient to use in tissue engineering [204, 205].
hES cells	Human embryonic stem cells (hES cells) were first reliably grown in culture in 1998 [206]. They have since started a new field of research with their ability to expand without any apparent limit in vitro. These cells have raised hopes that they could be a source of human cells for tissue engineering applications, where autologous cells were unavailable. Human embryonic stem cell-derived mesenchymal progenitors (hES-MP) are derived from HES cells by selecting for rapidly proliferating cells which proliferated in feeder free culture, over many passages [207]. These cell have the advantages of perpetual growth whilst removing some of the disadvantages associated with hES cells [207]. Much progress has been made in differentiating hES cells into multiple cell types [208-213] but the risk remains of transplanting undifferentiated hES cells into a patient.
hES-MP cells	hES-MP cells are differentiated from hES cells and retain their stemness and can be continuously differentiated in this state. The cell line has a restricted lineage however, differentiation is limited to forming bone, cartilage, and adipose tissues. This narrower section allows greater dependency on the resultant cell type, which makes their differentiation easier to predict and control. This is of great importance for use in tissue engineering. A main feature of hES-MPs is that they cannot revert back into hES cells [207]. hES cells can cause tumours to form when implanted into rats [207]; Karlsson *et al.* found that a similar injection of hES-MP cells did not appear to cause a teratoma and instead formed a homogeneous and well differentiated tissue.

1.7.4 Supplements used in culture of bone cells

The following supplements are routinely used in culture to stimulate osteoblastic differentiation [214]. β-glycerol phosphate (β-GP) is used as a phosphate donor to enable mineralisation and has an additional direct effect on cell differentiation by influencing intracellular signalling. The presence of just β-GP into culture media is still reported to produce mineralised ECM but when combined with Dexamethasone (DEX) the cells are able to produce mineralised deposits [214]. Ascorbate increases the volume and maturation of collagen deposited. The collagen produced then influences the cell

signalling causing increased alkaline phosphatase (ALP) activity. DEX is used in MSC systems to stimulate the differentiation of osteoblast cells.

1.7.5 The effect of hypoxia on cells

Hypoxia is an area of low oxygen concentration. Within the tissues of the body the level of oxygen is already very low, although this does depend on the specific tissue. Some cells are optimised to function in hypoxic conditions, like avascular tissues such as cartilage. The effect of hypoxia on cells is often dramatic. Many genes are switched on or off and the cell begins to release specific chemicals into the surrounding area that are designed to encourage vascularisation. Evidence is conflicted on whether hypoxia induces or inhibits osteoblast formation with Hirao *et.al* concluding from low (5%) O_2 culture conditions that osteoblasts and osteocytes differentiated preferentially in higher (20 %) O_2 environments [215]. However, Utting et al. documented that hypoxia inhibited the growth of osteoblasts in their studies [216]. Reports that hypoxia increases the recruitment and differentiation of osteoclasts is well established [217, 218].

1.7.6 Cell co-culture impact on differentiation

MSC cells have been found to become differentiated into osteoblasts, or upregulate osteoblast markers, when in the presence of either osteoblasts and osteocytes cells, even in the absence of osteogenic media [219-221]. It is not known if there is any contact between osteoblasts and MSC cells within the body but this effect has been shown to occur through culture in collected conditioned media [220]. Birmingham et al. found that osteocytes appeared to have a stronger osteogenic effect when co-cultured with MSC cells, although co-culture with osteoblasts also induced differentiation over a longer time frame. The group also found a synergistic relationship when both osteoblasts and osteoclasts were cultured with MSC cells [219]. However, there are some contrasting reports that only osteocytes can induce osteogenesis in MSC cells and not osteoblasts [222, 223].

1.8 Vascularisation of tissue engineered constructs

Despite appearances bone is a highly vascularised tissue with a high density of blood vessels passing through the entire structure. Bone also plays an essential role in blood component formation, with the bone marrow residing inside bone responsible for the formation of platelets and red blood cells. The ability of a scaffold used for bone tissue engineering can be used to determine the likely success of scaffold for bone regrowth [224-227]. A poorly vascularised area will prevent cells within the scaffold from acquiring nutrients and oxygen which will lead to cell death[227]. However, even with rapid blood vessel formation the time required for the blood vessels to penetrate the scaffold itself often leaves the cells without oxygen for too long, resulting in scaffold cell death. This places a limit on the potential thickness of scaffold currently used to that of the maximum blood vessel growth over the period cells can survive for. The absence of nutrients and oxygen can have a subtler influence on the construct by causing non-uniform differentiation of cells or causing cells to differentiate into unplanned cell types [228]. Any cell death within the scaffold will release the contents of the cell into the local area which has a deleterious effect on the surrounding cells. The inflammatory response of the body when it encounters a wound site increases the vascularisation of the area [77]. This response can lead to negative consequences if the reaction is severe.

1.8.1 Necessity for vasculature in tissue engineering

The main tissue engineering solutions which been used clinically, are for tissues such as cartilage and skin patches grown in-vitro [229]. These tissues are either thin or avascular in nature where the supply of blood is not critical or can be easily vascularised. Some researchers argue that the largest problem facing tissue engineers is that of ensuring a suitable blood supply for an implanted tissue [224]. The vessels within the body are usually no more than a few hundred μm apart with the diffusion limit of oxygen in tissue calculated to be around 200 μm

Larger tissues require the formation of rapid vascularisation when implanted in the body or risk becoming necrotic. Many strategies have been proposed for tissue engineering of large functional tissues and these will be discussed in the table 1.6. Before beginning it is important to define two concepts clearly, angiogenesis and vasculogenesis (figure 1.10). Angiogenesis is the sprouting of capillaries from existing vasculature [230, 231] whereas vasculogenesis is the spontaneous assembly of blood vessels where none existed before [232].

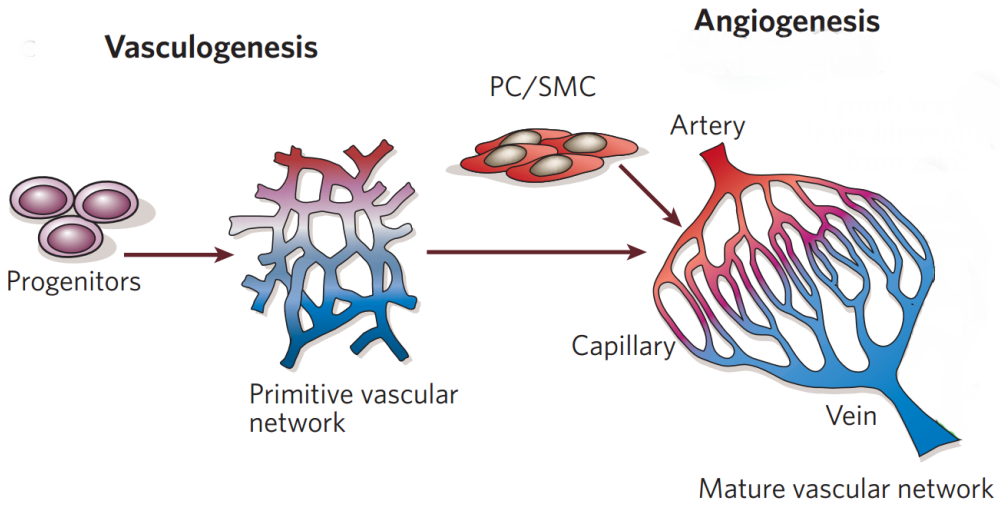

Figure 1.10. In vasculogenesis vessels spontaneously form from endothelial progenitors. Angiogenesis is the sprouting of vessels from existing vasculature. When vasculogenesis occurs, angiogenesis follows and causes the formation of a mature and organised vasculature network. Adapted, with permission from Nature Publishing Group, journal: Nature [233]. Copyright 2005.

1.8.2 Current strategies in vascularisation

The methodologies described below (table 1.6) describe the current approaches to vascularisation of a scaffold. These techniques are not always mutually exclusive and many can be combined for enhanced effectiveness.

Table 1.6. Table for different methods of vascularising tissue engineering constructs and scaffolds.

Technique	Description	Refs
In-vivo pre-vascularisation	Scaffolds can be implanted into a second site on a patient to allow for ingrowth of vasculature into the scaffold. This can then be removed and implanted into the desired site where it can re-connect with the existing vasculature. This allows for the implantation of a fully vascularised and functional scaffold. There are some problems with this technique as it requires 3 separate surgeries, two more than a standard implantation. One surgery is required to implant the scaffold into a secondary site and a second to then remove it and finally a third to implant into the actual defect/desired site.	[234, 235]
Growth factor and cytokine inclusion	Chemical and biomolecules can be included onto or into the scaffold via a variety of techniques that can speed up the vascularisation or angiogenic response. These molecules can be included within the scaffold if it is designed to degrade and release the molecules. They can be bound to the surface or simply contained within a porous structure to give rapid release upon implantation. Biomolecules such as VEGF are the most popular for engineering a vascular response.	[236]
Cell based vascularisation in-vitro	Adding specific cells such as endothelial cells and smooth muscle cells which form vasculature in the body can allow the formation of vessels in-vitro for pre-implanting. Often a bioreactor is required to produce flow that allows the vessels to form. When this technique is successful it meets some of the shortfalls associated with in-vivo pre-vascularisation although the vasculature formed in-vivo is often far superior due to the larger number of cells available and biomolecules at the artificial wound site.	[225]
Biologically derived scaffolds	Decellularised tissue preserves the structure of the vasculature and allows human cells to re-inhabit the existing vasculature for rapid vasculature formation. Both animal and cadaver tissues can be used however, there is an issue with reproducibility and the ever-present risk of disease transmission. Further problems exist getting endothelial cells to fully revascularise the tissue as capillaries are often so narrow it is difficult to get new cells to travel down these vessels to repopulate them. However, even if only the larger vessels are formed it is then much easier to grow new capillaries via angiogenesis than it would be to grow the complete vasculature by vasculogenesis or to encourage surrounding vessels to grow into the scaffold.	[236, 237]
Synthetically designed scaffolds	Taking inspiration from biological structures but removing the unpredictable nature and disease risk it is possible to assemble a computer design scaffold via additive manufacturing. This technique can produce vasculature templates such as channels throughout the structure which would then allow nutrients to enter the scaffold and allow endothelial cells to form vessels. It is possible to use dual headed printers to print both the scaffold and cells at the same time. Additive manufacturing can be a very time consuming and low yield process but this field is rapidly advancing and hold great promise.	[238]

1.8.3 Methods for testing vascularisation

To ensure that a scaffold can provoke an angiogenic response a variety of tests exist (table 1.7). Tests for the study of vascularisation can be split into in-vitro and in-vivo testing strategies. Using these before implanting a scaffold allows for a greater probability of success and allows the engineer to redesign or test additional variable that would not be possible in an in-vivo study.

Studying the stages of angiogenesis then allow tests to be designed which measure various stages of the process [230]. The first step is that endothelial cells break through the basement membrane to leave their standard location within the existing blood vessels. The endothelial cells then begin to migrate along a chemotactic gradient towards the stimulus of the angiogenic progress. The endothelial cells then begin to proliferate rapidly to ensure adequate numbers are available for the new vessels to form. The final step is for the endothelial cells to re-organise themselves into tubular structures to form blood vessels. With an understanding of these steps it is possible test whether a scaffold can stimulate any of these behaviours.

Table 1.7. Table for the most common methods for testing the angiogenic potential of a scaffold.

Technique	Description	Refs
Endothelial proliferation (in-vitro)	The first technique uses the knowledge of the increased proliferation of the endothelial cells during natural vessel formation by testing for this elevated proliferation rate. In comparisons with controls it can be observed whether endothelial cells proliferate and to what extent. One problem with this technique is what source of endothelial cells to use as different cell populations can react very differently.	[239]
Cell migration (in-vitro)	Cell migration assays demonstrate the ability of a scaffold to produce angiogenic factors which encourage the migration of endothelial cells. Scaffolds are separated from the endothelial cells by a filter and the endothelial cells can migrate through the filter. This allows analysis of the filter to analyse the distance of cells, although this can be a very time consuming method to analyse.	[240]
Vessel formation (in-vitro)	Tube formation of the endothelial cells can also be measured *in-vitro*. The cells can be combined with a collagen clot material such as Matrigel which emulates the 3D nature of an in-vivo model. Measurement of spontaneous vessel formation can then be measured.	[240]
Synthetic perfusable vascular network (in-vitro)	A novel method for investigating angiogenesis is using an artificial network construct of endothelial lined electrospun fibres formed over robocast sacrificial material. Ortega et al. developed a synthetic perfusable vascular network which showed vessel like organisations of endothelial cells over 5 days. The scaffold being tested for angiogenesis can be added to the areas in between the artificial vasculature and vessel formation can be measured growing out of the artificial vessels towards the scaffolds.	[241]
Organ culture assays (in-vitro)	Organ culture assays are as close to achieving the complexity of an *in-vivo* system, *in-vitro*, as it is currently possible to do. The most popular technique it to remove and segment the aortic ring from a rat and then measure outgrowth and abundance of vessel like growths from this explant towards the scaffold. However, the process of angiogenesis usually occurs in microvasculature, whereas this technique uses an aorta which therefore does not simulate the in-vivo situation as accurately.	[242]
Chorioallantoic membrane (CAM) assay (In-vivo)	A chorioallantoic membrane (CAM) assay involves implanting the scaffold under the shell and on the CAM of an embryonic chicken. The vascularisation response of the CAM after several days is analysed. We discuss this technique in greater detail below.	[243, 244]
Corneal angiogenesis assays (In-vivo)	Corneal angiogenesis assays are conducted by implanting the scaffold into a pocket on a living rat or rabbit cornea. An advantage is that as the scaffold is placed on the eye of the animal where it is possible to view the development of the vascular response by imaging the eye of the animal. The procedure to implant the scaffold requires considerable skill and this limits the number of animals which can be prepared at any one time for this assay. A further complication arises as it is very difficult to avoid the inflammatory response resulting from the implant.	[240]
Matrigel plug assay (in-vivo)	The scaffold is combined with matrigel and implanted into the subcutaneously. The scaffold-matrigel complex is removed from the animal after 7 to 21 days and the measure of vascularisation is analysed. The skill required for the surgery is less than that required for the cornea assay. It is however difficult to observe the process of vascularisation and requires animal subjects.	[245]

A CAM involves implanting the scaffold under the shell and on the CAM of an embryonic chicken (figure 1.11). The CAM is analogous to the placenta found in mammals and is heavily vascularised. The shell is opened and the scaffold is inserted onto the membrane and the shell is then resealed to prevent infection. The egg is then allowed to develop over 7 days before the shell is re-opened and the extent of vascularisation can be measured.

The CAM technique is popular as it relatively cheap cost and it is possible to conduct multiple tests on one CAM. In addition, the facile method of storage in an egg incubator allows a high number of sample testing possible. However, the technique is one which uses a chicken and does not use a mammalian species which does not make it ideal for testing. An in-ovo technique of the CAM assay has been adapted whereby the embryo is removed from the shell and kept inside a petri dish [246]. This allows the monitoring of the vascularisation response over time on the same samples and makes it easier to run several samples on one scaffold. While this has the appearance of an in-vitro test it is still utilising an entire animal and should be classified as in-vivo.

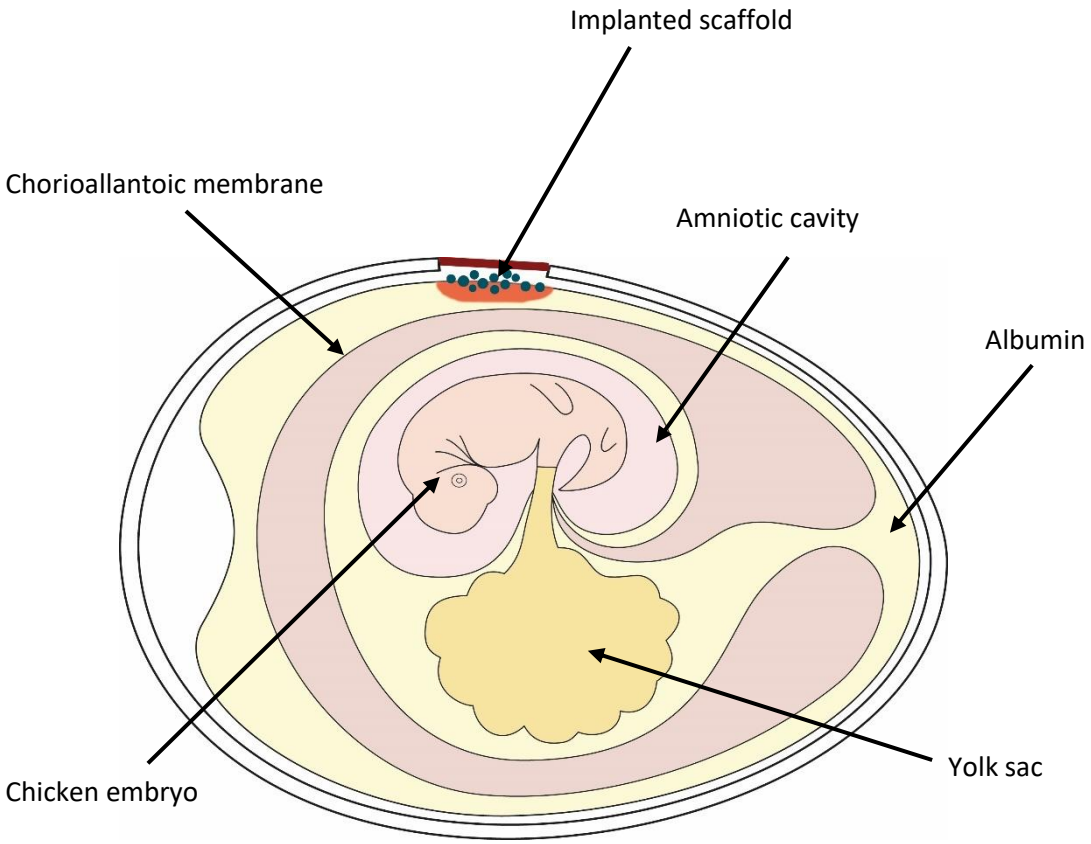

Figure 1.11. Diagram of the implanted scaffold on an chorioallantoic membrane within a chicken egg. This is used as an in-vivo assay to determine the angiogenic properties of a scaffold.

1.9 Findings from literature review

Currently used filler materials do not allow complete remodelling of a wound within the bone. At best, they allow minimal infiltration of the surrounding material and integration at the interfacial area between the bone and the implant. A tissue engineering solution could provide a superior treatment alternative to existing methods. Current tissue engineering solutions are usually monolithic scaffolds which require open surgery to implant. To circumvent this injectable scaffolds have been developed to obviate the need for surgery. These injectable scaffolds are a promising method to minimally invasively fill bones but the majority of these do not include cells, instead relying on cell infiltration from the surrounding wound bed. Injectable scaffolds loaded with cells require a rapid formation of vasculature to provide the scaffolds internal area with fresh nutrients and oxygen. In this thesis, it is proposed that a porous polyHIPE material which can be manufactured as microparticles suitable for cell loading and injection delivery has strong potential to meet these challenges.

1.10 Main aim:

1. Produce an injectable cell carrying microparticles system using bone as a model.

Specific aims:

1. Choose a fabrication system that will allow the best compromise between particle production speed and the ability to include customisable micro-features.
2. Test the biocompatibility of the materials used for the microparticles and elucidate the cell behaviours over long term culture.
3. Produce a biodegradable system of microparticles and compare biocompatibility and osteogenic potential to the non-degradable system.
4. Measure the injection potential of the microparticles and by assessing if they protect cells from the shear forces involved with injection.
5. Determine the microparticles angiogenic effect using various culture conditions in an in-vivo CAM assay.

The overall aim of the PhD was to produce an injectable particle system which can be used for non-load bearing tissue applications such as a bone filler material. The was tested up to the stage where it would be ready for an in-vivo study. Injectable tissue engineering solutions obviate the need for open surgery which will reduce the risk of infections, reduces risk of complications and increase recovery time to minimise hospital stay. Voids within bone lead to increased fracture risk and unless treated are likely to fill with fibrous tissue which will greatly reduce the ability of the bone tissue to regrow. Introducing a tissue engineering solution of MSC cells supported on microparticle scaffold should encourage the regeneration of bone. This would support regeneration at the point of contact between bone and scaffold and throughout the cell-laden scaffolds. This tissue engineered solution could be far more successful than traditional bone packing material due to the inclusion of cells and porosity. To determine the functionality of the proposed microparticle system various tests need to be undertaken such as the biocompatibility, osteogenic effect and ability to vascularise.

In Chapter 1 the existing literature will be explored around the research area. In Chapter 3 a variety of particle manufacturing methods are investigated and speed of production is compared against complexity and customisation of the particles produced. In chapter 4 the flexibility of the technique chosen in chapter 5 is evaluated terms of its ability to alter the microsphere size and porosity. In chapter 6 the biocompatibility and osteogenic potential of the microspheres are tested using an MSC like cell line. During this chapter, it is also found that the microspheres agglomerate together and that cells will penetrate the porosity and grow throughout the microsphere. These aspects are examined closely and evaluation of which differentiated cell types are present within the structure. In chapter 6 several biodegradable materials are trialled to determine if the agglomeration, ingrowth and biocompatibility occur in this new system. For chapter 7 an in-vivo CAM assay is used to determine angiogenic potential of the microspheres and both the degradable and non-degradable systems are compared this way. Finally, in chapter 8 the project is discussed in terms of the main milestones and

initial aims of project. Included in the appendix is an additional chapter which contains results from early experimentation on microspheres seeded with neuronal cells for a potential injectable neuro tissue engineering application.

Chapter 2: Materials and methods

2.1 Light based photocuring of monomers: Stereolithography

2.1.1 Laser based photocuring of monomers using a digital micromirror device

When combined with a laser source a digital micromirror device (DMD) allows the specific photocuring of monomers into a predesigned spatial pattern designated by the computer software. A DMD contains micromirrors which reflect incoming light either towards a photocurable monomer or a light block depending on their angle. Polymer particles were manufactured using this principle. A continuous wave 473 nm laser (150 mW output power, MBL) was set up with the lens and at distances shown in Figure 2.1. All lenses were purchased from Thorlabs (Germany) unless otherwise stated. The initial two lens set-up caused expansion and then stabilisation of the beam (Ø18.0 mm N-BK7 Plano-Convex Lens, 20 mm and 30 mm focal length respectively) before reflecting off the DMD (Texas Instruments Incorporated, TX, USA). The beam was focused through a second lens (Ø18.0 mm N-BK7 Plano-Convex Lens, 30 mm focal length) to stabilise the beam expansion of the DMD. This laser image was then reflected by a mirror (Broadband Dielectric Mirror) towards the monomer bath. A black and white image jpeg image created using Microsoft paint is uploaded to the DMD by its proprietary software (Vortran Laser Technology Inc, Sacramento, CA, USA) to allow for pattern projection.

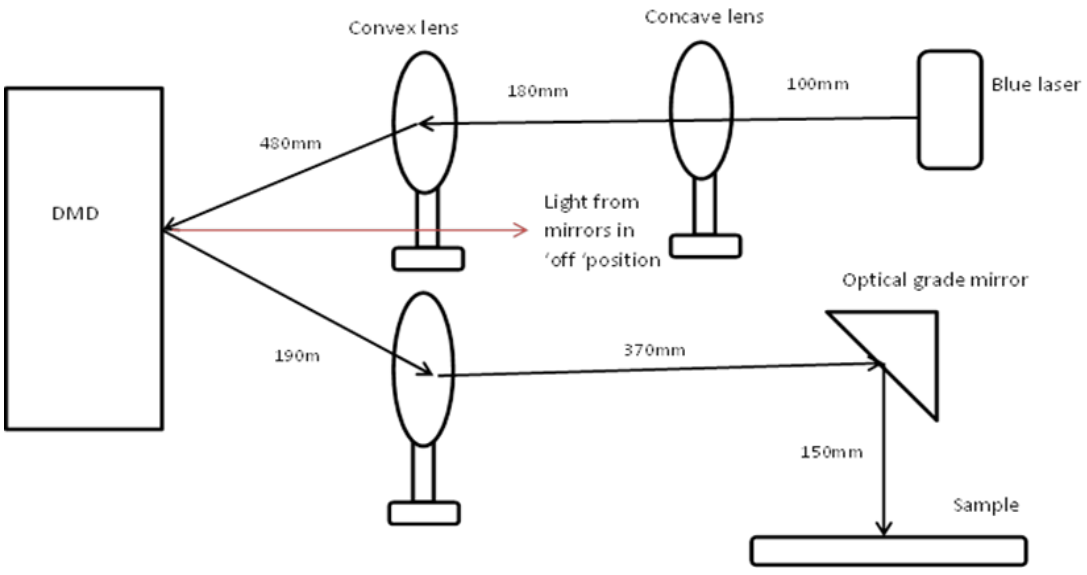

Figure 2.1. Schematic of DMD setup used to make the microparticles

2.1.2 Preparing a monomer solution of polyethylene glycol for photocuring

Photocurable polyethylene glycol (PEG) was prepared by mixing PEG monomer (MW=258, sigma Aldrich) with 4wt% photoinitiator 1:1 blend of Diphenyl(2,4,6-trimethylbenzoyl)phosphineoxide and 2-hydroxy-2-methylpropiophenone. The photocurable monomer was then kept in a photo-protective container (glass vial, 20 ml, wrapped in silver foil (Tesco, UK)).

2.1.3 Image design and production for software controlling digital micro mirrors

Images for the DMD were designed either in Autodesk inventor or Microsoft paint depending on the accuracy requirements. Images were formed in absolute black and white values and at 1024 x 768 resolution before uploading to the DMD.

2.1.4 Direct laser write of a photocurable monomer using single photon curing

Single photon (to differentiate from 2-photon) initiators requires the energy of a single photon to begin polymerisation. This technique allows the laser to move over a monomer bath causing polymerisation directly under its path. A passively Q-switched DPSS microchip laser, (Pulselas P-355-300), with a sub-nanosecond pulse duration and a variable repetition rate was used with an output wavelength set at 355 nm with a 0.5 ns pulse width and maximum power of 12 mW, 16.6 kHz repetition rate (Alphalas, Gottingen, Germany) was expanded and stabilised before being passed through a 10x Carl Zeiss 1.3A microscope objective onto a motorised stage. The motorised stage (ANT130-XY (Aerotech, UK) for xy translation & z translationPRO115 (Aerotech, UK) could move in the x, y and z directions and was programmable using G-code (A3200 Software-Based Machine Controlled (Aerotech, UK)). A well was made on a glass slide, which controlled the depth of the structure, and the photocurable PEG was added to the well. The stage was then programmed to write a line 25 mm long in the x direction. The size of the y direction changed depending on requirements and was between 300 µm and 2 mm.

2.1.5 Photo-polymerisation of computer designed objects using 2-photon manufacture

2-photon initiators require the simultaneous energy of two photons to begin polymerisation, this allows the creation of a voxel within the polymer. A 3D computer designed object (via the computer-aided design [CAD] software Autodesk Maya) was photocured within a monomer bath using this technique. A well was formed out of tape, with the centre (1 cm^2) removed, and applied onto a glass slide. 0.5 ml of PEGd was added to the well. A passively Q-switched DPSS microchip laser, Pulselas P-355-300, with 0.5 mW pulse duration and a variable repetition rate was used with an output wavelength set at 1064 nm and maximum power of 12 mW, 16.6 kHz repetition rate (Alphalas, Gottingen, Germany) was set at I = 2.05 and expanded up to fill the aperture of an x20 microscope objective (EC-Plan NEOFLUAR 10×, Carl Zeiss Ltd, UK). Using the SCA software and STL file is imported and sliced with the following settings slice DZ (0.009 mm), join distance (0.001 mm) and fill spacing (0.001 mm).

2.2 Microfluidic device manufacture and microsphere manufacture using said microfluidic device

2.2.1 Manufacture of a microfluidic device for fluid encapsulation

Microfluidic devices allow the manipulation of small volumes of liquid under highly laminar flow. These devices were manufactured to allow the fabrication of microparticles via encapsulation of one liquid within another. Lines photocured from PEG were formed using the same set up as in 2.1.4 using the design in figure 2.2. Lines were cured on a standard glass microscope slide and washed in isopropanol immediately after removal from the laser setup to removed uncured monomer. Polydimethylsiloxane (PDMS) (Sylgard 184) was prepared using a ratio of 10:1 of base to initiator, and the resulting mixture was stirred and then degassed in a vacuum for 15 minutes. The silanising agent tridecafluoro-1h,1h,2h,2h-tetrahydrooctyl trichlorosilane was added to the surface by vacuum deposition. The PDMS was then poured on the slide in a container, which controlled the total thickness to 14 mm. The PDMS was cured at 60°C for 3 hours and then removed from the container.

A 1 mm biopsy punch was used to create the input/output channels. The PDMS was bound to a glass slide by both surfaces being exposed to oxygen in a plasma rig at 50 W for 2 minutes, and then both surfaces being pressed together. Flexible silicon tubes (1.5 mm external 0.5 mm internal) were inserted into the channels.

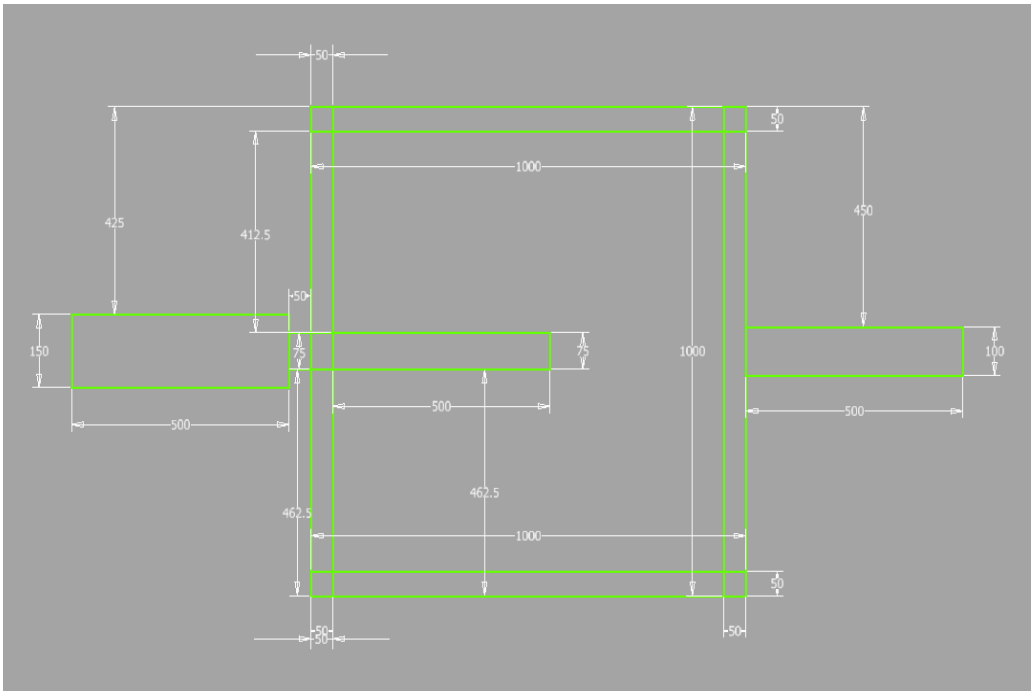

Figure 2.2. Schematic for microfluidic chip layout

2.2.2 Encapsulation of oil in water using the microfluidic device

Fluid encapsulation through microfluidics allows the manipulation of one liquid to surround another. Within the highly laminar flow of liquid in microfluidics the two liquids can be miscible as a boundary is maintained between the two solutions as they will only mix via diffusion. One syringe (50 ml) of dyed water and another (20 ml syringe) of mineral oil were prepared and plugged into the microfluidic device. The oil went through the central channels and the water from the two intersecting channels. A syringe pump (Genie-plus) was set at 5 ml/min for the water and 5 ml/hr for the oil phase. An optical microscope was used to record the formation on the encapsulated droplets.

For the manufacture of PEG microspheres and EHA/IBOA polyHIPE microspheres same method as the encapsulation above is used with the photocurable polymer replacing the mineral oil phase. A UV lamp (350 mW) was placed downstream on the microfluidic chip to photocure the polymer. EHA/IBOA was dispensed at a slower rate of 3ml/hr.

2.2.3 Iterations of microfluidic device to produce high yield continuous production with minimal user input during operation

The final method of microsphere production went through a few iterations until a continuous manufacturing system was produced. Originally a microfluidic chip and syringe system was used to for the microspheres (figure 2.3). This was then simplified to a T-junction microfluidic and the requirement of a microfluidic chip was removed. Using syringes for the water flow required repeated halting of the system to add more water, due to the much higher flow rate (ml/min) of water when compared to the flow rate of the monomer (ml/hr). The final iteration was a closed loop system that recycled the water used but filtered out the microspheres. A curing chamber was included to allow extra curing time for the microspheres which allowed the used of very high flow rates.

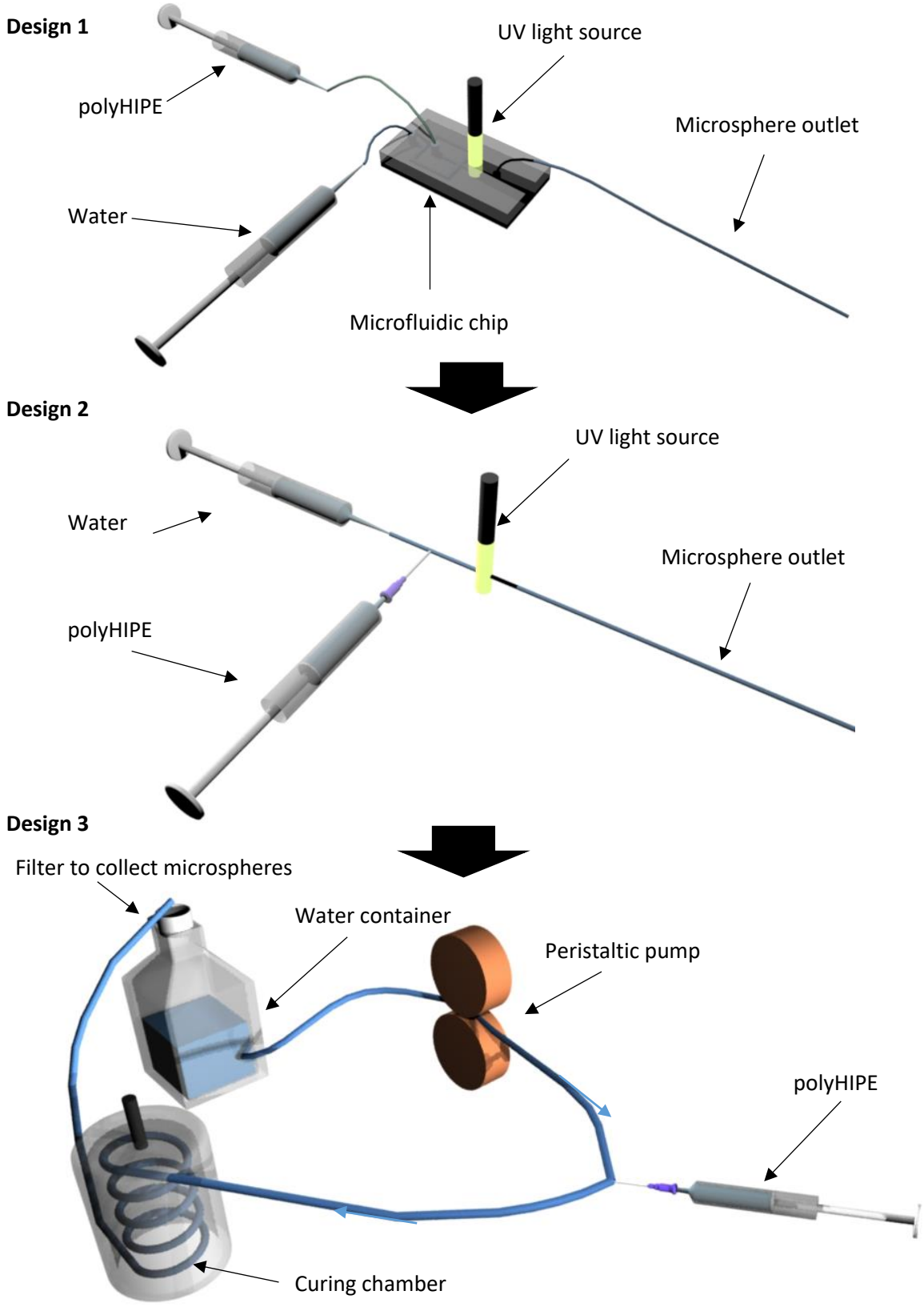

Figure 2.3. The 3 main iterations of design for microsphere manufacturing. (a) Microfluidic chip device used for encapsulation with syringes. (b) Simplified design using T-junction microfluidic design principles. (c) Continuous flow T-junction setup not requiring operator interaction during manufacturing process.

2.3 Polymerising photocurable emulsions into microspheres and thin films

2.3.1 Water in oil (EHA/IBOA copolymer) mixing to form a high internal phase emulsion

All the chemicals were purchased from Sigma-Aldrich (Poole, Dorset, UK) and used as supplied unless otherwise stated.

A high internal phase emulsion (HIPE) is an emulsion of two immiscible liquids with a high internal phase percentage. If the encapsulating phase is formed from a photocurable monomer, then this HIPE can then be polymerised into a solid and highly porous structure. The HIPE was prepared by mixing the monomers isobornyl acrylate (IBOA, 3.66 g) and 2-ethylhexyl acrylate (EHA, 1.56 g) with the crosslinker trimethylolpropane triacrylate (TMPTA, 1.41 g) using an overhead stirrer. The surfactant Hypermer B246 (0.21 g, Croda) was added and the solution mixed until it was dissolved. The photoinitiator diphenyl(2,4,6-trimethylbenzoyl)phosphine oxide/2-hydroxy-2-methylpropiophenone blend (0.35 ml) was added before the addition of the water.

As the external phase is a photocurable polymer it is possible to cure the HIPE into a highly porous structure and to drain the internal water phase to leave open voids. To prepare a polyHIPE with 80% porosity, 28 ml of deionised water was added over 5 minutes in a drop-wise fashion into a 100 ml capacity beaker whilst the solution was stirred at a stir speed in between 300 and 1260 rpm using an overhead stirrer (IKA Lab Egg). After complete addition of the water, the emulsion was left to stir for a further 5 minutes. The specific stir speed used to investigate resulting porosity at different stirring rates were 320, 540, 765, 870 and 1260 rpm at room temperature. The emulsion was stored in an amber glass vial (Supelco) and used within 6 hours of preparation. The emulsion remained stable for 48 hours although literature states that the pore size changes over time due to Ostwald ripening. To investigate the effect of heat on porosity the waters temperature was kept stable at 4, 15 and 30°C before addition to the monomer to form the HIPE at 320 rpm.

2.3.2 Reaction for polycaprolactone methacrylation to form a photocurable monomer

Commercial PCL was methacrylated within the lab to form a photocurable PCL monomer which could be used in forming polyHIPE structures. Hydroxyl terminated PCL (30.0 g, Sigma Aldrich) was dissolved in a solution of dichloromethane and trimethylamine (120 ml and 17.4 g respectively) and cooled in an ice bath to 1°C. Methacrylic anhydride (28.2 g) was added dropwise and the reaction was brought to room temperature and left to react for 24 h. The excess solvent and unreacted reagents were then removed under reduced pressure using a rotary evaporator and the methacrylated PCL was purified by in isopropanol and precipitating at -20 °C 3 times.

2.3.3 Water in oil (polycaprolactone) mixing to form a high internal phase emulsion

Photocurable PCL monomer can be used to form the encapsulating phase of a HIPE to produce PCL polyHIPE structures after photocuring. Thiol-ene, TMPTA, PCL and the surfactant Hypermer B246 are combined in a vessel at 40 °C until the surfactant has dissolved. Once returned to room temperature the photoinitiator, chloroform and toluene are added. Water is added in a dropwise fashion over 5 minutes with the solution stirred at 350 rpm. A more detailed description is given in Dr. Colin Sherborne's thesis ("The development and characterisation of biocompatible emulsion templated foams for additive manufacturing", Sheffield University).

2.3.4 Water in oil (Thiol-ene) mixing to form a high internal phase emulsion

Photocurable thiol-ene based monomer can be used to form the encapsulating phase of a HIPE to produce thiol-ene based polyHIPE structures after photocuring. Trimethylolpropane tris(3-mercaptopropionate) (2.33 g) is added to TMPTA (1.74 g) and the surfactant Hypermer B246 (0.23 g, Croda). The reactants and then dissolved into 5.2 g of chloroform and stirred. Finally, the photoinitiator diphenyl(2,4,6-trimethylbenzoyl)phosphine oxide/2-hydroxy-2-methylpropiophenone blend (0.1 g) was added and the solution is protected from light by a foil covering. For 80% porosity 28 ml of deionised water is added in a dropwise fashion with a magnetic stirrer bar rotating at 360 rpm over 2 minutes.

2.3.5 Photocuring HIPE into porous microspheres using the closed tank stir reactor method

The first main method employed within this thesis to form a double emulsion (water in oil in water) is by that of closed tank stir reactor CTSR (figure 2.4). The HIPE solution is separated by shear within a container of water to form droplets of HIPE which can then be photocured, producing polyHIPE microspheres. A 100 ml capacity beaker (50 mm diameter, 70 mm height) containing deionised water (40 ml) was set stirring at a defined rate using an overhead stirrer (Lab Egg, IKA). HIPE (2 ml) was added to the beaker in a drop-wise fashion with continuous stirring. The resulting double emulsion (w/o/w) was left to stir for 2 minutes. Stirring was subsequently stopped and the microspheres were cured immediately using the UV output of a mercury lamp (Omnicure S1000, 100 Watt) for 60 seconds.

When the effect of water temperature was investigated, the temperature was set at points between 5 and 60°C whilst maintaining a stirring rate of 320 rpm. The water temperature was controlled using a thermostatically controlled water bath (Stuart hotplate CD162, Stuart equipment) or an ice bath as appropriate. Constant temperature was maintained for 5 minutes before addition of the room temperature HIPE. For the investigation of how stir rate effects the resulting microsphere size distribution different stirring rates were investigated. The stirring rates used were 320, 540, 765, 870, 1260 and 1500 rpm. After photocuring with UV light the microspheres were removed by filtration, washed in water 3 times for 15 minutes and then stored in ethanol.

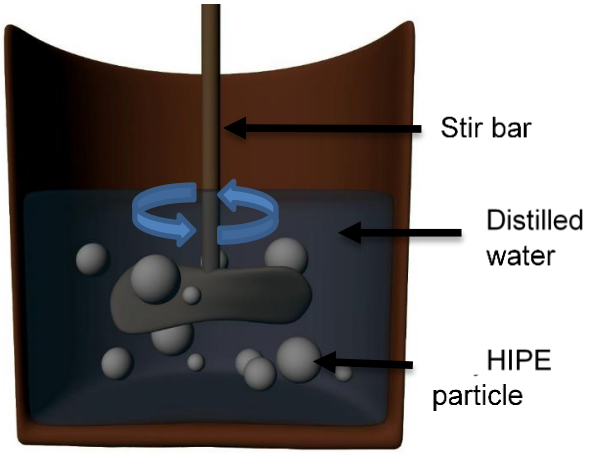

Figure 2.4. Diagram of experimental set-up used to produce polyHIPE microspheres via the double emulsion technique. Photocurable HIPE is added to a stirred solution which disperse into spherical droplets which are then photocured by UV light into polyHIPE microspheres.

2.3.6 Photocuring HIPE into porous microspheres using T-junction microfluidics

The second method employed within this thesis to form a double emulsion (water in oil in water) is by that of T-junction microfluidics (figure 2.5). The HIPE solution is injected into a continuously flowing stream of water which buds off the HIPE droplets as they leave the needle entry point. The droplets are then photocured, producing polyHIPE microspheres. For the T-junction device, a small internal diameter (0.15 – 0.51 mm, Nordson EFD) dispensing tip was used to inject the photocurable HIPE into a 6 mm diameter silicone tube (Advanced Fluid Solutions) through which a continuous flow of deionised water was driven via a peristaltic pump (Masterflex L/S tubing pump, Cole-Palmer). The resulting droplets were immediately cured by the UV emission of a mercury lamp (Omnicure S1000) which was directed via a liquid-filled light guide (Figure 2.4). The water flow rate was controlled by altering the rotation rate of the peristaltic pump. The flow rate of the HIPE was controlled via a syringe pump (GeniePlus, Kent Scientific). The system was allowed to run for 30 minutes to stabilise and then microspheres were collected. A continuous stream of microspheres were produced, which were then collected in a 40 µm sieve (40 µm cell strainer, BD Falcon).

To investigate manufacturing conditions on resulting microsphere size 3 parameters were altered. Monomer flow rate, water flow rate and dispensing tip internal diameter size all influence microsphere size. The effect of monomer flow was investigated by keeping other settings constant whilst being altered to 1, 3, 5 ml/hr. The effect of water flow was investigated by keeping other settings constant and altered from 100 rpm to 600 rpm in 100 rpm increments. The combined effect of these two settings was investigated by using 3 different monomer flow rates (1, 3, 5 ml/hr) at each water rpm setting (80, 160, 240 rpm). Finally, the effect of the diameter of the dispensing tip was investigated by changing the tip to 0.15, 0.25, 0.51 mm whilst keeping the other parameters constant at 3ml/hr HIPE

flow and 200 rpm water flow. To produce the smallest microspheres possible, we used a HIPE flow of 0.25 ml/hr, 600 rpm water flow rate and a 0.15 mm tip size.

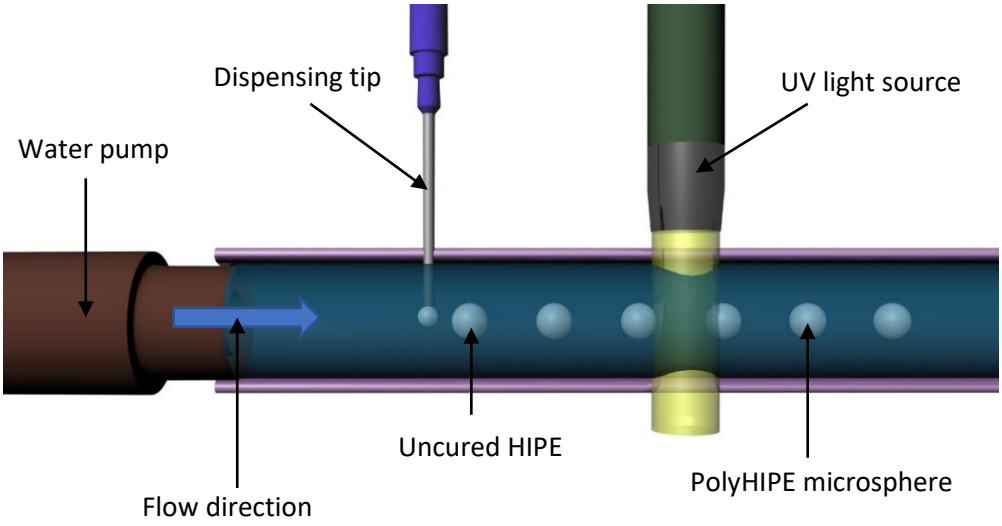

Figure 2.5. Diagram of experimental setup used for microsphere production via the microfluidic technique. T-junction microfluidic setup introduces HIPE via a dispensing tip which buds of once attaining a certain size, exact size dependent on other properties such as flow rate and viscosity. HIPE droplets are carried from the dispensing tip via continuously flowing water and are then cured via UV light into polyHIPE microspheres.

2.3.7 Photocuring HIPE into thin films over glass coverslips

Thin and flat layers of polyHIPE material was used for initial cell culture work before progressing onto culturing on microspheres. A 500 µl of HIPE/monomer was added to a 13 mm glass coverslip and then cured with a mercury lamp for 30 seconds. 80% porosity EHA/IBOA monomer blend was used as was a 0% porosity (non-porous) EHA/IBOA monomer. The lack of porosity was caused by not adding the water phase to the monomer during stirring.

2.4 Imaging of microspheres and analysis of both microsphere and pore diameter

2.4.1 Imaging of porous microspheres using optical microscopy

To understand how the manufacturing methods influenced the population of microspheres it was necessary to capture images of the microspheres so that they could be measured using software. PolyHIPE microspheres were imaged using a reflected light optical microscope (Miotic B5 professional series) and measured in ImageJ using a calibrated scale from a stage micrometre (imaging apparatus). Microsphere diameter was measured using the measure function on ImageJ and excel was used to calculate statistics (see 2.14).

2.4.2 Imaging of porous microspheres using scanning electron microscopy

To measure the porosity of the microspheres and to observe them at a higher magnification it was necessary to image them using a scanning electron microscope (SEM). Samples were mounted on aluminium stubs using adhesive carbon tabs and sputter coated with gold (SC500, emscope) with a 15 mA current for 2 minutes at 0.05 atm. Images were then acquired using a SEM (Philips/FEI XL30 ESEM) operating with 15 eV electron beam energy. To determine pore size, microspheres were sectioned using a cryostat (Leica CM1860 UV) to 40 µm sections in Tissue Freezing Medium (Leica) which was allowed to evaporate for mounting and gold coating. Pore sizes were measured from the SEM images using the inbuilt measurement feature of ImageJ software (NIH, USA), measuring all the pores in four fields of view for each condition.

2.4.3 Methods used to measure microsphere diameters

Microspheres were imaged under an inverted light microscope and a jpeg saved of the viewed microspheres. A stage micrometre was used at the same magnification to set the scale later in ImageJ. More than 3 images (for each measured >50 microspheres) were taken of each condition in a population.

2.4.4 Methods used to measure microsphere internal pore size

Pore sizes were measured from the SEM images using the inbuilt measurement feature of ImageJ software (NIH, USA). The scale was set according to the burnt in data bar with ImageJ's scale functionality. A line was then drawn across each pore and the ImageJ function 'measure' was used. The resulting data table was then exported into excel for further data analysis and comparison.

2.4.5 Degradation study of polycaprolactone microspheres with standard and accelerated degradation

A degradation study was required to determine whether the PCL microspheres would degrade and over what time scale. For the accelerated degradation study 0.2 g of microspheres were added to a glass container and weighed. 1 ml of either 0.1 M Sodium hydroxide (NaOH) or dH_2O was added depending on the sample. NaOH was used for accelerated degradation and dH_2O was used for standard degradation. Samples were also kept in air as a control. Samples were kept in a 37 °C dry incubator for 60 days. The solution was then removed and the samples allowed to dry. Samples were then re-weighed to determine the material lost over the time period.

2.4.6 Manufacturing of solid polycaprolactone microspheres

Solid microspheres were produced in the same manner as the polyHIPE microspheres but without the addition of the water during the HIPE step. Solid microspheres were required for both the injection study and for the CAM assay study for use in comparison to standard porous microspheres. Both microsphere populations were made via the T-junction microfluidic method (see 2.1.3). The photocurable solution used to produce the solid microspheres was formed using the following method. Thiol-ene, TMPTA, PCL and the surfactant Hypermer B246 are combined in a vessel at 40 °C until the surfactant has dissolved. Once returned to room temperature the photoinitiator, chloroform and toluene are added. No water is added as would be used for a polyHIPE, the solid microspheres are made up the identical chemical components.

2.5 Surface modification through plasma coating

2.5.1 Plasma coating of polyacrylic acid

In preparation for cell culture, the surface chemistry of the polyHIPE microspheres was modified by inductively coupled plasma polymerisation of acrylic acid. The process was conducted using a custom-made apparatus consisting of a cylindrical borosilicate glass chamber with stainless steel endplates connected to vacuum pump (RV8, Edwards). Chamber pressure was detected by an active Pirani gauge (APG-L-NW25 Edwards) and manually controlled by a needle valve regulating the flow of monomer vapour (Edwards LV10K). The flow of monomer vapour (acrylic acid) was established through the chamber at 2.4 cm^3/min. The electromagnetic field was generated by a coil wrapped around the chamber connected to a radiofrequency generator (Coaxial power systems limited). The power to the coil was manually adjusted to 15 W and the polymerisation occurred- under these conditions for 20 minutes. Microspheres were spread out evenly on aluminium foil within the chamber. After the power to the coil was switched off, the monomer vapour flowed for a further 5 minutes before the flow was halted. The chamber was then opened to the atmosphere and the microspheres were removed.

Previous studies have used plasma polymerisation to encourage cell adhesion [247, 248] to control cell differentiation [249]. Plasma deposition allows the binding of chemical groups such as -COOH (acrylic acid) to surfaces [250]. Other methods of adding acrylic acid to HIPEs has been achieved by blending acrylic acid into the aqueous phase [247]. The deposition of a –COOH group has been shown to increase cell attachment and is also a useful substrate for further chemical/surface modification. [248]

2.6 General cell culture techniques

2.6.1 Freezing cells for storage in liquid nitrogen

For long term cell storage cells were frozen with a cryoprotectant and stored in liquid nitrogen. The freezing solution was prepared by adding 20% Dimethyl sulfoxide (DMSO) to 80% foetal Calf serum (FCS). The cells were then centrifuged and counted using a haemocytometer and 1 ml of freezing solution was added for every 1 million cells. Cells were then aliquoted into cryo-vials which are inserted into controlled freezing devices (Mr. Frosty, Thermoscientific) which regulate the cooling temperature change to -1°C a minute. The device was placed in a -80°C freezer for 12 hours before vials were removed and placed in a liquid nitrogen dewar.

2.6.2 Defrosting cells from liquid nitrogen for use in cell culture

When cells were required they were removed from the stores and thawed before being plated up for passaging and then use. Cells in cryo-vials were removed from the liquid nitrogen store and defrosted by a water bath set at 37°C. The vial was removed from the water as soon as the media had defrosted to preserve cells. Cells were then transferred to a T-75 flask containing 12 ml of media and this was placed into the incubator. 24 hours later the media was removed from the flask and exchanged with fresh media.

2.6.3 Supplement inclusion into media for the culture hES-MP cells

Human embryonic stem-cell derived mesenchymal progenitor (hES-MP) cells (Cellartis, Sweden) are an established cell line originally derived from human embryonic stem (hES) cells. hES-MP cells were maintained with Alpha Modification of Eagle's Medium (AMEM, Lonza) supplemented with 100 mg/ml penicillin-streptomycin, 10% foetal calf serum (FBS, Labtech, UK) and L-glutamine at 2mM concentration (Sigma Aldrich, UK). hES-MP cells were maintained with an additional supplement during passaging: human basic fibroblast growth factor (βFGF) at 4 nM (Life technologies) to maintain stemness. Further supplements were added for specific media formulations as described in the table below.

Table 2.1. Table of media supplements for cell specific media

	Media supplement				
Media condition	FCS/Penstrep/L-glutamine	Ascorbate-2-phosphate	B-Glycerol Phosphate	Dexamethasone	hFGF
Growth	10%, 100 mg/ml, 2mM	----------	----------	----------	4 nM
Supplemented	10%, 100 mg/ml, 2mM	50 µg/ml	5 nM	----------	------
Osteogenic	10%, 100 mg/ml, 2mM	50 µg/ml	5 nM	10 nM	-----

2.6.4 hES-MP culture and standard maintenance between passages

hES-MP were removed from cryo-storage at passage 3 and grown in Alpha MEM (AMEM, Lonza) media supplemented with human fibroblast growth factor (hFGF). T-75 flasks were pre-coated with 0.1% gelatine solution (porcine, type A) for 5 minutes prior to cell cultivation. Every 2 days, 80% of the cell media was replaced and the cells were passaged once every 7 days in a split 1:6.

2.6.5 Passage technique for hES-MP cell expansion

Cells were passaged to increase cell number, for hES-MP cells all work done with differentiation analysis was conducted on passages less than 10 and for experiments measuring cell viability, passages under 15 were always used. Media was removed from the T-75 flask and samples were rinsed once with phosphate buffered solution (PBS). Trypsin (0.25%, 2.5 ml) was added to the flask which was then kept in incubator and checked regularly for cell detachment. Cells were persuaded to detach from the flask with gentle taps to the side of the flask. Once cell detachment was confirmed via a light microscope 10 ml of warmed media was added to the flask to block the trypsin from functioning. This media was then added to a centrifuge tube and centrifuged at 1000 rpm for 5 minutes. Media was then removed via motorised pipette to leave the cell pellet undisturbed at the bottom of the tube. 3 ml of fresh media was then added and using a 1 ml Gilson pipette the media was resuspended to disperse the cells.

2.7 Culture of hES-MP cells on microspheres

2.7.1 Microsphere sterilisation in alcohol before cell culture

To prevent microbial or fungal infection in the culture it was necessary to sterilise the microspheres before beginning the cell culture experiments. Microspheres were sterilised by soaking in 70% ethanol for 1 hour. The ethanol was then removed and the microspheres were then washed 3 times in dH_20 for 15 minutes and finally soaked in Alpha Modification of Eagle's Medium (AMEM) media for 1 hour.

2.7.2 The culture of hES-MP cells on a thin film

Before working with microspheres, the biocompatibility of the material was tested using a flat surface, this increased the attachment of cells as they could land directly onto the material. hES-MP cells dispersed above the scaffold when seeding. 20,000 cells per well (24 well plate, Corning) was used. Samples were moved to a new well plate before any tests to prevent contamination with other cells.

2.7.3 Technique used to seed hES-MP cells onto microsphere

To grow the cells onto the microspheres a method was developed to ensure the greatest opportunity for cells to bind to the microspheres. hES-MP cells were detached from T75 flasks with trypsin, which was then inactivated with AMEM media. Cells were centrifuged at 1000 rpm for 5 minutes before the media was replaced with fresh AMEM media. 100,000 cells were suspended via gentle pipetting and added to the 0.2 g of microspheres in media. This cell-microsphere mix was placed on a cell rocker for 45 minutes at 12 oscillations per minute. Samples were then kept in the incubator for a further 2 hours before microspheres were removed and added to a new T25 flask. They were then very gently rinsed with PBS to remove unattached cells before adding new media.

Media was replaced every 2-3 days by removing 80% of the media and replacing it with fresh media. This prevented the loss of microspheres associated with attempting to remove all the media and prevented any damaging forces experienced by the cells through suction.

2.7.4 hES-MP culture on microspheres for a time course study of ingrowth

To understand the behaviour and interaction of cells and microspheres over time in culture, a time course study was conducted. For the time course imaging, uniform microspheres were produced to keep the diameter of microspheres constant (figure 2.6). Samples were taken at days 1, 4, 7, 11, 15, 20, 25 and 30 fixed in 3.7% formaldehyde solution for 1 hour and then frozen in optimal cutting temperature compound (Fisher) and stored at -80°C. Samples were then sectioned and stained with haematoxylin and eosin stain (H&E) or imaged with a confocal microscope. Distance of cell penetration was measured using ImageJ and averaged over several microspheres for each condition. Separate samples of microspheres were grown in AMEM + beta-glycerol phosphate (βGP), AMEM + ascorbate-

2-phosphate (A2P) and AMEM + βGP + A2P to determine which supplements supported cell migration. These microspheres were fixed and imaged as above at days 15 and 30.

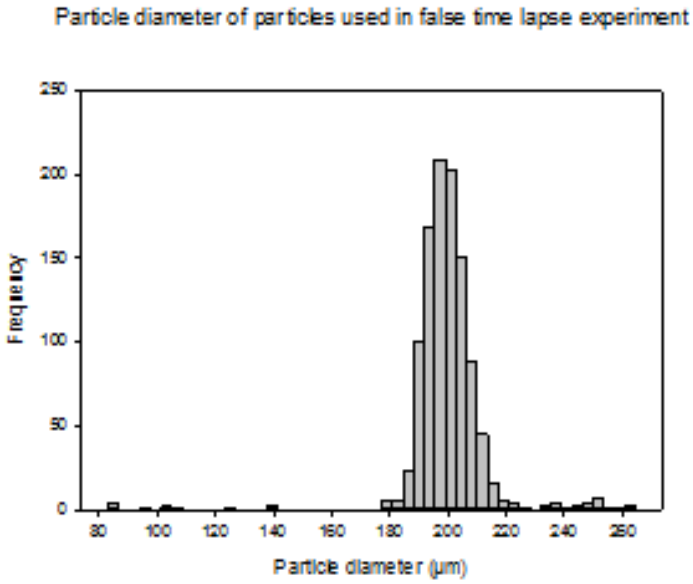

Figure 2.6. Distribution of microsphere diameters used for the time course experiment via microfluidic T-junction.

2.7.5 Survival study: injection of hES-MP cells bound to microspheres from a syringe

To investigate if porosity in microspheres provided a beneficial effect in cell survival when injected, an injection study was conducted. A monodisperse population of PCL microspheres with an average diameter of 400 µm were filtered to remove any microspheres with a diameter above 500 µm using a fish tank plankton filter mesh. HES-MP cells were cultured on this microsphere population for 4 days in growth media in a T-75 culture flask. Each flask was split in half, with half going to a centrifuge tube and the remaining half prepared for injection. Microspheres were drawn up slowly into a 20 ml syringe before a 510 µm internal diameter microlance was fitted to the syringe. At a steady rate (2 ml/s) the syringe contents were dispensed into a centrifuge tube by hand. Both centrifuge tubes (injected and control) were treated in the same manner for the rest of the procedure. The centrifuge tube was centrifuged at 1000 rpm for 5 minutes and the media was removed and washed with PBS. A second centrifuge, under the same conditions, and trypsin was added to the tube. Tubes were left for 5 minutes to allow all cells to be removed from the scaffold. The suspension was removed from the microspheres and centrifuged a final time. The trypsin was removed and the cells suspended in 100 µl of media and 100 µl of trypan blue. The number of live to dead cells was measured in triplicate from each sample. The number of live cells obtained from the injected microspheres was normalised against the control microspheres. n = 3 for each condition. 20,000 hES-MP cells were classed as ‘loose cells’ were treated in an identical manner as the microspheres.

2.8 Quantitative analysis of cell growth and differentiation on microspheres

2.8.1 Cell activity measurements using the Resazurin salt assay

Cell growth was assessed by using an assay to measure cell metabolism at different time points to observe any changes in overall cell energy use. The assay chosen to measure cell metabolism was a resazurin salt assay. The risk of this assay is that fluorescence from one test may linger to the next to give a false reading and that resazurin is toxic to cells and might damage them. Resazurin salt was made at 3.8 μg/ml in cell culture medium (AMEM). Individual experiments differed and are described in each chapter but the general method was as follows. Resazurin salt in media was added to each container or well of cells and left to incubate for between 1 and 4 hours depending on the experiment (but kept constant throughout one experiment). After the time had elapsed, the Resazurin salt was removed from the cells, which were washed in PBS 3 times before fresh culture media is added. 200 µl of Resazurin salt was added to a 96 well plate in triplicate (3 wells per sample) and was read by a fluorescent plate reader. Excitation was at 535 nm and emission measured at 615 nm.

2.8.2 Total sample DNA and Alkaline phosphatase production measurements

Alkaline phosphatase is an early indicator of MSC differentiation to osteoblasts and can be measured using an enzymatic ALP detection test. As different quantities of cells would skew the ALP data, all data is normalised to the total DNA from a sample. To obtain the activity of ALP in a sample the following assay way used. Media was removed and samples washed 3 times with PBS. Cell digestion buffer was made up using 10% TE buffer (10 mM Tris-HCL, 1 mM $ZnCl_2$, 1 mM $MgCl_2$, in distilled water, (pH9)), 1% triton X-100 and water. Samples were left at 4 °C for 12 hours in the cell digestion buffer. Samples were broken in two using scissors and put in a 1.5 ml micro-centrifuge tube. Samples placed at -80 °C for 10 minutes then at 37 °C in a dry incubator for 15 minutes. This step was repeated 3 times. Samples were vortexed for 15 seconds and then centrifuged for 5 minutes at 10,000 rpm. Alkaline Phosphatase yellow liquid substrate for ELISA Kit (APYLS) was made up with 1ml APYLS and 4ml dH2O and one tablet to make up 5 ml solution. 190 µl of APYLS was added to the well of a 96 well plate and 10 µl of cell lysate was then added. On a plate reader 30 readings were made at one minute intervals measuring absorbance at 405 nm.

Using the same lysate, a picogreen assay was used to determine DNA quantity within each sample. PicoGreen solution was made up in dH_2O with picogreen (1:200) and TE buffer (TE buffer (10 mM Tris-HCl, 1 mM ethylenediaminetetraacetic acid (EDTA), pH 7.5, 1:20). 180 µl of picogreen working solution and 180 µl of cell lysate were added to a 1.5 ml centrifuge tube and wrapped in foil. Samples were vortexed for 5 seconds and incubated at room temperature for 10 minutes. 100 µl was added to a well in a black 96 well plate in triplicate for each sample. The well plate was read using a spectrofluorometer using an excitation wavelength of 480 nm and reading the emission at 520 nm.

2.9 Cell cultured microsphere sample preparation and sectioning

2.9.1 Fixing cells

When using fluorescence or SEM on biological samples, they can be 'fixed' to increase the mechanical robustness of the samples. To 'fix' a sample the cells are killed and the proteins within the sample are crosslinked. Microsphere samples were washed 3 times in PBS for 1 minute and fixed in 3.7% formaldehyde solution for 50 minutes and then washed again with PBS thrice. The elongated time period was to allow for the fixation agent to diffuse into the centre of the microspheres to ensure the whole structure was fixed. Thin samples were treated as above but were left in 3.7% formaldehyde for 15 minutes.

2.9.2 Cryostat microtome

For imaging thin slices of samples, they must be sectioned finely using a microtome. Samples were frozen in tissue freezing medium (Leica) by dipping in liquid nitrogen. Samples were then stored in a -80°C freezer for a minimum of 24 hours. Sections were obtained from a cryostat (Leica CM1860 UV) at -24°C with at 6, 10, 15 or 40 µm thickness. Samples were stained with haematoxylin and eosin (H&E) or alizarin red and imaged under an optical microscope (B5 professional series, Miotic). Microspheres not seeded with cells were embedded in wax and cut in 6 µm slices with a microtome (Leica RM2145) at room temperature.

2.9.3 Hexamethyldisilazane treatment of samples for imaging of cells using scanning electron microscopy

For imaging samples using an SEM it must first be treated with hexamethyldisilazane (HMDS) to remove any water from the sample. After samples were sectioned and placed on 12 mm glass coverslips PBS was used to remove the tissue freezing media. Samples were then treated with the following solutions to dehydrate the sample for SEM. 15 minutes in each solution of 35%, 60%, 80%, 90% and 100% ethanol in distilled water. HMDS and ethanol (1:1 weight concentration) for one hour then 100% HMDS for 5 minutes twice. The HMDS is then removed and the samples allowed to air-dry for 1 hour. Samples were then gold coated and imaged with an SEM as in 2.4.2.

2.10 Fluorescent microscopy of cell cultured microsphere samples

2.10.1 Cell wall permeabilization using detergent

Once a sample is fixed the cell wall must be permeabilised using a detergent if the target proteins for staining at within a cell membrane. After fixing, the samples were soaked for 15 minutes in a solution of PBS and 0.1% triton X-100 and then washed 3 times with PBS.

2.10.2 Staining of f-actin filaments using a phalloidin-fluorescein isothiocyanate stain

Imaging actin filaments provides detailed information on cell structure and compliments DNA/nuclei staining in 2.10.3. Phalloidin- Fluorescein isothiocyanate (FITC) stains were made up at 1000:1 dilution in PBS and added to the samples in PBS for 1 hour at 4°C whilst covered. Samples were washed with PBS to then stored in PBS and imaged within 48 hours. FITC is a green fluorescing stain. FITC Phalloidin was excited using a 488 nm laser (4% transmission) and emission detected above 505 nm.

2.10.3 Staining of cell nuclei filaments using a 4',6-diamidino-2-phenylindole stain

Imaging DNA/nuclei is an effective way of observing every cell within a sample and acts as control to compare against cells stained with other markers. 4',6-diamidino-2-phenylindole (DAPI) was added via two methods depending on the experiment. 3D scaffolds were immersed in 1:1000 dilution DAPI in PBS for 20 minutes before being rinsed three times. This was often in combination with other stains. DAPI staining for sectioned samples was added via the ProLong antifade fixing mountant, of which one drop was added and the coverslip was then mounted. DAPI is a stain for nuclear material and stains both live and dead cells. DAPI was excited using a 760 nm laser (16% transmission) and emission detected between 435 and 485 nm.

2.10.4 Confocal/fluorescent microscope set-up for imaging

Images of 1756×1756 and 1024×1024 pixels were obtained using a Zeiss LSM 510META upright confocal microscope with either a 10× objective (Achroplan 10x/0.3 W, Carl Zeiss ltd, UK), 20x objective (20x/0.45 W, Car Zeiss ltd, UK) and a 40x objective (Achroplan 40×/0.75 W, Carl Zeiss Ltd, UK).

2.10.5 Imaging of Live & dead cells on a microsphere through staining

Live/dead imaging allows the fluorescent live imaging of whether a specific cell has membrane integrity or not (which indicating cell death). Media was removed from the samples and incubated for 20 minutes with fresh media containing Ethidium homodimer-1 (1:1000) and Calcein AM (1:250) at 37 °C. Following incubation samples had fresh media added once the media containing the dyes had been removed. Samples were imaged using an upright Zeiss LSM 510 confocal microscope with an argon ion laser (488 nm) for Calcein AM (488 nm, 12% power and emission collected with a LP 505 filter) and a helium-neon laser (543 nm, 31 % power, and emission collected using a LP 560 filter) for Ethidium

homodimer-1 (λ_{ex} = 536 nm / λ_{em} = 617 nm). Images taken at 1024 by 1024 pixels using W N-Achroplan 10x/0.3 objective with a 1.6 µs pixel dwell time.

2.10.6 Imaging of mature collagen through Second Harmonic Generation imaging

Second harmonic generation (SHG) is a fluorescent imaging technique which allows the imaging of mature collagen fibre within a biological sample. Samples were cut at 40 µm thickness from frozen sections of day 30 microsphere cultures from the time-lapse experiment. Sectioned samples from microspheres cultured in growth media, supplemented media and osteogenic media. No previous staining had been administered to samples before SHG work. dH_2O was added to samples and a coverslip was added (ensured that there were no bubbles). A drop of oil added to top of coverslip for use of an oil immersion lens (x40). Excited with 2-photon at 950 nm and accepted filter light at 469 – 480 nm (light where SHG/mature collagen should emit). In addition, two filters were set either side of target wavelength to make sure the light received in key filter region was not overspill from another source such as auto-fluorescence (SHG light should only be in that narrow range). The other filters sets used were at 447 – 469 & 480 – 501 nm. Images were taken at 512 by 512 pixels.

2.11 Staining of cell cultured microsphere samples for optical microscopy

2.11.1 Haematoxylin and Eosin staining

Staining with Haematoxylin and Eosin (H&E) allows the identification of cell nuclei, cell structure and the presence of some ECM. As samples were frozen hydrated samples did not need to undergo the rehydration steps typically involved with histology. Slides were rinsed in water to remove remaining cryostat optimal cutting temperature compound (OCT) medium for 1 minute. Slides were submerged on a rack in haematoxylin for 60 seconds before being placed in a container with a constant flow of tap water and left until the flow ran clear. Slides were then submersed in Eosin for 5 minutes and then dipped twice in separate tap water containers to remove excess stain. Samples were dipped in 70% industrial methylated spirits (IMS), dipped in 95% IMS and left for 30 seconds submerged in 100% IMS to dehydrate the sample. Samples was then dipped in two separate containers of xylene before being removed for fixing.

2.11.2 Calcium staining using Alizarin red

The presence of calcium deposits is a reliable indicator of osteoblast formation and can be detected using an alizarin red stain [251]. 1ml of 1mg/ml alizarin red in dH2O, adjusted to pH 4.1 by adding ammonium hydroxide, was added to the sample for 20 minutes. The sample was washed with dH2O until all unstained dye was removed. Samples were then rehydrated as above (see H&E) and then fixed. Alizarin red is a stain for calcium/mineral deposits which in turn is a useful indicator of cell state as only particular cells deposit minerals into their surrounding area.

2.11.3 Collagen staining using Sirius red

While there are more cell types that produce collagen than which deposit calcium it is an additional indicator when detected with calcium of osteoblast differentiation. Sirius red solution was made by dissolving 1mg/ml of Sirius red powder in saturated picric acid. 1ml of Sirius red solution was added to the samples on the slide via pipette and left for 30 minutes before being rinsed until the water rand clear. Samples were then rehydrated as above (See H&E) and then fixed. Sirius red is used to stain collagen (red) and other connective tissues (yellow).

2.11.4 Polysaccharide staining using Toluidine Blue

The presence of polysaccharides within the sample and can indicate the formation of chondrocyte cells. Toluidine blue stain (1g Toluidine blue [1%] and 0.5 g sodium borate [0.5 %] in 100 ml of distilled water) is added to the samples using a pipette for 5 seconds. Samples are then rinsed very gently with tap water until the water runs clear.

2.11.5 Antibody staining for sclerostin using 3,3'-Diaminobenzidine staining for optical microscopy imaging

Sclerostin is present in mature osteocyte cells and is a popular marker for differentiating between osteoblast and osteocyte cells. A 3,3'-Diaminobenzidine (DAB) kit was purchased from Abcam - Mouse and Rabbit Specific HRP/DAB (ABC) Detection IHC kit (ab64264) and the relevant components were used for this study. Sectioned samples of microspheres, cultured for 60 days in osteogenic media, were protein blocked for 10 minutes, washed and then submerged in hydrogen peroxide block for 5 minutes and then washed again. Rabbit anti-Sclerostin antibody (ab85799, Abcam) was added to buffer (PBS and 1% bovine serum albumin) at 1:350 and added to the samples for 12 hours at 4 °C. Samples were washed 5 times with PBS for 5 minutes. Biotinylated anti-rabbit goat (ab64256, Abcam) (1:300) in buffer was added to the samples for 1 hour before removal and washing 3 times in PBS for 5 minutes. The DAB stain was then added to the samples for 5 minutes precisely and then washed off and rinsed with PBS 3 times for 5 minutes. Sections of Wistar rat tibia imbedded in paraffin were dewaxed in xylene before undergoing the same process as above. Controls with every step except secondary and controls with no primary was also processed as above.

2.12 In-vivo study of vascularisation response using a Chorioallantoic membrane assay

2.12.1 Preparing the Chorioallantoic membrane model for implantation of scaffolds

The Chorioallantoic membrane (CAM) assay was used to assess the vascularisation response of the microspheres in an in-vivo environment. This assay was performed according the published procedure [252]. Fertilised chicken eggs (*Gallus domesticus*) purchased from Medeggs (UK) were incubated from day 2 of fertilisation until day 8 at 37°C in a humidified egg incubator (R-COM Suro20). At day 8 a window was cut into the shell of the egg (5 mm^2) and the implants was injected into the opening using a 5 ml syringe with a 1.1 mm internal diameter needle tip. Masking tape was used to secure sterilised (in ethanol, 30 minutes) parafilm over the implantation site to prevent infections.

2.12.2 Implantation of EHA/IBOA microspheres into a Chorioallantoic membrane model for angiogenic potential assessment

Each egg was implanted with one of the following samples or controls. 0.5g of EHA/IBOA polyHIPE microspheres cultured for 3 days in osteogenic media with hES-MP cells were washed and injected in PBS for implantation. 0.5g of EHA/IBOA polyHIPE microspheres soaked in osteogenic media for 3 days without cells were washed and injected in PBS for implantation. 100,000 hES-MP cells cultured in growth media (P4) were injected in PBS into the egg. A control was used where the egg was opened and then resealed without the addition of any foreign objects.

2.12.3 Implantation of polycaprolactone microspheres into a Chorioallantoic membrane model for angiogenic potential assessment

Each egg was implanted with one of the following samples or controls. 0.5g of PCL polyHIPE microspheres cultured for 3 days in osteogenic media with hES-MP cells were washed and injected in PBS for implantation. 0.5g of non-porous PCL microspheres cultured for 3 days in osteogenic media with hES-MP cells were washed and injected in PBS for implantation. 0.5g of PCL polyHIPE microspheres cultured for 11 days in osteogenic media with hES-MP cells were washed and injected in PBS for implantation. 0.5g of PCL polyHIPE microspheres cultured for 11 days in growth media with hES-MP cells were washed and injected in PBS for implantation. 100,000 hES-MP cells cultured in growth media were injected in PBS into the egg. A control was used where the egg was opened and then resealed without the addition of any foreign objects.

2.12.4 Scaffold Retrieval from the Chorioallantoic membrane assay and in-situ imaging

The chicken eggs were incubated until day 14 when the scaffolds were retrieved and the eggs were terminated. The chicken eggs were removed from the incubator one by one as they were processed. Angiogenesis was quantified by taking light microscope pictures just before scaffold retrieval (Miotic)

and using histological images of the retrieved scaffolds. Data on the density and bifurcations of the blood vessels was obtained by analysing a 2 cm^2 area around the implant over a series of images.

2.12.5 Staining techniques used on the tissue samples removed from the Chorioallantoic membrane

To view the histological properties of the area around the microsphere implants some of the CAM assay was extracted, stained and imaged. The area around the implant was then extracted from the egg using tweezers and scissors and placed into 3.7 % formaldehyde for 30 minutes to fix and were then washed for 15 minutes in PBS thrice. H&E was used to stain these samples for imaging using an optical microscope (Miotic). FITC Phalloidin and DAPI were used to image the samples under confocal (see section 2.10.4). Natural red fluorescence of the chicken eggs red blood cells were also used in fluorescent imaging (emission: 488 nm 12% transmission, filter low pass 505).

2.13 Digital techniques used on images

2.13.1 Computer generated trace of cells within microsphere sections

To aid the visualisation of cells within the microspheres a model was created using CAD software. Autodesk Maya was used to trace over an image of hES-MP cells inside a section of a microsphere. Polygons were created face by face using the 'Create polygon faces' tool over first the internal structure of the microsphere and then in a separate layer the cells were traced over. The polygon was then smoothed (mesh -> Smooth – settings to Exponential and division levels set at 2).

2.13.2 False coloured scanning electron microscopy images

To aid the visualisation of cells of images taken using an SEM false colour was manually added using Photoshop (Adobe). Layer masks were used for each colour channel and the paintbrush tool was used to change these layers to incorporate the desired structures. No automated software was used to detect features and all structures are subject to the author's interpretations of the image.

2.13.3 Manipulation of image stacks from confocal microscopy: Z-stack

Images taken on the confocal microscope could be taken at different depths, when these images were taken through a sample they were assembled into a z-stack of images. Z-stack images (1024 by 1024 pixels) were obtained using the same settings as single plane images but repeated images were obtained of the same area, translated 11 µm in the z direction after each capture.

2.13.4 Manipulation of image stacks from confocal microscopy: Stereoscopic image

A stereoscopic (3D) picture of the microspheres was produced that can be viewed without any additional hardware (glasses). Using the software Zeiss image LSM browser a z-stack of images were processed with the projection function (number of projections = 64, difference angle =6). Two images were selected at a slight difference in rotation between the two. Skytopia software was then used to optimise the position of the two images side by side for easy viewing.

2.13.5 Manipulation of image stacks from confocal microscopy: Z-project

Combinations of the images taken on a z-stack were often converted into one image to easily display all the captured information in a single frame. The z- project function on ImageJ was used on z-stack confocal data. With less than 10 layers the average intensity function was used. Above 10 layers the max intensity function was used.

2.14 Statistical analysis

2.14.1 Unpaired students T-test

Unpaired students T-test is a statistical method for comparing two sets of data and to determine statistical error. Care must be taken when using this test as the chance of a false positive occurring increases quickly with multiple comparisons. It is ideally suited for only comparing two sets of data, which is the only times it is used in this thesis, most comparisons were undertaken using an ANOVA test. T-tests were conducted using GraphPad Prism 6 using the default T-test settings.

2.14.2 ANOVA multiple comparison test

The ANOVA test was used to compare multiple sets of data to determine if significant differences were present. This test helps eliminate the risk of false positives being returned as significant. ANOVA tests were conducted using GraphPad Prism 6 using the default ANOVA settings with the multiple comparisons setting 'Compare the means of each column with the mean of every other column'. Significance was denoted by a * symbol (* $p < 0.05$, ** $p < 0.01$, *** $p< 0.001$, **** $p <0.0001$). However, despite the * denotations, each test was tested only against $p = 0.05$ and increased significance was not directly tested for.

2.14.3 Microsphere data analysis and method of displaying data on Tukey boxplot

Data analysis on the physical attributes of the microspheres is shown throughout this thesis as a boxplot. It is important to understand that the graphs describe the variance in microsphere size and do not denote error or a variance from a specific value. Put another way, if infinite microspheres were analysed the data would remain (roughly) identical to what is presented and would not be reduced to a single value.

Microsphere diameter was measure in ImageJ and then transferred to excel. Measurements from each microsphere in a condition were added together to form a single data set. These data sets from different samples were then compared against one another as either histograms or as boxplots. Tukey boxplots were used with the highest datum within 1.5 interquartile range (IQR) of the upper quartile, the lowest datum at 1.5 IQR of the lower quartile, first and third quartile making up the box and the media making the bar within the box. The upper and lower bars were microsphere diameter values closest to the calculated theoretical value of where the bar would lie.

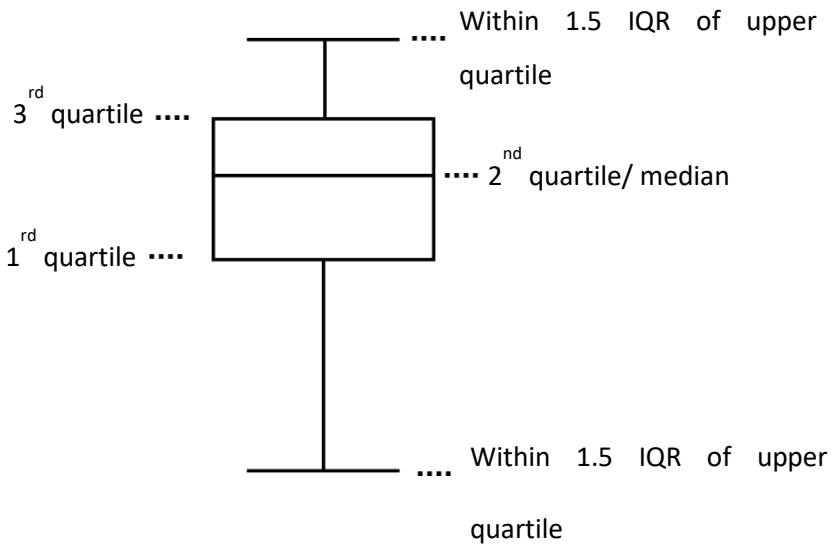

Figure 2.6. Explanation of the Tukey boxplots used to visually compare microsphere diameter and microsphere pore size.

2.14.4 Analysis of the SHG data from images captured using the confocal microscope

The SHG imaging of collagen was analysed to determine any significant difference in the intensity between samples (denoting different quantities of collagen). The images used in the analysis of SHG had been kept at original intensity so can be compared to each other. Cell fluorescence was measured using ImageJ. Regions of interest (of where the microsphere was located) were measured using ImageJ and the area, integrated density and the mean grey value were obtained. Three control region was obtained from an area with no fluorescent activity and later averaged. The corrected total cell fluorescence (CTCF) was calculated by the following formula.

$$\text{CTCF} = \text{Integrated Density} - (\text{Area of selected fluorescence} \times \text{Mean fluorescence of background readings})$$

The data was then compared using an ANOVA test to determine significance.

2.14.5 Method used to assemble data on the cell infiltration into microspheres over time

This is the method used to analyse the cell ingrowth and penetration into microspheres over time when cultured in different mediums. To calculate number of cells in each slice a z-stack was taken from each slice and combined as a z-project in ImageJ. Particles were only selected for if the diameter was great than 170 µm and if largely intact (undamaged). Cells were counted within each particle slice when a DAPI nuclei stain was seen. The maximum penetration was found by measuring each cell inside the particle from the centre of its nuclei stain the nearest edge using the measure function on ImageJ. For each particle slice the 5 particles with the greatest penetration were taken and the mean average was taken for the penetration distance. 95% confidence limits were used for both sets of data. The data was then compared using an ANOVA test to determine significance.

2.14.6 Measurement of cell nuclei alignment on polycaprolactone microsphere agglomerations.

Cell alignment was measured from a z-stack of images of hES-MP cells growing over PCL microspheres in an agglomeration. For each image, ImageJ was used to measure the alignment of the elongated nuclei to an arbitrary 0° base. The distribution of cell alignment was then plotted on a spider plot on excel.

2.14.7 Techniques use to analyse the vascularisation response to the implants

Data on the density and size of blood vessels in proximity to the scaffold was obtained from both the imaged of the implant in situ and of the sectioned samples of the scaffolds. Data on the density and bifurcations of the blood vessels was obtained by analysing a 2 cm^2 area around the implant over a series of images. Blood vessel diameter was measured using ImageJ and the widest point of vessel was imaged. Each bifurcation with the 2 cm^2 area was counted, as were and additional bifurcations downstream of the same vessel. Blood vessels that left the area and then re-entered were only counted once when recording frequency of blood vessels. Samples were compared using an ANOVA test.

Chapter 3: Fabrication methods for particle manufacture

3.1 Chapter aims

1. Evaluate the manufacture of microparticles using photocurable based materials
2. To investigate methods of structuring microparticles incorporating porosity
3. Produce a set-up to manufacture a continuous and rapid production of microparticles

3.2 Introduction

The initial step of the project involved identifying the microparticles that would be used for the scaffold. A variety of stereolithography and photocuring methods were available. Choosing the microparticle for the injectable scaffold was a balance of control over the structure of the particle and the speed of production. However, no matter the level of detail achievable, if the speed of manufacture is too slow to produce an appreciable number of particles the process is not suitable for large scale production. Control over the particles shape is a highly desirable feature of the manufacturing process. Being able to alter the porosity and shape of the object will allow for greater innovation in both assemble and directing/supporting cell growth, differentiation and vascularisation [253]. A brief review of the techniques and materials from literature follows.

3.2.1 Photocuring monomers: Lithography techniques

Photolithography utilises photocurable materials to rapidly form solid objects from a pre-polymer liquid. For a polymer material to be photocurable, a photoinitiator is added. The photoinitiator absorbs light, and the resultant loss of an electron results in the formation of a free radical. This then initiates free radical polymerisation, causing the monomers around it to solidify. The use of lasers has allowed for rapid and precise triggering of photocurable materials, producing features down to the nano-scale [254].

Photolithography is the direct write with a laser, where the beam is scanned over the surface of a photo-curable polymer, which then cures [255]. While this method is slower in making objects than photo-mask printing (including DMD projection) methods it is much faster at mid-operation alterations to the design of the microfluidic. Changes can be made after each production without the need to print out more transparencies or create new moulds. This allows direct write to reduce the waste involved with development and removes delays involved with altering traditional production methods [256]. This technique is slower than other laser based methods when it comes to producing objects as the whole structure is not formed immediately, but built up line by line.

Two-photon polymerisation relies on the selective photocuring of a voxel within the monomer solution [257]. For the free radical formation, the photoinitiator for a two-photon polymerisation requires the excitation of two electrons simultaneously. This double arriving of a photon effectively combines two

photons, hence with twice the energy (half the wavelength), which is sufficient to liberate an electron from its atom and thus begin the polymerisation [258]. This allows the laser to cure features below the diffraction limit of light which is the limit of other photocuring techniques [257]. Two-photon printing allows nanoscale structures and patterning and can be used to produce high levels of detail and structuring [259]. With a two-photon technique it is possible to manufacture true 3D structures. Two-photon laser polymerisation can be used to produce 3D components for a microfluidic device such as micro-porous filters [260] which be used for applications such as filtering components of the blood [261].

Microfluidic channels can be used to turn what is essentially a batch process of particle manufacturing into a continuous process. Liquid pre-polymer passes through the channel whilst a light source cures the polymer as it passes [136-139]. These channels are formed from polydimethylsiloxane (PDMS), a silicone-based organic polymer, and the standard for microfluidics. This material has an advantage for photocurable applications as it forms a competitive oxygen layer a few microns thick from its surface, which prevents free radical polymerisation[136]. This prevents the polymers from curing and adhering to the channels walls. There are many variations of this technique reported in the literature [141]. An example is of a single channel, which is patterned with DMD projection, curing objects within the monomer flow [141-144].

3.2.2 Microparticles: their manufacture and applications in tissue engineering

Porous particles confer a significant advantage for cell survival, since they allow the cells to bind to the interior of the particle, away from external forces during implantation [67, 106]. Cells on the inside or in surface depressions are better able to resist shear forces [107]. Porous materials also provide a higher surface area for cells to grow on, and allow for increased perfusion through particles if the porosity is interconnected [262]. There are many methods available for producing porous particles but not all can be combined with microfluidics or laser curing.

Being able to control the shape and porosity of particles is difficult. To then produce a system which requires high numbers of these particles reduces the viable options for particle manufacture. Unshaped particles are usually spherical in nature due to the formation of a shape for minimal surface tension. There are many techniques for forming spherical particles [69, 263-265], but less alternatives exist for forming particles in specific shapes [136]. Being able to design and tailor the shape of each particle is important as creating the desired microarchitecture allows us to influence cell behaviour [266].

3.2.3 Polymers and materials used within chapter 4

Polymer: Polyethylene glycol

Polyethylene glycol (PEG) is used for many applications in the medical industry such as for non-fouling surfaces and relative bio-inactivity [267, 268]. PEG is a polyether compound and can be modified to form a diacrylate (PEGd), for use in free radical polymerisation reactions [269]. When combined with a photoinitiator the mixture will react to light by polymerising, as the photoinitiator begins a free radical polymerisation reaction. Photo-absorbers can be added to attenuate the polymerisation reaction [270]. PEGd is a popular material for 3D printing using lasers (microstereolithography), partially due to its transparency and its non-toxicity to biological tissue [262, 271].

Emulsion: Polymer high internal phase emulsion

Polymer high internal phase emulsions (polyHIPE) are an example of a highly porous material which can be cured in a particle form [272, 273]. PolyHIPEs are emulsions of water and an hydrophobic monomer, which can be formed with up to 99% interconnected porosity [150]. When the water content is greater than 70%, waters droplets start deforming to allow higher porosity [151]. A surfactant is added to the monomer which lowers the interfacial tension of the droplets, allowing them to form interconnected porosity [150]. It has been postulated that when the material dries the polymer shrinks, which acts to open interconnecting pores in the thin walls between pores [274]. When combined with a photoinitiator, some polyHIPEs can be used as a photocurable material, forming structures with high interconnected porosity.

3.3 Results

3.3.1 Photocuring of shaped objects using controlled laser based radiation

A 407 nm laser was utilised with a digital micromirror device (DMD) to project patterns onto a bath of photocurable PEG monomer. Structured/shaped microparticles were produced in a batch style processing technique (figure 3.1). Different projections were used to produce microparticles with different structures. Incorporation of porosity of different sizes into the microparticle designs were successfully manufactured as physical structures. Over-curing is evident in some locations (blue arrows), although features are well formed. Over-curing often causes the rounding of corners on objects. Particles were formed with internal structuring, demonstrating the versatility of using the DMD for image projection. The SEM micrographs reveal the surface topology of the particles (figure 1d -g). The particles appear micro textured from the micromirrors on the DMD. This can be seen from the dimpled surface of the particles. The polymer 'tail' on the particles was caused by a slight overspill of laser light, it is also visible on the side of the particles (red arrow). The proportions of the hexagon in Figure 3.1f appear distorted and are not identical to the image loaded into the DMD software to form the shape.

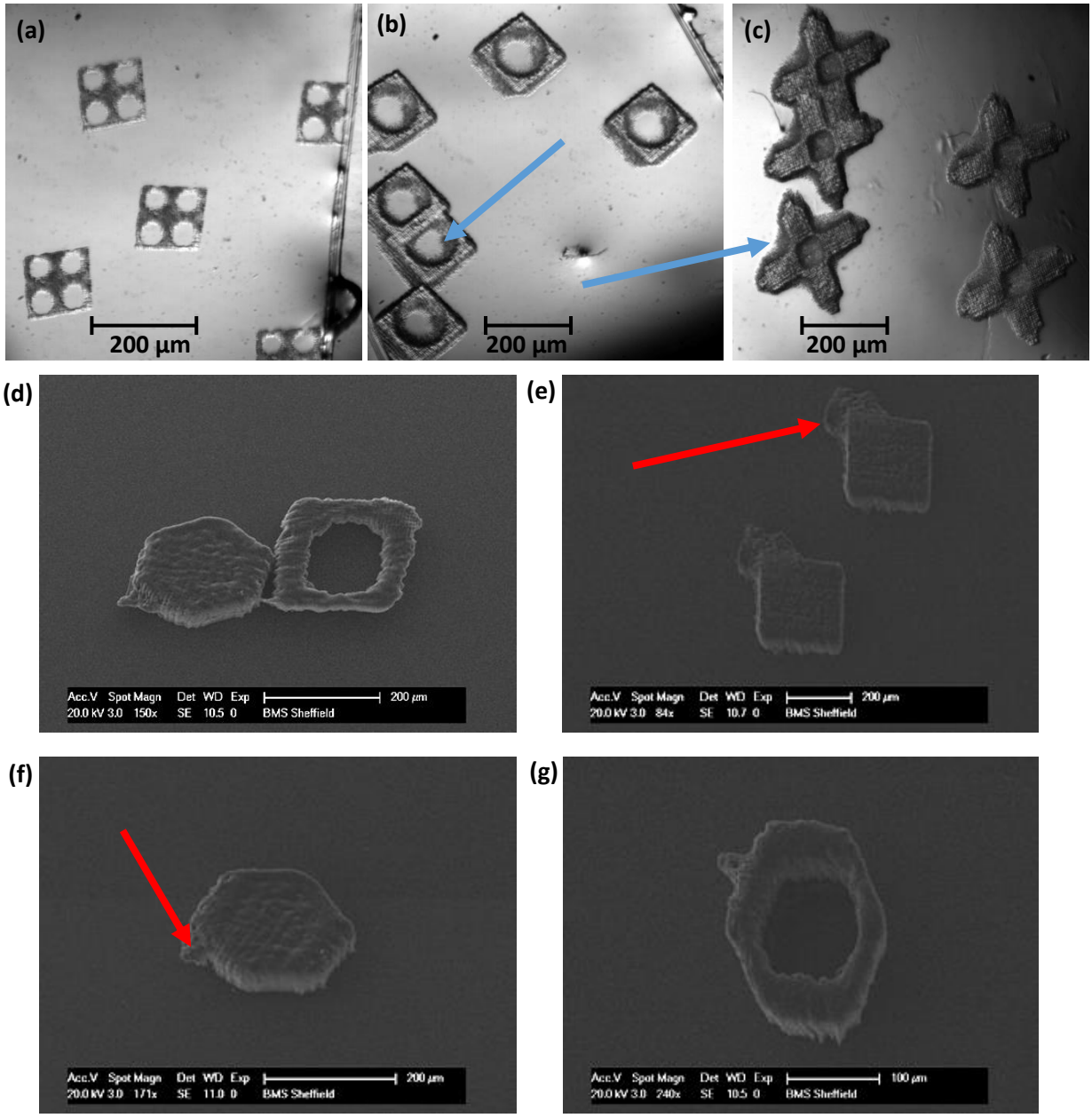

Figure 3.1. Particles formed using the DMD setup projecting onto a glass slide containing photocurable PEGd. DMD projector used to produce shaped particles, in a batch process. (a-c) Optical micrographs of photocured PEG microparticles. Each particle has internal porosity designed into its structure. (a) Square particles with small internal porosity. (b) Square particles with large internal porosity. (d-g) SEM micrographs of particles formed using the DMD projector and photocurable PEG. (d) Hexagonal particle alongside a square particle with large internal pore. (e) Solid square particle. (f) Solid hexagonal particle. (g) Hexagonal particle with a large internal pore. Blue arrows denote overcuring and red arrows show laser overspill regions.

3.3.2 Two photon laser photocuring (manufacturing) of CAD designed microparticles particle

Before manufacturing the calibration tests for the 2-photon direct write allowed us to determine the power and speed settings required for producing a voxel of a particular size (figure 3.2). While this exact data is individual to the specific setup it does illustrate the effect that speed and laser power

have on the voxel area of polymer curing. Increasing the speed had the greatest effect and reduced the cured polymer height while increasing the power increased the height of the cured polymer.

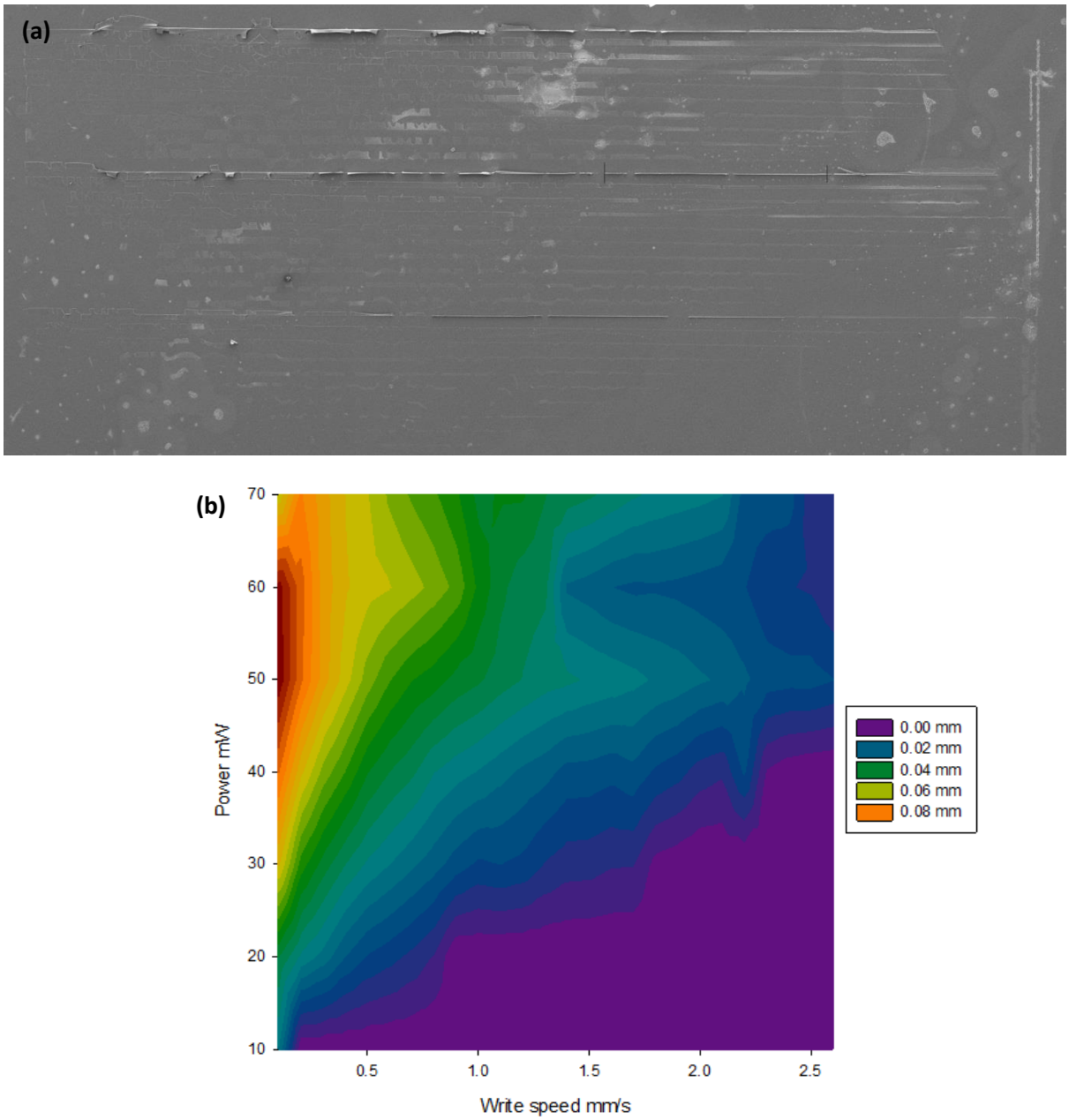

Figure 3.2. (a) Lines formed by 2 photon polymerisation when photocuring PEGd. For each line the stage travelled in both the x and z axis to form a gradient. Each line in a set was at a different stage speed and each set was done at a different power. Measuring the size of the resulting photocured feature allowed for the creation of a settings library. (b) Data gathered from (a) and displayed onto a graph relating laser power and stage write speed to the feature size produced. 0.00 mm = no structure formed.

Having calculated the voxel size, it was then possible to manufacture a CAD designed micro-particle with specific features through 2-photon photocuring (figure 3.3). The internal structure shows the path of the laser as it cured the monomer. The complete structure (Figure 3.3d) does not resemble the CAD file exactly. The pores in the sides of the microparticle have not been formed. A slight curve over the

upper surface of the microparticle is also observable. Features of 50 µm diameter were successfully formed and the pores extended through the structure. Both the large (90 µm) and small pores (35 µm) were created in the particle.

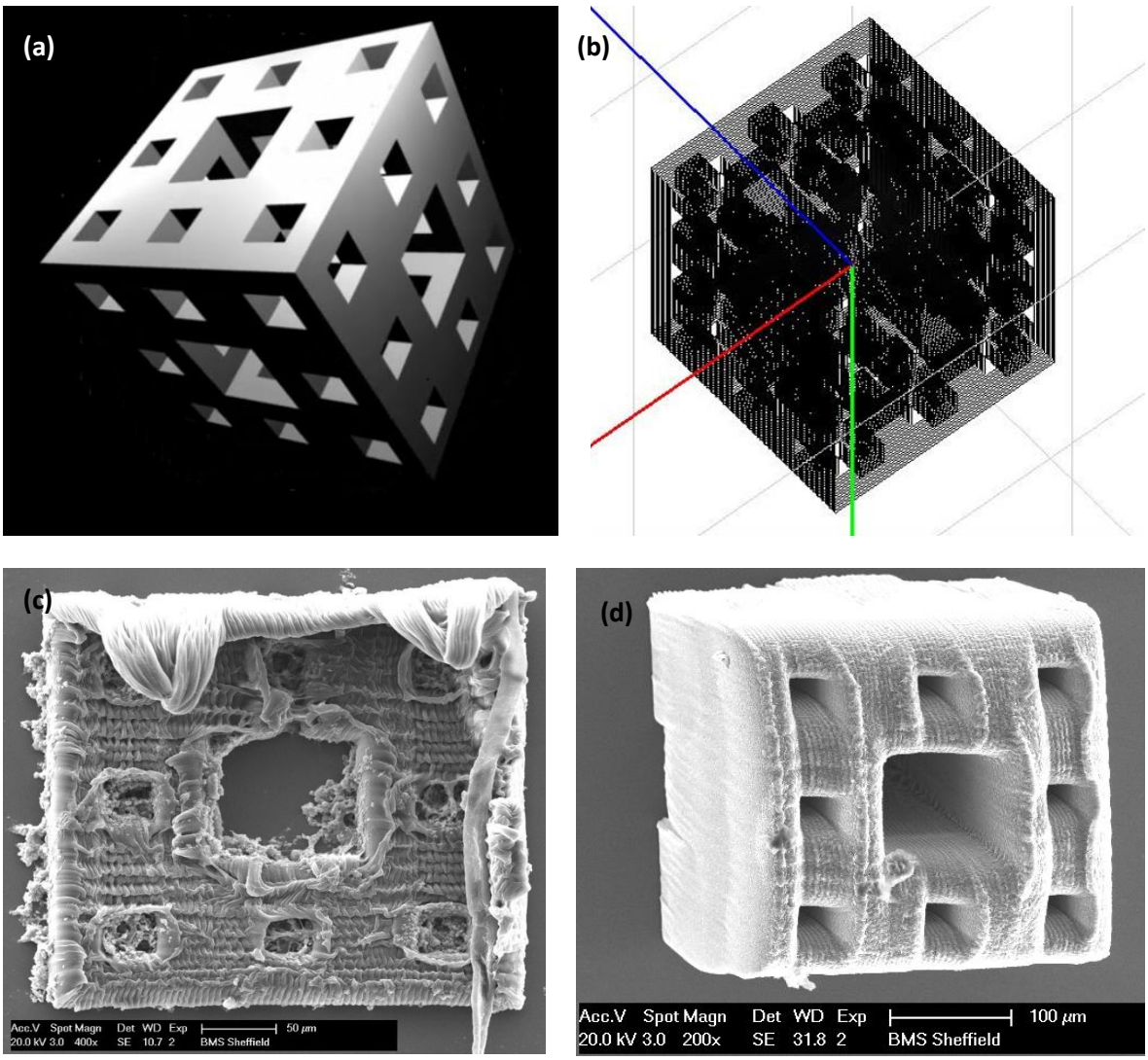

Figure 3.3. (a) STL file for particle design containing both large and small pores. (b) Computer generated laser path for curing of microparticles by STA software. (c) Aborted attempt at micro-particle showing the internal features of the structure. (d) Micro-particle structured via 2-photon polymerisation over 4.5 hours.

3.3.3 Producing microspheres through encapsulation of oil phase in water phase using a microfluidic device

Single photon direct write was used to cure the microfluidic template in PEGd. PDMS was used to create an imprint of the PEG template and bonded to glass to form a microfluidic chip (figure 3.4). The power and speed of the laser changed the width of the cured PEG on the glass slide but did not change the height of the polymer. The height could be altered by changing the depth of the monomer inside the monomer bath. The images in Figure 3.4 demonstrate the range of channel sizes that could be

produced by this technique. Increased channel diameters further could be achieved by curing two or more lines in parallel.

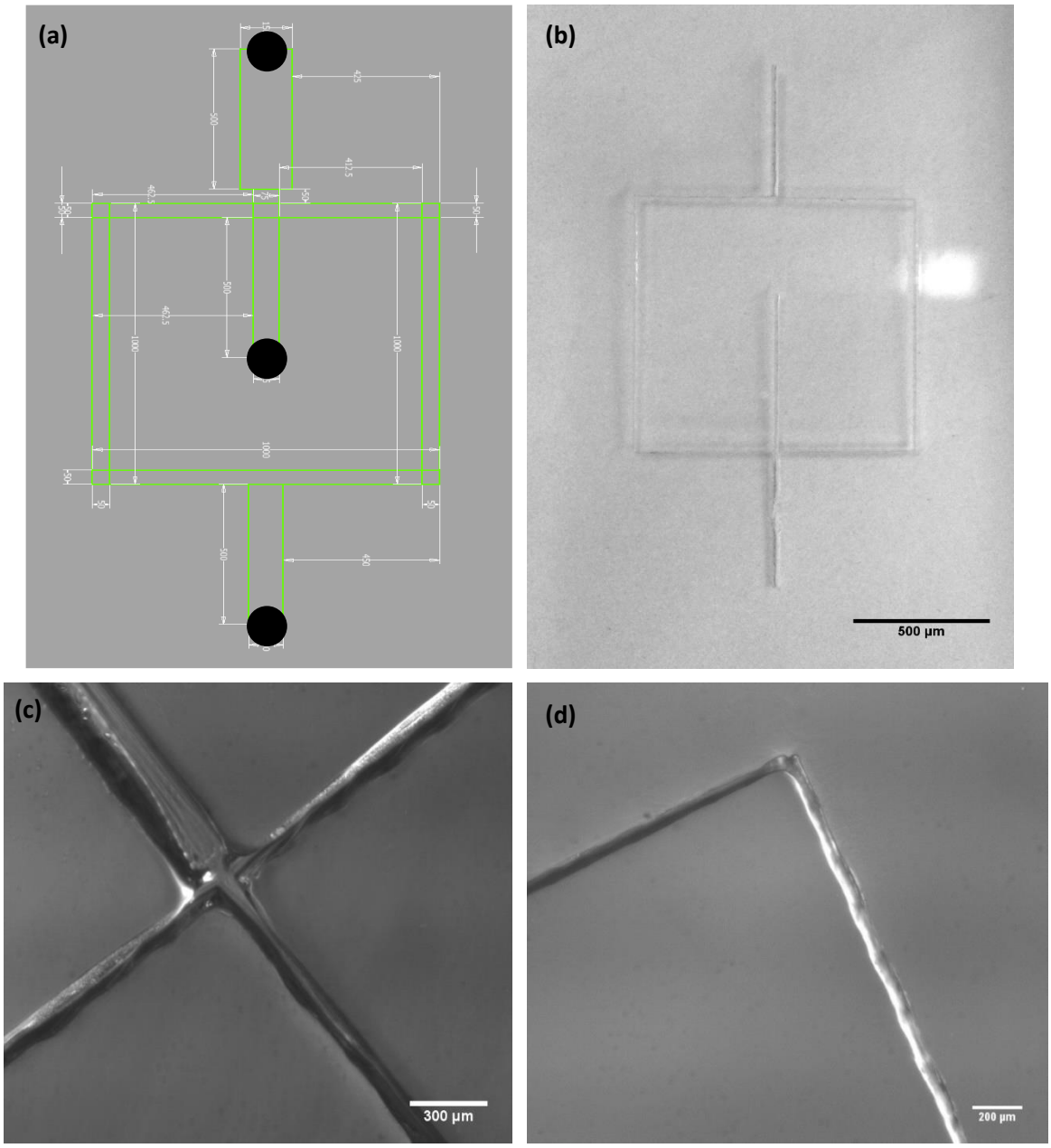

Figure 3.4. (a) CAD design file for the microfluidic channel. Black circles indicate where a hole would be punched into the PDMS for input and output feeds. (b) PEG structure of the microfluidic channel on a glass slide. (c) PDMS mould of the microfluidic device focusing on the encapsulation area of 160 µm (d) Corner of the microfluidic PMDS channel with a channel width of 80 µm.

Encapsulated oil phase droplets were produced by the microfluidics. Figure 3.5 demonstrates the successful application of the microfluidic chips. Dyed water and oil were used to establish the flow rates required to produce the microdroplets in two non-miscible solutions. In Figure 3.5a laminar flow can be seen when the two differently dyed waters first interact and remain distinct and don't mix. On the left of the image the effect of mixing can be observed as the two flows begin to intermingle (black circle, Figure 3.5a).

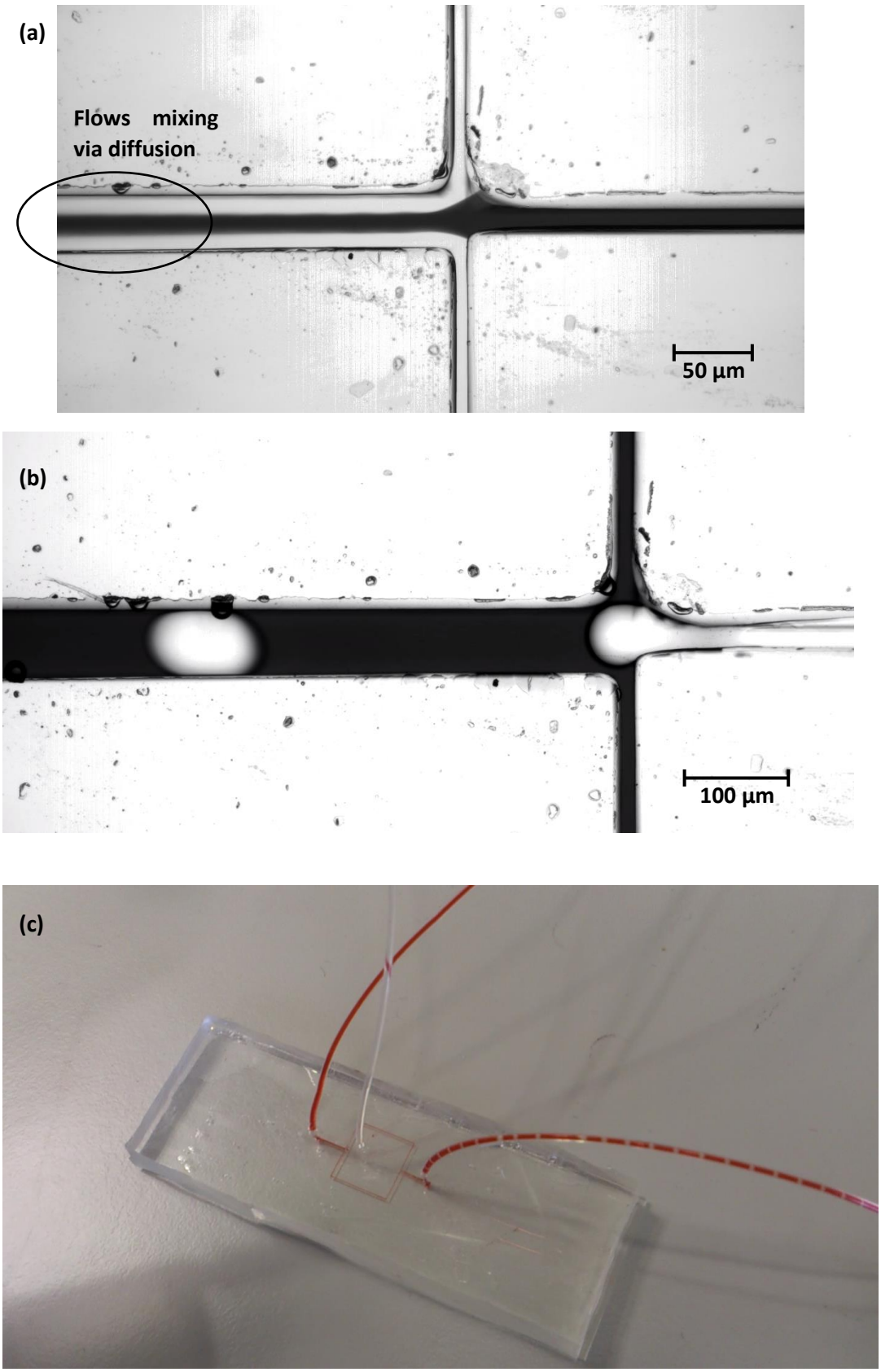

Figure 3.5. (a) Laminar flow within the microfluidic chip of two inputs of differently dyed water. (b) Optical microscope image of oil and dyed water in microfluidic chip producing encapsulated bubbles of oil. (c) Same experiment as (b) but showing the setup of the experiment.

Using PEG photocurable monomer, water and the encapsulation microfluidic it was possible to form spherical microspheres of PEG (figure 3.6). Changing the flow parameters changed the size of the microspheres. Decreasing the PEG flow caused small microspheres to form and increasing the flow rate of the water had a similar effect. These microspheres were very rapid to manufacture but do not include any porosity or structuring. We then combined this method with a materials processing method (polyHIPE) to include porosity within the microspheres.

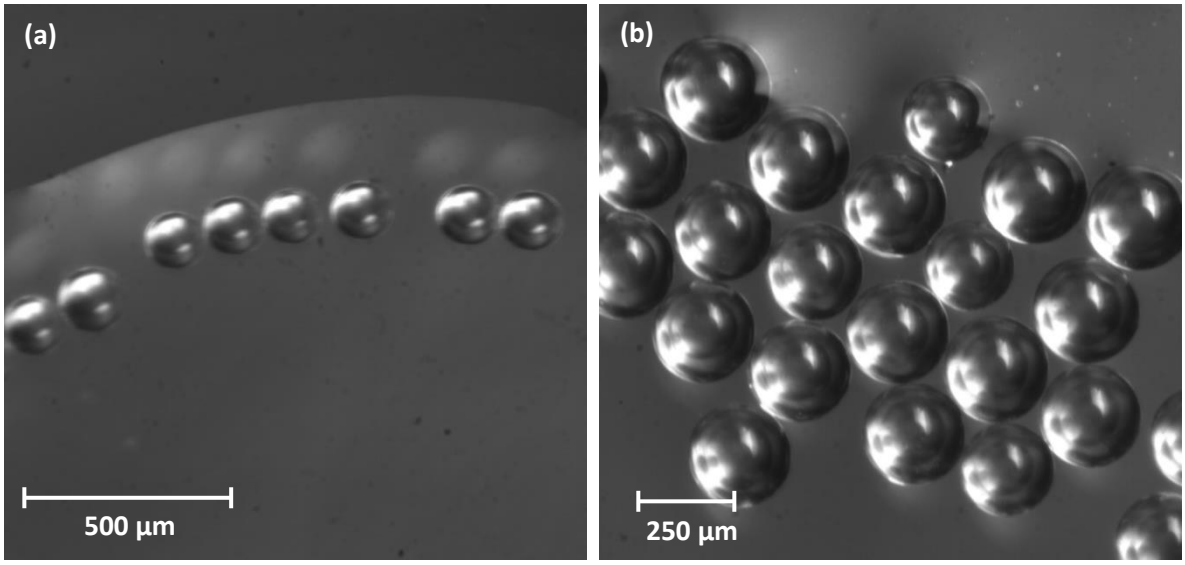

Figure 3.6. PEG microspheres formed by the microfluidic chip. Different flow settings were used to achieve the different sized microspheres. (a) 3 ml/hr monomer flow. (b) 10 ml/hr monomer flow.

3.3.4 EHA/IBOA polyHIPE microspheres manufactured using the microfluidic device, via encapsulation and photocuring

EHA/IBOA polyHIPE microspheres were formed using the encapsulation microfluidic chip (figure 3.7). The polyHIPE system will be expanded on and discussed in detail in the following chapter. The HIPE used is an oil based emulsion (w/o) and when combined with the microfluidic chip the system becomes a double emulsion (w/o/w). Once cured these microspheres were highly porous and formed a uniformly sized population. Flow rate alterations had the same effect as those used for PEGd in Figure 3.7. The microspheres have an open surface porosity (figure 3.7a) which allowed the water used in the HIPE formation to leave the microsphere when drying. Production rate of the microspheres was 180 microspheres per minute.

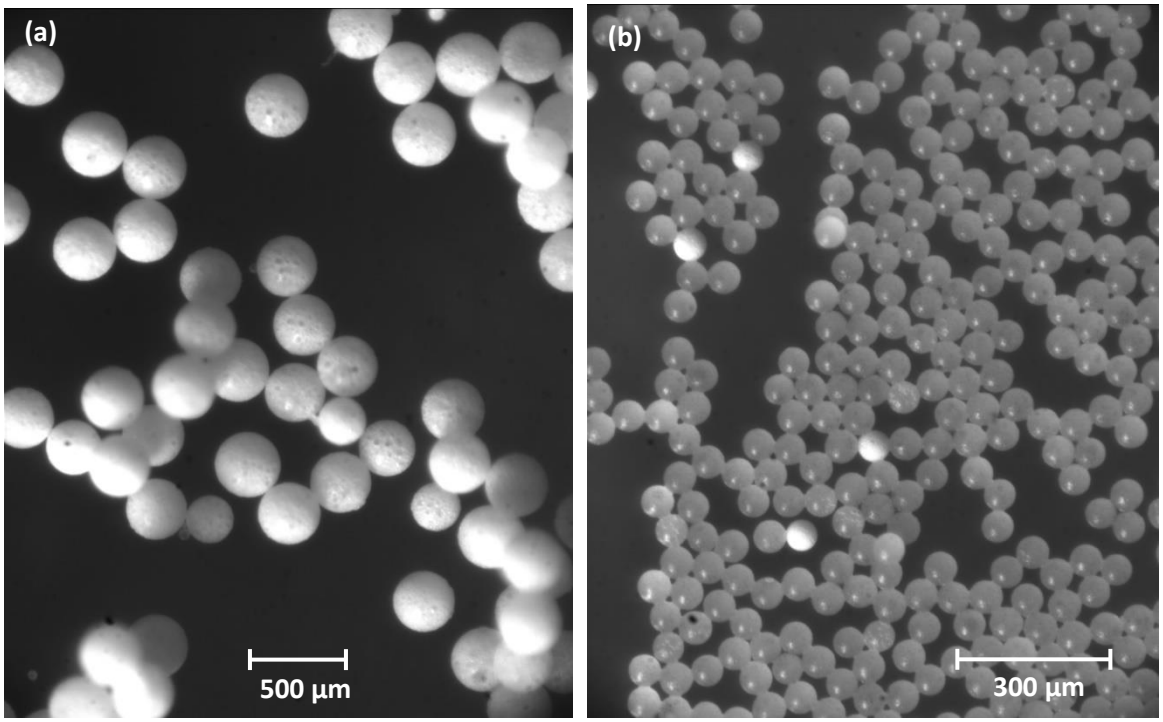

Figure 3.7. polyHIPE EHA/IBOA microspheres formed by the microfluidic chip. Different flow settings were used to achieve the different sized microspheres

3.4 Discussion

The DMD system was used to manufacture shaped particles by allowing precise shaping of the laser light using the image uploaded to the DMD's software [275]. Problems with the set-up or irregular laser intensity can cause distortions to the projected image which in turn effects the cured polymer structure. Scattering from the polymer can cause a wider area to photocure than is desired and the corners of objects often cure faster than other areas, leading to over curing. The microtextured topology seen on the SEM images of the particles in Figure 4.1 show a dimple effect. This is formed from the individual micromirrors or more specifically the gaps between the mirrors [276]. This can be reduced by increasing the number of mirrors to make a single structure. However, while this will reduce the size of the topology but does not eliminate it. This surface topology may be advantageous, as it increases the surface area of the particle and provides a topology for interaction with cells [277], both on the micrometre scale and on the nano scale.

Porosity can be included in particles, both by designing voids into the structures or by designing the particles to not fit together seamlessly. When randomly assembled, cross shaped particles will allow the formation of a higher percentage of porosity than square particles. Through this method both the external porosity and any internal pore size can be controlled. The particles produced in Figure 4.1 were designed to produce a controlled pore sizes in this way. Controlling pores size is essential for controlling cell and blood vessel ingrowth. Too few or small pores can result in low cell/vascularisation ingrowth to occur. Whereas when pores become too large the material can become too mechanically weak to support load.

Depending on the photocurable material, some cured objects can only be formed in 2.5D when using the DMD system, this can be offset by structuring the particles to form seudo-3D structures through interlocking. A void was left in the centre of the particles to allow the particles to slot together, forming 3D structures. See Figure 3.7 for an example of how these particles are theorised to fit together. In materials, which are transparent, the laser light passes all the way through the monomer bath, curing the entire depth of the monomer. This allows for the 3D design of the x and y axis but no control in independently designing the z axis. An opaque solution, or one with photo-absorbers, can be built up in multiple layers using a motorised stage in the z-axis in a similar way to many 3D printing technologies [278]. Changing the particle shape can go a long way to overcoming the shortcomings of a 2.5D scaffold.

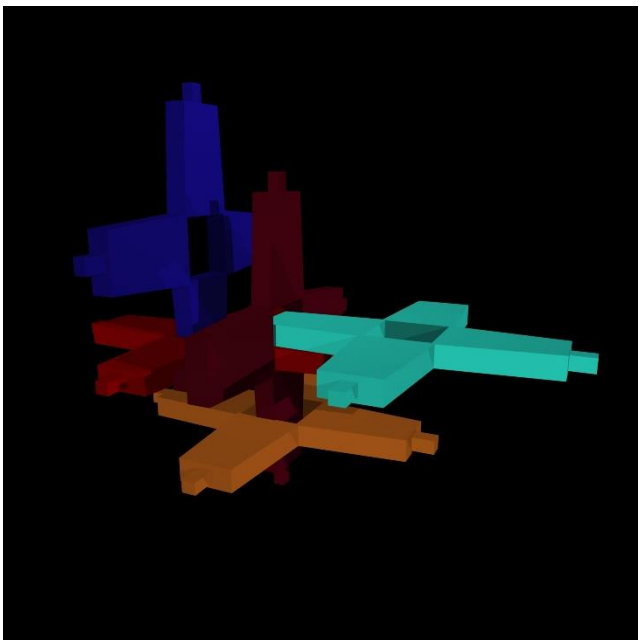

Figure 3.7. CAD generated image of interlocking particles showing the potential open 3D structures of particles when mixed together randomly.

The use of 2-photon polymerisation allows the manufacture of intricate and highly detailed particles with a true 3D structure. Using this system, it is possible to fully reproduce the 3D structure designed on CAD software. As the object is supported in the liquid during formation it is able to support the formation of overhangs without the requirement of a secondary support material. Exact control over pore size, distribution and nano-scale topology is possible using the technique which can be utilised to guide cell alignment and differentiation [279, 280]. Sub 100 nm resolution has been achieved by the research community [281] with many groups such as Misawa et. al. producing structured geometries with a high degree of complexity [282]. However, the particle in Figure 4.5 required 270 minutes to manufacture. This is approximately 1200 times slower than particles formed with the DMD. This is an issue which exists for all freeform fabrication manufacturing methods and is only exacerbated as the line width used to lay down material is reduced.

The speed of particle manufacture is an important aspect for consideration, as a complete implant may require tens of thousands of particles [283]. Producing particles slowly in the lab may be possible and even translatable to small scale in-vivo experiments but when scaling up for industry this would quickly become non-viable. Modifications have been suggested which can be made to increase the production rate. Output can be increased by splitting laser beam with mirrors and then focused on different parts of the monomer on the stage, so that the particle is built in a parallelised way. Increased levels of photoinitiator and increased laser power can be used to increase the write speed and reduce printing times. Despite these methods for speed and yield increases the production of highly complex true 3D structures is currently very time consuming. If it were possible to increase the output of the technique

of the particles sufficiently, the technique would become the gold standard for producing particles for bottom up tissue engineering.

Microfluidic systems can be combined with DMD or direct write manufacturing techniques to manufacture particles for tissue engineering [139, 141, 145, 284]. The encapsulation microfluidic chip is used in biotechnology to encapsulate biomolecules or cells within a sphere which can then be used as a cell carrier [131, 285], micro incubator/reactor [286] or as a printable bio-ink [106, 287, 288]. Using a single photon (standard direct write) lithography system to form the microfluidic device was chosen due to the reduced manufacturing time. As this microfluidic is designed in 2 axes there was no need to control the curing in the z-axis with the laser. The depth could be controlled by the quantity of monomer used. Changing the speed and power of the laser changed the width of the microfluidic channel. This reduced the complexity of the program required to control the stage. For channels larger than the laser could produce, multiple lines were added in parallel next to each other. Once formed a template could be used many times to produce PDMS moulds until the templates became damaged from repeated use [289].

Using the microfluidic systems, spherical particles (microspheres) were photocured by combining two immiscible solutions within the chip and forcing one to encapsulate the other phase. It is possible to use this microfluidic system to form microspheres without photocuring. For example using an alginate solution and a aqueous calcium solution, to set the alginate into uniform spherical droplets [290]. Here we use a photocurable liquid as the oil phase which can be photocured by a radiation source after the droplets have been formed [291]. Microspheres formed from PEGd were the initial microspheres formed by the microfluidic device. Similar manufacturing processes have been reported in the literature, forming PEGd microspheres down to 40 µm in diameter [292]. There is very little control over the structure of the microsphere formed from these devices. The microfluidic tube can be shaped to flatten a droplet or to elongate it [272] but the finer control offered by the DMD or the 2-photon polymerisation is not currently possible. Where this technique stands out compared to the previous methods discussed the rapid speed of microsphere manufacture. The rate of microsphere formation was 3 particles per second. This is a substantial speed increase when compared to the DMD production rate.

The microfluidic system allowed for rapid manufacture but confirmed no method to include complexity or porosity into the microspheres. The loss of control over the microfeatures and porosity of the particles was compensated for using the polyHIPE material. This emulsion based material which photocured as a porous polymer, the properties of which could be tuned independently of the microfluidic system. This is discussed in detail in the following chapter. The polyHIPE material is full of air/water interfaces from the internal liquid droplets which scatters laser light [293, 294]. This is not an issue when the suspended spherical HIPE monomer is cured under a UV lamp as the entirety of the

microsphere need to be solidified. However, when used with the DMD the scattering nature of the material reduced the thickness of the resulting structure. Additionally, with the increased scattering, resolution was greatly reduced, as the laser light scattered and cured a larger area of monomer.

3.5 Conclusion

In this chapter, different techniques to produce particles were investigated. An association was found with the amount of control over the particles structure, and the time required for fabrication. Increasing the customisation required longer manufacturing times. 2-photon polymerisation could replicate true 3D objects from CAD files but required many hours per particle. DMD based particle fabrication was much more rapid and offered 2.5D control over the particles structure but required operator input in a batch process. Both techniques allowed for the design on internal porosity within the particle, which is essential. The final method used, the microfluidic device, had very little control over the shape of the particles produced but could manufacture hundreds of particles in the same time as a single batch of particles from the DMD. This continuous process and the speed of manufacture was essential for producing the volume of particles necessary for a scaffold. The use of a polyHIPE material allowed for the inclusion of porosity within the particles produced, and allowed us to use this final technique for the remainder of the project.

Chapter 4: PolyHIPE microsphere production

4.1 Chapter aims

1. Produce porous microspheres from the EHA/IBOA polymer blend

2. Investigate effects of processing conditions on both internal porosity and on microsphere size distribution.

3. Compare the microspheres produced via two techniques: controlled stirred tank reactor (CSTR) and the microfluidic T-junction.

4.2 Introduction

4.2.1 Microspheres and their application in tissue engineering

Porous and non-porous microspheres are utilised for many applications in tissue engineering such as microcarriers for cell expansion [295, 296], release of bioactive agents [297], and as building blocks for (self-assembled) scaffolds [298, 299]. The advantage of using microspheres for these applications is that they can be delivered as injectable materials, thus bypassing the requirement for open surgery. Additionally, porous microsphere-based cultures can be used as an ink for 3D cell printing. As a 3D cell support matrix for cells, porous microspheres have many advantages over their non-porous counterparts; they can provide enhanced nutrient diffusion, a 3D culture environment and greatly increased surface area [296, 300]. Many techniques have been used to develop porous microsphere systems including supercritical CO_2 [126], thermally induced phase separation [128], freeze thaw cycles [129], solvent evaporation [130], microsphere leaching [131] and polyHIPE formulations [132].

4.2.2 Photocured emulsions: The polyHIPE

A polyHIPE allows precise control of the degree of porosity within the microspheres as well as control over the degree of interconnectivity and to some extent pore size [301]. The defining feature for an emulsion to be classified as a HIPE is when the internal phase volume contributes greater than 74% of the total volume, corresponding to the maximum packing density of equal sized spheres [150, 302]. If the continuous phase is composed of suitable monomers and cross-linker, a highly porous foam (polyHIPE) can be produced upon curing of the HIPE. A polyHIPE can have a porosity with interconnected pores of up to 99% [150]. This interconnected network of pores is created by the contraction of the thin monomer film surrounding the droplet phase during curing [303]. PolyHIPEs are increasingly being used in tissue engineering applications (including bone tissue engineering) and as cell culture substrates due to their highly porous nature and interconnectivity [185, 302]. In addition, we have recently demonstrated that the mechanical properties of this copolymer system can be finely tuned by changing the ratios of the monomer [304].

4.2.3 Turning the emulsion into microspheres: manufacturing techniques

In this chapter porous microspheres were prepared from a HIPE via photocuring [305]. The microspheres were produced by two methods; (i) double emulsion of photocurable HIPEs to produce water-in-oil-in-water (w/o/w) emulsions in a continuous stirred-tank reactor (CSTR) which were then photocured and dried [302, 306, 307] and (ii) the Gokmen method employing T-junction fluidics/droplet microfluidics [132, 147, 263, 308]. These methods produce very different microsphere size distributions. The latter method provides the ability to produce a very narrow distribution of microsphere size which allows greater control over the scaffold. This is important for delivery as the microsphere size will dictate the bore size of the injection needle while a narrow microsphere size distribution will ensure no blockages can occur from unexpectedly large microspheres. Additionally, controlling the microsphere size allows the control of pore size between microspheres when packed together. Controlling this pore size could allow control over nutrient diffusion and could induce or inhibit angiogenesis (through lack of large enough spaces for blood vessel formation). Monodisperse spherical microspheres present a maximum packing density of 74% (with hexagonal close packing) while a polydisperse microsphere distribution allows for a higher packing density [309].

Photocurable HIPEs allow near instant formation of porous microspheres by curing under UV light. In the double emulsion technique, the HIPE is added dropwise into rapidly stirred water. The mechanical force breaks up the added HIPE into smaller spherical droplets to create a suspension of HIPE droplets in a large volume of water to create a w/o/w emulsion. The spherical HIPE droplets are then rapidly photocured, and the water removed by filtration and evaporation. For the microfluidic method, HIPE is introduced into rapidly flowing water within a silicone tube, via a dispensing tip inserted into the side of the tube. The flowing water ‘buds’ off the HIPE feed stock into droplets. The microsphere size can be controlled by altering the flow rate of water/HIPE or changing the needle tip diameter [132, 263]. The two main advantages of this method are that it produces microspheres with a narrow size distribution, and that it is a scalable continuous manufacturing process (e.g. by (i) increasing the number of silicone tubes and (ii) by adding HIPE injection sites into the tubes) [132, 263, 308] .

4.3 Results

4.3.1 The effect of manufacturing parameters on the internal porosity of the polyHIPE

The polyHIPE material has both an external porosity and an internal porosity along with interconnecting porosity between the pores (Figure 4.1). The polyHIPE material used for these experiments is a blend of the monomers EHA and IBOA. The polyHIPE is expected to be 80% porous as the proportion of water added to monomer is 80:20 (by weight) for the HIPE process. The average size (mean) of the interconnectivity is 2.0 µm and the median is 1.7 µm. There are both micron scale and nano scale interconnecting porosity with the largest pores up to 5.5 µm and the smallest observed being 160 nm. This microporous material scatters the light significantly giving the material a white appearance (Figure 4.1c) despite the transparent materials used in its formulation.

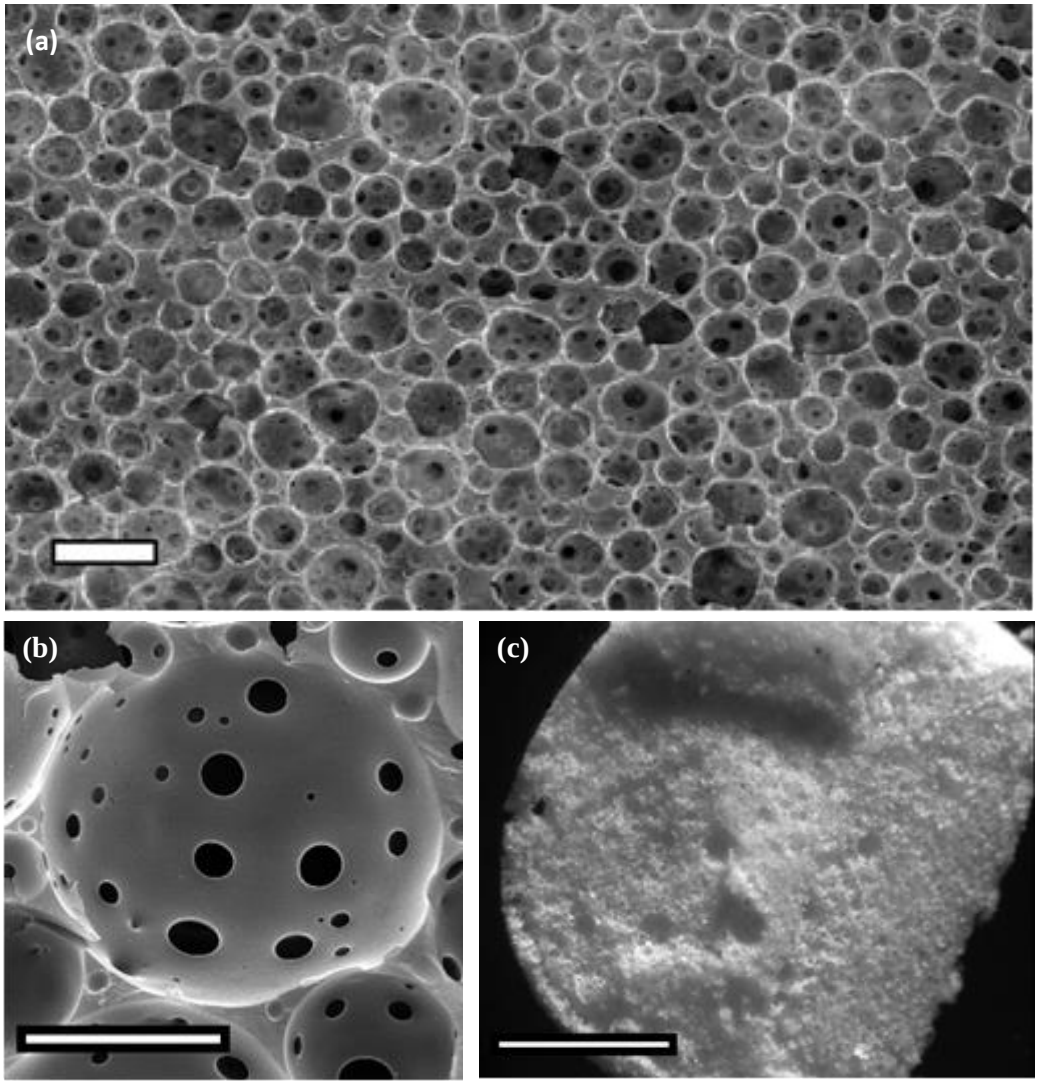

Figure 4.1. EHA/IBOA blend PolyHIPE material with 80% porosity and internal interconnected porosity between larger pores. (a) SEM micrograph of polyHIPE surface displaying open porosity with pores up to 35 µm in diameter. Scale bar is 20 µm. (b) SEM micrograph of interconnectivity between pores in the polyHIPE. Scale bar is 20 µm. (c) Optical micrograph from reflected light microscope of the white appearance of the polyHIPE. It is possible to see some of the larger pores on the surface as a rough texture. Scale bar is 1 mm.

Temperature change influenced the size of the pores within the polyHIPE with increasing temperatures resulting in the formation of larger pores (Figure 4.2). The water was added to the monomer solution at a specific temperature during the w/o emulsion forming stage. The resulting materials were imaged using an SEM and the pores were measured using ImageJ. As temperature increased the average pore sized increased along with an increased spread of pore sizes. At 30 ºC the largest pores measured were up to 70.0 µm in diameter while at 4 ºC the largest was 34.7 µm (≈ 50 % decrease). The average (mean) pore size decreased by 55% from 22.3 µm at 30 ºC to 10.0 µm at 4 ºC. 15 ºC was closer to 30 ºC in values with a 3 µm decrease in mean average (≈ 15 % decrease) and the largest pore size recorded at 65.6 µm (≈ 6 % decrease).

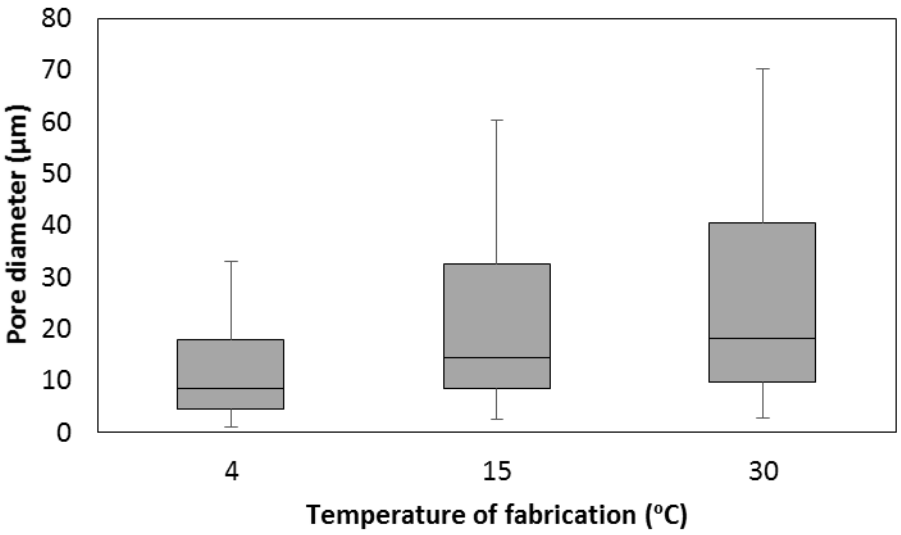

Figure 4.2. The relationship between the temperature of the water during the initial HIPE mixing (w/o) mixing stage and the resulting pore sizes measured in the polyHIPE material, by SEM images. Increasing temperature increases the maximum pores size along with an increase in medium pore size. The temperature change does not change the minimum pore size found in the material. This data has been show on a Tukey boxplot. A Tukey box plot presents interquartile range with the centre line as the median, whiskers represent maximum and minimum microsphere/pore diameter. The temperature of the water added to the monomer is controlled. n > 315.

Increasing the speed of the paddle stirring the monomer as the water is added to form a HIPE decreases the resulting size distribution of pores in the polyHIPE (Figure 4.3). As the rate of stirring used to form the material is increased the pore size initially decreases, until it plateaus at 765 rpm. After this speed there is very little difference in the pore size distribution at the faster stir rates. This effect can be observed in the SEM micrographs (Figure 4.3b) with decreasing pore sizes at higher stirring speeds. Between the slowest stir rate, 320 rpm and the fastest rate, 1260 the mean average pore size decreased by 70% and maximum pore size decreased by almost 80%. The largest interconnected area between pores measured at 320 rpm was 24.1 µm while the largest measured in 1260 rpm was 8.9 µm. These stir rates were chosen as they were the set speeds on the lab egg stirrer used to stir the solution.

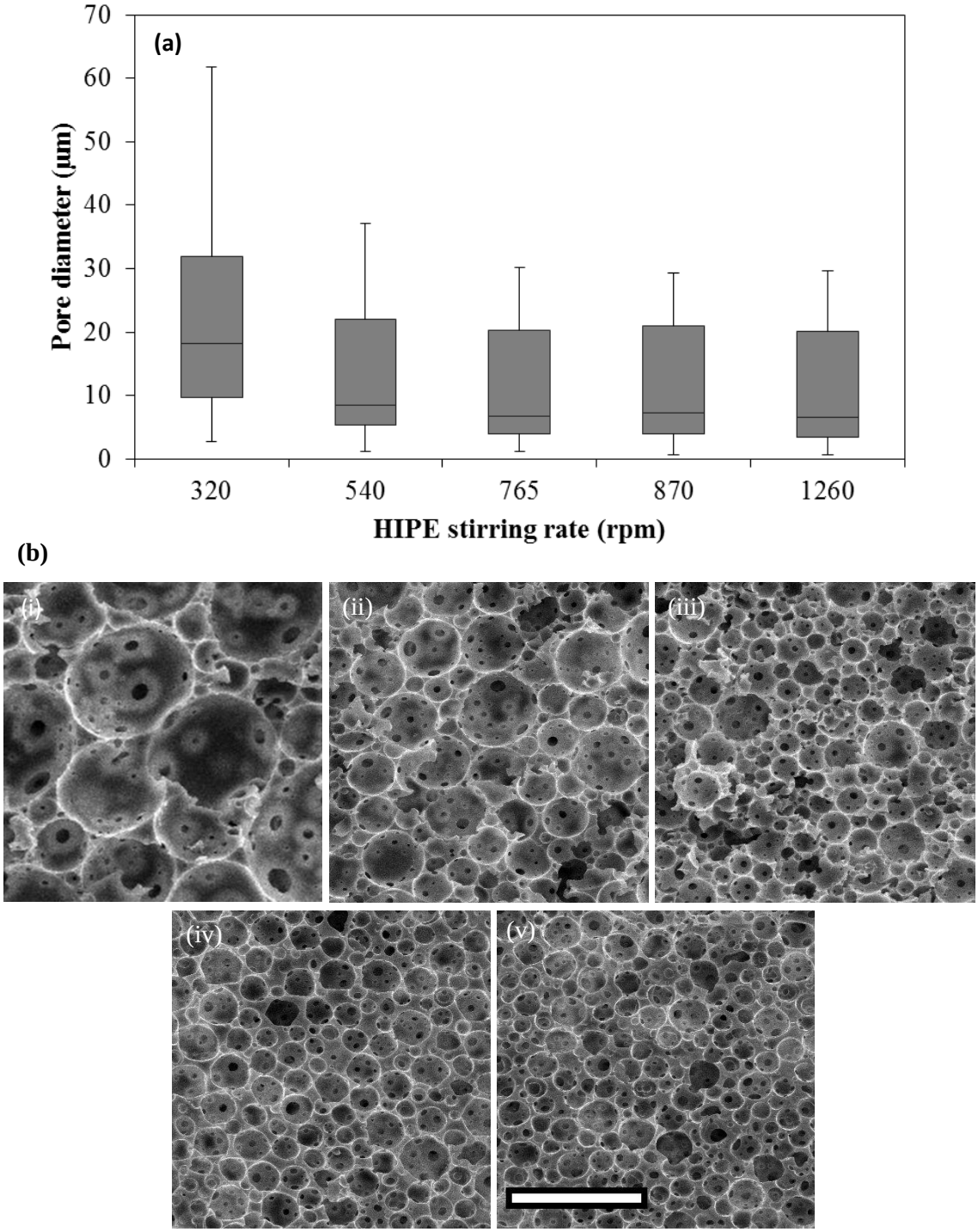

Figure 4.3. The monomer was stirred at different rates during the water addition process (w/o) and the resultant pore sizes was measured. (a) Box plot of pore sizes from each material formed at different stir rates. With increasing stirring rate, the median pore diameter within the polyHIPE decreases, along with the distribution of pore sizes. After 765 rpm there is little effect on the pore size with each increasing stir rate. (b) SEM micrographs of sectioned polyHIPE blocks to show internal porosity. These images, among others, were measured to produce the graph (a). (b i) 320 rpm, (b ii) 540 rpm, (b iii) 765 rpm, (b iv) 870 rpm, (b v) 1260 rpm. The scale bar is 100 µm. n > 384 per condition.

4.3.2 Porous microspheres manufactured via double emulsion and the effect of processing parameters on resulting microsphere size

Microspheres produced via controlled stir tank reactor (CSTR) are formed with a wide distribution of sizes within a single batch, with interconnected pores throughout the material (Figure 4.4). Porous microspheres with a disperse microsphere size distribution were prepared by double emulsion of photocurable HIPE to produce a W/O/W emulsion which was then photocured. A large volume of water was stirred continuously and the HIPE was added dropwise over several minutes. Micrographs in Figure 4.3a-d displays microspheres at different sizes found from a single batch of microspheres produced via double emulsion. Porosity can be found throughout the microsphere (Figure 4.4e) in a homogeneous state and interconnections are visible between the pores.

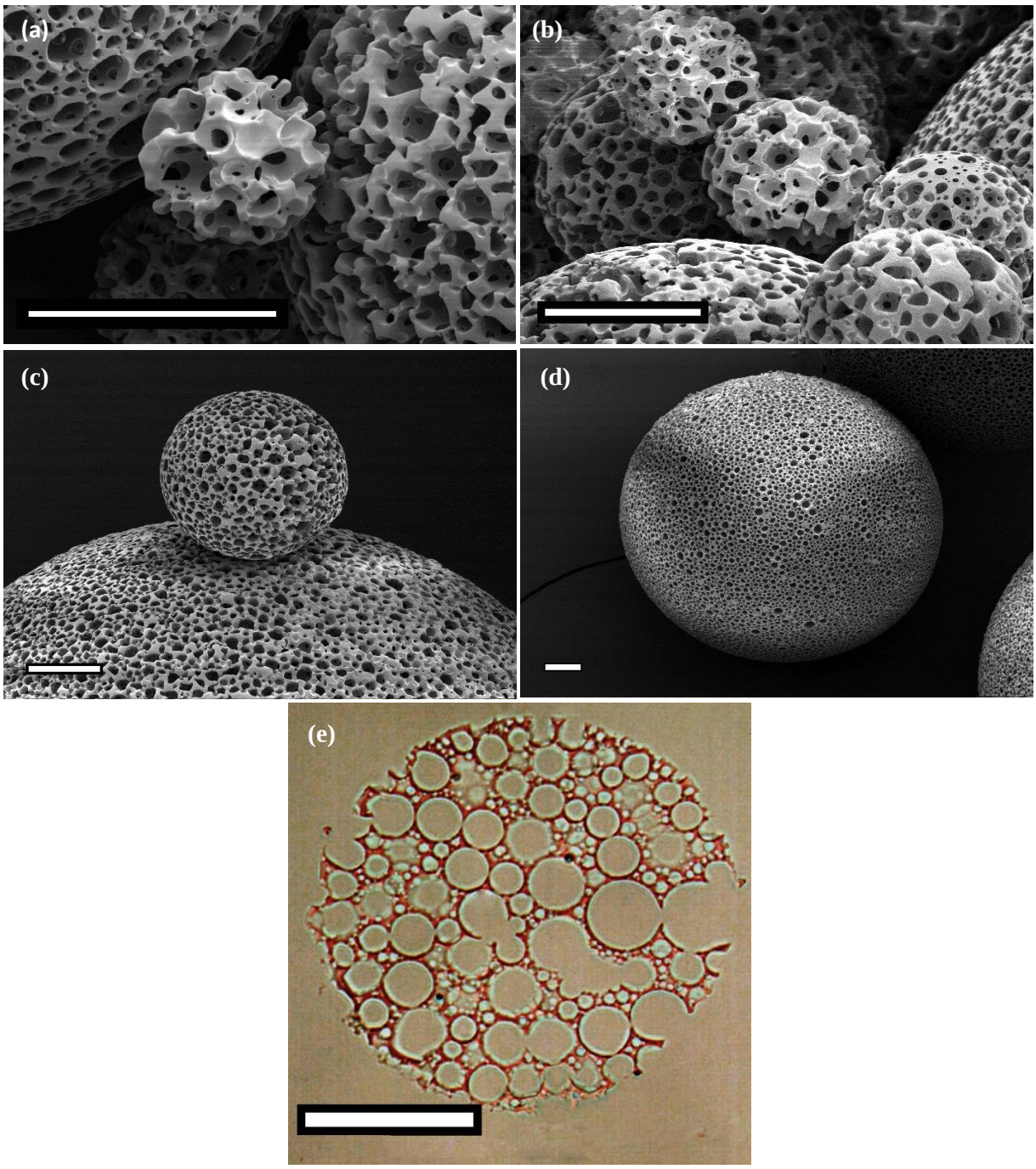

Figure 4.4. PolyHIPE microspheres formed by the double emulsion technique (w/o/w). EHA/IBOA blend PolyHIPE material with 80% porosity and internally interconnected porosity between larger pores. (a – d) SEM micrographs showing the range of sizes present in a microsphere population produced from this technique. (e) Optical micrograph of a 6 µm thick slice of a sectioned microsphere. It is possible to observe the interconnectivity between the pores. Scale bar is 100 µm in images.

Increasing the temperature of the water to which the HIPE was added to widened the distribution of microsphere sizes formed (Figure 4.5). Microspheres formed at the lowest temperature of 4°C had an IQR of 125 to 285 µm whereas the highest temperature of 60°C has an IQR of 275 to 922 µm (an increase of 305%). There appears to be a linear increase in microsphere median size over the observed range of temperatures. Figure 4.5d presents the skewed distribution found all microsphere populations in histogram form. It is important to note that a higher number of lower diameter

microspheres does not correlate to a higher total volume than a lower number of larger diameter microspheres. When comparing Figure 4.5b and 4.5c is can be observed the increased in diameters found at the higher temperature but the consistent spherical nature of the microspheres at the lower temperature.

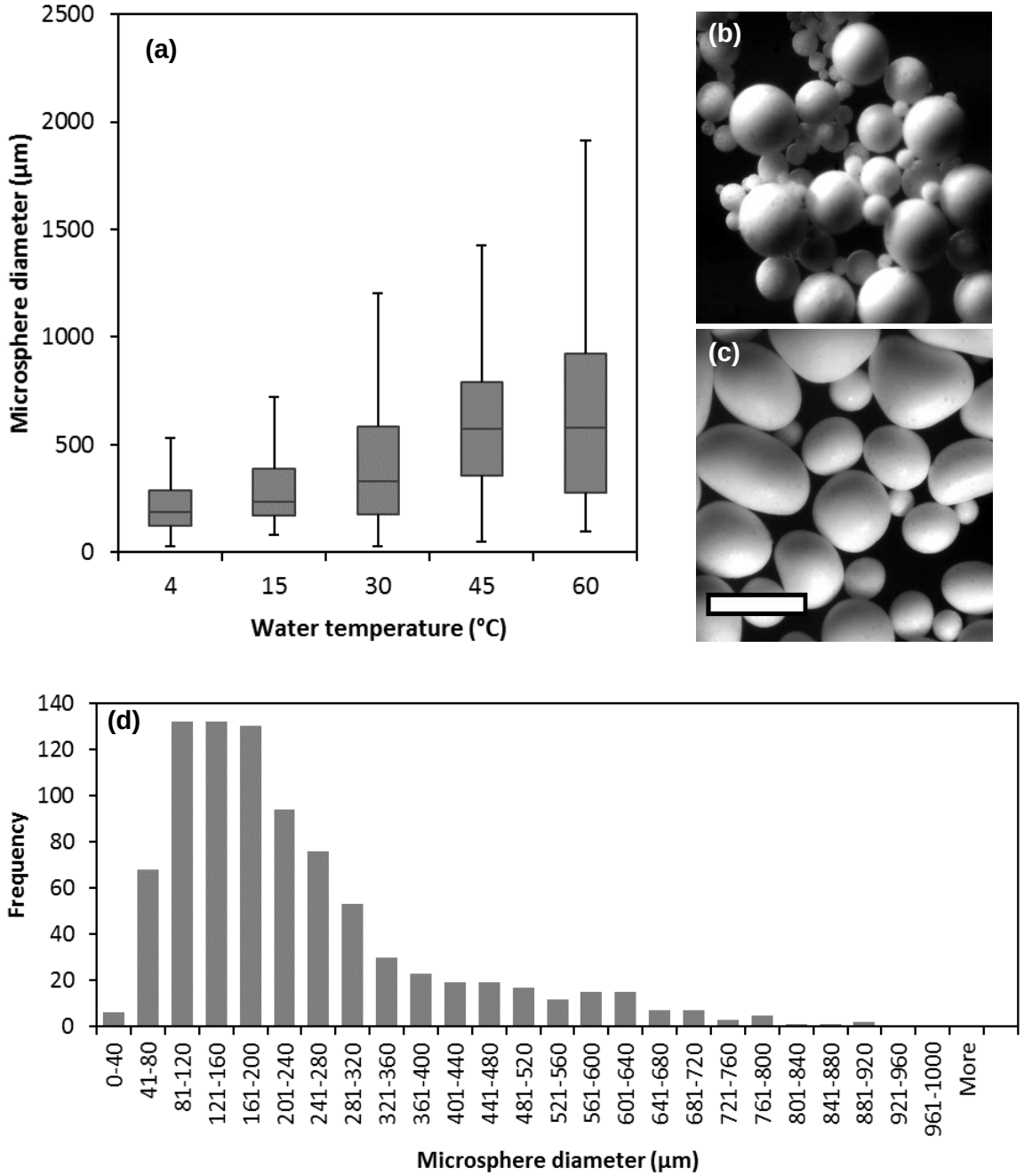

Figure 4.5. The effect of temperature of the water to which the HIPE is added to, on microsphere size distributions from the double emulsion technique. (a) The effect of the water temperature during the process microsphere diameter. Higher temperatures resulted in higher microsphere average diameter and broader distributions of microsphere size. For all temperatures the stir rate of 320 rpm was used. n > 72 particles per condition. (b) Optical micrograph of microspheres formed from double emulsion at the 14°C condition. (c) Optical micrograph of microspheres formed at the 45°C condition. Scale bar is 1 mm. (d) Distribution of microsphere diameters formed at the 4°C condition. n = 617

Temperature of the water to which the HIPE is added to for formation of the double emulsion (w/o/w) does not appear to impact the porosity of the resulting polyHIPE (Figure 4.6). The pore diameter analysis is conducted on the same microspheres as those analysed in Figure 4.5 for microsphere diameter. Figure 4.6a suggests no overall trend of the temperature influencing microsphere porosity. Figure 4.6c again shows no observable trend in microsphere pore size between different temperatures.

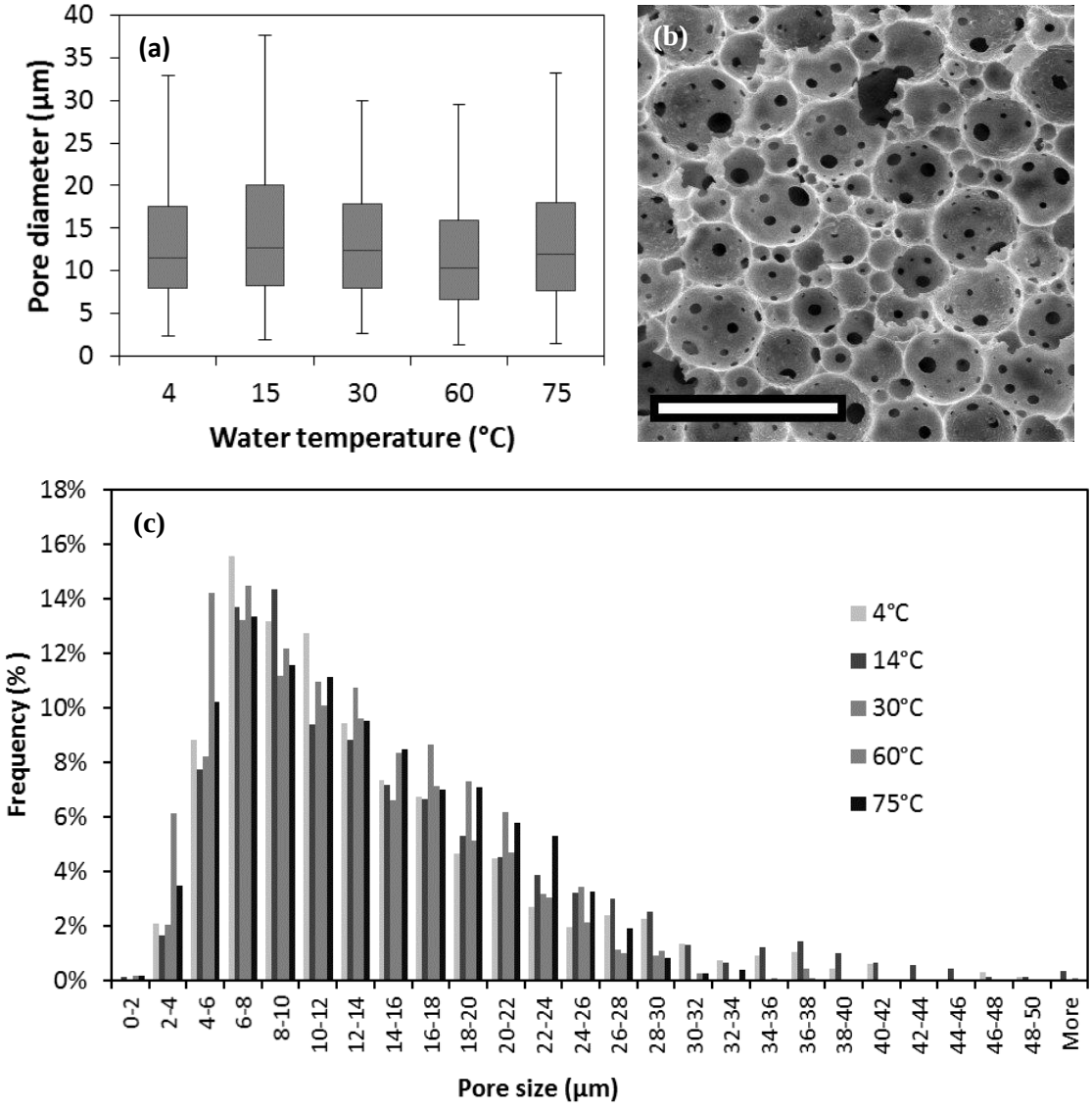

Figure 4.6. Relation between pore diameter, measured in SEM micrographs of sectioned polyHIPE material, formed at different temperatures during fabrication (w/o/w). (a) Tukey boxplot of pore diameter with varying temperature. Centre line corresponds to median size, upper and lower box for upper and lower quartile respectively, lowest bar for lowest datum still within 1.5 IQR of lower quartile and upper bar for highest datum within 1.5 (IQR) of upper quartile. n > 104. (b) SEM micrograph of sectioned polyHIPE with porosity formed at 75°C, scale bar is 50 µm. (c) Same data as (a) but displaying the data as a histogram for clearer observation of pore size comparison between different temperatures.

Both the median microsphere size and the width of the size distribution decreased with increasing stirring rate (Figure 4.7). At the slowest stirring rate, the median diameter was 408 µm with a large interquartile range (IQR) of 276 to 690 µm. At the fastest rate the median microsphere diameter decreased to 131 µm (67% decrease) with a much narrower IQR of 81 to 166 µm (80% decrease). At the slowest speeds microspheres begin to lose their spherical shape which observed in Figure 4.7bi. In Figure 4.7bi-iv the microspheres are spherical in shape and the overall decrease in microsphere size can be observed between the images as the stir speed increases from 350 rpm (Figure 4.7i) to 1500 rpm (Figure 4.7iv). A similar increase in average size can also be observed in the picture series.

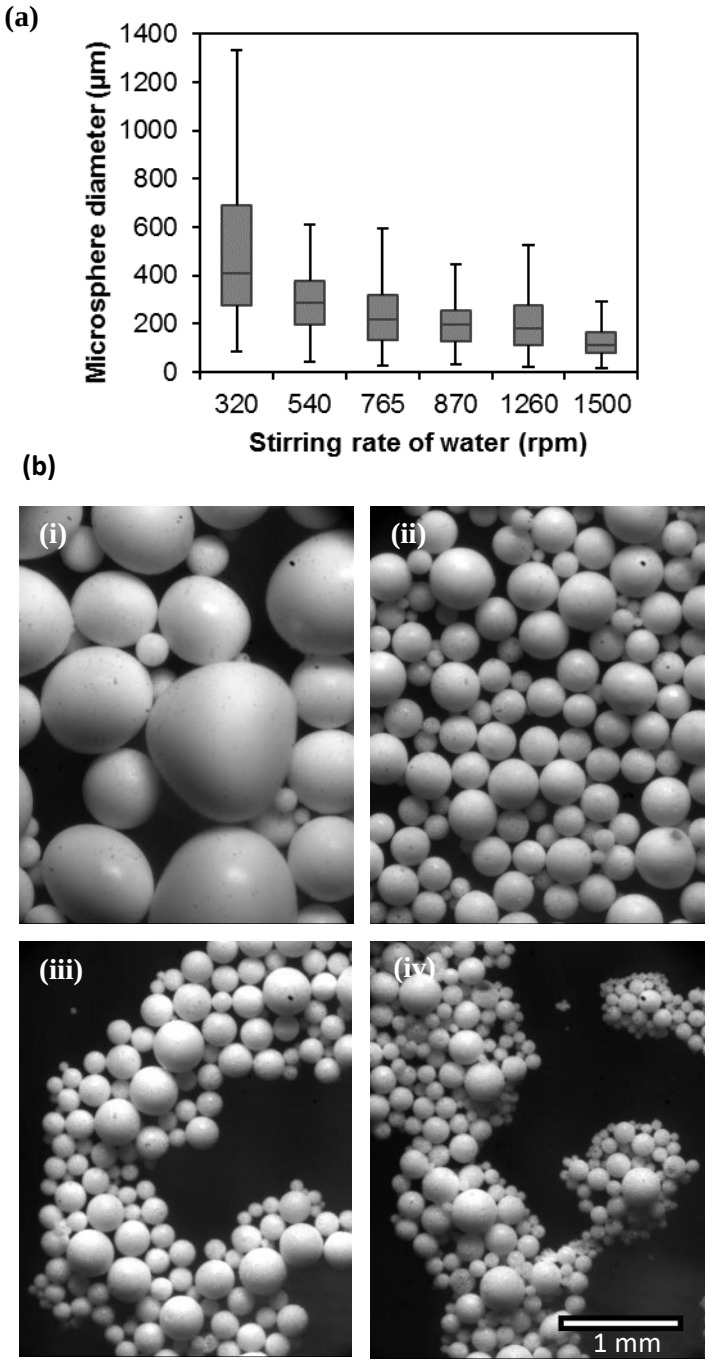

Figure 4.7. The effect of the stir rate applied to the water, to which the HIPE is added to, on microsphere size distributions from the double emulsion technique (w/o/w). (a) Box plot of effect of the stirring rate when mixing the double emulsion on microsphere diameter. With increasing rate, the median diameter of the microspheres is lower as is the distribution of sizes. n > 800 per condition. (b) Optical micrographs of microspheres formed produced at different stirring rates from the double emulsion. The largest microspheres (which form at the slower rate) are less spherical. (b i) 350 rpm, (b ii) 540 rpm, (b iii) 1260 rpm, (b iv) 1500 rpm.

4.3.3 Porous microsphere manufactured via microfluidics and the effect of processing parameters on resulting microsphere size

A T-junction microfluidic device was devised to produce porous microspheres with a narrow size distribution, all of which contained interconnected porosity (Figure 4.8). Uncured HIPE is injected into a channel of continuously flowing water. Under stable conditions, droplets of a certain size bud off from the injection needle. The droplets then pass under the UV output of a mercury lamp which photocures the HIPE. The resulting porous microspheres are then collected. These images also clearly show that the exterior of the microspheres is open pored.

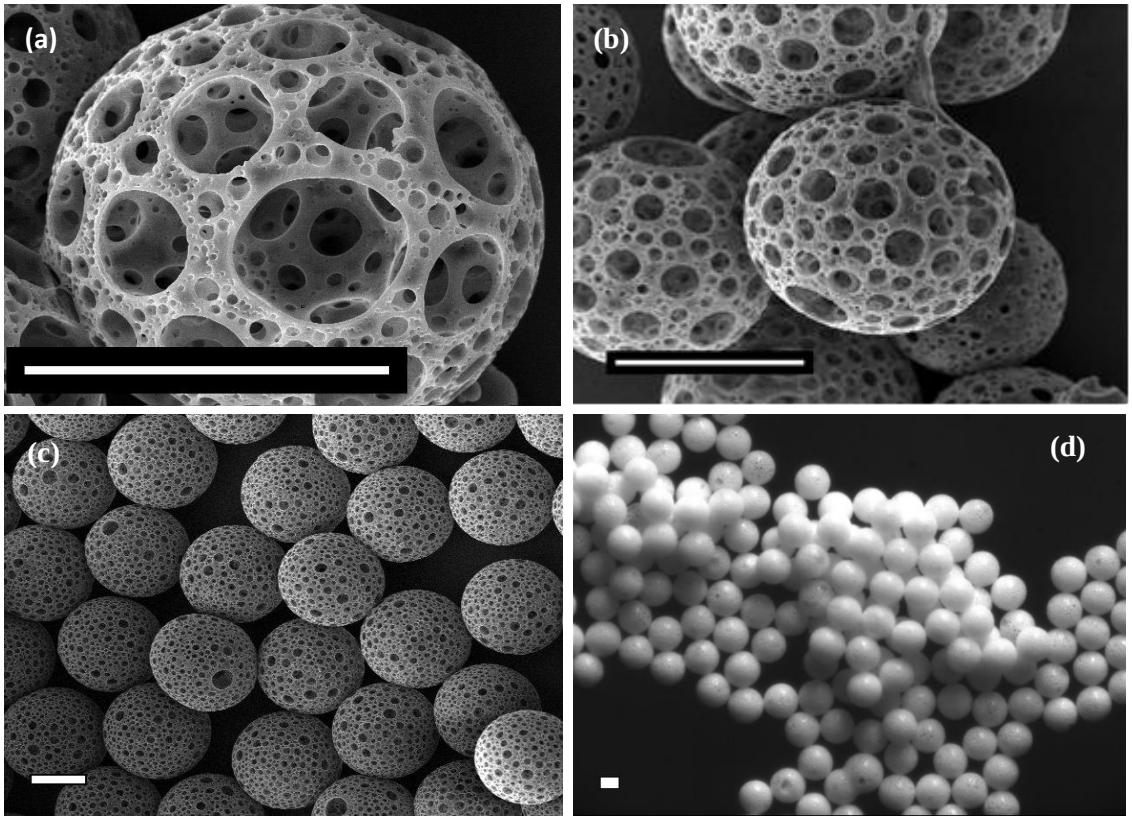

Figure 4.8. Microspheres produced by the microfluidic technique. The resulting microsphere population is highly monodisperse. (a-c) SEM micrographs of microspheres produced by microfluidic technique, microspheres can still be produced in different sizes (compare (b) to (c)) but are monodisperse populations. (d) Optical images of a monodisperse microsphere population produced from the T-junction microfluidic. Here, microspheres vary from 185 µm to 215 µm and average ≈200 µm in diameter. All scale bars are 100 µm.

Increasing the monomer flow into a constant stream of water led to an increase in the microsphere diameter (Figure 4.9). Here the flow of HIPE from the needle into a steady stream of water was altered and the effect on microsphere populations was observed. The uniformity of the microsphere size can be seen in the optical microscope image in Figure 4.8. Increasing the monomer flow increased the volume of microspheres produced by the system. A narrower distribution in microsphere size was observed at the lower monomer flow rate compared to 5 ml/hr (Figure 4.9b).

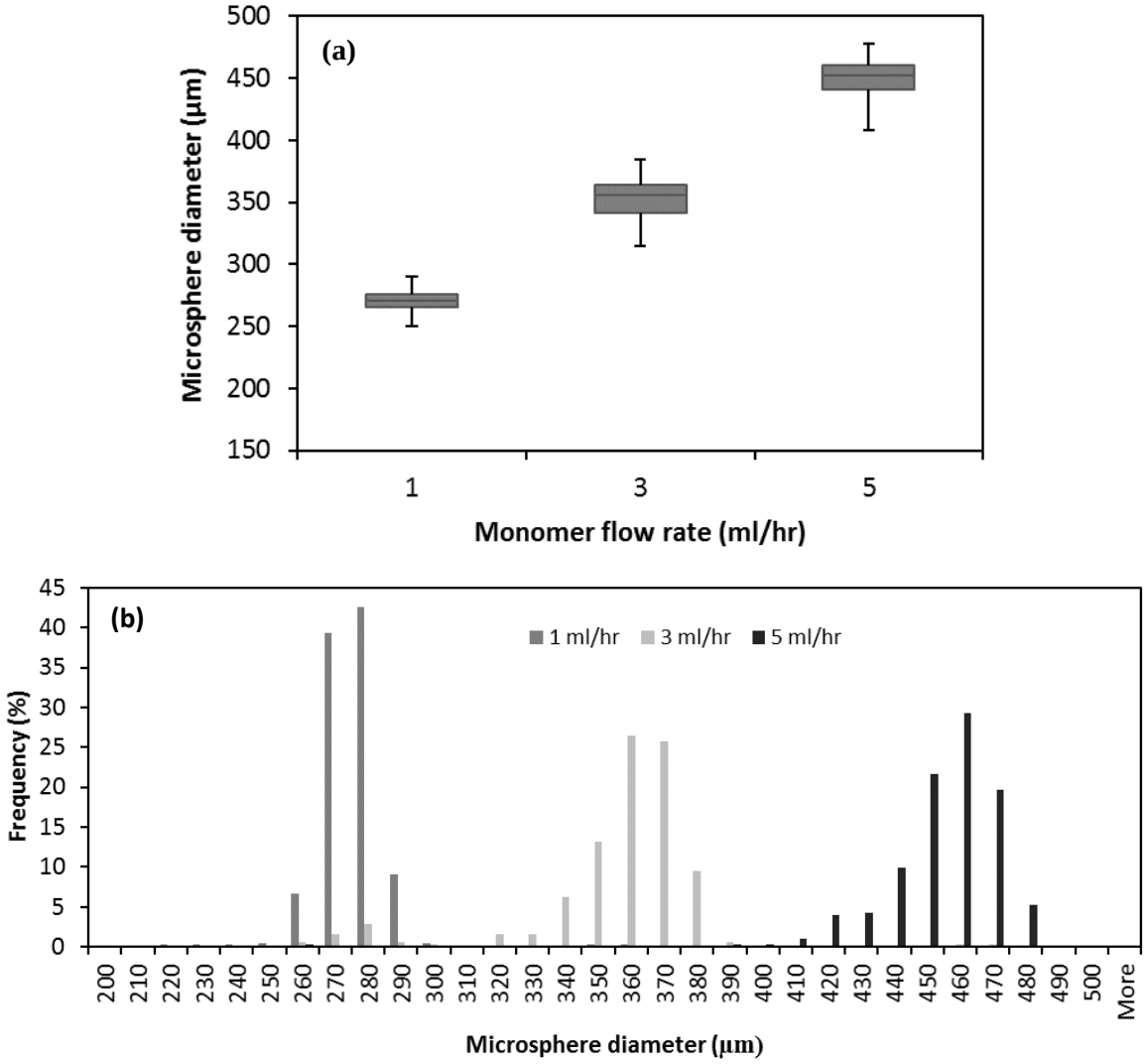

Figure 4.9. (a) The effect of both water flow rate and monomer flow rate on the resulting size distributions of microsphere size formed from a microfluidic T-junction device. Higher monomer dispersion rates produce a greater volume of microspheres per unit of time. n > 192 per condition. (b) Same data as (a) displayed as a histogram. Microsphere sizes are produced in distinct distributions of size.

Increased flow rate of water, to which the HIPE was injected into, decreased the average microsphere diameter dramatically at lower speeds but had diminishing returns as flow rate was increased further. The effect of water flow rate on the microsphere size and size distribution is shown in Figure 4.10. Except for the slowest water pump rate (125 ml/hr) the range of the microsphere size distribution appeared constant irrespective of pump rate. At higher speeds, less variation is observed between the size populations, although there is still a slight difference. 745 ml/min was the fastest flow speed the pump could achieve with the setup.

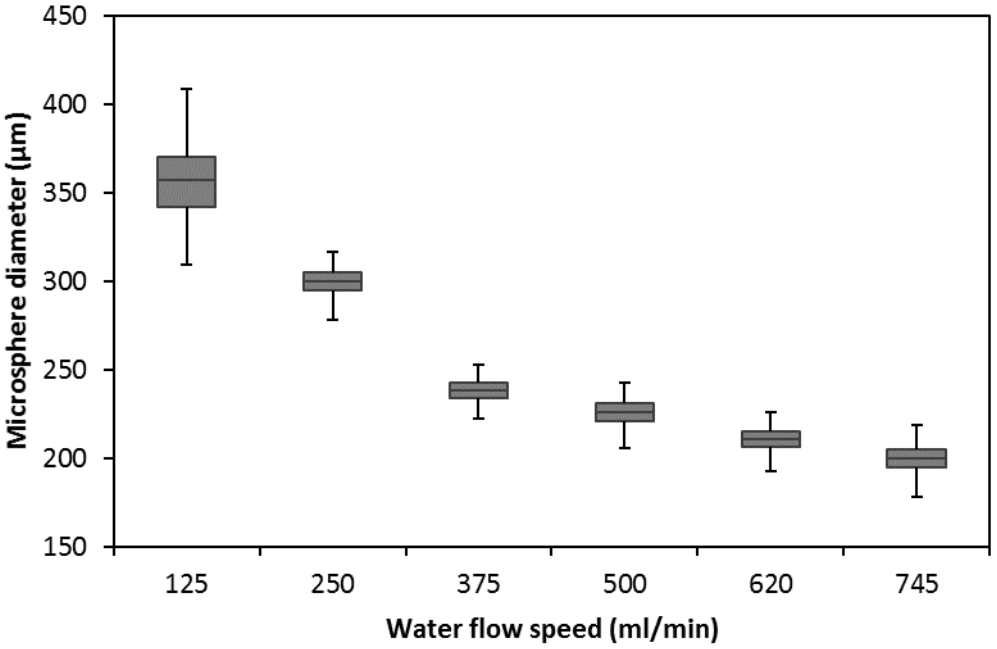

Figure 4.10. The resulting microsphere size distributions produced when altering the rate of water flow through the microfluidics T-junction while keeping monomer flow rate steady. Increasing the water speed reduced the median diameter. Similar microsphere distribution sizes are observed in all speeds except for the slowest rate (125 ml/min). n > 63 per condition.

The combination effect of water speed and HIPE monomer flow rate can be combined to produce different microsphere populations. Increasing water rate decreases microsphere size and decreasing monomer flow also decreases microsphere size. At 5 ml/hr HIPE flow rate and a water speed of 100 ml/min a comparatively large microsphere size distribution is observed. Between 3 and 5ml/hr HIPE rate at 200 ml/min water speed the two microsphere populations are approximately similar in size distribution and median microsphere size.

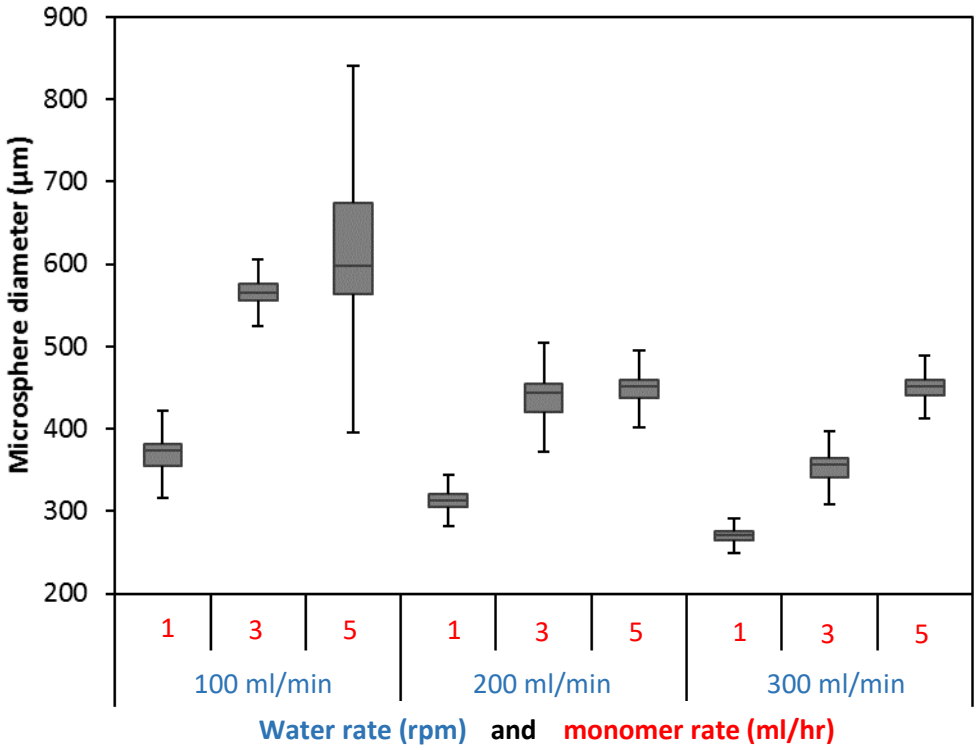

Figure 4.11. The effect of both water flow rate and monomer flow rate on the resulting size distributions of microsphere size from a microfluidic T-junction device. Decreasing monomer rate and increasing water flow both allow the formation of smaller microspheres with the inverse having an opposite effect. n > 118 per condition

Utilising smaller internal diameter dispensing tips decreased the median microsphere size in comparison to larger dispensing tips. The size distribution between 250 and 510 µm is similar whereas the size distribution at the smallest tip diameter is larger. Microspheres over 1 mm in size were formed from the 510 µm dispensing tip and microspheres down to 400 µm formed from 150 µm dispensing tips.

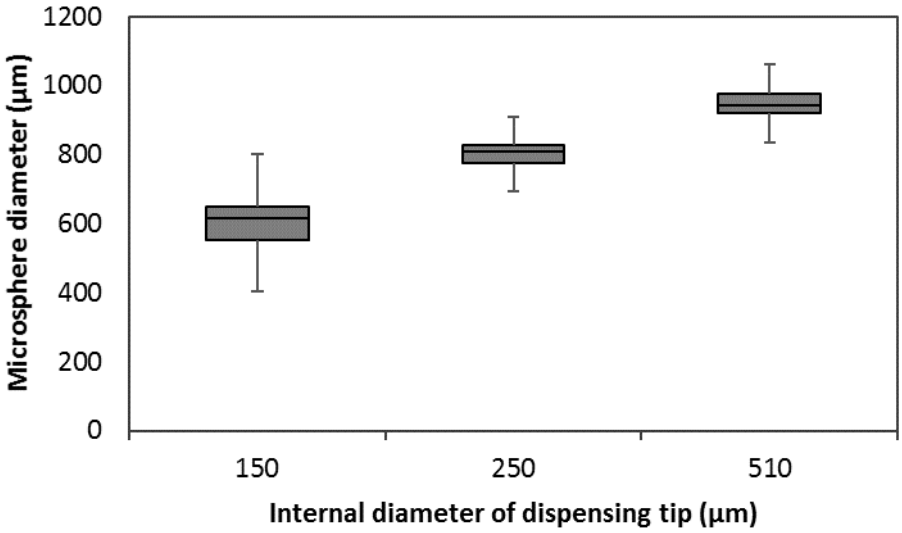

Figure 4.12. Relationship between altering the internal diameter of the dispensing tip and the resulting change in microsphere size distribution of microspheres formed in a microfluidic T-junction device. Utilising smaller internal diameter dispensing tips decreased the median microsphere size in comparison to larger dispensing tips. It was possible to form very large microspheres with the larger dispensing tips. n > 15 per condition

4.3.4 Direct comparison of both manufacturing techniques on microsphere pore size, diameter distribution and structure

Despite the differences between the two porous microsphere production methods, it has been demonstrated that they both produce microspheres containing internal pores of similar size, and distribution (Figure 4.13a). SEM images of a thin section of a microsphere prepared using a microtome (Figure 4.3b-c), show that the porosity is consistent throughout the whole structure. A small difference

in pore size can be observed; the microspheres prepared by double emulsion contain a larger number of 4 and 6 µm pores.

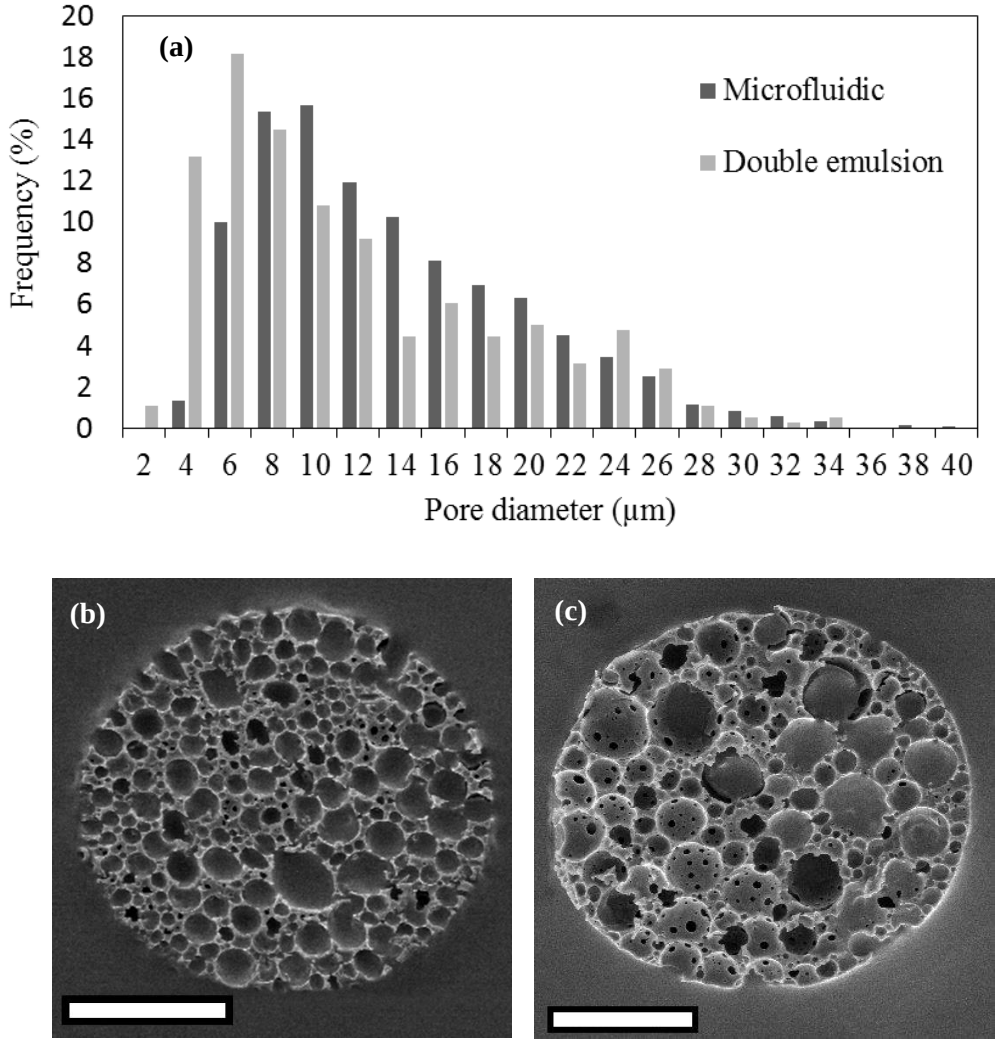

Figure 4.13. Comparison of the effect from production techniques on the internal porosity of polyHIPE microspheres from the same HIPE monomer batch. (a) Spread of pore diameter of microspheres formed from microfluidics and double emulsion compared on a histogram. n > 1474 per condition. (b) SEM micrograph of a sectioned microsphere formed via the microfluidic T-junction device. (c) SEM micrograph of a sectioned microsphere formed via the double emulsion method. Scale bar is 100 µm for both micrographs.

Microspheres produced by the CSTR technique produce a disperse range of sizes whereas the microfluidic technique produces microspheres with a size narrow size distribution (Figure 4.14). SEM microscopy was carried out to analyse the overall microsphere shape and microsphere pore size (Figure 4.14). The bar plot in Figure 4.14(a) summarises the size distribution. All microspheres exhibited open surface porosity along with smaller inter-pore windows connecting larger pores.

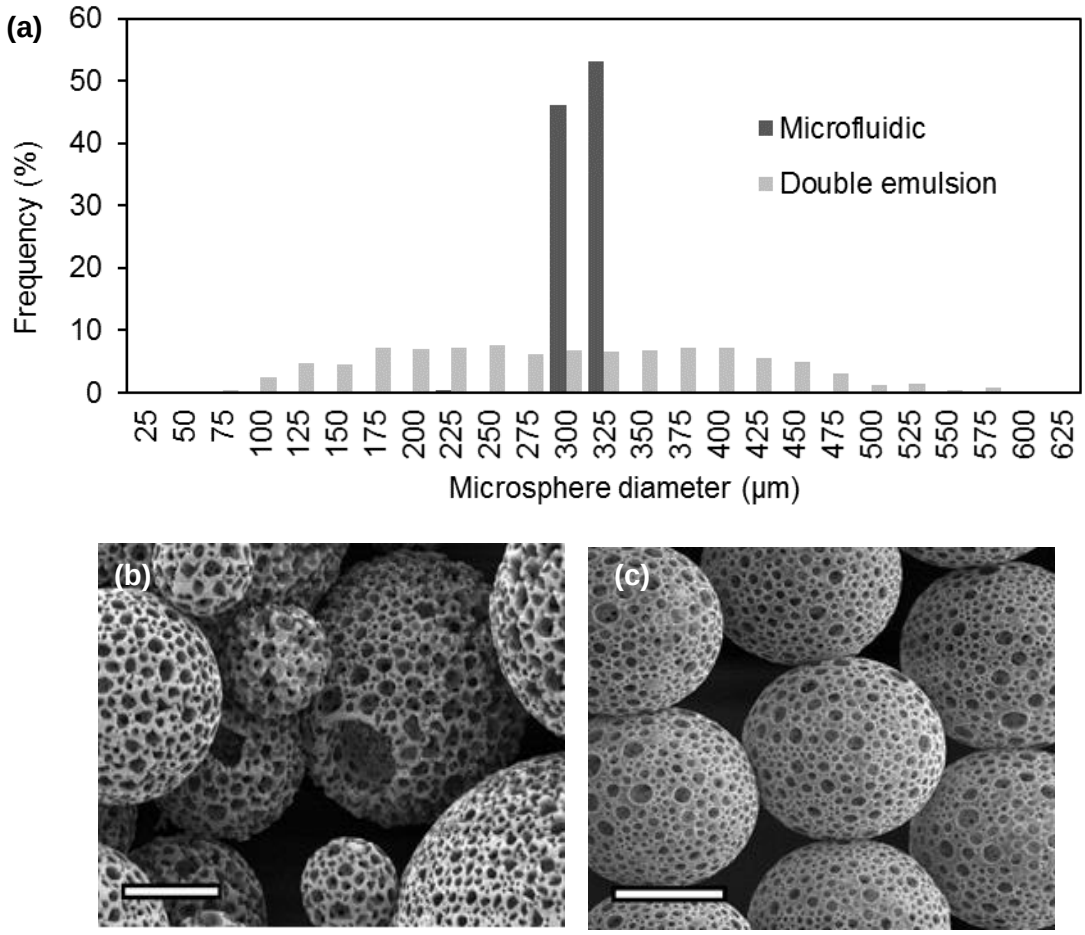

Figure 4.14. Comparison of the distribution of microspheres sizes formed from both techniques with a similar mean microsphere size. (a) Graph showing the microspheres from the microfluidic technique (narrow size distribution) with microsphere sizes from the double emulsion (broad size distribution). n > 676 per condition (b) SEM micrograph of polydisperse polyHIPE microspheres formed via double emulsion. (c) SEM micrograph of microspheres formed via a microfluidic T-junction. Scale bars are 100 µm.

4.4 Discussion

This chapter investigated the parameters and methods that can be used and altered to control microsphere median size and size distribution. The use of porous microspheres in tissue engineering requires control over the microsphere size and the pore size arising from the method of manufacture. This tight control is necessary to produce microsphere-based scaffolds with reproducible properties which can be used as injectable scaffolds. Producing microspheres with specific morphological properties allows rational design of scaffolds by altering the total available surface area and changing the void sizes between microspheres to control substance diffusion. Porosity is required in tissue engineering constructs to allow the ingrowth of cells and the diffusion of nutrients into the scaffold [93]. The surface porosity of a polyHIPE can also influence the cell attachment and cell differentiation of cells, such as hES-MP cells [310].

The polyHIPE material contains biologically relevantly micro and nano scale porosity. Nano-scale features, including porosity, have been found to increase cell attachment and influence cell behaviour [279, 280]. The larger pores found in the polyHIPE material allow cells to grow in a 3D environment. A 3D environment alters the behaviour of cells when compared to 2D culture of the same material [300]. This is due to the biological similarity of 3D environments in-vitro to the actual biological niche of the cell in the body and its 3D environment. If a surface feature is too large it will be interpreted by cells as a 2D environments [300]. The pores in the polyHIPE are between 2 to 70 μm in size, of which are the correct scale to act as true 3D environments.

The interconnectivity shown in Figure 4.1 would facilitate the exchange of nutrients and waste removal for cell culture [262]. Interconnectivity smaller than the size of a cell can still allow passage of the cell due to a rearrangement of its cytoskeleton. This process is highly dependent on cell type and on cell mobility for example keratinocytes have been reported to squeeze through gaps only 500 nm in diameter [311] while osteoblasts are reported to require larger pores (~40 μm) for ingrowth [312].

Both temperature and stir rate were found to affect the diameter of pores formed during the initial emulsion step (w/o). The effect of stir rate on microsphere size becomes negligible at faster speeds and greater at the lower speeds. It is expected that larger changes in speed would be required to observe further changes. The effect of water temperature on the pore size distribution was also investigated. Lower temperatures formed smaller pores whereas higher temperatures formed larger ones (Figure 4.2). Less variation was found between 15 and 30°C than 4 and 15°C in a similar pattern to that observed in the stir rate experiment.

Larger voids and interconnecting windows in the PolyHIPE can be created through a controlled destabilisation of the emulsion by increasing the temperature of the droplet phase to 80°C [313]. The emulsion stability is dependent on a range of factors including the temperature during both the HIPE

formulation and polymerisation stage [247]. This elevated temperature will increase the kinetic energy of the molecules in both phases. This has a double effect on the emulsion destabilisation to produce larger pores within the PolyHIPE. The water molecules will increase their kinetic energy and will be more likely to break through the barrier layer. Also, the viscosity of the continuous film will be decreased, making it more fluid like and prone to destabilisation.

Both temperature and stir rate influenced the resulting microsphere size with CSTR microsphere manufacturing. Increasing the stir rate reduced both the median pore size and the size distribution of the PolyHIPE microspheres (Figure 4.7). At the high stirring rates of 765, 870 and 1260 rpm, there was a small decrease in the median microsphere size range. This is attributed to a small increase in stirring speed in relation to the total stirring speed, so the observed difference is minimal. Increasing the temperature of the water to which the HIPE was added, had a significant effect on the distribution of microsphere sizes formed Microspheres formed at 320 rpm at the lowest temperature of 4°C had a narrow IQR whereas the highest temperature of 60°C has a much greater IQR (an increase of 305%). There appears to be a linear increase in the median size over the observed range of temperatures. Microspheres formed at the highest temperature of 60°C were aspherical in shape, this was also observed for microspheres produced at the slowest stirring rate (Figure 4.7). This can be clearly observed in Figure 4.7 where the microspheres are aspherical in shape. Aspherical shapes formed because of the short time frame between the end of mixing where the HIPE is broken up into droplets and the rapid photocuring of the monomer. The water was still moving around in the beaker when the microspheres were cured causing the resulting distended shape to be formed.

Microspheres at larger sizes (greater than 800 µm) began to deform in shape regardless of temperature or stir rate. This maximum spherical microsphere size has been reported to be dependent on the viscosity of the HIPE material [302]. To aid in the formation of microspheres from higher viscosity emulsions many labs have reported that water may be replaced with a solution of polyvinyl alcohol [273].

Pore size remained independent on microsphere size and it can be observed (in Figure 4.4a & b) that both the smaller microsphere and larger microsphere appear to contain surface porosity of similar size. The pore diameter did not alter significantly within the microspheres, regardless of the stirring rate of the water or the water temperature as also been reported by Boo et al [307]. This allows pore size to be controlled independently of conditions used to affect microsphere size. It is of note that internal pore size distribution can be controlled independently to the conditions used to control the microsphere size. There was no significant difference between the internal porosity when the emulsion was subjected to different water stirring rates, or water temperature, during the w/o/w fabrication process. These observations concur with the results reported by Boo et al [307]. This allows pore size to be controlled independently of conditions used to tune microsphere size.

While it is more difficult to produce a defined microsphere size distribution via the double emulsion method, it is possible to approximately control the median microsphere size. The process is however very sensitive to changes in the environment, such as temperature, as well as the nature of the CSTR. The microsphere sizes produced at a particular stir rate appear to form a skewed distribution, as also noted by Zhang et al [130]. Other groups similarly reported that the average microsphere diameter decreased with increasing stirring rate [263, 264].

When utilising the microfluidic manufacturing method, it was possible to produce microspheres with a narrow size distribution and to control the median microsphere size. All three parameters, monomer flow rate, water flow rate and dispensing needle internal diameter all played inter-dependent roles in controlling the microsphere size distributions and median size. Both the HIPE monomer flow rate and water speed can independently control the PolyHIPE microsphere size. It can be decreased by either increasing the water flow rate, or by decreasing the monomer injection rate. From Figure 4.11 it is possible to use the combination of parameters to create a microsphere population with a median anywhere between 500 and 280 μm.

The T-junction fabrication technique produced excellent microsphere size distribution for the EHA/IBOA polymer blend, however it may not be the best methods for less stable polyHIPE solutions. Sung-Wook Choi et *al.* showed that their HIPE began to separate out into multiple phases soon after formation [314] and this phase separation was exploited to produce microspheres with variable pore size. Over time the emulsion gradually destabilises as the suspended water droplets merge together to form larger ones in a process known as Ostwald ripening [315]. This is less applicable in the CSTR as it is a batch process where only small volumes of HIPE are used at any one time, therefore fresh HIPE can be made up at regular intervals.

Changing the water flow rate was the simplest method of altering microsphere size while the most difficult was changing the pipette diameter. Changing the monomer flow rate was effective but it took the system a longer period of time to regain stability due to the viscoelastic nature of the monomer causing a gradual change in the flow rate. Changing the water flow rate had an instantaneous effect on the microsphere size. The most difficult parameter to change during an experiment was the dispensing tip as this required the experiment to be halted and exposed to light, risking accidental photocuring. While changing both water flow rate and dispensing tip diameter the volume of microspheres produced is constant. When changing the monomer flow rate the total yield is effected, producing smaller microspheres often required low monomer flow rates, greatly reducing the yield over a certain period of time. However, these are only of concern when establishing the microsphere size.

At high monomer injection rate and a slow water speed, a large microsphere size distribution is observed. At faster monomer injection flow rate at and faster water speed, the microsphere populations are approximately similar in their size distribution. The larger distribution is caused by the flow being too slow for the volume of monomer that was being expelled from the dispensing needle. Especially at the slower speed the peristaltic pump had a very noticeable (slow) peristaltic flow pattern which allowed monomer to bud off from the dispensing tip at greatly different quantities depending on the local flow conditions and the volume of monomer waiting to be removed from the dispensing tip.

The narrow distribution of microspheres sizes formed from T-junction microfluidics allows greater control over the scaffold as a whole. This is important for delivery as the microsphere size will dictate the bore size of the injection needle, and a narrowly controlled microsphere size distribution will ensure no blockages will occur from unexpectedly large microspheres during injection or bioprinting. Additionally, controlling the microsphere size allows the control of the spacing between microspheres when packed together. Controlling this packing arrangement would allow control over nutrient diffusion and could induce or inhibit angiogenesis (through lack of large enough spaces for blood vessel formation). Monodisperse spherical microspheres present a maximum packing density of 74% (with hexagonal or cubic close packing) while a polydisperse microsphere distribution allows for a higher packing density [309].

For both techniques, the internal pore size distribution can be independently controlled to the conditions used to control the microsphere size. There were small differences between the internal porosities when the emulsion was subjected to different water stirring rates, or water temperature, during the fabrication process. These observations concur with the results reported by Boo et al [307]. The slight difference observed in Figure 4.13 is not of great importance for cells as the pore sizes which are different (4 and 6 μm) are unlikely to be colonised by cells. The larger pores which are more relevant to cell behaviour are mostly equal in frequency. This statement should not be confused with interconnecting porosity in which pores of 4 and 6 μm could be essential for cell passage between larger pores.

There is a clear difference in surface pore architecture of the microspheres produced by the two methods. In the CSTR method the emulsion droplets are continuously surrounded by water while in the T-junction microfluidic set-up the emulsion is dispensed through a small diameter (0.15-0.5 mm) metal syringe which will influence the surface porosity of the HIPE. Both the small diameter of the syringe and the contact of the HIPE with the metal can have an effect on the final surface porosity of the produced polyHIPE microspheres. Indeed, the surface porosity of polyHIPEs is highly affected when curing them on different surface energy materials [150].

Both broad and narrow distribution sizes could desirable depending on the requirements of the application. Microspheres produced in a broad distribution of sizes would allow for a higher random packing density which could reduce the size of the voids between microspheres, this would reduce the space available for vascularisation to occur [316]. For microsphere populations featuring a monodisperse size distribution, the lower packing density would allow the engineering of pore diameters between the microspheres to best manage the void size between adjacent microspheres. It is possible to precisely control the size of the microspheres prepared using the microfluidic device by small alterations to the processing conditions. When increasing the HIPE dispensing rate, the microsphere size distribution does increases slightly. This is therefore not the parameter recommended for controlling microsphere size as water pump rate and needle tip size provide better control with less size variation. It is worth pointing out however that the HIPE dispensing rate is linearly correlated with the rate of microsphere production. Increasing the dispensing rate to increase yield of spherical microspheres appeared to work only to an upper limit before the size distribution increased too much to be considered monodispersed. However Gokmen *et al.* found that when the monomer dispensing rate is very high, long streams of monomer are ejected from the needle leading to rod-like elongated shapes [264].

4.5 Conclusion

Porous microspheres were produced using the EHA/IBOA polymer blend system. Microspheres were produced in sizes from 40 µm to 600 µm. CSTR and T-junction microfluidics allow to produce both narrow and broad size distribution of microspheres, respectively. Changing the temperature of the water after the formulation of the polyHIPE does not greatly affect the pore size but has a dramatic effect on the microsphere size in CSTR. This allows porosity to be engineered independently of microsphere size, and allows for tailoring of the porosity parameters. Altering the stir rate of the w/o emulsion changed the pore size within the polyHIPE and altering the stir rate of the continuous water phase in the double emulsion (w/o/w) altered the microsphere diameter. The use of microspheres in tissue engineering requires control over the microsphere size and the porosity dimensions. This tight control is necessary to produce microsphere-based scaffolds with reproducible properties which can be used as injectable scaffolds. Producing microspheres with specific morphological properties, surface area, interconnectivity and packing arrangement will allow for customisation over the range of porosity parameters towards a tailored porous support structure for cells.

Chapter 5: Cell culture on EHA/IBOA polyHIPE microspheres

5.1 Chapter aims:

1. Measure cell growth and behaviour when cultured on microspheres.
2. Test for differentiation of osteoblasts when hES-MP cells are cultured on the microspheres.
3. Analyse the cell mediated aggregation of microspheres into a proto-tissue over time.
4. Measure the cell ingrowth into the microspheres and determine the differentiated cell type found within the pores.

5.2 Introduction

5.2.1 Chapter introduction

Chapter 5 investigated the manufacture of porous, non-degradable polyHIPE microspheres. A variety of median diameters and population size distributions were produced in a controllable manner. The polyHIPE microspheres contained small interconnecting windows between the larger pores, allowing for completely interconnected porosity within the structure. Within this chapter the potential of these microspheres was investigated for bone tissue engineering.

5.2.2 Human embryonic stem cell-derived mesenchymal progenitor cells

Human embryonic stem cell-derived mesenchymal progenitors (hES-MP) cells are derived from human embryonic stem (hES) cells. These cells were originally derived by multiple passages of hES cells on gelatine whilst retaining the adherent cells. They are very similar to mesenchymal stem cells in terms of the expression of markers and the cell morphology [207]. hES-MP cells are able to give rise to populations of osteogenic [317], chondrogenic [318] and adipogenic [207] cells. In the original paper no markers of undifferentiated hES cells were identified in the hES-MP cell population [207]. These hES-MP cells have been chosen for this work for a number or reasons. They are of human origin, they are a non-cancerous cell line and they express the same markers as MSC cells and exhibit very similar behaviour.

5.2.3 Mesenchymal stem cells and their osteogenic differentiation

Differentiation along an osteogenic cell lineage can be characterised by the expression of markers, composition of the ECM and cell morphology [319]. In vivo mesenchymal cells differentiate to pre-osteoblast cells, to mature osteoblasts and then to either osteocytes or to lining cells [320]. A more detailed review of the cell types can be found in chapter 2. These cells form part of the cycle of bone remodelling by producing bone. Osteoblasts lay down collagen and mineral deposits and osteocytes

act as monitoring cells and help regulate the remodelling process in response to mechanical stimulation or damage [197].

5.2.4 Media supplements used in the culture of bone cells

For this chapter, it is crucial to understand the different media used for the cell cultures. The different media will be referred to by their assigned names throughout the chapter without reference to their key components. These media formulations are commonly used in the literature, but are sometimes referred to by different labels. All the media are formed from a base of AMEM with human fibroblast growth factor (hFGF), Penicillin-Streptomycin and L-glutamine. Details of concentrations used can be found in the experimental protocols chapter (2.6.3)

Growth media: Basic media described above with the addition of hFGF. hFGF increases the rate of cell proliferation (mitogenic growth factor) and is used to help prevent the hES-MP cells from differentiating [207].

Supplemented media: Basic media with the addition of βGP and A2P. βGP is used as a phosphate donor to enable mineralisation and may have a direct effect on cell differentiation by influencing intracellular signalling [321, 322]. A2P increases the volume and maturation of collagen deposited and increases alkaline phosphatase (ALP) activity [323, 324].

Osteogenic media: Basic media with the addition of βGP, A2P and DEX. DEX is used in this media to stimulate cells along the osteogenic lineage [324, 325]. Osteogenic media is supplemented media with the addition of dexamethasone. Dexamethasone is a corticosteroid and is used in MSC systems to stimulate the differentiation of osteoblast cells.

5.3 Results

5.3.1 Culture and proliferation of hES-MP cells on EHA/IBOA copolymer

Cell viability was compared on a flat polyHIPE surface both with and without a coating of acrylic acid along with a gelatine coating (figure 5.1). A resazurin assay was used to compare cell viability of hES-MP cells on flat sheets of material (porous and non-porous). Samples coated with gelatine performed similarly to uncoated samples and all samples coated with poly acrylic acid (pAA) were found to have a greater cell metabolism reading (figure 5.1a). When comparing coated and uncoated polyHIPE topology a significantly difference was observed. Significant increases were observed at each time point when comparing polyHIPE coated with pAA (figure 5.1b). There was no significant increase in cell metabolism for uncoated samples of polyHIPE, even between day 1 and day 7. Cells can be observed growing on flat and porous surfaces using fluorescent microscopy on samples stained with FITC and DAPI (figure 5.1c & d). hES-MP cells on the porous material can be observed growing in the pores whereas on the flat sample the cells are elongated on the surface.

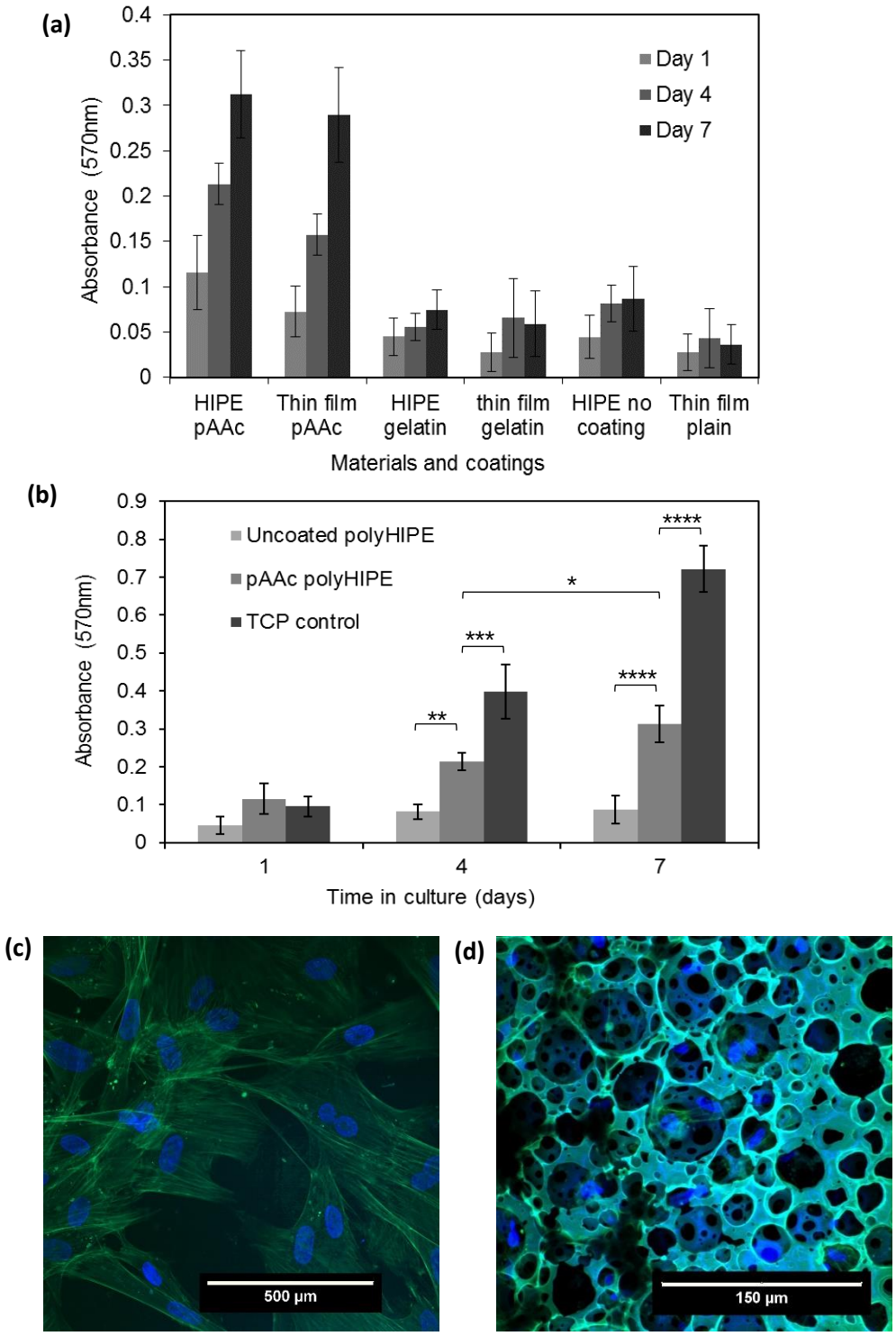

Figure 5.1. hES-MP growth study using thin films with different topologies, of which half were coated with pAA, and in which proliferation was measured indirectly via resazurin assay. (a) Graph showing all conditions tested at day 7. (b) Same data as (a) graph displaying the results of the polyHIPE samples along with the TCP control with growth over 7 days. Significant differences between samples were apparent from day 4 and were repeated with the results from day 7. A significant difference was found between coated and non-coated samples (ANOVA multiple comparison). (c) Confocal image of hES-MP cells growing on a poly acrylic acid coated (pAAc) non-porous surface at 7 days in culture. (d) Confocal z-stack of hES-MP cells growing on a pAAc porous (polyHIPE) surface at 7 days in culture. FITC-Phalloidin (green – actin) and DAPI (blue – Nuclei) were used as fluorescent stains for these samples. ANOVA < 0.0001. n = 4, N = 4 Data is mean ± SD.

After determining growth on 2D substrates hES-MP cells were then cultured on microspheres coated with acrylic acid to determine scaffold viability (figure 5.2a). hES-MP cell growth was measured on microspheres over 30 days using resazurin salt to measure cell activity at each time point. Cell activity increased to day 11 after which the cell activity remained relatively constant. No continuous statistical difference was observed between the two mediums used to culture cells over the 30 days. hES-MP cells began forming bridges between microspheres which, over time, bound the microspheres to one another (figure 5.2b & c). Figure 5.2c shows a fluorescent image of a 40 µm thick sectioned sample showing the cells attached to a microsphere after 30 days in culture. There is both a layer of several cell-layers deep surrounding the microspheres and cells within the internal porosity of the microsphere.

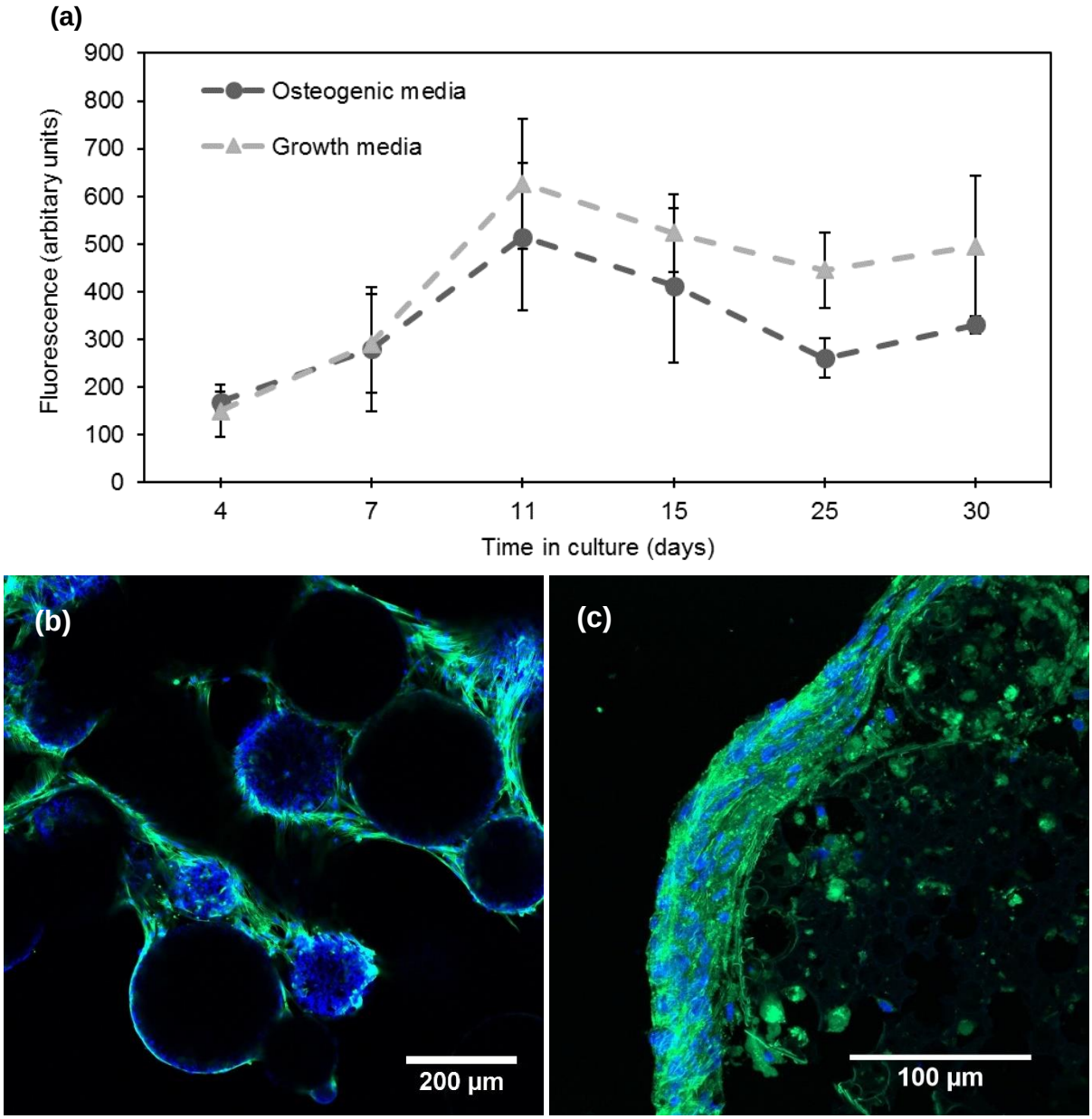

Figure 5.2. (a) hES-MP cell metabolic activity for 30 days of cell culture on polyHIPE microspheres, measured using resazurin salt assay. Cell activity increases until day 11 after which the metabolic activity plateaus. Error bars ± standard deviation (b) Confocal image (z-stack) of microspheres and hES-MP cells at day 11 stained with DAPI (blue) and FITC-phalloidin (green). Microspheres can be seen auto-fluorescing blue. By day 11 the microspheres were observed to have formed into a several large agglomerations within the flask, of a cell-microsphere structure. (c) Microspheres at the day 30 timepoint and stained as in (b) with microspheres fluorescing green. By day 30 a much larger cell layer is visible under microscopy and the microsphere agglomerations are larger than at day 11. n = 3, N =2 Graph data is mean ± SD.

Confocal z-stack images show two microspheres, one of which has cells bound to the surface and the other does not (Figure 5.3). The auto-fluorescence of the microsphere can be observed and compared to a microsphere on which hES-MP cells are attached. The microspheres were imaged alongside each other and it is not obvious as to why one has many cells and the other has no cells bound to it.

Interestingly, the presence of green fluorescence on the left most microsphere is absent from the microsphere without cells. Villanueva et al. found that cellular debris did non-specifically bind with Phalloidin which may explain this [326]. The stereoscopic 3D image in Figure 5.3b provides a simple way for a reader to view one of the cell covered microspheres in 3 dimensions. To enable viewing stereoscopic glasses are not required.

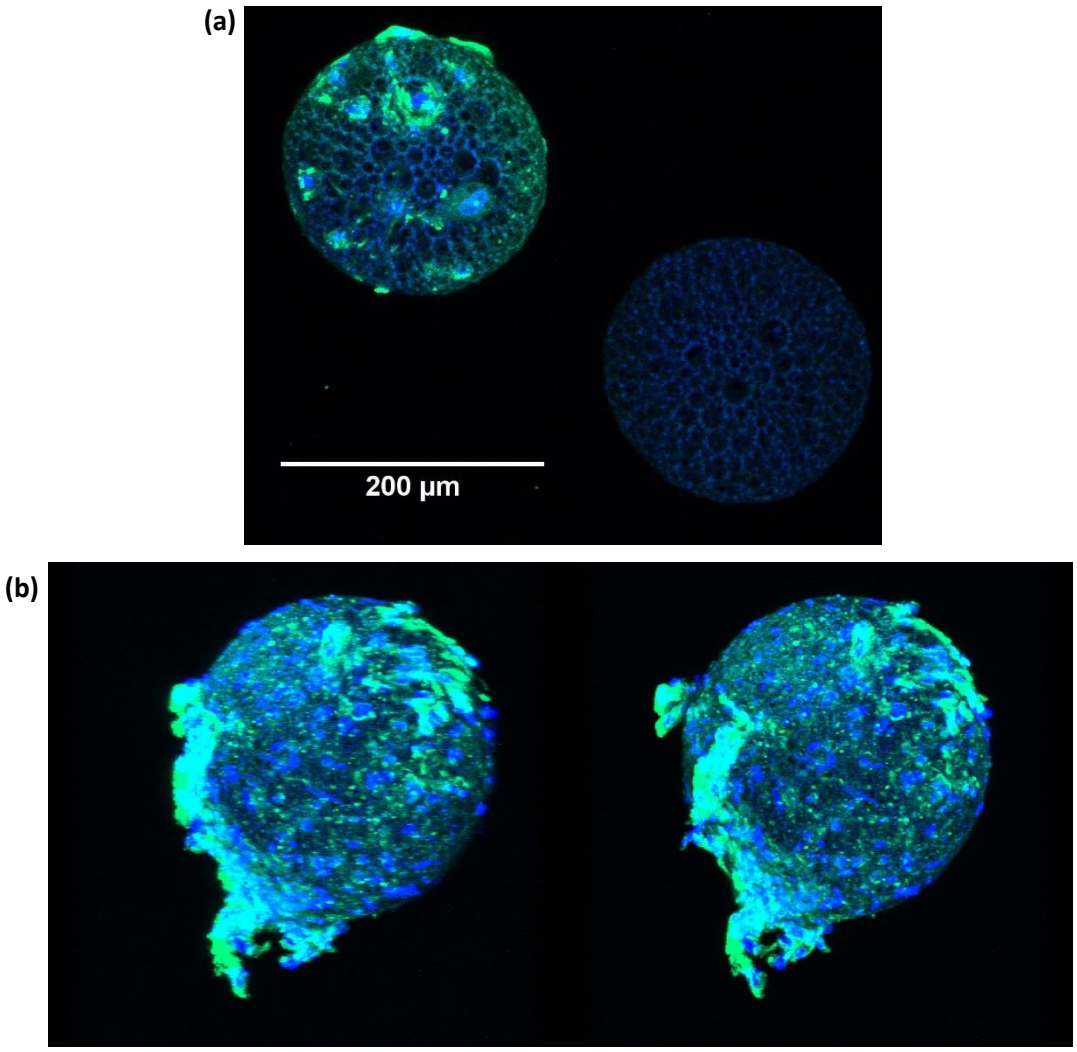

Figure 5.3. Confocal z-stack image of cells attaching to the outer surfaces of the microspheres after 3 days in culture. Microspheres & hES-MP cells were stained with DAPI (blue) FITC-phalloidin (green). (a) Two microspheres, one without cells and one with hES-MP cells attached to its surface. It is possible to see some cells residing inside the surface porosity. (b) Stereo-graphic image of microspheres similar to (a). It is possible to resolve (b) into a 3D image by crossing one's eyes slightly until both individual images overlay each other. If visualised correctly the images convey spatial 3D data not easily shown using 2D images. More detailed instructions can be found online at http://www.instructables.com/id/How-to-view-stereo-graphic-images/?ALLSTEPS.

5.3.2 Agglomeration of EHA/IBOA microspheres and hES-MP cells which form over time

Further work was undertaken to examine the agglomeration formation more closely to understand what might happen *in-vivo*. Confocal z-stacks were taken of microspheres forming cell initiated aggregations at different time points during the culture (figure 5.4). It is possible to see both the

increasing size of aggregations and the increasing numbers of cells on and around the structures. Initial formation of many smaller units, formed from a few microspheres, are observed. These smaller units gradually combined to form larger agglomerations. After 30 days in culture only one or two entities would be visible within the culture flasks. These agglomerations were robust and could be easily handled with tweezers without breaking apart. Cells were observed within the pores of the microspheres, especially at day 60. This lead to the following experiments investigating ingrowth of cells into the microspheres.

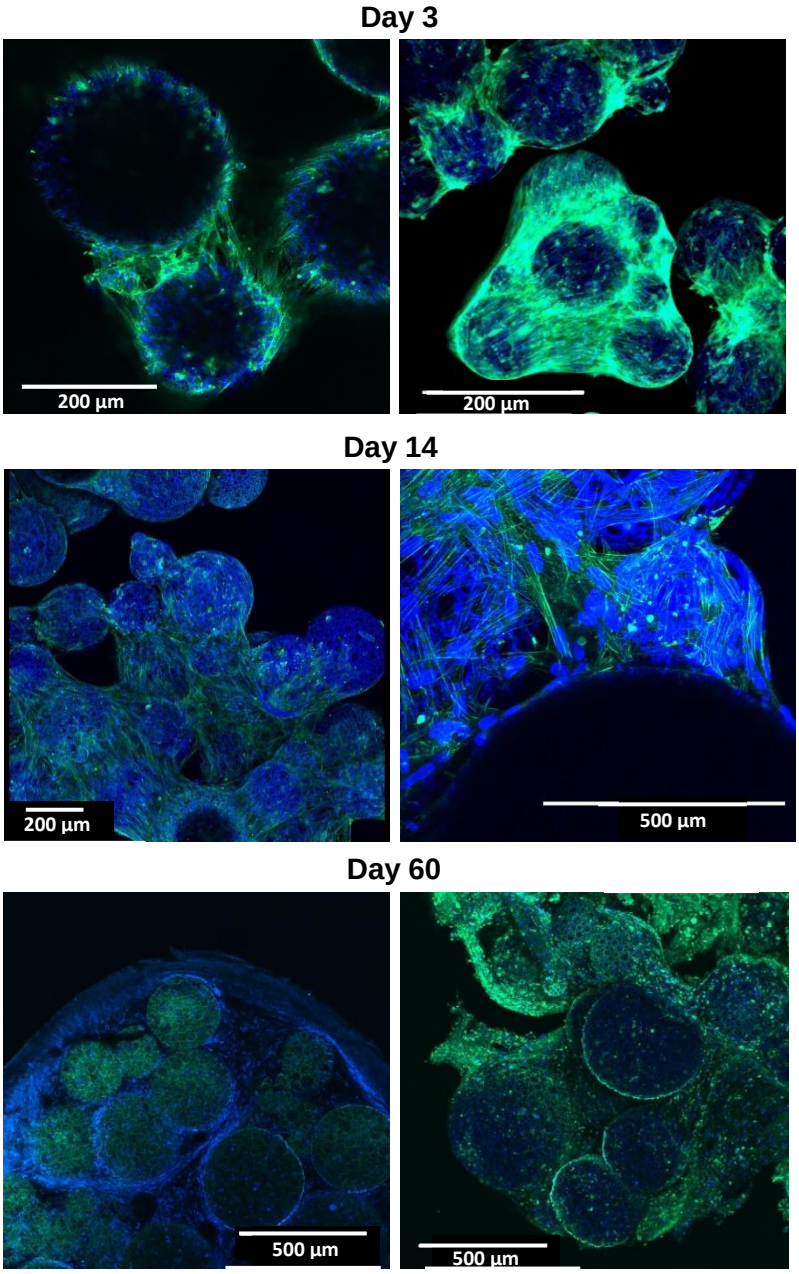

Figure 5.4. Microspheres in culture with hES-MP cells over a 60-day time period. Initially many aggregations of a few microspheres are found at day 3 and by day 60 all the cells have formed into a single larger structure. Increased cell number on the agglomerations can be observed by day 60. Images are confocal z-stack images of DAPI (blue) and FITC-Phalloidin (green). Images from the day 60 time point are from 50 µm thick sectioned samples. Cells appear to be present within the porosity of the microspheres at day 60.

SEM imagining of a sectioned microsphere agglomeration was examined to understand the structure of the surrounding ECM (figure 5.5). ECM build-up between cells and microspheres after 60 days in culture can be observed in the SEM images. The red line in Figure 5.5a shows the boundary of ECM around the microspheres. The ECM extending between two microspheres together can be observed in figure 5.5b and in false colour in figure 5c. The ECM spans the distance between the two

microspheres with a fibrous appearance. It was also possible to see biological material within the internal porosity which we further analysed using staining to ascertain its identity.

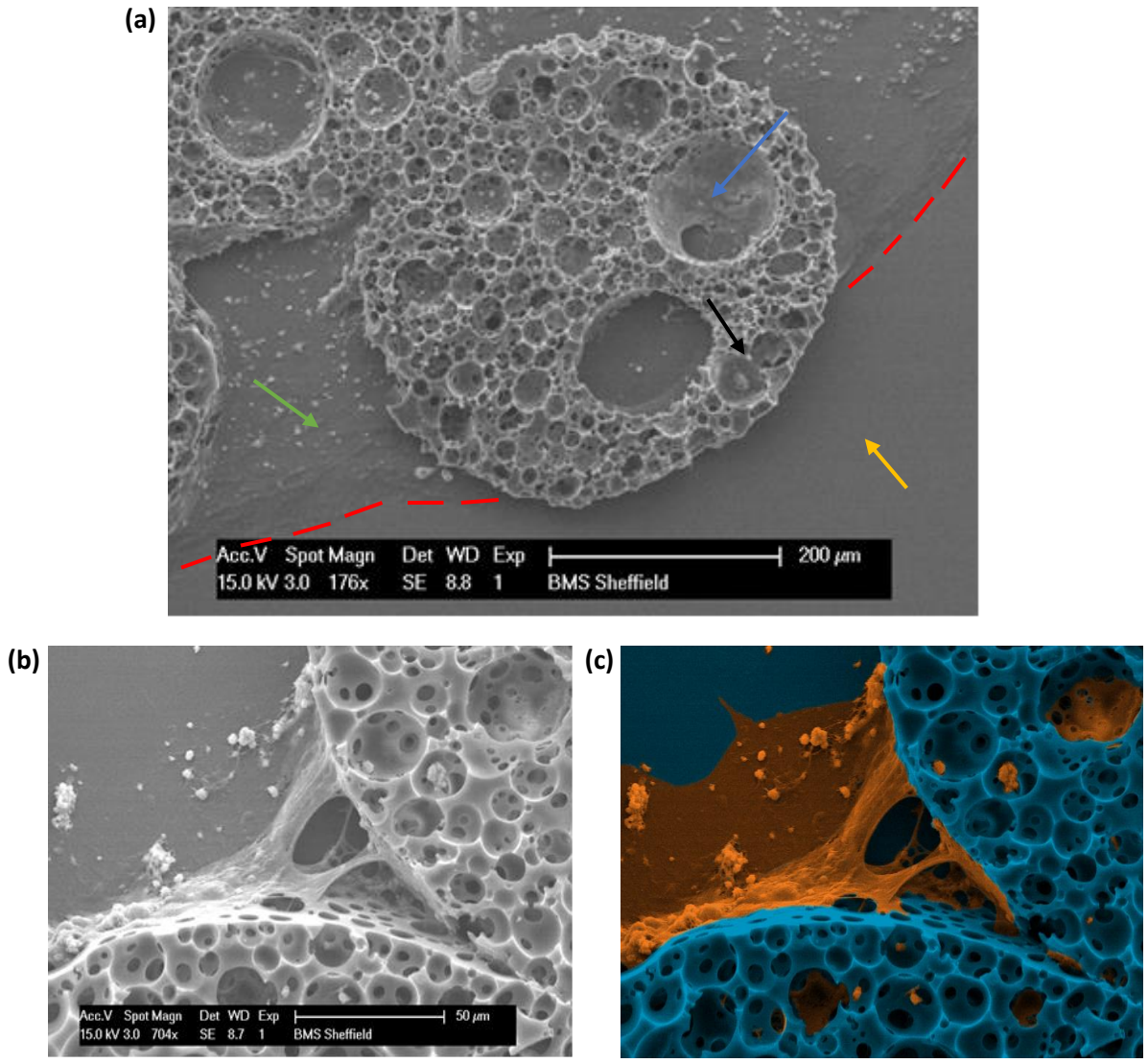

Figure 5.5. SEM images of 50 µm thick sections of polyHIPE microspheres fixed after 60 days in culture with osteogenic media. (a) SEM image of a microsphere on the periphery of the agglomeration. The red line indicates where the boundary of the cells/ECM extended to. The black arrow is indicating the area imaged for figure 9. The yellow arrow is indicating an area between microspheres containing cells and ECM material. The purple arrow is indicating the area outside the agglomeration. The blue arrow is indicating a large pore over 60 µm in diameter covered in cells. (b) SEM image of the ECM binding two microspheres together along with the cells and ECM extending out beyond the microspheres. (c) False colour SEM image of (b).

H&E stained sections of hES-MP cell culture on microspheres, at different time points, can be seen in figure 5.6. The histological stain H&E was chosen to identify cell nuclei to determine if the biological material within the pores contained cells. Few cells are observed in the day 3 image and many microspheres are still independent. By day 15 cells surround each microsphere many are bound together into small clusters (figure 5.6b). By day 30 all the microspheres have combined into one single structure and cells appear to have fully inhabited the internal pores of every microsphere (figure 5.6c).

A thick of ECM can be seen building up around the exterior of the agglomeration which increases in volume and depth by day 60 (figure 5.6d). At day 60 the cells within the internal porosity take on a more osteocyte like morphology and significant numbers of dendrite-like protrusions are observed between cells.

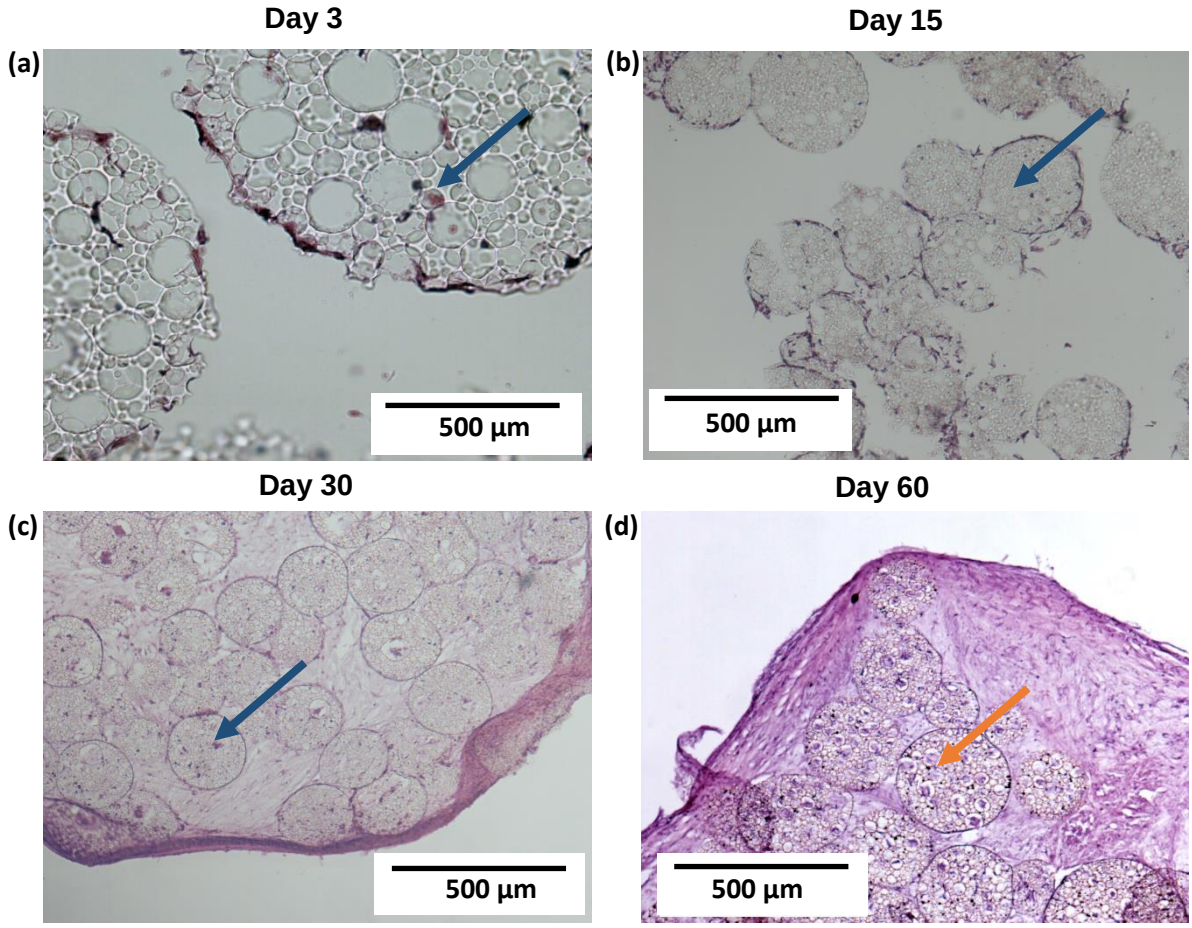

Figure 5.6. H&E stains of 15 µm thick sections of microspheres, at different time points, from microspheres cultured in osteogenic media. Cells are visible inside the microspheres, especially at the later time points (blue arrows). At day 60 the interior of the microspheres appears saturated with cells (orange arrow). H&E also highlights the continual build-up of ECM around the microspheres. In the day 60 section a large area to the right of the microspheres appears to be exclusively ECM.

One experiment to examine cell survival within the agglomeration is shown in figure 5.7. A live dead stain has been imaged with multiple slices using a confocal microscope and assembled into a 3D image. The agglomeration is one from 60 days of culture with osteogenic media. The microsphere agglomeration has been cut along the right side of the image (green arrows) exposing the internal structure. At the external surface of the microsphere there is a higher proportion of living cells than dead (red) cells. Within the microsphere, a higher proportion of dead cells are present but there is still a high presence of live cells. Microspheres can be seen auto-fluorescing green in the image with one is illustrated by the yellow dash-line circle.

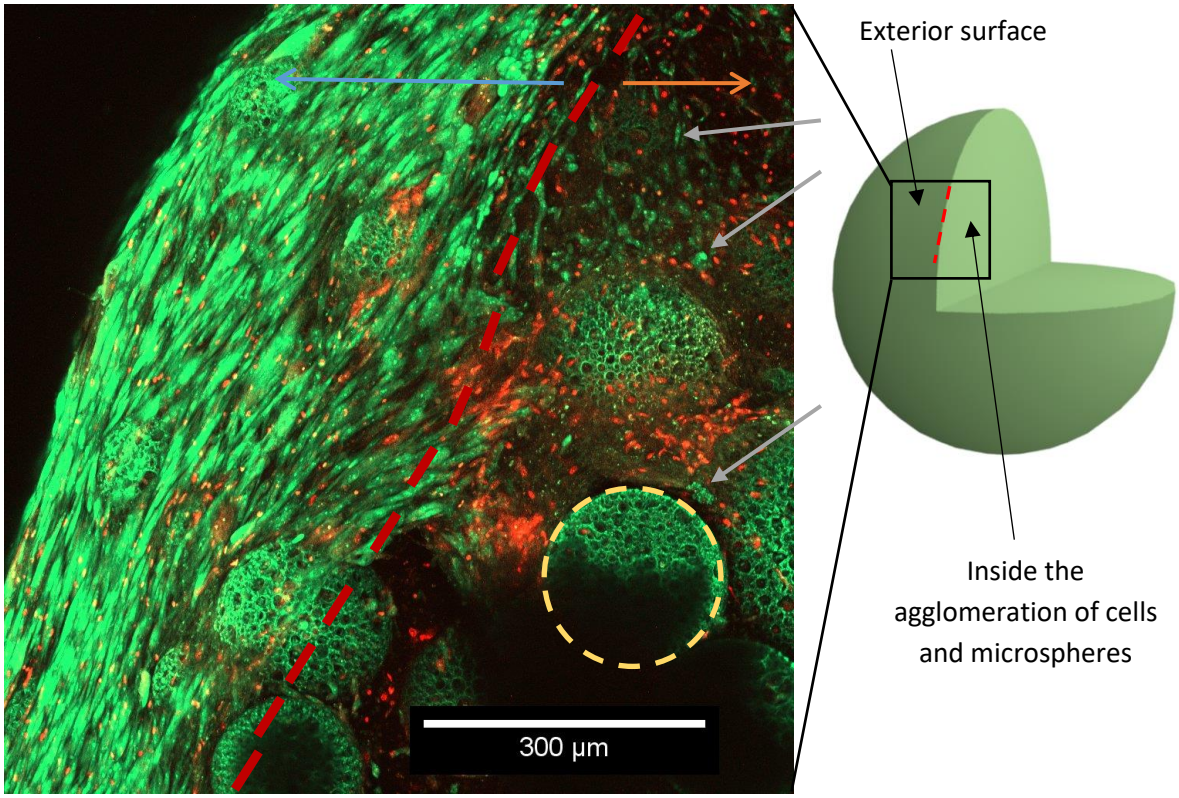

Figure 5.7. Live dead confocal z-stack of a microsphere agglomeration at 60 days. The structure was cut in half using a scalpel and the edge of the cut section was imaged to capture both interior and exterior structure. The white circular dotted line shows the outline of one of the 'embedded' microspheres. On the left of the red dotted line (blue arrow) is the external surface of the agglomeration and to the right of the line (orange arrow) is the inside of the microsphere agglomeration. Green cells represent living cells whereas red indicates dead cells. On the surface of the agglomeration there is a much higher number of living cells than in the interior. However, living cells are observable within the structure along with the dead cells (green arrows indicate some of the living cells visible).

5.3.3 Cell growth and migration into EHA/IBOA microspheres from long term culture

The SEM images (Figure 5.8) offer an additional technique for observing the cells within the porosity of the microspheres. Cells and ECM can be seen within the macro-porosity and forming connections between pores through the interconnecting porosity. Figure 5.9b shows a false colour image highlighting the cells/ECM which can be seen in the original greyscale (Figure 5.9a). The size of the interconnecting pores between the macro-porosity in which the cell/ECM has extended through is measured in Figure 5.9c. None of the connecting pores are larger than 12 µm wide. It should be noted that the process required to prepare samples for SEM requires dehydration of the cells using ethanol and HMDS evaporation and may have some effect on the cell structure. However, Braet et al. found no difference in structure between samples prepared with the more commonly used Critical Point Drying and drying by the evaporation of HMDS [327].

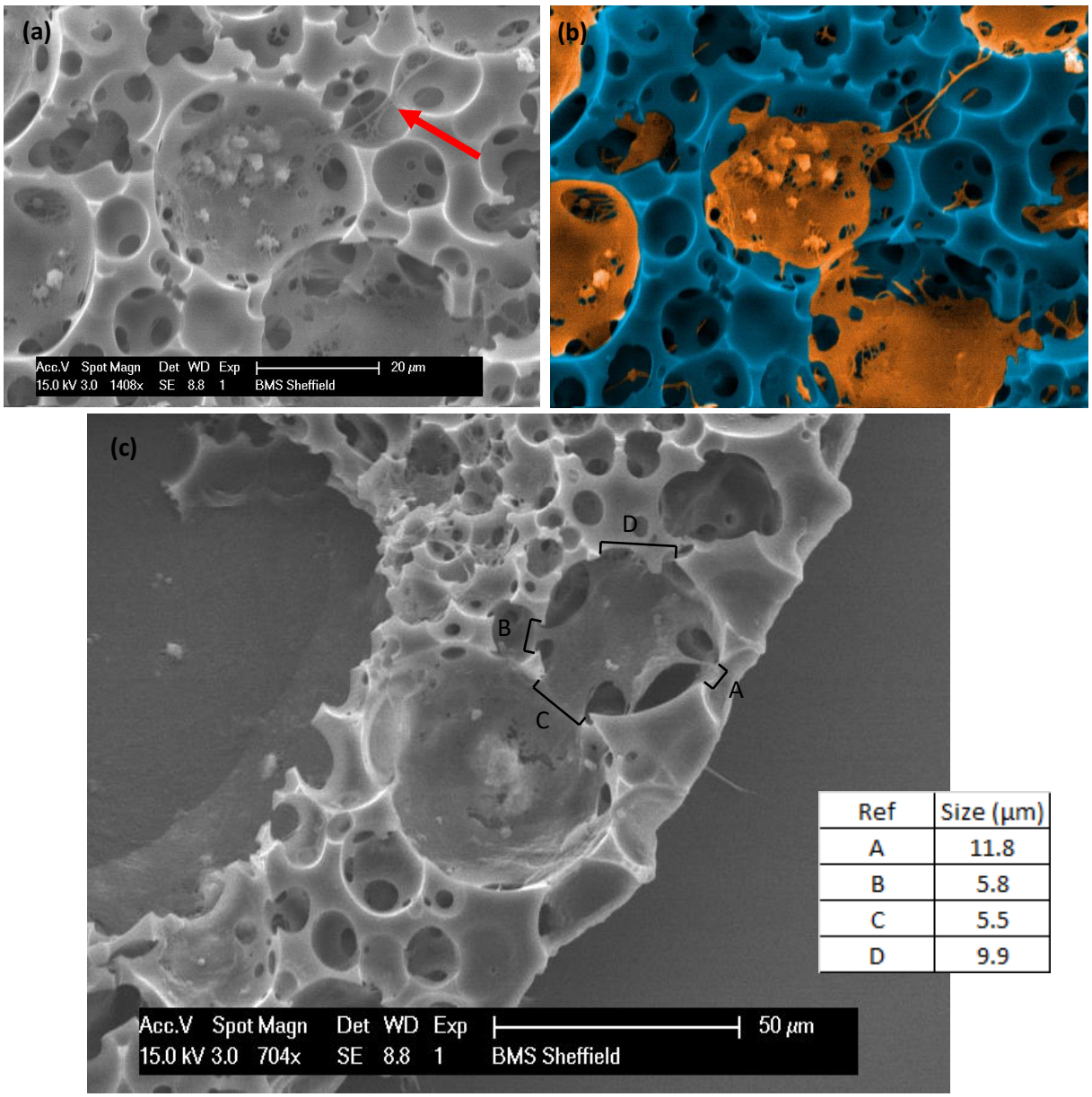

Figure 5.8. SEM images taken of 50 µm thick sections of microspheres cultured with hES-MP cells at the day 60 time-point. (a) SEM micrograph showing cells inside the pores, with fibres or cell extrusions projecting from one pore to another (red arrow). (b) False coloured SEM image of (a) using photoshop. The cells are coloured in orange while the scaffold material is coloured blue to enhance contrast. The outlines of the cell were determined by visual inspection. (c) SEM image of pores on the external edge of a microsphere. Measurements are included to show the dimensions of all (visible) openings to the central pore.

Cells were found to grow/infiltrate into the porosity of the microspheres over time, with those cultured in osteogenic media growing in faster and deeper than those cultured in growth media. Cells were found to begin infiltrating the microspheres by the 4th day, when cultured in osteogenic media. There was comparatively less penetration depth observed into microspheres cultured in growth media over the entire experiment. In growth media, some of the largest pores showed signs of cell infiltration, but there was no penetration into the smaller pores as observed with the osteogenic media. Analysis of the microspheres showed that the medium microsphere diameter was 200 -205 µm. This standard size

allowed us to image all the microspheres at their maximum circumference to ensure we could build up a coherent picture at this microsphere size.

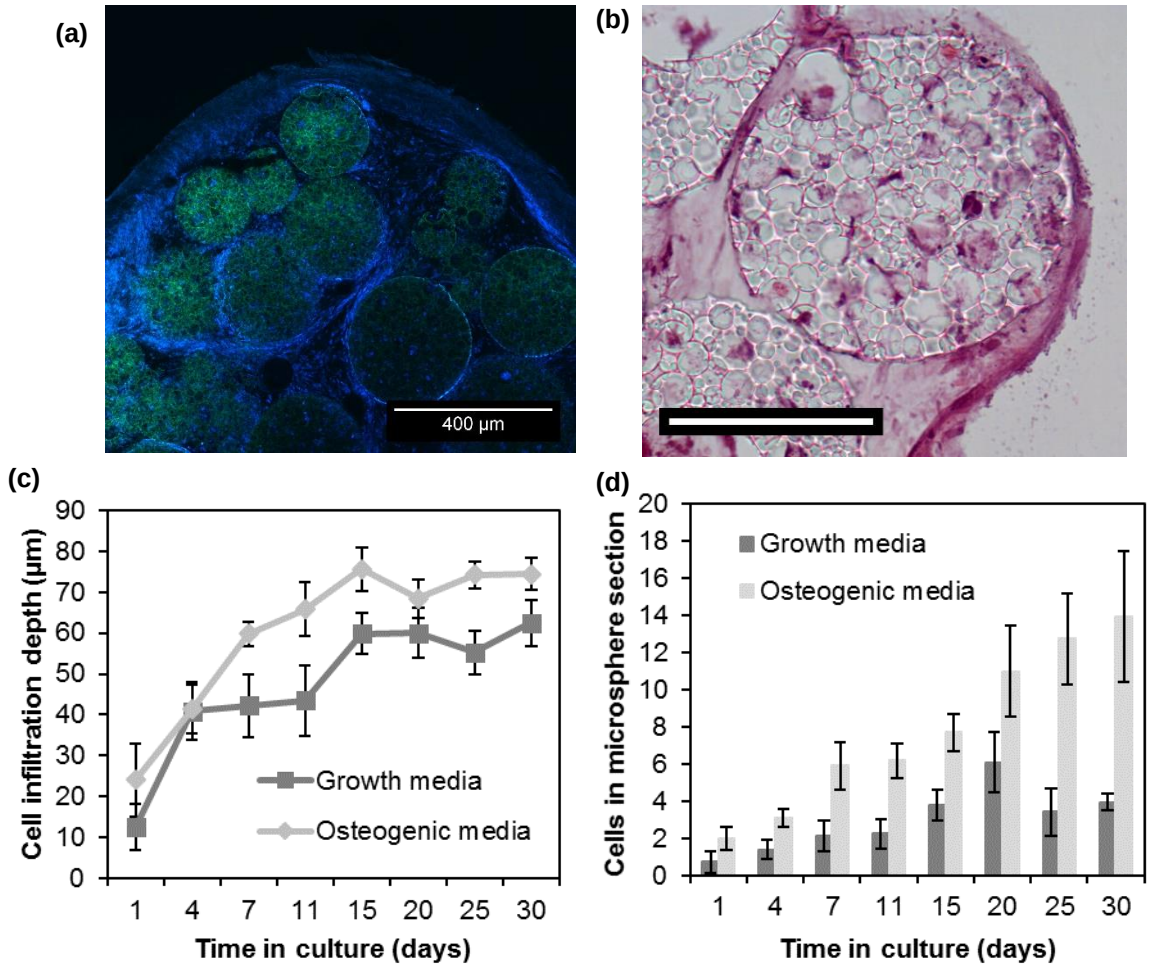

Figure 5.9. (a) Confocal image of a scaffold after 30 days, sectioned at 40 µm thickness. Scaffold stained with FITC-Phalloidin and DAPI with the microsphere fluorescing green. (b) A H&E stained 10 µm section of the in-vitro study at day 30 showing a representative image (of those cultured in osteogenic media) of cell ingrowth into the microsphere. Scale bar is 100 µm (c) The maximum penetration of cells into the particles of the entire data set. As particles are at most 200 µm wide the greatest penetration is at 100 µm. The deepest 20 cells were selected from each data set and 95% confidence limits were used. (d) Average number of cells within each particle over time using 95% confidence limits. n > 6. N = 2 Graph data is mean ± SD.

5.3.4 The effects of media additives on ingrowth of hES-MP cells into microspheres within an agglomeration

Osteogenic media caused the largest increase in ALP production with supplemented media stimulating greater ALP than growth media (Figure 5.10). The amount of ALP produced by hES-MPs after 14 days in culture was standardised against µg/ml of DNA. There is no significant difference found between any of the materials cultured in the same class of media. Significant differences between the different media types were observed for each material, except for TCP. There was no statistical relationship

between the ALP produced and the quantity of DEX added to the media, when considering similar surfaces (data not shown, 10, 20, 50 and 100 nM used).

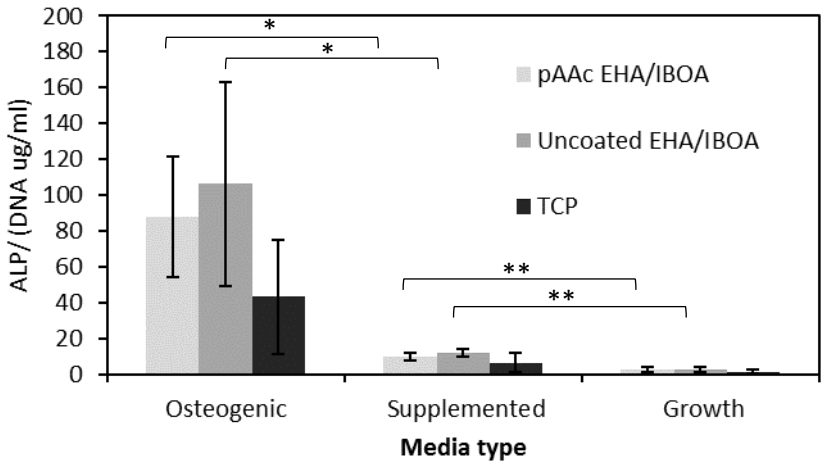

Figure 5.10. ALP/DNA assay on day 14 flat samples and cultured in 3 different media compositions. Differences in ALP production were observed between different media on the same material; except for TCP for which no statistically significant difference was found between any of the media compositions. One-way ANOVA (p<0.0001) and multiple comparison, n = 3. N = 1 Graph data is mean ± SD.

Different levels of cell ingrowth were observed depending on the type of media the microspheres and cells were cultured in, with those in osteogenic and supplemented supporting the fastest ingrowth rates (figure 5.11). The number of cells within the microspheres were counted and their distance from the outer surface of the microsphere was measured. The samples were 40 µm thick and the area measured made up 30% of the total microsphere volume. This was used to extrapolate the total number of cells per microsphere. From Figure 5.12 it can be observed that the cells within the growth media culture did not penetrate in high numbers into the microspheres. The furthest distance the cells were found to penetrate was 40 µm. Culture in growth media containing either βGP or A2P appeared similar to each other but had significantly more cell infiltration into microspheres than culture in just growth media. A huge increase in internal cell numbers was observed when cultured in growth media with both βGP and A2P. On average a 100% increase in internal cell number when compared to media containing either βGP or A2P. Interestingly the addition of DEX into the media to form osteogenic media did not appear to affect this specific phenomenon with no significant differences found between osteogenic and supplemented media. No difference was found between growth media and media containing only ascorbic acid when measuring number of cells within the microsphere but a difference was observed when considering the penetration distance of cells into microspheres.

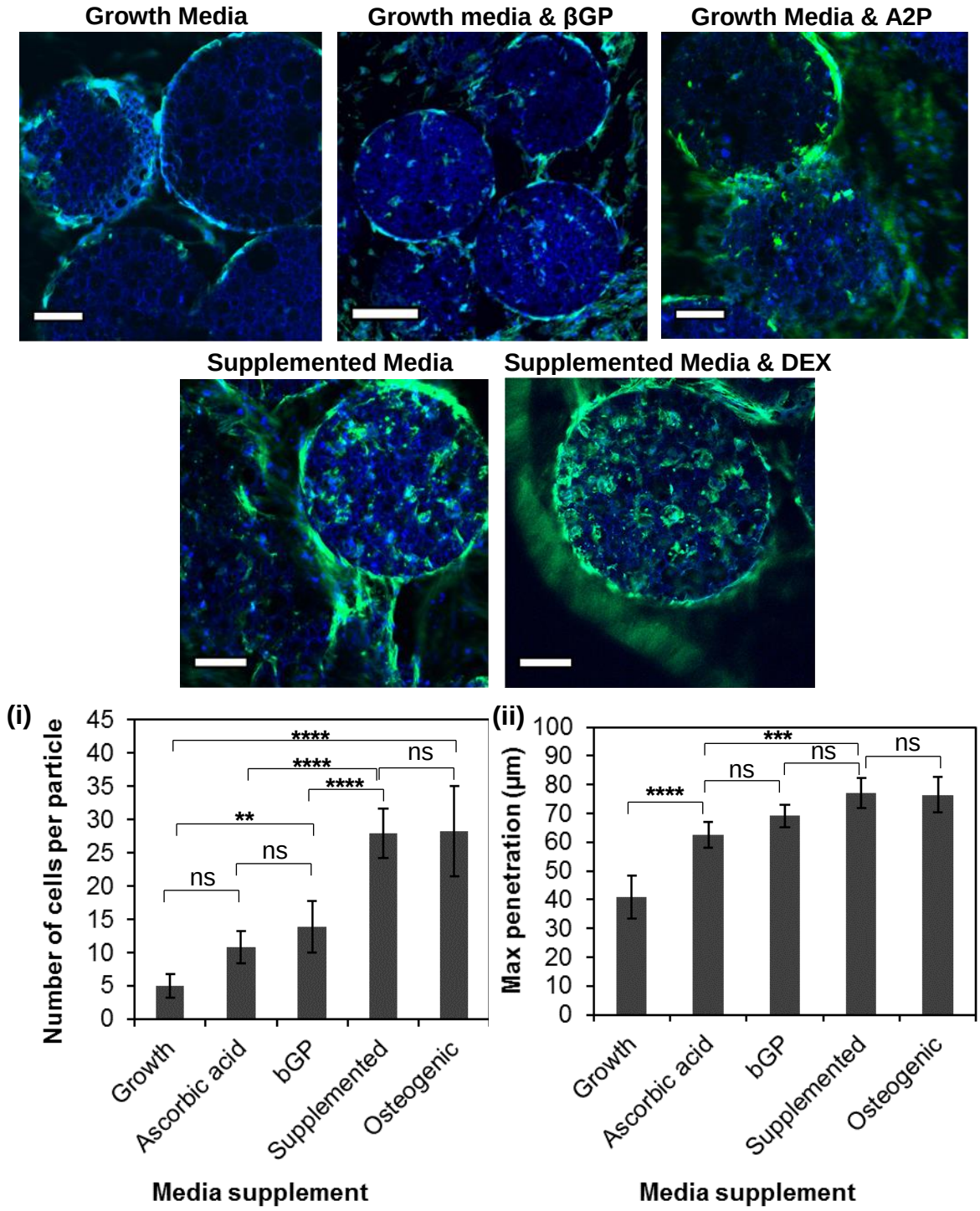

Figure 5.11. Fluorescent images of hES-MP cells penetration into microspheres, after 30 days, when cultured in different medium. Monodisperse polyHIPE microspheres sectioned into 30 µm thick slice and stained with DAPI and FITC-Phalloidin. Microspheres autofluorescence blue in all images. Scale bars are 50 µm. Graph (i) Average number of cells per 40 µm slice with 95% confidence limits. Using ANOVA ($p < 0.001$) and multiple comparisons no significant difference was found between ascorbic and βGP or between supplemented media with and without DEX. Significant difference was found between growth media and all other variables except ascorbic acid. Supplemented media with and without DEX was significantly higher than any other media type when measured by number of cell infiltration. Graph (ii) Average maximum penetration (of 5 cells with greatest penetration into each microsphere slice) with 95% confidence limits. ANOVA ($p < 0.001$). $n > 7$. $N = 2$ Graph data is mean ± SD.

5.3.5 The effects of media supplements on the extracellular matrix production of hES-MP cell cultured with microspheres

ECM is visible inside the microspheres, within the pores where the cells have migrated to (Figure 5.14). Collagen detected by SHG is in greatest abundance in osteogenic media. There was no significant difference between collagen produced with supplemented media and growth media. This in turn contains significantly more than cells cultured in growth media. The intensities from the SHG images were measured and Figure 5.14b shows a graph of the results. There seems to very little overlap in the filters which means that the green that is seen is certainly SHG/mature collagen. Calcium deposited can be seen in both media which contained βGP but not in the growth medium. Particularly strongly stained areas appear to be around the exterior of the microsphere and inside the microspheres for osteogenic media.

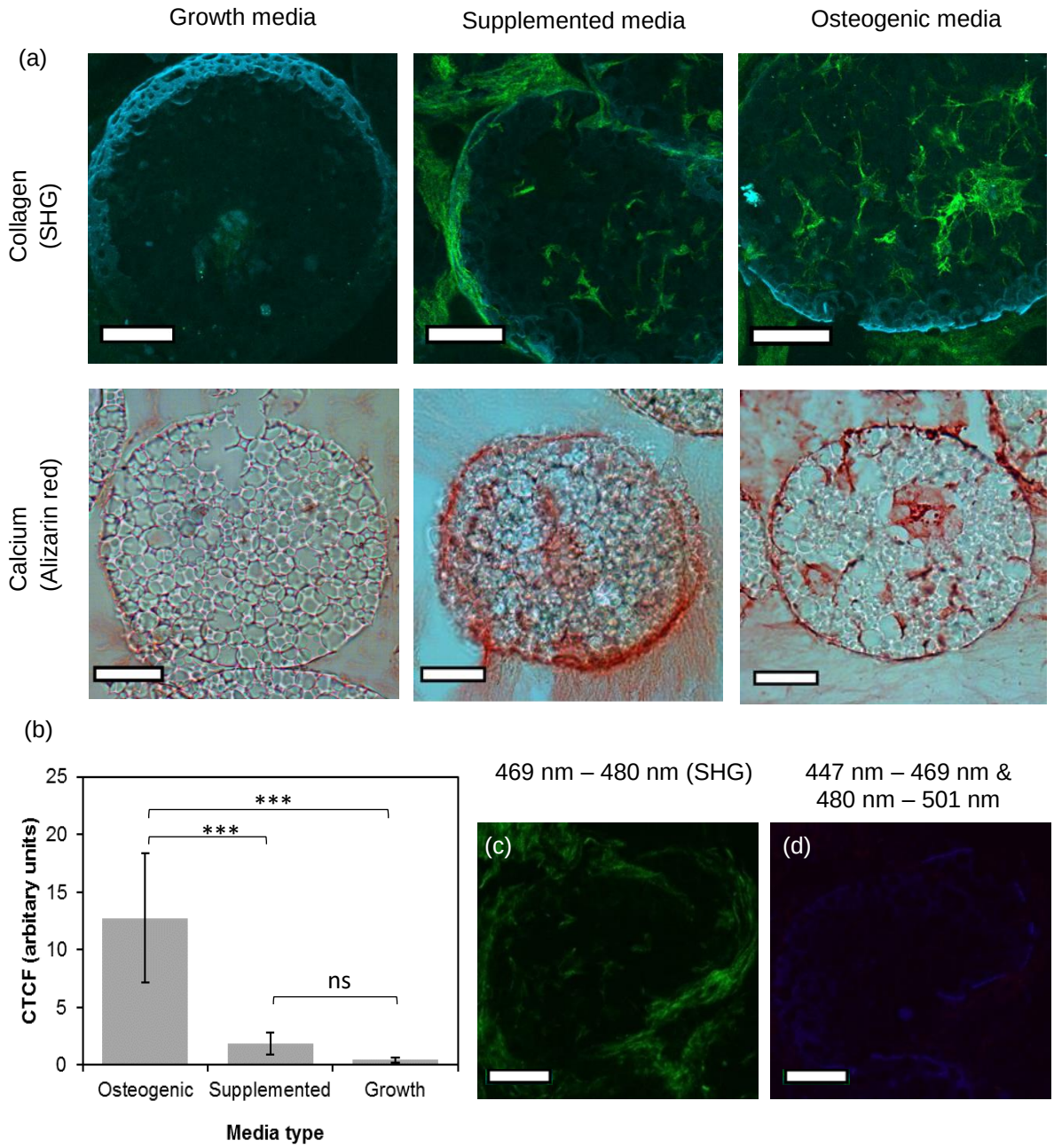

Figure 5.12. (a - Above) z-stack from confocal microscope converted to a single image by ImageJ z-project function. Images are of second harmonic generation (SHG) imaging which identifies mature collagen. Osteogenic media sample shows large amount of collagen formation in contrast with supplemented media. Growth media shows almost no return of the SHG signal. (a - Below) Optical images of sectioned microspheres from the day 30 time point. Samples have been stained with alizarin red to stain calcium deposits. The samples cultured in growth media show little positive staining whereas those cultured in osteogenic media shows a strong positive. The cells cultured in supplemented media shows levels of staining similar to those found in the positive control. (b) shows the corrected total fluorescence (CTF) within the particle. DEX influences the production of mature collagen. Image (c) shows the narrow band filter used to capture the SHG signal and the image (d) shows the two bands either side of the SHG region which demonstrates that the majority of the signal within the 469 nm – 480 nm band is from SHG and not overspill from nearby wavelength regions. All scale bars are 50 µm. ANOVA < 0.0001. n = 8. N = 2 Graph data is mean ± SD.

Small quantities of collagen staining can be observed in cells cultured in growth media with larger deposits of collagen are observed around the samples cultured in supplemented media but the

greatest density of collagen is in samples cultured in osteogenic media (figure 5.13). The area around the microspheres appears to contain more collagen than the centre of the sample. Collagen is observed within the pores on all samples not cultured in growth media. Calcium is less abundant than collagen and is only detected strongly on those microspheres cultured in osteogenic media. The strongest staining is surrounding the microsphere agglomeration suggesting osteoblast formation. A smaller amount of calcium is visible within the pores of the microspheres from osteogenic media culture. The presence of glycoproteins, as detected by toluidine blue assay, was observed on the samples. The strongest areas of the stain were around the exterior matrix of the agglomeration. Cells within the pores of the microsphere were also stained, indicating at least a low level of glycoproteins. In the 60 day culture the strongest glycosaminoglycan (GAG) signals are detected close to the edge of the agglomeration where the nutrient level would be highest.

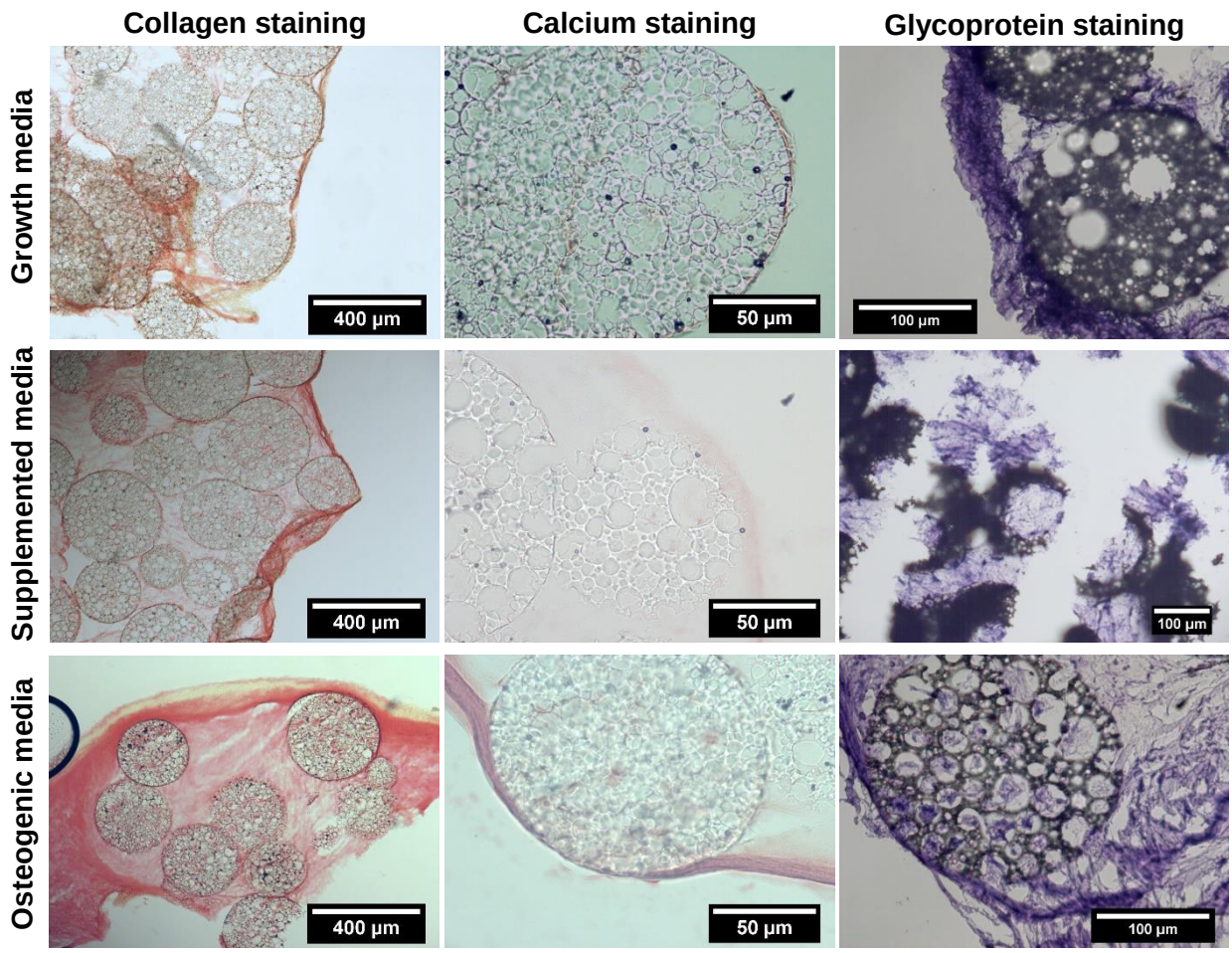

Figure 5.13. Optical images of 15 µm thick sections of polyHIPE samples from the day 60-time point. Samples have been stained with Sirius red to stain collagen, alizarin red to stain calcium and toluidine blue to stain for glycoproteins. Collagen is visible in all samples but appears most predominantly in samples cultured in osteogenic and supplemented media. Calcium is only strongly visible in osteogenic media with the brightest area surrounding the microsphere. In osteogenic culture cells within microspheres show evidence of Toluidine blue staining.

5.3.6 Investigation into the identity of cells within pores of the polyHIPE microspheres

After 60 days in culture thick ECM can be observed around the microspheres and cells can be seen within almost every pore of the microspheres (figure 5.14). A higher magnification image (Figure 5.14b) shows the morphology of the cells more clearly within the porosity. The dendritic like appendages linking cell to cell through the interconnected porosity can also be seen in this image. The images in Figure 5.14c and 14d show digitally constructed images which highlight the porosity and the H&E stained areas.

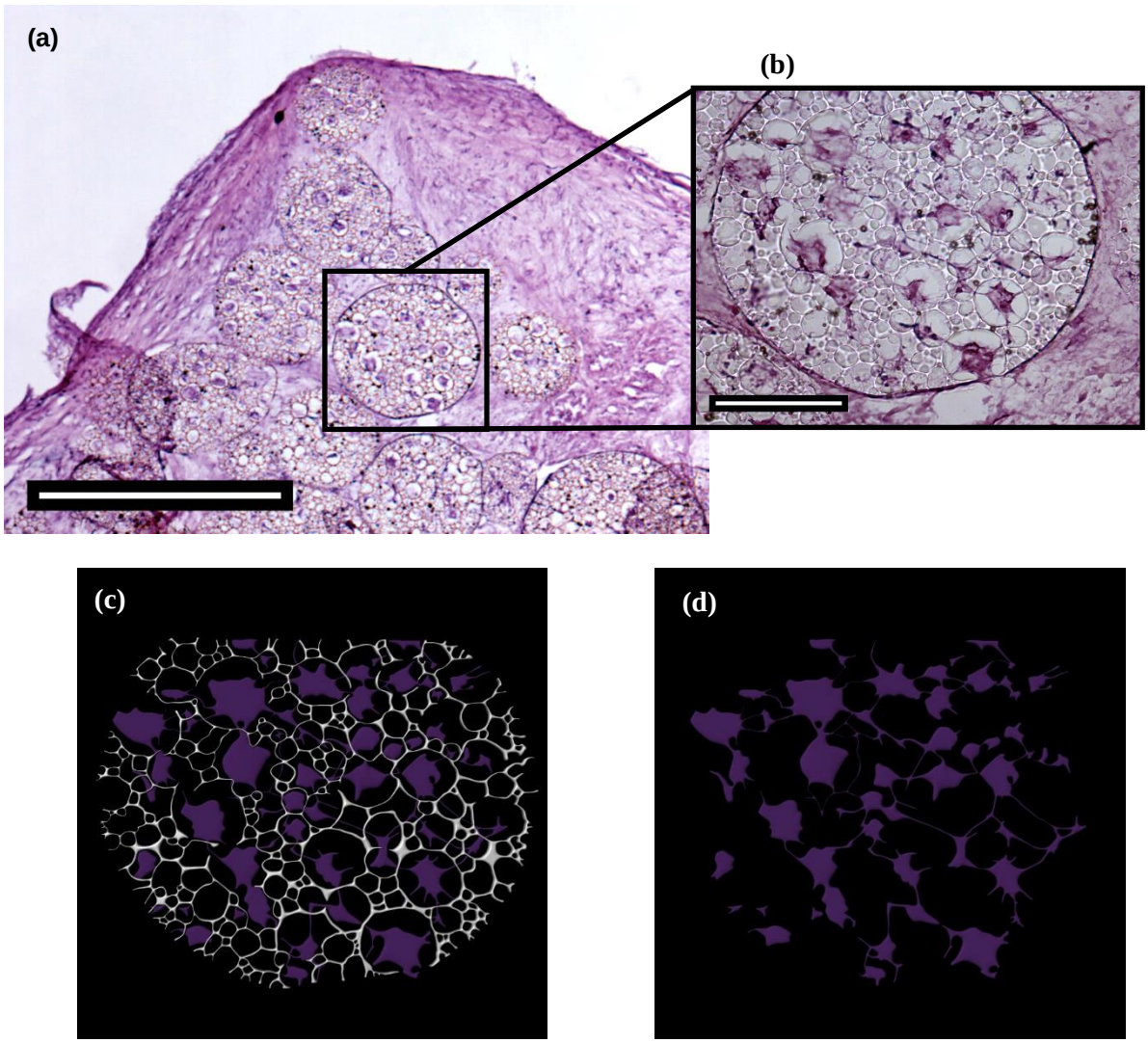

Figure 5.14. Optical image of a representative 15 µm thick microsphere slice, sectioned on a microtome. Sample was stained with H&E staining. It is possible to see cells within the microspheres internal porosity, linked cell to cell by cell processes or dendrites. Large quantities of ECM and cells can be seen encircling the microspheres forming a large structure. Section was a day 60 sample cultured in osteogenic media. (a) Scale bar is 500 µm. (b) Scale bar is 100 µm. (c & e) Images produced on Autodesk Maya via tracing and should be considered a guide only, but demonstrate potential connections between cells.

The biological material visible within the pores of the microspheres as a morphology similar to that of an osteocyte cell and contains deposited collagen, calcium and polysaccharides (figure 5.15). Originally the H&E staining appeared to show cell morphology similar to that of an osteocyte (Figure 5.17c). However later more specific tests such as SHG and Sirius red showed that these structures were at least partially formed of collagen (Figure 5.17a & 5.17b). The SEM image in Figure 5.17e shows a structure stretched across the pore, anchored to surrounding area. On this supporting structures are small granular like materials. This is a 2D like section of a sample and it should be noted that this shape existed in 3 dimensions within the pore. The toluidine blue stain indicates that there is the additional

presence of proteoglycans within this structure whereas alizarin red indicates the additional presence of calcium deposits.

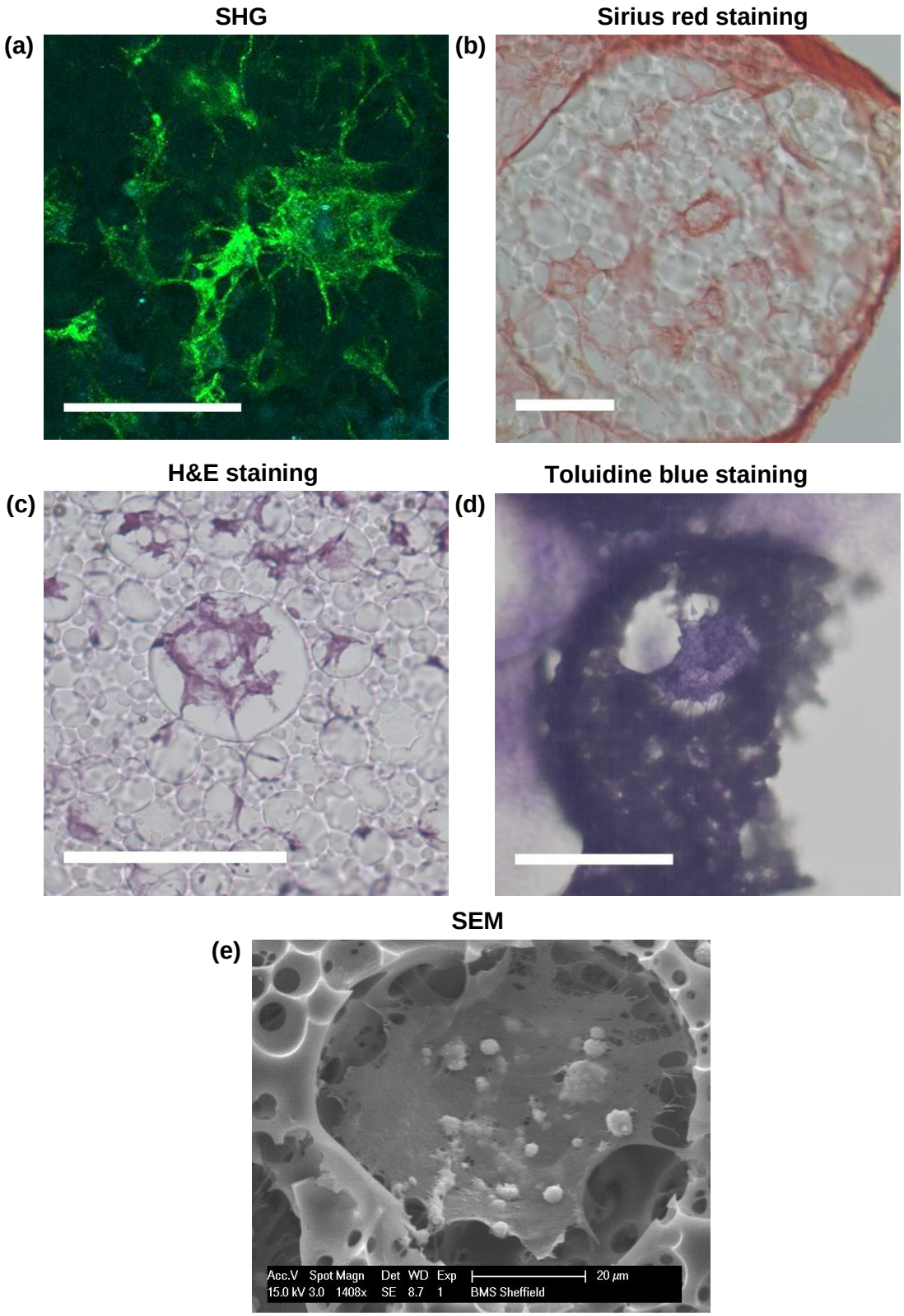

Figure 5.15. Images comparing cells/ECM within pores, found within the microspheres. Both (a) and (b) are specific collagen stains (SHG and Sirius red respectively) and (c) stains for general ECM material (H&E). (d) Toluidine blue stain for proteoglycans. All scale bars are 50 µm. (e) SEM micrograph of the effect captured at high magnifications.

Sclerostin is a marker found in mature osteocytes located within osteons within the bone. Positive staining was observed for Sclerostin within the pores of the microspheres (figure 5.16). The positive control showed staining in an adult rate bone where osteocytes are expected to be present. Not all cells within the microsphere stained positive for sclerostin.

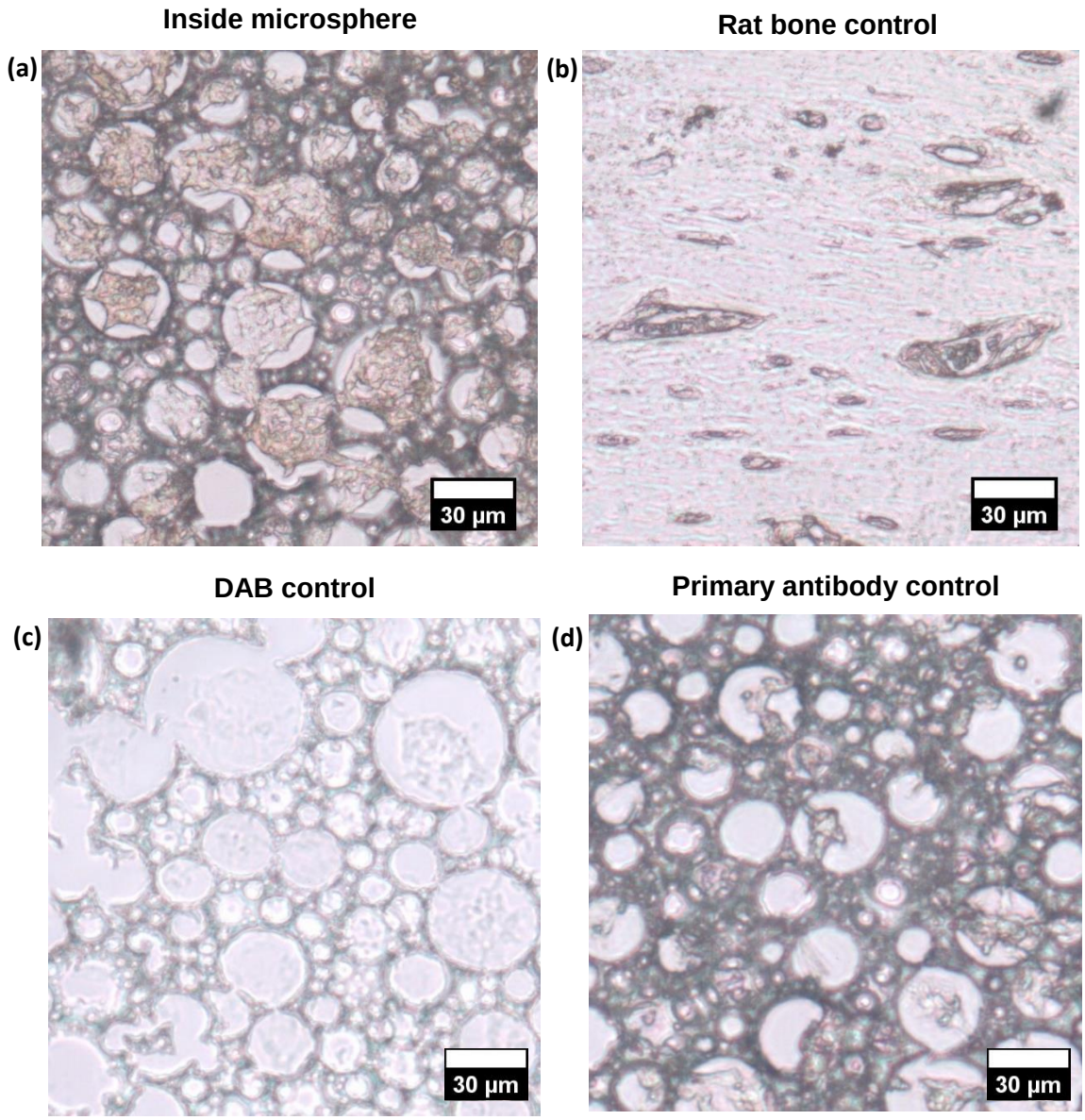

Figure 5.16. (a) DAB stain for Sclerostin on 15 µm sections of EHA/IBOA microspheres after 60 days in culture with osteogenic media. (b) Dab stain for Sclerostin on sections of adult rat bone sections showing stained cells where osteocytes would be expected. (c) Control using only primary and secondary antibody but no DAB stain. (d) Control using no primary antibody but including secondary antibody and DAB staining.

5.4 Discussion

Cells grew preferentially on EHA/IBOA thin films when surfaces were coated with acrylic acid and increased levels of metabolism was observed over 7 days in culture. On uncoated and gelatine coated samples no increase in metabolic activity over 7 days was observed, indicating limited cell proliferation. Gelatine is used successfully to culture the hES-MP cells for passage, and as results were similar to uncoated surfaces, it is likely that the coating method failed to adhere gelatine to the surface of the material. Viswanathan et al. also found that the attachment of hES-MP cells was dependent on surface chemistry [310]. The low cell attachment and growth on uncoated polyHIPEs is likely due to the hydrophobicity of these materials while depositing acrylic acid increases the hydrophilicity resulting in higher cell growth. Similar effects were observed in a recent study by the Claeyssens group using a polyHIPE 3D scaffold built by additive manufacturing show enhanced growth by plasma coating of acrylic acid and also demonstrate enhanced osteogenic differentiation on these surfaces [304]. Malayeri et al. demonstrates a similar level of enhanced growth of MG63 cells on EHA/IBOA polyHIPE surfaces [328]. Acrylic acid coatings are widely used as they are both highly hydrophilic and biologically recognisable to cells through protein absorption, and allows greater cell viability on the coating than hydrophobic surfaces [247, 329, 330]. No difference in cell metabolic activity was observed on surfaces with and without porosity, regardless of coating. This is again consistent with what Viswanathan et al. found, with the attachment of hES-MP cells dependent on surface chemistry but independent of porosity [310]. Differences in cell morphology were observed however with cells taking a more elongated shape on non-porous surfaces.

The culture of hES-MP cells on microsphere showed an increase in cell activity over the first 11 days after which total cell metabolism remained stable. There were no significant differences over the first 11 days between the different media indicating that early hES-MP proliferation is similar on these microspheres with and without differentiation cues in the media. Osteogenic media is used to differentiate MSCs into osteoblast like cells. When differentiating into osteoblasts there is usually a reduction in metabolic activity after an initial period of 1 - 4 days [192]. This was not observed for the culture on microspheres indicating that either the tests were insufficiently sensitive to pick out the difference or that most of the cells had not begun to differentiate and were still proliferating. When seeding onto microspheres, a lower number of cells attach to the surface as many cells fall past them in the culture. This results in greater free area around the cells which then does not induce contact inhibition. This lack of inhibition allows cells to freely proliferate instead, perhaps at the expense of differentiation.

Over time it was observed that cells began to form agglomerations incorporating the microspheres, until all microspheres were aggregated together in one large mass. The cells and microspheres combining after a period of time to form large cell-microsphere aggregates, as was also observed by

Zhang *et al.* [265]. Within the T-flasks, multiple small aggregate nuclei were formed after a few days, which then increased in size, as single microspheres and other small aggregates combined. After 30 days, only a few very large aggregates remained but these would no longer merge without exterior intervention in pressing them together. Aggregates forced into contact for a length of time would then merge. By day 60 the microspheres are surrounded by a large amount of ECM, in some areas there is almost 400 μm of this ECM between the microspheres and the nearest edge of the agglomeration. The 3B's group in Portugal have shown that it is possible to form aggregates in a faster fashion by increasing the cell and microsphere contact area by growing them within an PCR tube [331]. This suggests that forcing microspheres together, such as would occur upon injection into the body, would allow aggregate formation to occur more rapidly than we have seen in-vitro. Aggregates remain as a solid structure and cells would continue to proliferate on the exterior. Over time, this outer layer increased in thickness. Microsphere-cell aggregates were firm enough to be handled and required cutting with a scalpel to prepare them for imaging.

Cells were found within the internal porosity of the microspheres having migrated in from the external surface through the interconnected regions. When samples were section and stained, it became apparent as to the extent of the infiltration of cells within the microspheres. We were surprised that cells did indeed grow into the polyHIPE material due to the small size of the pores, especially the interconnecting pores, of the material. Many studies state that the optimal pores size for ingrowth is far larger at larger than 100 μm [97, 332] whereas the average porosity of the polyHIPE was around 25 μm with few interconnecting pores being larger than 7 μm. Lu *et.al* studied the culture of osteoblasts in porous ceramics and found that within their interconnected porous system osteoblasts/bone ingrowth required interconnecting pores larger than 20 μm in diameter [333] which is larger than those in the polyHIPE material. Internal cell numbers and ECM quantities can be seen increasing within the microspheres when comparing two time points indicating cell still viably within the scaffold. MSC differentiated cell types which can survive within a low oxygen environment are osteocyte or chondrocyte cells. Other groups had observed cell infiltration into porous microspheres with a recent study by Huri et al. showing cell ingrowth of adipose derived stem cells into salt leached PCL (polycaprolactone) microspheres [334]. Previous studies with hES-MP cell growth on polyHIPEs have focussed on scaffolds with larger pore sizes [310], whereas in this study we concentrated on pore sizes more comparable to the studies of Cosgriff-Hernandez who studied the growth of hMSCs on similar porous microparticles [335]. Pores at the smaller end of the scale (roughly 50 μm) are reported to work well in-vitro in producing osteoblast like cells [336]. This pore size was chosen so we could examine the effects of osteogenic differentiation *in-vitro*.

Culturing cells in osteogenic media caused faster cell ingrowth into the microspheres, when compared to non-osteogenic media. We found that in osteogenic media cells had reached the centre of the

microspheres by around day 15 in lower numbers, with cell numbers inside increasing up to the end of the experiment at day 30. After 60 days cells appeared to inhabit most of the pores within samples grown in osteogenic media. In comparison when cultured in growth media cells remained closer the external surface than in osteogenic media and fewer cells were observed within the microspheres. Most cells within microspheres cultured in growth media were close to surface of the microsphere. Osteogenic media is formulated to induce MSC like cells to differentiate into osteoblast cells. Figure 5.10 shows that osteoblast cells are formed on this material when using osteogenic media, as indicated by increased ALP levels. These results could indicate that osteoblast like cells are more inclined to migrate into scaffold than the cells found when cultured with growth media. Both MSCs [101, 102] and osteoblasts [337, 338] have been shown to migrate and MSC cells have also been known to migrate through smaller pores when stimulated by certain chemicals [103]. Therefore, a specific chemical from the media may be responsible for the cell ingrowth by causing MSC ingrowth. Osteogenic media is formed from the addition of several additives which are absent in growth media. An additional experiment was then conducted to examine is a specific additive, or additive combination, within the osteogenic media was causing cells in migrate further into the microsphere.

Different levels of cell ingrowth into microspheres was observed when using media containing different combinations of the additives used in osteogenic media, with dexamethasone appearing to have no effect on ingrowth. Results showed that both ascorbate-2-phosphate and βGP caused a small increase in cell ingrowth when used independently but that they worked synergistically together for far greater cell ingrowth. Ascorbate-2-phosphate is known to promote ECM secretion (collagen and glycosaminoglycan) from the cells [339]. βGP is reported to promote the formation of mineralized bone by providing a surplus of phosphate ions to osteoblasts and stimulates ALP production through surface bound activators [340, 341]. Neither effect would suggest a direct reason for cells to grow into microspheres. β-GP or ascorbate-2-phosphate could coat the surface of the microsphere or acts on the cell to allow/encourage them to enter the microsphere. Ascorbate-2-phosphate and βGP both aid in the formation of ECM which could itself enhance cell migration. The presence of DEX appeared to have little effect on infiltration. Similar ingrowth was observed for media containing ascorbic acid and β-GP with and without dexamethasone. MSC cells have been shown to migrate when stimulated by TGF-β [342] and while no TGF-β was added to the media, DEX is reported to enhance TGF-β2 binding in a dose dependent manner [343] which may increase the sensitivity of MSC cells to any TGF-β released within the system. There is no evidence however that TGF-β enhanced migration would cause MSC to migrate into small pore systems.

The use of the different additive combinations in media resulted in different levels of ECM production in both the microspheres themselves and in the agglomeration with dexamethasone having an impact on observed composition. ECM is produced by all cells but some cell type produce specific ECM. In this

study, we have hES-MP cell and potentially osteoblasts cells within the microspheres. The role of an osteoblast is to lay down ECM and to facilitate the production of bone whereas the primary role of the stem cell is self-perpetuation. This is why, and as we observed, that ECM deposition and mineralisation of a scaffold is an indicator of the presence of osteoblasts [192]. Less calcium is observed in systems without cultured without βGP which was predicted as without βGP there are very low levels of mineral available to deposit. Increased levels of collagen are observed in media containing ascorbic acid as ascorbic acid plays a key role in collagen maturation. When looking at the intensity of the SHG a statistical difference was found with the addition of dexamethasone to the culture media. While supplemented media formed osteoblasts (due to the presence of calcium) a significant increase in both collagen and calcium was observed with the addition of dexamethasone to the media. This is likely due to an increased number of osteoblast or more developed osteoblasts as dexamethasone is known to promote osteogenesis. From this it appears that the ingrowth of cells into the microspheres is not directly related to the formation of osteoblastic cells but from the availability of both βGP and ascorbic acid.

There are many indications that the cells within the porosity of the microspheres are osteocyte cells including shape, antibody staining and ECM composition, but it is not possible to rule out the possibility of chondrocytes being present. Few cells can survive under hypoxic conditions expected within the microspheres pores. This is an indicator that cells have differentiated to a cell type which can survive in hypoxic conditions. Osteocyte cells survive and perform in areas distant from blood supplies [344]. Osteocytes have been documented preferably differentiating under hypoxic conditions [215] although there is still some debate on whether osteoblasts are enhanced or inhibited under those same conditions [215, 216]. Another cell type which is often formed under hypoxic conditions is chondrocytes [345-347], which have also been reported forming in small pores similar to these, in both *in-vivo* [348] and *in-vitro* [349] experiments. Literature has shown that hES-MP cells can be differentiated into chondrocytes, although usually only in chondrogenic media [207]. Osteocytes have a spindly appearance, which is observed within the microspheres, whereas chondrocytes have a more spherical appearance. Dendritic like extensions were observed running between pores and cells within the microsphere at day 60. The formation of dendrites is observed on osteocytes but not on chondrocytes [350, 351]. Both cell types would be surrounded by collagen as we observed from the Sirius red staining. The deposition of calcium deposits is usually an indicator of osteoblastic activity but chondrocytes can also deposit bone under certain conditions, usually when they are hypertrophic [352]. Hypertrophic chondrocytes begin to deposit bone but once surrounded by bone they usually die due to the lack of nutrients, leaving behind cavities for bone cells to inhabit [353]. This might explain the decreased levels of GAG within internal pores at day 60 indicating that any chondrocytes that were formed have been replaced by osteocytes in hypoxic areas. Positive staining for Sclerostin was also

found on some of the cells at day 60 within the microspheres. Sclerostin was initially used to determine osteocytes from osteoblast as the antibody is only present in osteocytes [354]. Sclerostin inhibits osteoblasts and prevents the deposition of new bone and is found to be secreted by osteocytes when they first form the osteon [355]. This could therefore indicate that the osteocytes are recognising the pore as an artificial osteon.

5.5 Conclusion

From the first results chapter where we looked at manufacturing, this chapter looked at the culture of cells (mainly hES-MP cells) with these microspheres. The study was taken further by looking at the long-term culture of hES-MP cells upon the microspheres where it was found that the cells assembled the microspheres into a large aggregation. The mesenchymal cells grew into the porosity of the microspheres and formed anchor points between microspheres. This allows a larger scaffold to self-assemble, made from numerous microspheres, allowing for the formation of larger pores between the microspheres that could enable vascularization. The binding of the microspheres by cells shows that it will be possible to create a continuous scaffold from individual microspheres over time. Cells were found to penetrate the microspheres when grown in media with containing supplements. The ability to create uniform sized microspheres allows us to create a time course to view cell ingrowth into microspheres. The supplemented media (βGP and ascorbate-2-phosphate) appear to work synergistically to stimulate cell infiltration into the microspheres. Adding Dexamethasone did not appear to have any impact on the cells abilities to grow into pores. However, adding dexamethasone to supplemented media increased ALP production in cells and greatly increased deposits of collagen and mineralisation. All of these factors confirm the presence of osteoblast formation. On balance, from looking at cell morphology and sclerostin staining, it appears that osteocytes are also forming within the internal porosity although there is some difficulty in differentiating between osteocytes and chondrocytes.

Chapter 6: Degradable polyHIPE microspheres

6.1 Chapter aims

1. Investigate the potential of the thiol-ene material for polyHIPE microsphere applications.
2. To utilise the new emulsion technique for forming a HIPE using PCL, recently developed in our lab, for polyHIPE microspheres
3. To investigate if the previous results with the EHA/IBOA polyHIPE can be replicated using a biodegradable polyHIPE microsphere system.

6.2 Introduction

In the previous chapter a non-degradable polyHIPE microsphere system was investigated and positive results were found from the cell ingrowth data. As a non-degradable polymer, it would be suited for studying cell growth and infiltration in-vitro but could not be used for an injectable implant in the clinic. The key to this project was to re-produce these results in a fully degradable system that could then be used as an injectable and degradable bone filler. In this chapter, we consider two systems, thiol-ene and PCL polyHIPE microspheres that have the potential to meet the requirements of the project.

6.2.1 Degradable materials and their use within the body

Degradable materials are an essential aspect of a successful tissue engineered solution [67]. As the cells included on and surrounding a scaffold begin differentiating and producing ECM material the scaffold should resorb at the same rate as growth, until no scaffold remains. Degradable materials should be able to be completely removed by the body's natural pathways. A non-degradable material risks eventual negative immune responses and prevents the formation of a completely natural and functional tissue. Sometimes it is possible to remove a non-degradable implant, in situation such as nerve regrowth [356], but this is never desirable due to the necessity of a second surgery and associated risks and costs. For most tissue engineered solutions the scaffold is an integral part of the implant and cannot be removed without removing the newly formed tissue.

6.2.2 Thiol-ene polymer as a polyHIPE

Thiol-ene reaction is one between a thiol and an alkene which results in an alkyl sulphide bond. It is possible to use a photoinitiator for this reaction [191]. Thiol materials such as trimethylolpropane tris(3-mercaptopropionate) (trithiol) are sufficiently hydrophobic to be formed into an emulsion but are also able to degrade within the body. Some studies have now been published using this material although few investigate the full biodegradability of the polymer [160, 190, 191].

6.2.3 Polycaprolactone polymer as a polyHIPEs

PCL is a biocompatible and biodegradable material [357] and is as close to a FDA approved material as possible, if the FDA did not operate on a case-by-case approval system. PCL is a polyester with a very slow degradation rate (3 – 4 years) that degrades to products which the body can easily remove [357]. The mechanical properties of PCL are not suitable for load bearing applications although the polymer is very popular in other fields of tissue engineering and also for non-load bearing bone applications [67, 358, 359]. The polymer itself is very well studied and relatively inexpensive to buy. Until recently the only PCL polyHIPEs which could be formulated were formed of PCL blends or with porosities below the 74 % limit [302]. These materials often had undesirable qualities with the blend polymer often being non-degradable [186, 360]. PCL has a comparatively lower hydrophobicity [186] that makes it unsuitable for polyHIPE manufacture, coupled with a high viscosity during emulsification. Recently Sherborne *et al.* succeeded in producing a true PCL polyHIPE using a dual solvent system and elevated temperatures. This polyHIPE is investigated within the chapter.

6.3 Results

6.3.1 The manufacture of Thiol polyHIPE microspheres and hES-MP cell growth on both microspheres and flat sheets

The thiol-ene based formulation was successfully processed to form a polyHIPE material and this material was then formed, using a w/o/w emulsion, in microspheres (Figure 6.1). From Figure 6.1a it is possible to see the highly porous nature of the material. The median pore size is around 40 µm and very large pores can be observed in the material, some greater than 100 µm in diameter. This high porosity is not apparent when looking at the external surface of the thiol polyHIPE microsphere (Figure 6.1b). On this exterior, the pore size diameter average is around 20 µm, a result repeated in Figure 6.1c & 1d. A significant proportion of the microspheres surface topology is smooth and lacking in surface roughness and pores.

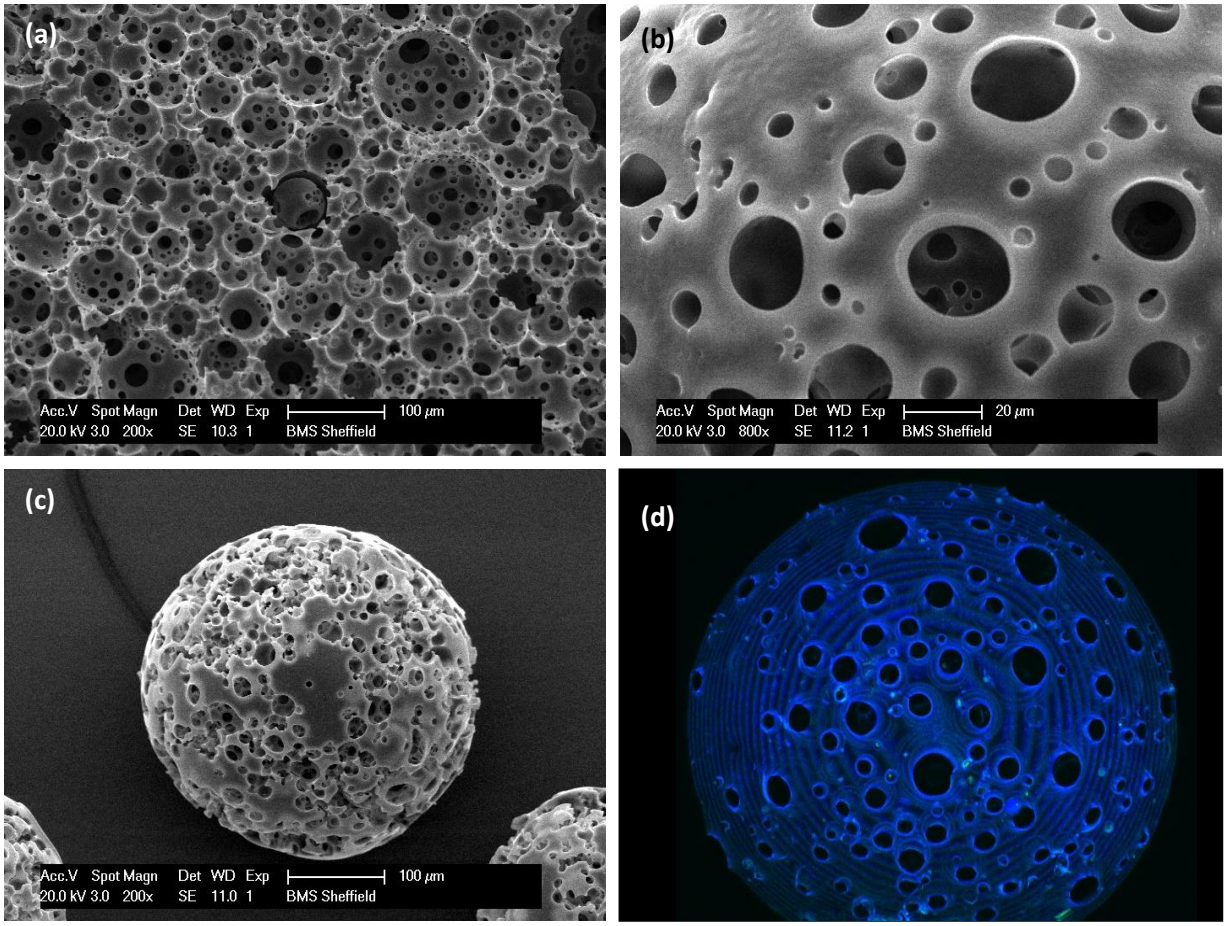

Figure 6.1. Thiol-ene material formed as an emulsion to produce a polyHIPE. (a) SEM micrograph of a flat sheet of thiol polyHIPE. (b) Exterior surface of a thiol microsphere. (c) 3oo µm thiol polyHIPE microsphere. (d) Auto-fluorescence z-stack image from a confocal microscope showing the exterior of the microsphere when wet.

hES-MP cell growth on thiol microspheres was investigated and cells were found to attach to the surface of the material, although no ingrowth was observed (figure 6.2). Cells can be seen binding to the exterior surface of the microspheres (Figure 6.2a & 2b) after 3 days in culture. After 10 days in

culture significantly more cells can be seen growing on the poly acrylic acid coated (pAAc) thiol microspheres (Figure 6.2d) than on the uncoated microspheres (Figure 6.2e). pAAc coated microspheres, when cultured with hES-MP cells still formed agglomerations of microspheres. When sectioned and stained it was observed that very few cells grew into the internal structure of the microspheres.

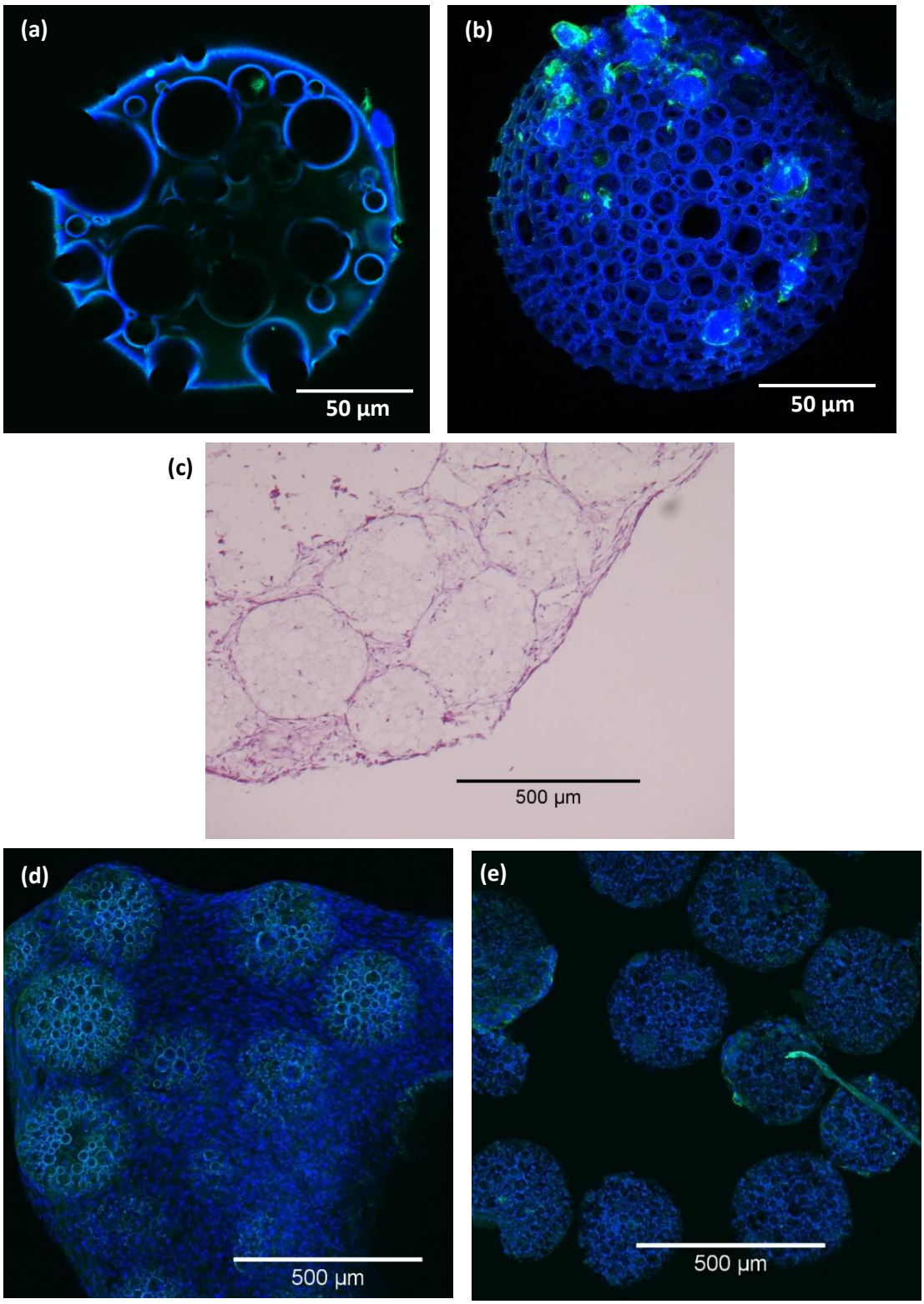

Figure 6.2. hES-MP cell growth on thiol-ene polyHIPE microspheres. All fluorescent images are stained with DAPI for cell nuclei and FTIC-Phalloidin for F-actin. (a) Fluorescent image of an uncoated thiol-ene microsphere after 3 days in culture with hES-MP cells. A cell can be observed attached to the side of the microsphere. (b) Z-stack image from a confocal microscope of a pAAc thiol-ene microsphere after 3 days in culture. (c) H&E stained imaged of a 15 µm thick section of a thiol-ene microsphere/cell agglomeration. (d) Z-stack image from a confocal microscope of a pAAc thiol-ene microsphere after 10 days in culture. (e) Z-stack image from a confocal microscope of an uncoated thiol-ene microsphere after 10 days in culture.

DNA and ALP recordings of hES-MP cells cultured on flat sheets of thiol-ene polyHIPE showed low levels of DNA in all three mediums but an increase in ALP activity for those cultured in osteogenic media (Figure 6.3). A slight increase in cell numbers is observed with pAAc when compared to uncoated particles, in osteogenic media. There is no significant difference between any of the media used when culturing on the thiol-ene polyHIPE. A difference was observed on the TCP between the different media. When considering ALP production, the media did have a significant effect. There was no significant difference between any of the different surfaces when cultured in the same media.

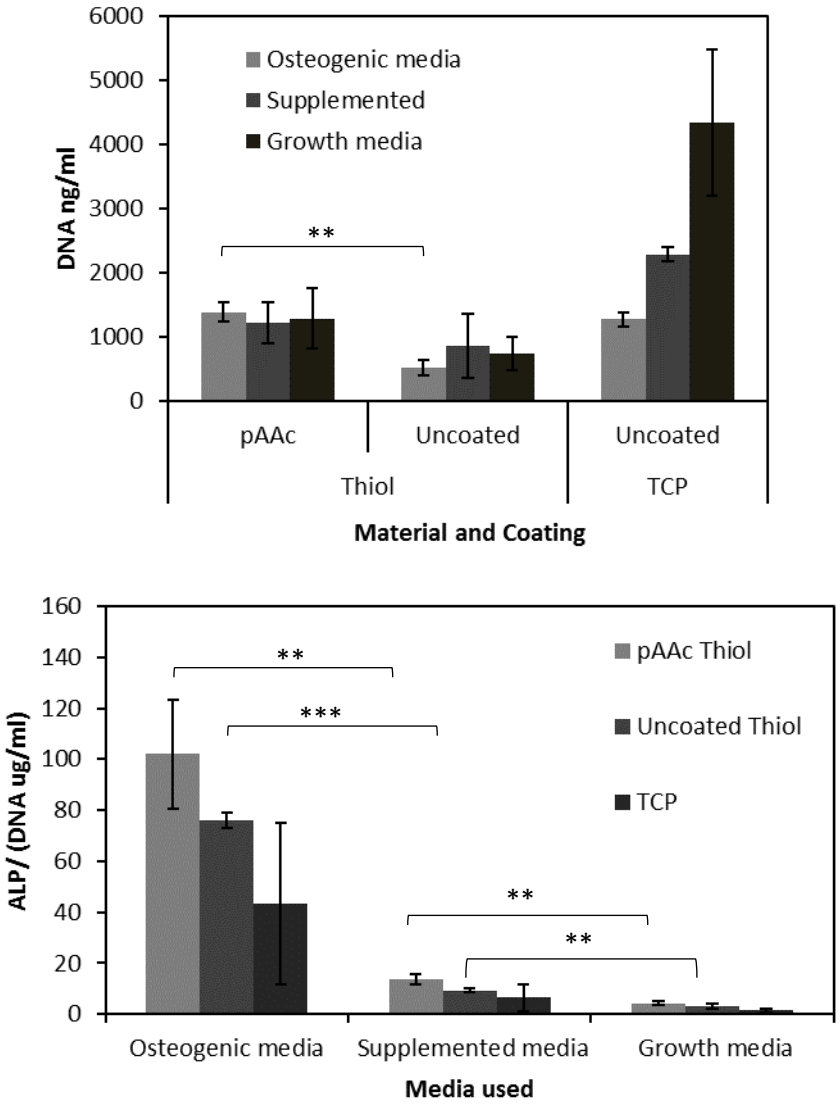

Figure 6.3. (a) Picogreen assay to detect the quantity of DNA on a flat scaffold after 14 days in culture in different media. (b) ALP production per unit of DNA measured for the same materials as in (a). No significant variance was found using an ANOVA between any of the materials cultured in a specific media. Significant difference was observed between the different media ANOVA. n = 3. N = 2 Graph data is mean ± SD.

6.3.2 Manufacturing polycaprolactone based polyHIPE microspheres

Highly porous microspheres were successfully manufactured from a PCL based polyHIPE material (figure 6.4). The PCL microspheres were more difficult to make compared to other polyHIPE systems used due to their lower stability. Two distinct surface morphologies were observed in the produced PCL microspheres, exhibiting different surface roughness (Fig 6.4d). The rougher morphology appears to have a higher degree of surface porosity. The distribution of microspheres formed from the stir emulsion manufacturing technique is a similar left leaning skewed distribution observed in chapter 4.

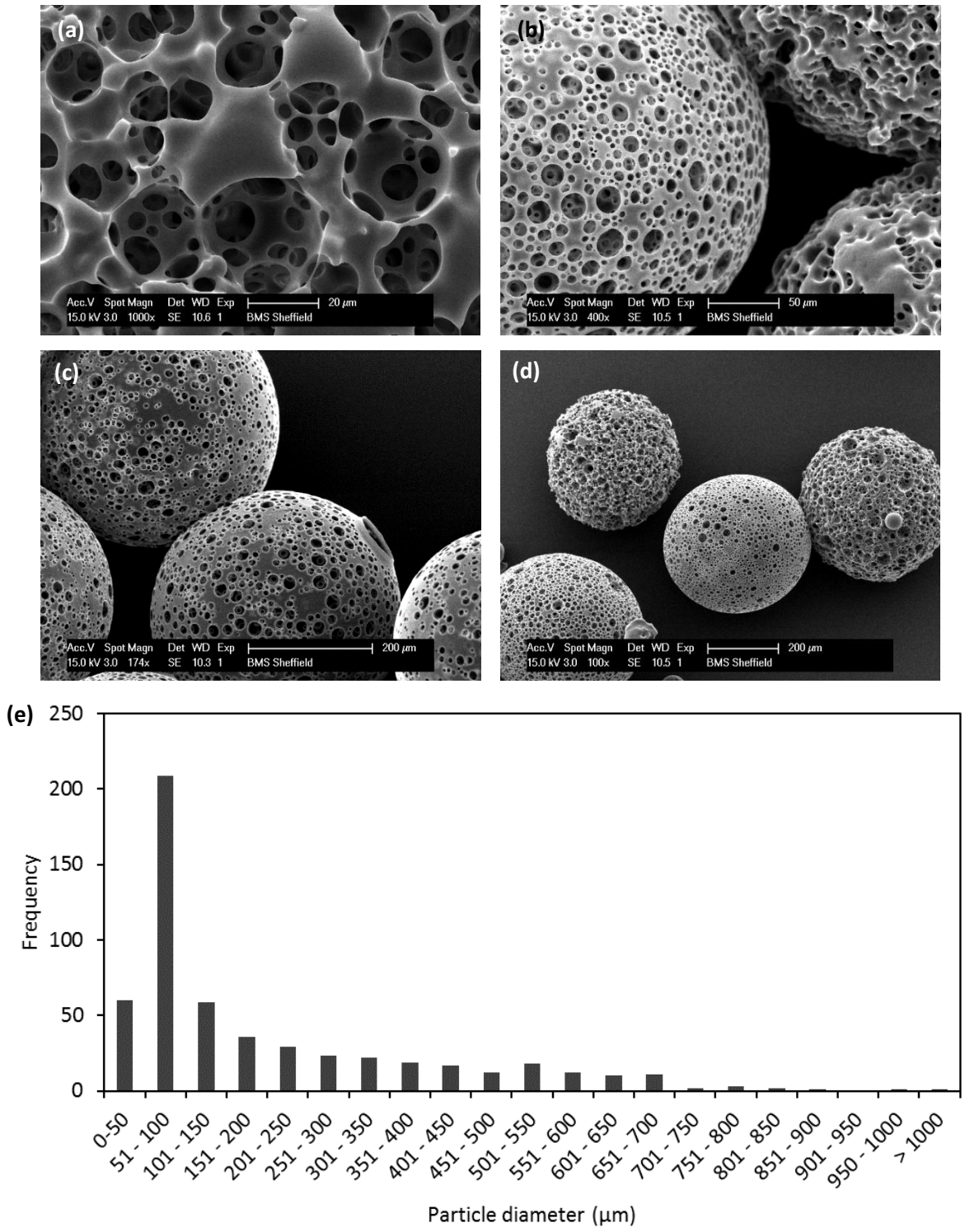

Figure 6.4. PCL polyHIPE microspheres formed by w/o/w emulsion. (a) SEM micrograph of surface skin of a microsphere. (b & d) SEM of PCL microspheres with different surface morphologies. (c) SEM of PCL polyHIPE microspheres. (e) Histogram of the size distribution of microspheres produced using the stir tank reactor method (w/o/w). n = 547

The internal structure of the PCL microsphere is highly porous and can be seen to include interconnecting pores between the larger pores (Figure 6.5). A wide distribution of pore size within the microsphere is described in Figure 6.5b. The largest pore recorded was 55 μm in diameter, although the majority of recorded pore diameter were less than 30 μm.

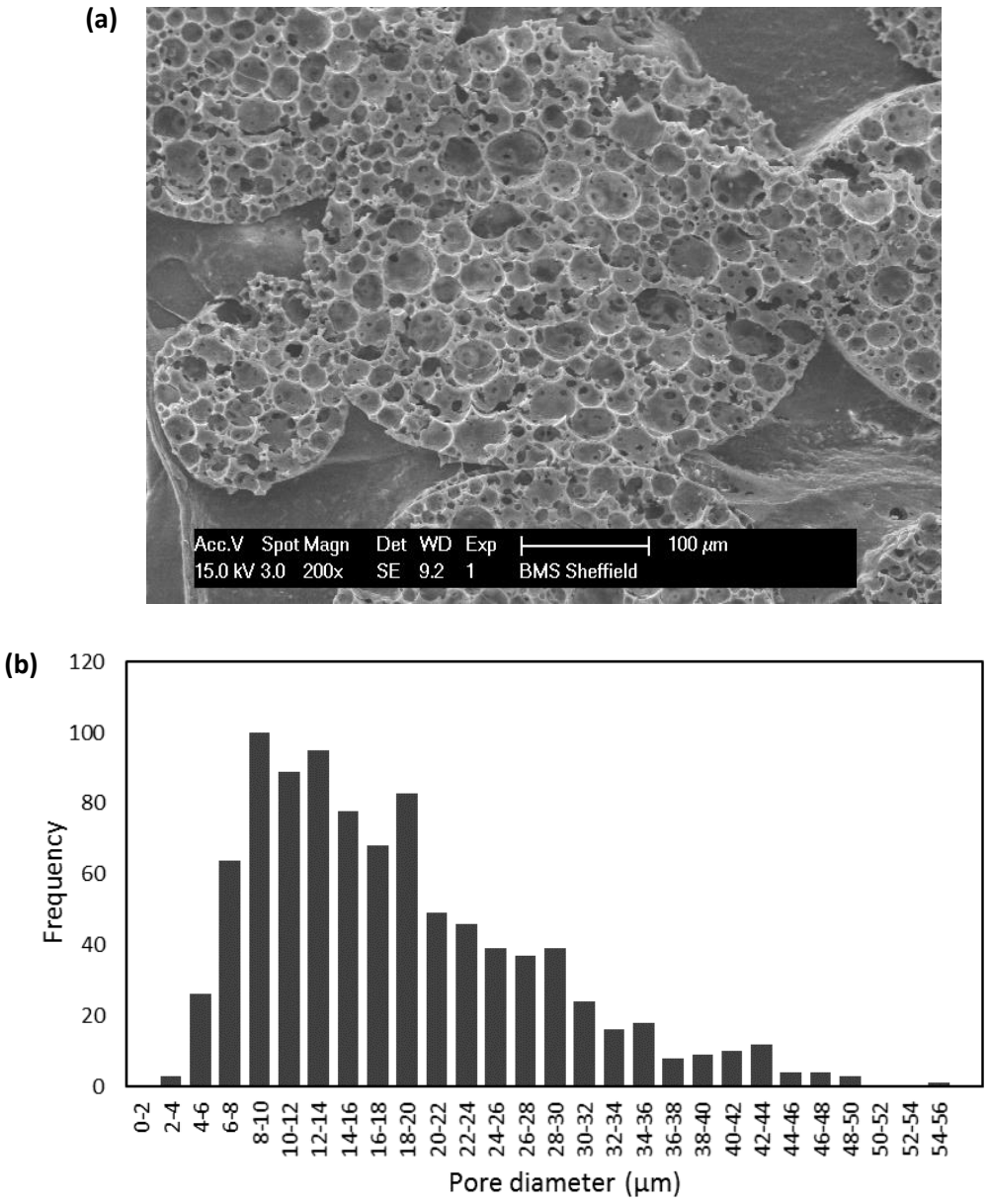

Figure 6.5. (a) SEM image of 40 µm thick section of a PCL polyHIPE microsphere showing the internal porosity of the structure. (b) Pore size diameter distribution from PCL polyHIPE microspheres measured from SEM images such as the one in (a). n = 312.

Internal pore size of the PCL microsphere was very similar to that of the EHA/IBOA microsphere system. PCL polyHIPE appears to have a slightly greater number of the smallest pores and significantly less of the largest pores recorded in the EHA/IBOA system (those pores greater than 35 µm). When comparing SEM micrographs of the microspheres produced from EHA/IBOA and PCL systems (Figure 6.6b & 6c) the appearance of both are relatively similar. EHA/IBOA polyHIPE microspheres appear to have slightly more open surface than the PCL microsphere which have a slightly more closed appearance.

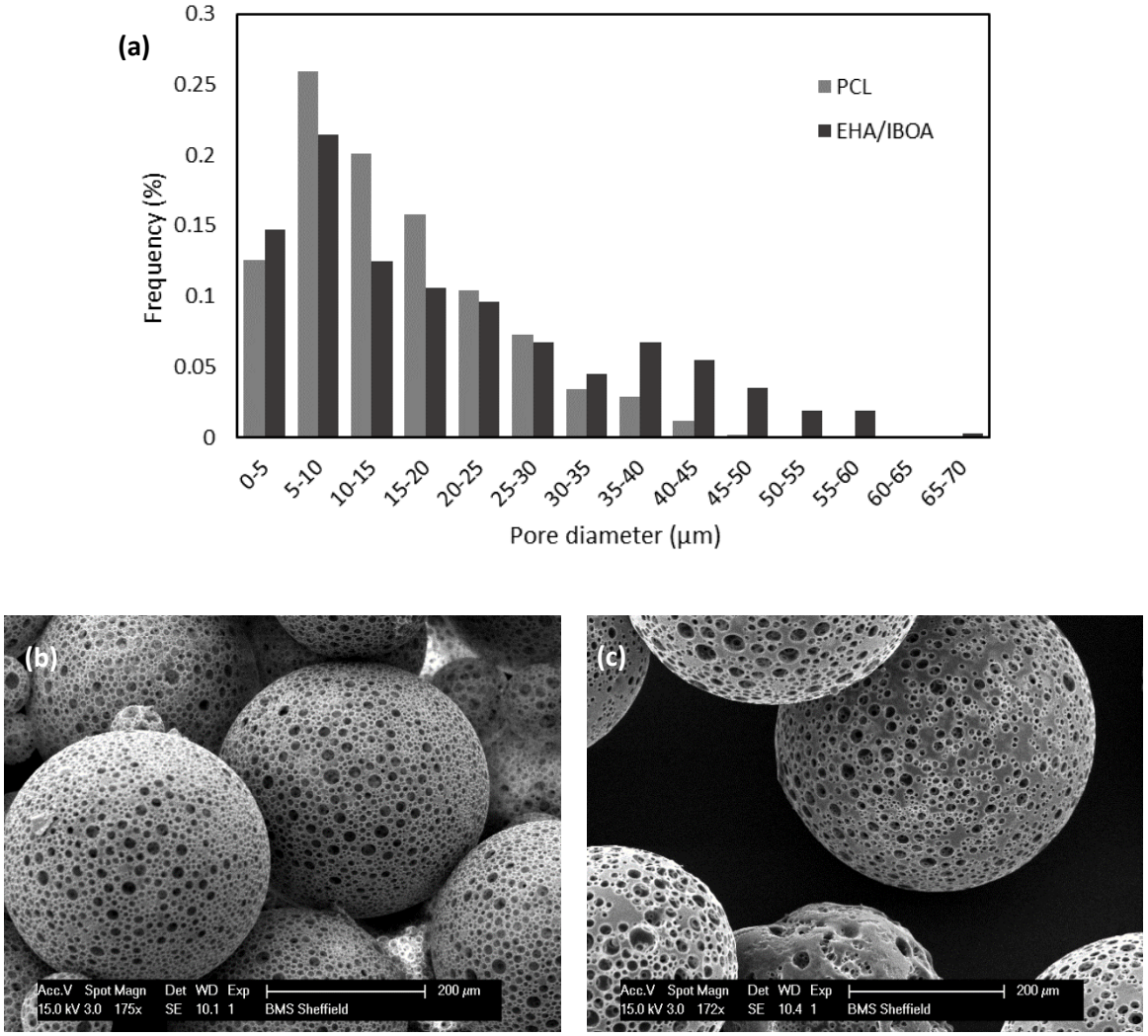

Figure 6.6. Comparison of PCL and EHA/IBOA microspheres. (a) Distribution of internal pore size diameters from both PCL and EHA/IBOA microspheres. Microspheres formed from the different materials were formed using the same processing conditions (at the same temperature, water content and stir rate). (b) SEM micrograph of an EHA/IBOA polyHIPE microsphere. (c) SEM image of a PCL polyHIPE microsphere. n = 312.

6.3.3 Accelerated degradation of polycaprolactone polyHIPE microspheres over a 60 day time period

Over the 60 days the microspheres stored in NaOH lost over 80% of their weight and the ones degrading in water lost roughly 25% of their original weight (figure 6.7). Microspheres were stored within a glass container for 60 days in designated solution. Degradation of the PCL polyHIPE as microspheres was conducted over 60 days, both in an accelerated form using NaOH and at a slower rate using distilled water. The microspheres stored in dry air did not reduce in weight over the 60 days.

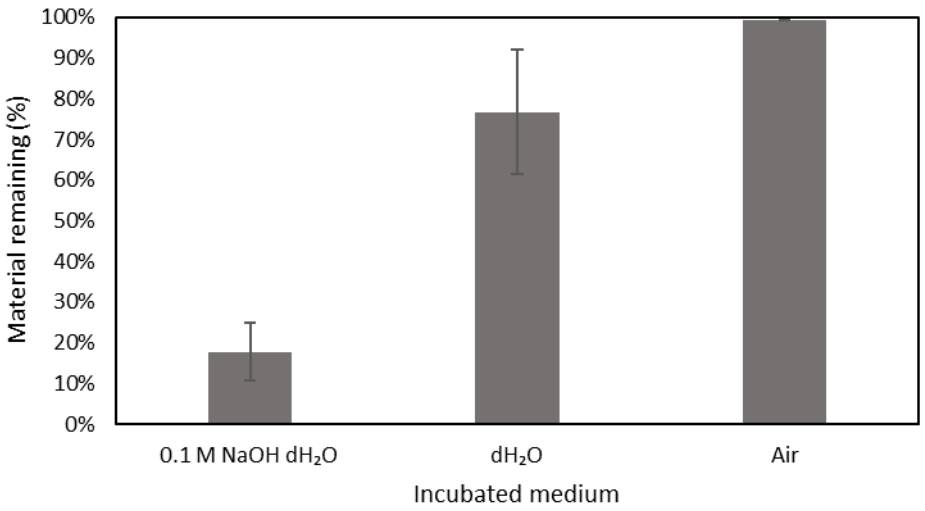

Figure 6.7. Accelerated degradation study of the PCL material as polyHIPE microspheres over 60 days at 37°C. Graph is showing remaining mass of the material as a percentage of the total mass. The accelerated test (NaOH) resulted in an 80% loss of mass and microsphere submerged in water lost around 25% of mass in the same time period. Samples kept dry lost 0% mass over the 60 day experiment. n = 4, N = 1.

6.3.4 Culture of hES-MP cells on polycaprolactone microspheres and the formation of cell enabled agglomerations

hES-MP cells successfully grew on the PCL microspheres and formed agglomerations by day 5 of culture (figure 6.8). HES-MP cells were found to form connections between each microsphere and then adhere them together. This slowly increased the size of the agglomerations as more and more cell coated microspheres met one another. The microspheres were used without any surface treatment. Embarrassment

Day 5 in Osteogenic media

Day 5 in growth media

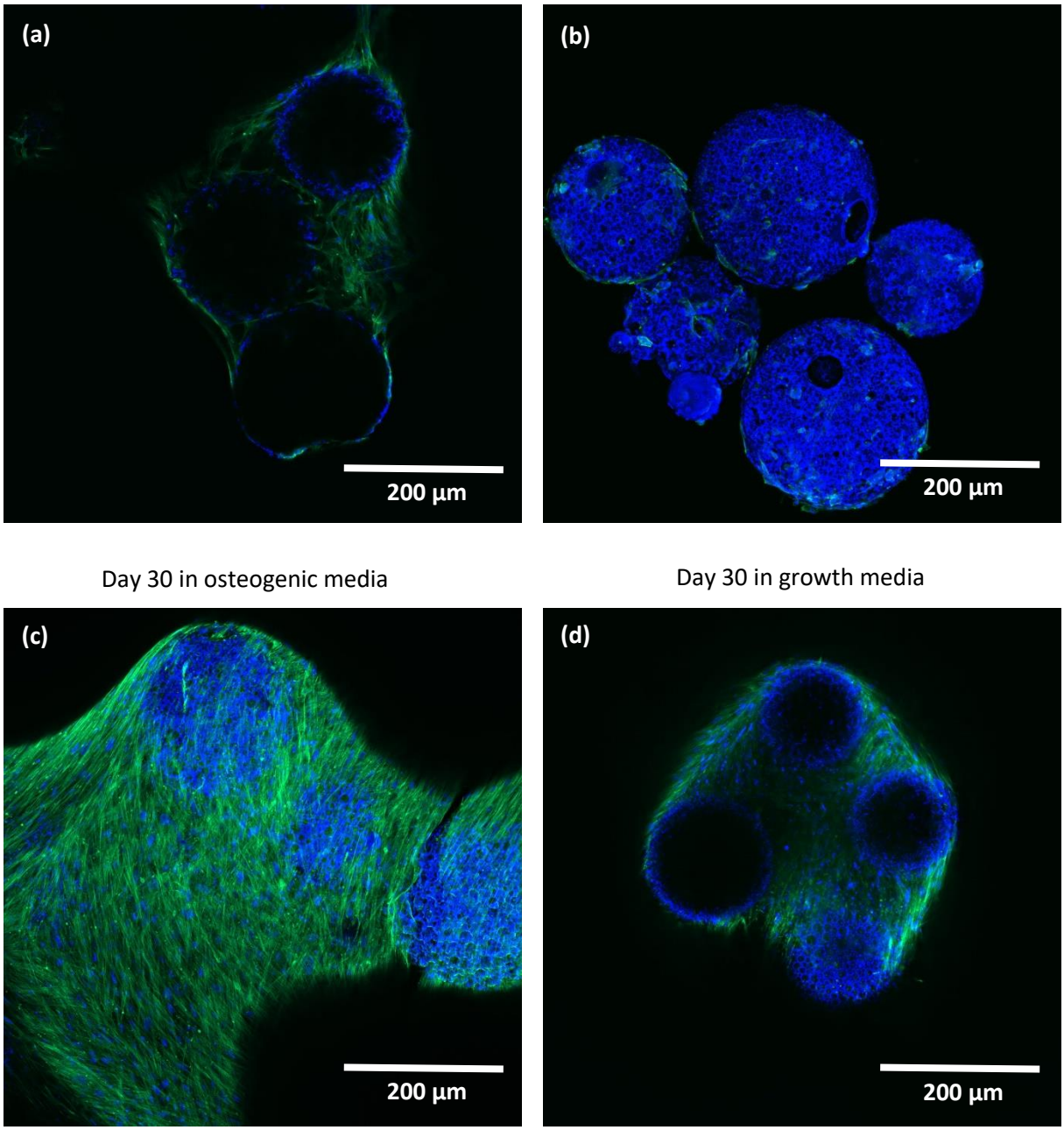

Figure 6.8. Confocal z-stack images of uncoated microspheres cultured in two different media at two time points. DAPI (blue) stains the cell nuclei and FITC-Phalloidin (green) stains the F-actin of the cytoskeleton. Cell initiated microsphere aggregation can be clearly observed at the later time points (c & d).

The cells binding the microspheres together can be seen more clearly in the confocal images using only the F-actin stain FITC-Phalloidin to image the cell's cytoskeleton (Figure 6.9). In Figure 6.9a & 10b it is possible to observe the cells growing over the microspheres and the initial stages of bonding between the microspheres. In Figure 6.9c cell bodies can be clearly seen extending between microspheres, adhering to each other or to an adjacent microsphere. At this early stage in culture it is possible to see this supporting structure. At later time periods, it is obscured by high levels of cell proliferation growing on the original supporting structure.

Day 5 in Growth media

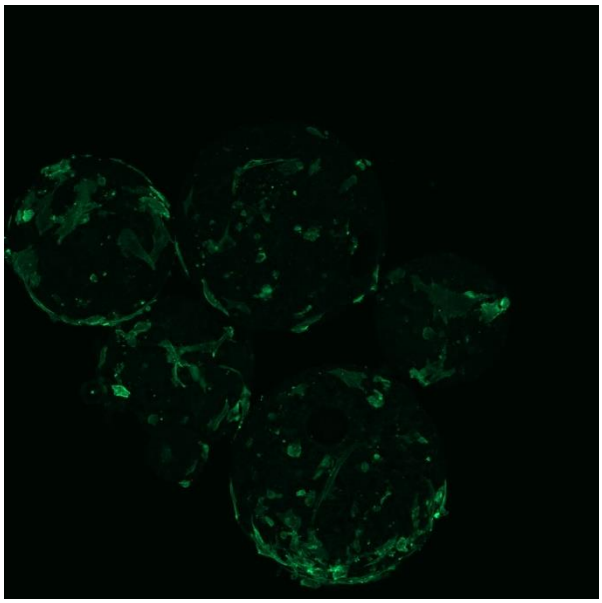

Day 5 in Supplemented media

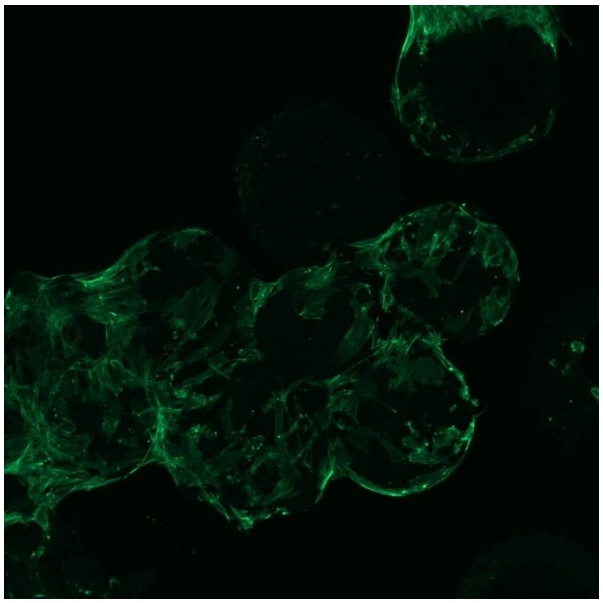

Day 5 in Osteogenic media

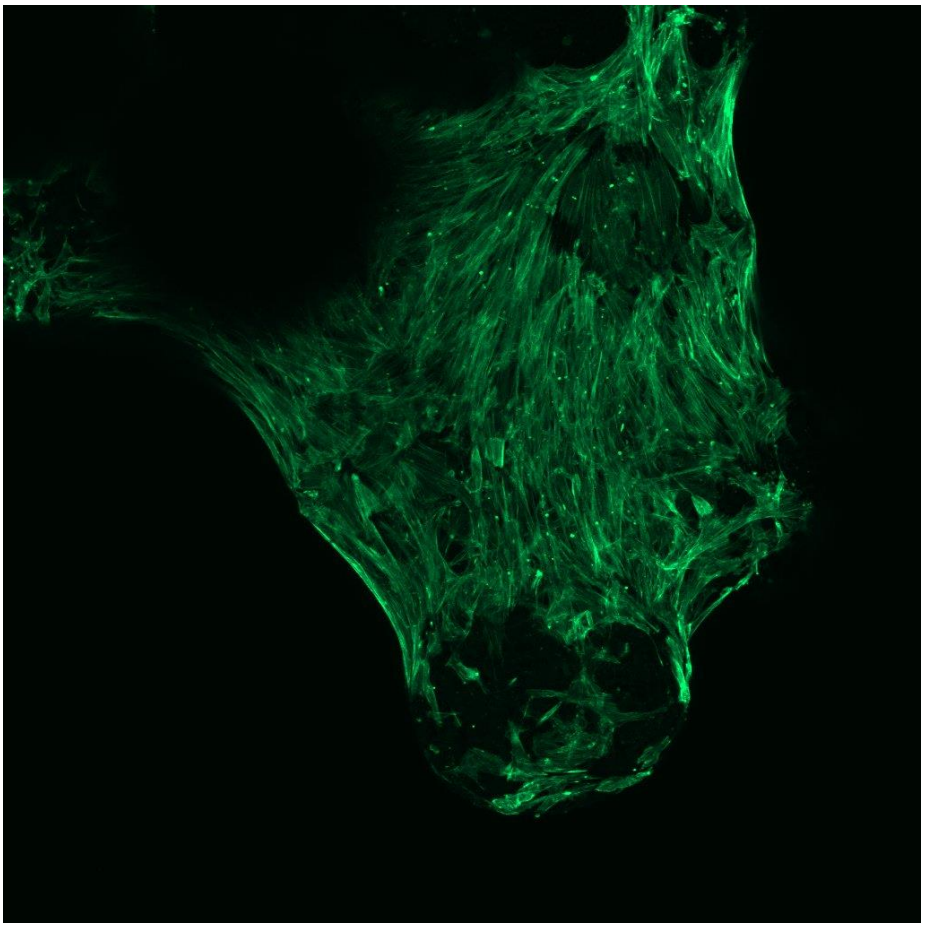

Figure 6.9. PCL polyHIPE microspheres cultured for 5 days in media with different additives and imaged with a confocal microscope. Only the FITC Phalloidin stain for f-actin (green) is shown here to highlight the structure of the cells cytoskeleton as they grow over and bind the microspheres together.

At the later time point of day 30 large numbers of cells can be observed covering the PCL microspheres (Figure 6.10). It is evident from the confocal images that the cells are highly aligned with each other in orientation. This is most notable in the deconstructed florescence images in Figure 6.10a & 10b. Even the nuclei (blue) have taken an elongated shape that follows that of the cell body (green). The histogram in Figure 6.10d shows a high level of alignment in the elongated nuclei from within the cells. This has been confirmed by measuring the nuclei orientation which can be observed in Figure 6.10d & e.

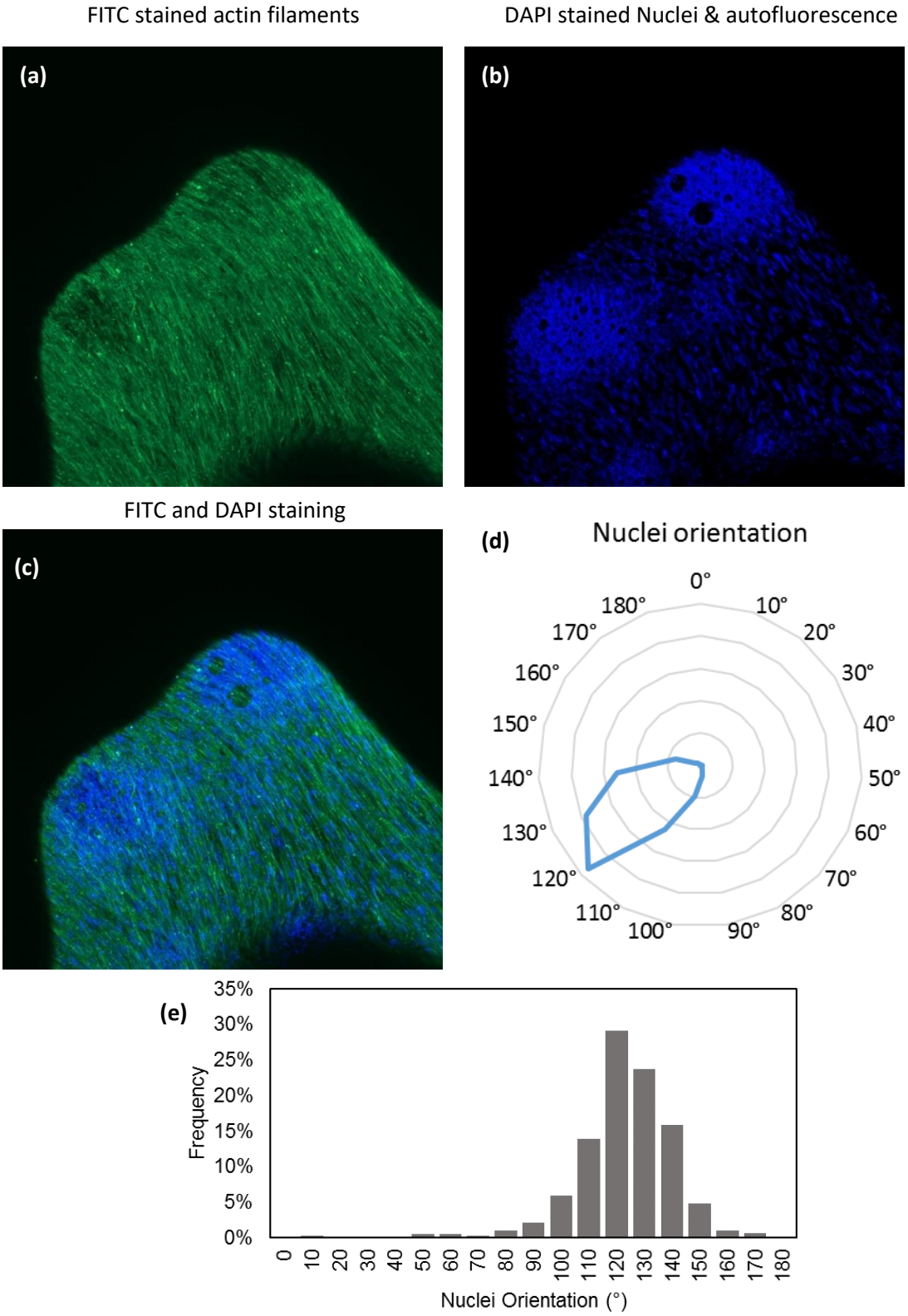

Figure 6.10. Confocal z-stacks of cells cultured on PCL polyHIPE microspheres after 30 days in culture and imaged with a confocal microscope. FITC and DAPI stains were used to stain the f-actin and nuclei respectively using fluorescence microscopy. (a) Actin filaments of cells growing on the PCL microspheres. (b) Nuclei of cells growing on the PCL microspheres. (c) Actin filaments and nuclei of cells growing on the PCL microspheres. (d & e) Radial and histogram plot of orientations of the nuclei found in (with respect to horizontal axis of image) (b) using cumulative frequency. n = 30. N = 4.

6.3.5 Cell ingrowth into polycaprolactone polyHIPE microspheres over time

Cells were found to grow into the PCL microspheres during culture with hES-MP cells (figure 6.11). Cells are observed within the microsphere's porosity by day 30 of culture. The morphology of the organic material within the internal porosity appears suspended between the edges of the pores Figure 6.11a & 11c). Fibres or cell protrusions can be observed running between pores, connecting the organic material within each pore to their neighbours (blue arrows). ECM/cell material which encases the microspheres and helps to bind them together into an agglomeration (Figure 6.11c & 11D). Figure 6.11 e shows an entire section of one of the microsphere-cell agglomerations. The ECM/cell network can be seen surrounding the microspheres.

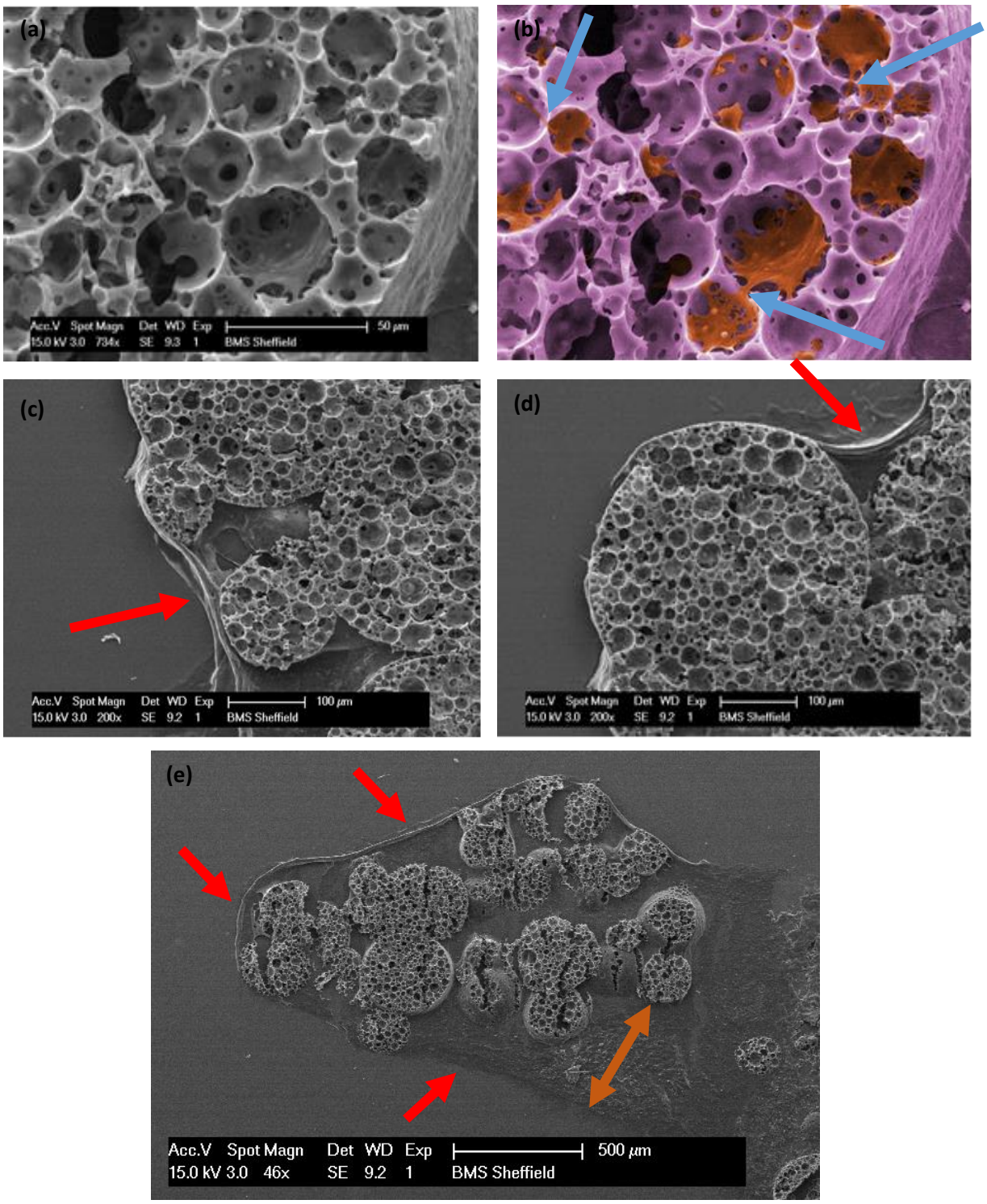

Figure 6.11. SEM micrographs of PCL microspheres cultured with hES-MP cells after 30 days in osteogenic media. Samples were sectioned to 40 µm thick and then imaged. (a) Cells/ECM is visible within the pores of the PCL microsphere. (b) False colour image of (a) with all biological matter coloured orange and the PCL material coloured pink. Blue arrows show where there are protrusions between porosity connecting cells. (c & d) SEM images showing the ECM build up around the microspheres which bound them into the agglomeration. (e) Low magnification image of an entire section of the clump. Microspheres can be seen within, surrounded by ECM material (red arrows). In some areas the microspheres are close to the surface of the ECM and in other areas there are several hundred microns between the microspheres and the edge of the ECM (orange arrow).

Cells infiltrated the microspheres over the 30 day culture (Figure 6.12). Samples were removed from culture a regular time intervals and the number of cells within the microspheres was measured. The different media the cells were cultured in appeared to influence the number of cells and the speed of which the cell grew into the microspheres. Cells cultured within growth media had the least cells within the microspheres and a significant difference was found between growth media and almost all the other media. Osteogenic media was significantly different to media containing ascorbate-2-phosphate with growth media. Cells cultured in growth media do not appear to increase significantly in number over time (Figure 6.12b).

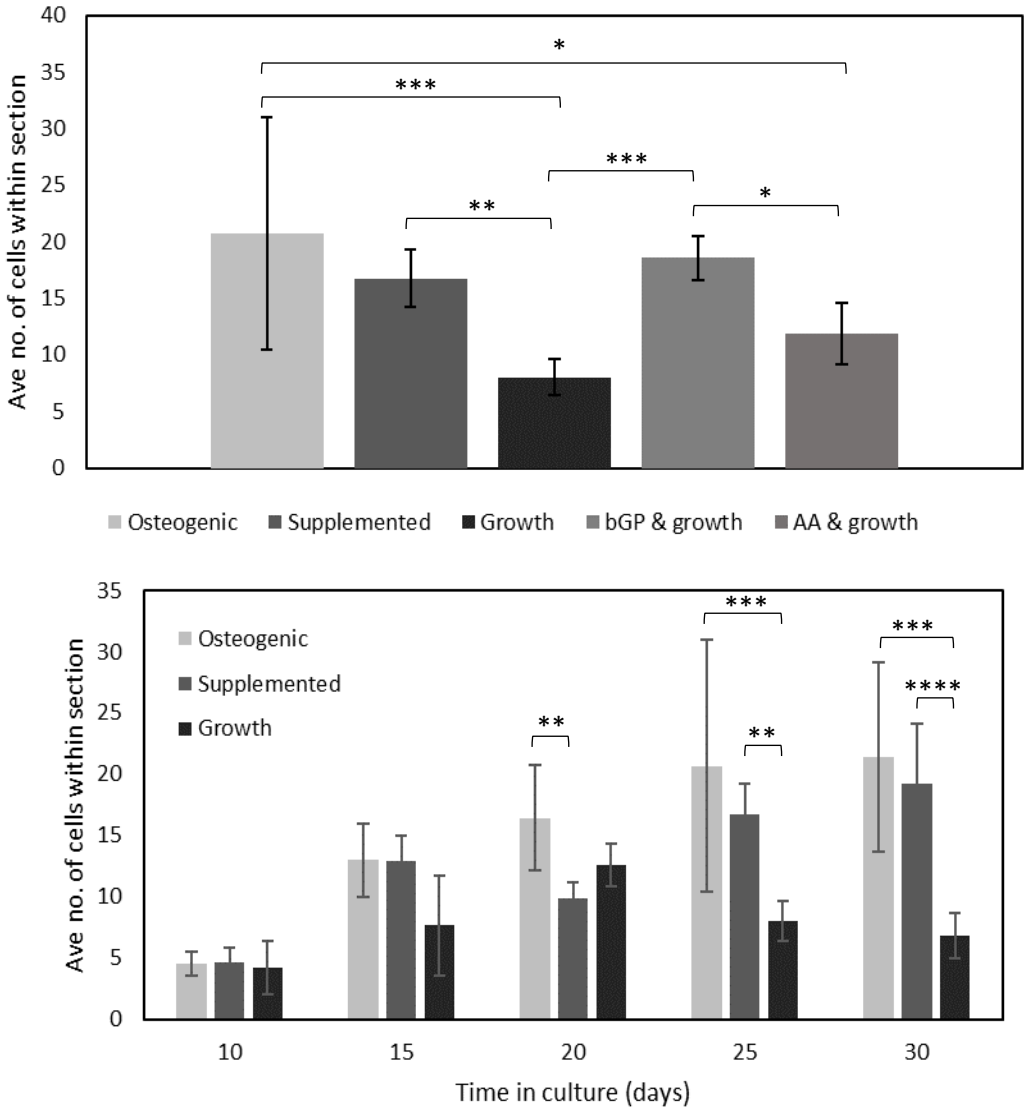

Figure 6.12. Microspheres were removed from culture at regular time points, sectioned and then the number of cells within each microsphere was counted. (a) Culture time point day 25 and investigating the effect of media additives on number of cells within the microspheres. ANOVA $p < 0.001$. $n = 6$, $N = 2$ Graph data is mean ± SD. (b) Cell ingrowth over time when cultured in 3 different mediums ANOVA $p < 0.001$. $n = 6$, $N = 2$ Graph data is mean ± SD

The culture medium used on the microspheres appears to have less of an effect on penetration distance of cells into the microspheres than on cell numbers within the microspheres (figure 6.13). Using osteogenic media will force cells to become osteoblasts. Supplemented will provide the minerals for osteoblasts but provides no impetus to differentiate. Growth media will hinder osteoblast formation due to the lack of minerals needed for that cell type. These 3 mediums are used to compare the effects of osteoblast formation on resulting cell migration. The depth of the cells into the microspheres did not increase significantly past day 10. This was followed up by investigating the ECM produced during cell culture.

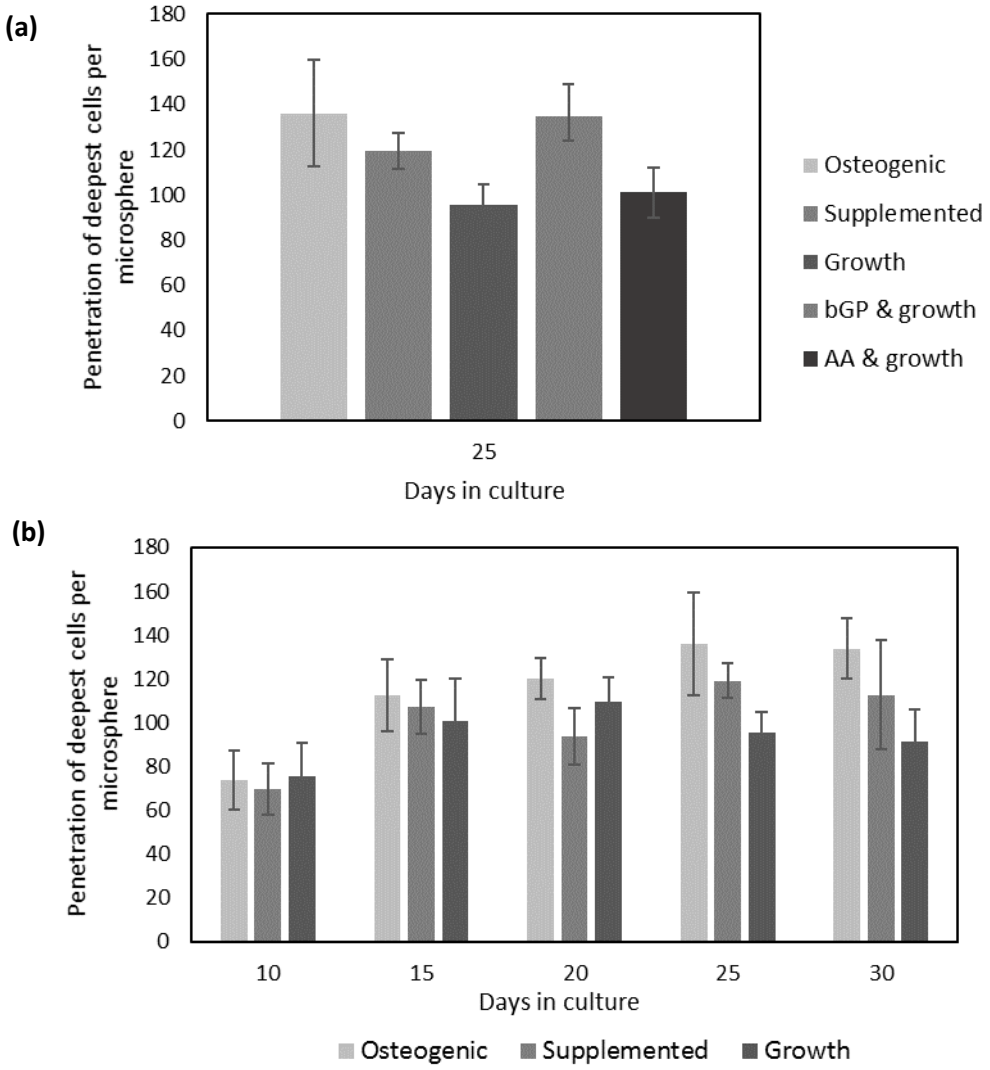

Figure 6.13. Microspheres taken at regular time points from culture, sectioned and stained with H&E to measure the distance of cell ingrowth. Cells were measured from their position within the microsphere to the nearest edge. (a) The effect of different media on cell ingrowth distance at 25 days in culture. (b) Cell ingrowth distance over time when cultured in three different media conditions. n =6. N = 2 Graph data is mean ± SD.

6.3.6 Measure of extracellular matrix within agglomerations of microspheres and cells cultured in media with different additives

H&E staining of the sectioned microsphere agglomerations show the microspheres are both bound by, and grown into, by the cells (Figure 6.14). At 30 days in culture it is apparent that most of the pores contain a cell/ECM construct. The structure observed in Figure 6.12e is reminiscent of those found within the pores of EHA/IBOA microspheres from chapter 5.

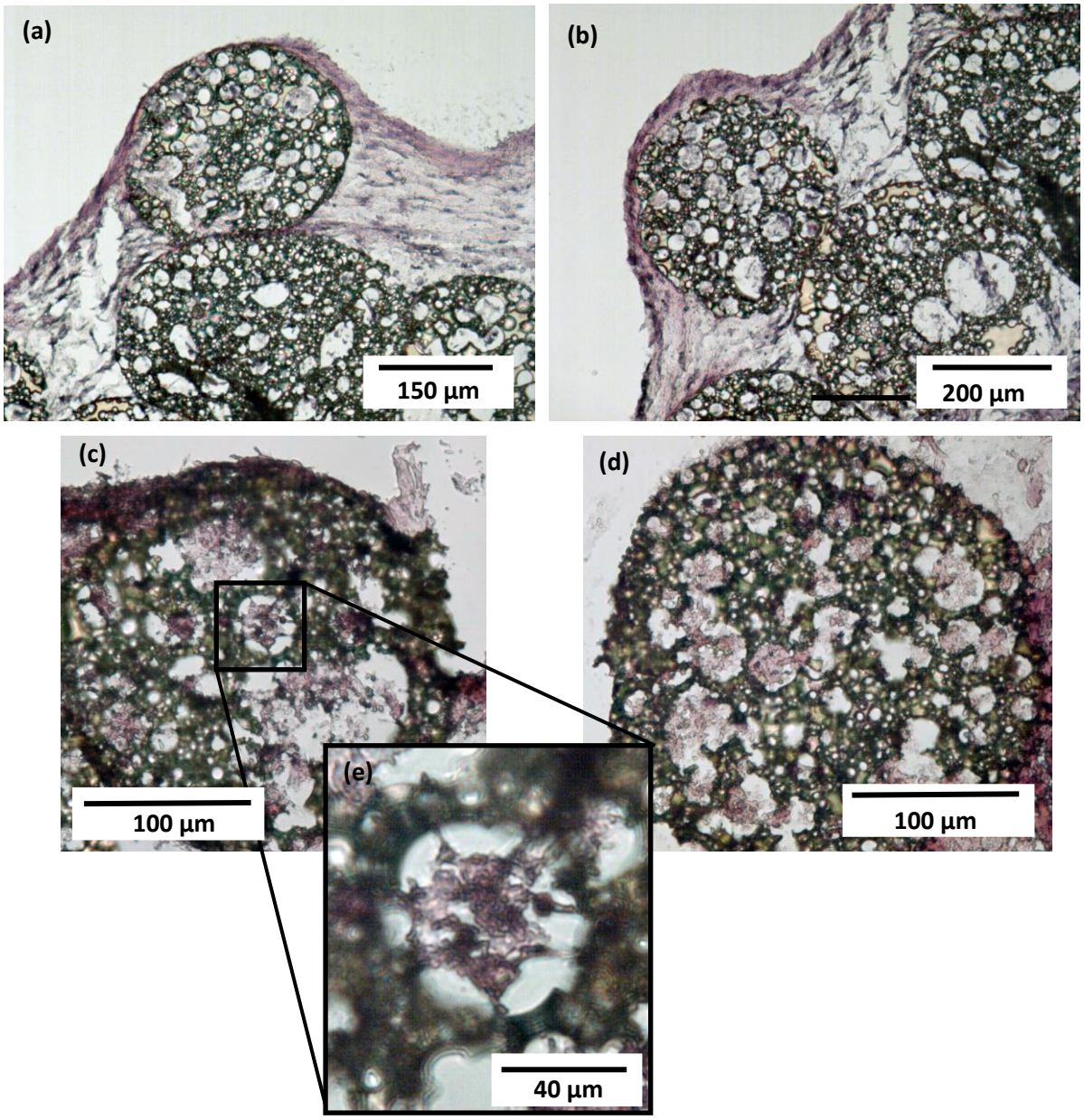

Figure 6.14. H&E stains of 10 µm thick sections of the aggregations formed with hES-MP culture on microspheres. (a & b) 15 days in culture using supplemented media. (c) Inside a microsphere after 30 days in culture with osteogenic media. (d) 30 days in culture using growth media containing βGP. (e) Higher magnification image of the cell/ECM morphology within the porosity of the PCL microsphere.

Collagen deposits are most prominent in the sample cultured in osteogenic media and least prevalent in those cultured in growth media (figure 6.15). Collagen is detected within every sample, regardless

of media condition with the brightest intensities found in 6.15e) High levels of collagen are present within the internal porosity of the microspheres (Figure 6.15f).

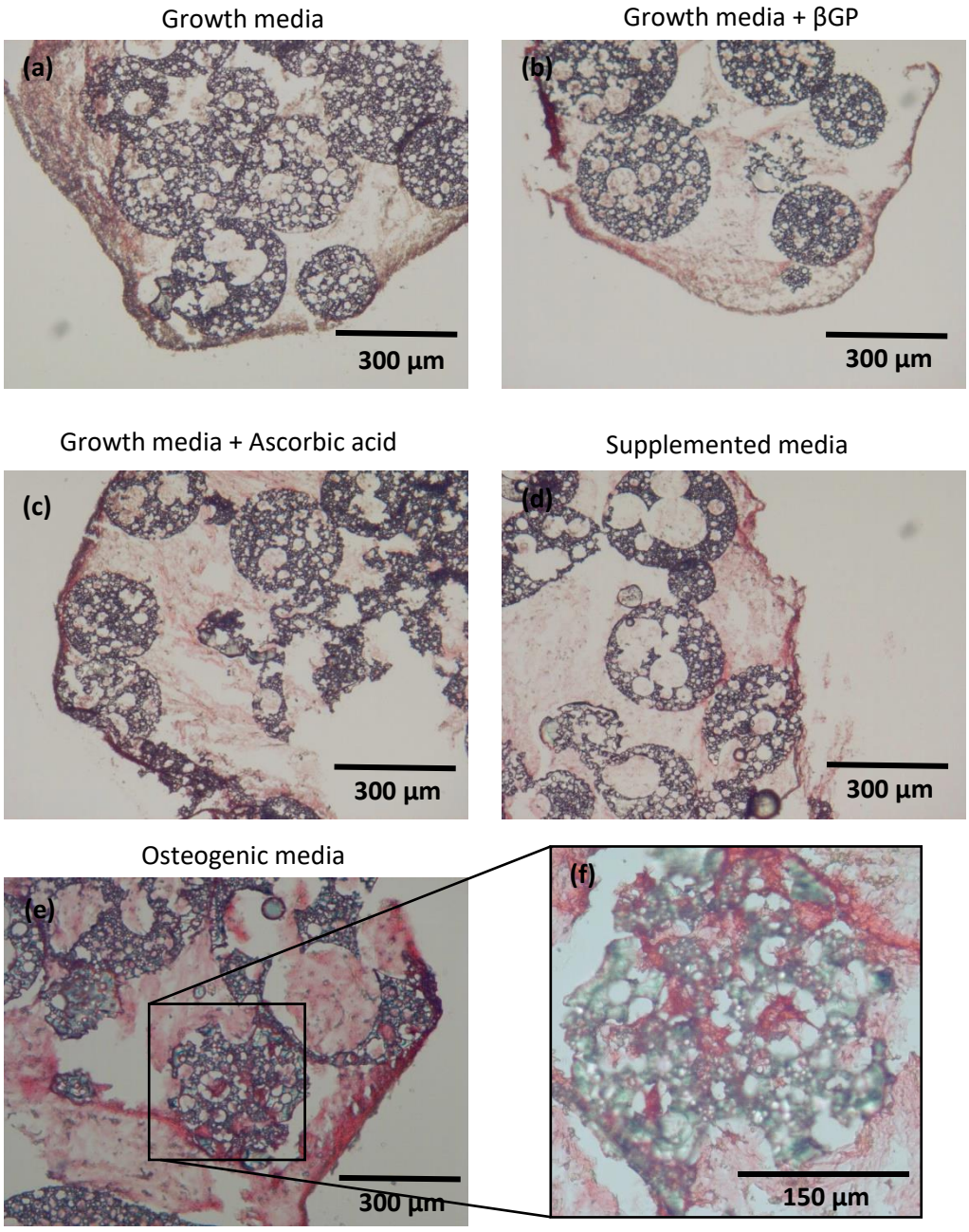

Figure 6.15. Sirius red staining for collagen deposits on sectioned microsphere agglomerations from day 30 of cell culture. Sections are 10 µm in thickness.

The alizarin red staining in shows the presence of calcium strongly in the cells cultured in osteogenic media but not in those samples cultured in any other media (Figure 6.16). Some positive staining can be observed around the microspheres cultured in osteogenic media (Figure 6.16e) with most of the

detected calcium surrounding the microspheres. Calcium can be observed deposited within the pores of the microspheres grown in osteogenic media (Figure 6.16f).

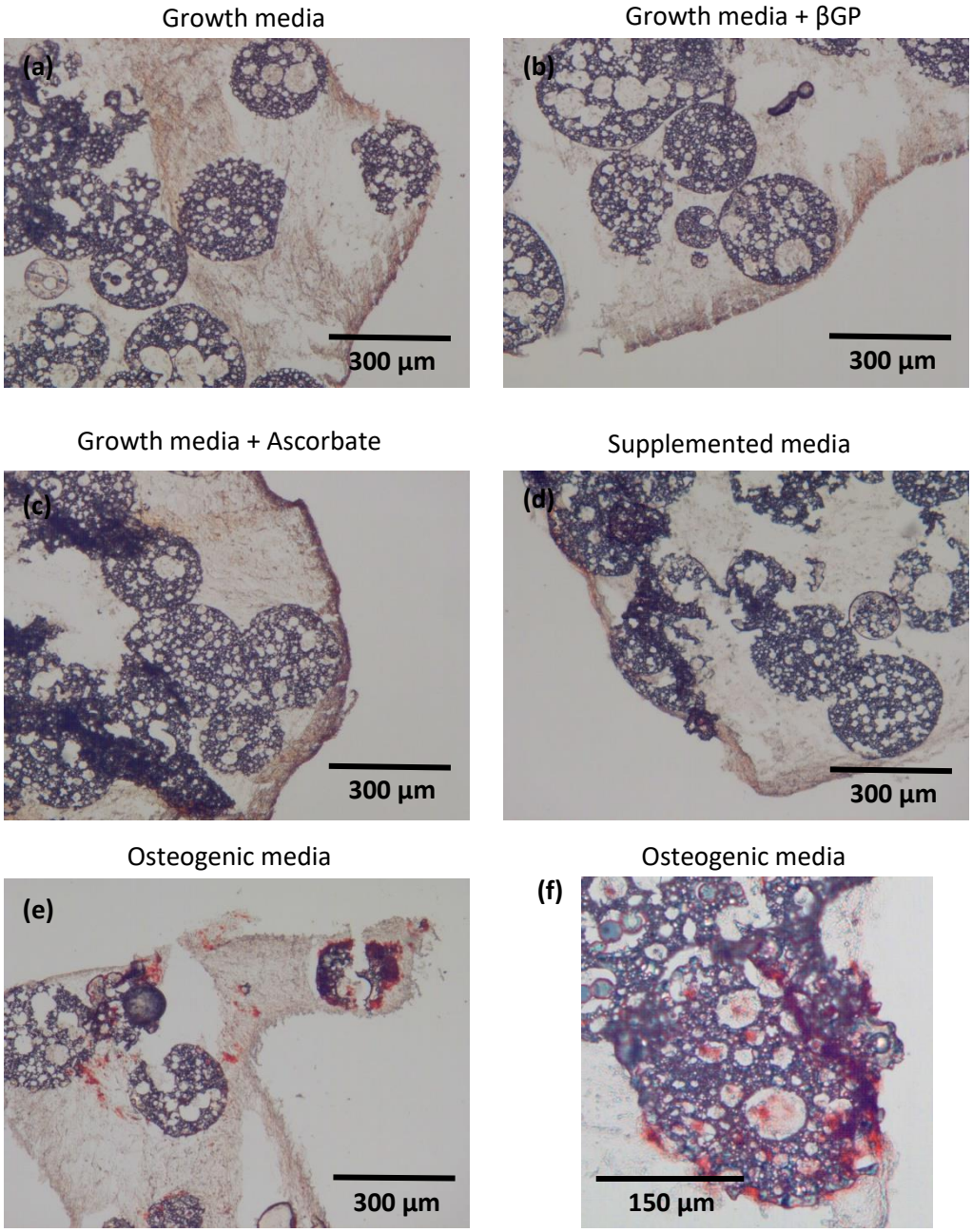

Figure 6.16. Alizarin red stain of calcium deposits within the microsphere agglomeration removed from culture after 30 days. Sectioned samples for 10 µm thick.

The toluidine blue stain shows that most of the proteoglycans present can be found outside the microspheres and it is equally evident for each media condition (Figure 6.17). Far less proteoglycans can be detected within the pores, unlike the results found previously with EHA/IBOA microspheres where a high intensity was observed within the pores.

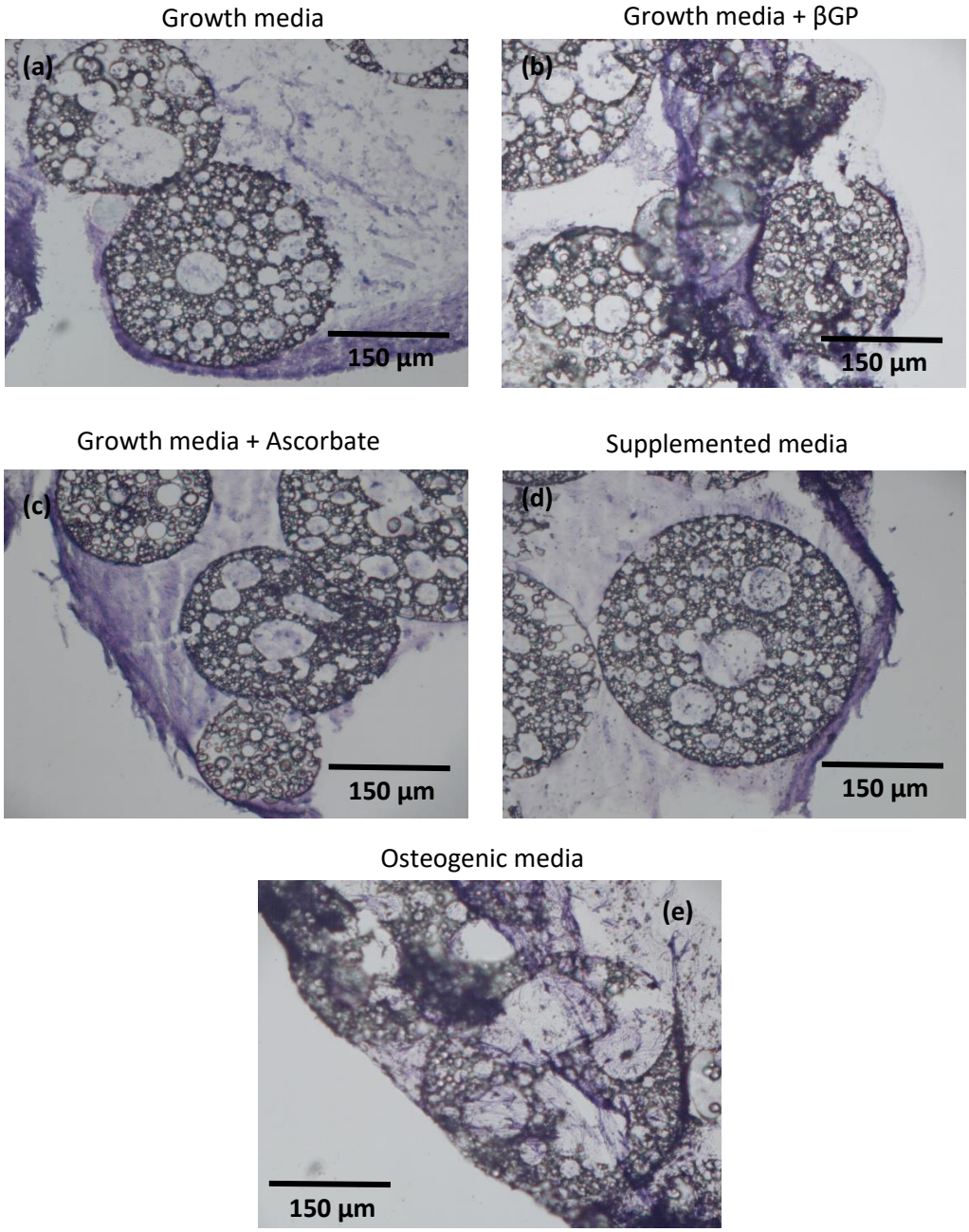

Figure 6.17. Toluidine blue stain of proteoglycans within the microsphere agglomeration. Samples removed from culture after 60 days. Sectioned samples using cryo-microtome at 10 µm thick.

6.4 Discussion

To the best of our knowledge a thiol-ene based polymer has not yet been used to form polyHIPE microspheres but the material has been used to form monolithic structures before. The formulation of thiol-ene polyHIPE material and its potential use in tissue engineering was first reported on by Caldwell *et al.* in 2012 [191], although a few years previously a 70 % porous material was produced by Gong et al. using thiol-ene polymers [361]. Gong et al. used their material to produce microspheres with porosity below 70% (and pedantically therefore not a polyHIPE) and without any interconnections between the pores [361].

The material initially looked promising for our application but a combination of difficulty in processing the material and inability to fully degrade prevented further use. The emulsion was highly stable, if more viscous than the EHA/IBOA material which made processing a little more difficult. This was especially true for attempting to form the microspheres with a T-junction microfluidic device. The experiment has not been included in this thesis but the resulting microsphere diameter distribution was high. The material was highly porous and contained larger pores than we had produced using the EHA/IBOA system. The material is also reported to be biodegradable [191], although it was only shown to degrade by 19% over 15 weeks. This would make it problematic to build a fully resorbable scaffold with the thiol-ene material. The incomplete degradation is an issue with all the photocurable polyHIPE materials, even with the PCL material. For while the PCL will completely degrade away it will leave behind the crosslinker, photoinitiator and any surfactant that was not removed from the polyHIPE during post processing. Biodegradable photo-initiators are available which could be used to replace the non-degradable one used in this application [362, 363].

Microspheres formed from the thiol-ene emulsion possessed surface topology that did not reflect the internal porosity being predominantly smooth skinned with pores occupying the minority of the surface area. This topology would make it more difficult for initial cell attachment, as the smooth surface could make it harder for the cell to adhere to initially [364, 365]. This surface porosity was also very small, with the upper pore size observed not much greater than 20 µm. As we observed in chapter 5 this would not prevent cell ingrowth but it might make it more challenging for the cells to begin to grow into the material. Despite this smaller surface porosity, the pores observed in the microspheres when sectioned appears similar to that of monolith polymer.

The thiol material supported hES-MP cells, when coated with pAAc, but there was no improvement over the EHA/IBOA polymer blend material alongside a lack of cell ingrowth. While the material did support cells, the results we obtained from the PCL material were superior in terms of cell growth, even without a coating. Cells were observed binding to the thiol-ene microspheres and the microsphere-cell agglomerations was successfully formed (Figure 6.2). Significant cell growth only

occurred on microspheres which had been coated with pAAc, those without a coating only supported limited cell growth. A critical finding was the lack of cell ingrowth into the microspheres after 14 days in culture, possible due to the reduction of open surface porosity. It is possible that on a longer time scale the cells may have grown into the microspheres but further experimental work was not undertaken once we began to use the PCL polyHIPE material.

Less cells were observed attaching initially to the microspheres during early culture which appeared to prevent cells from growing on the uncoated microspheres which had shown some success when using flat surfaces. When we initially conducted cell culture on the thiol-ene material (on a flat sheet) cells adhered to the non-coated scaffold. This result was not repeated when we moved onto culturing with microspheres. When culturing on flat sheets cells have longer to attach to the surface when seeding than for microspheres. When seeding on a flat sheet the cells fall and rest on the scaffold which gives them time to attach to the scaffold. A problem with microsphere culture is that the cells usually only have a brief time of contact with the microspheres while seeding. Thus, we often used a great many more cells in our 3D cultures than we did for 2D culture (not unexpected). Many other authors using 3D materials use large numbers of cells and not just for microsphere culture [366].

When culturing hES-MP cells with osteogenic and non-osteogenic media there was no impact on the amount of DNA collected, but the ALP/DNA was strongly impacted by the different media. The control showed a standard growth profile, with the slowest growth for the cells in osteogenic media and fastest for those in growth media. Conversely there was no difference between the DNA quantity for cells cultured in the different medias on the material. However, when we looked at ALP production per unit of DNA, we find that the media does have a profound effect on the cells. Cells cultured in osteogenic media produced significantly more ALP than those cultured in supplemented media, and these had significantly higher ALP production in turn when compared to growth media cultured cells.

The benefits of using the PCL polymer as a material for the microspheres is in the fully degradable nature of the material and its long history of use in the medical device industry [357]. Its degradability is especially suitable for bone, due to its long term degradation profile to minimise the quantity of acidic degradation products over a period of time and allow the inclusion of a high degree of porosity without degrading faster than bone can regenerate [357]. Usually the poor mechanical properties of PCLs prevent it from being used in load bearing applications but this does not hinder its use for our application. There are few fully degradable polyHIPE materials [367], with those reported on often being only partially degradable [360, 368].

In addition to the biological benefits of the material, PCL can be more easily processed into a polyHIPE as it is hydrophobic. This hydrophobicity is required for forming an emulsion with water as the internal phase. The opposite to a w/o does exists in an oil-in-water emulsion, where the bulk phase is a

hydrophobic oil material and the polyHIPE is formed from hydrophilic materials. Considerable post processing is required for these polyHIPEs as large quantities of oil need to be removed from the polyHIPE before use. PCL is not an ideal material polyHIPE manufacturing as it forms a far more viscous emulsion than those used previously in this study. It is thought that this property made the emulsions far more unstable, although it is difficult to pinpoint a definite explanation.

The microspheres produced from the photocurable PCL emulsion were open pored and the porosity extended throughout the entire scaffold. A higher number of pores can be found on the exterior of the PCL microspheres than was observed for thiol-ene microspheres. Both CTSR and T-junction microfluidics were used to form the microspheres. The emulsion was unstable which made it unsuitable for storage greater than an hour and would have made it unsuitable to thermal curing. This imposed limitations on the T-junction microfluidic method as fresh emulsion was required regularly.

The surface topology of the microspheres where not identical within the population, some appear smooth, while other are very rough, yet both are highly porous. This was also observed in populations of EHA/IBOA microspheres formed from the CSTR method. The difference this could make for cell attachment is significant, with the rougher surface providing a greatly increased surface area for cells. The difference in surface topology is likely due to the different flow velocities within the CSTR. Solution close to the stirrer when compared to that around the edge of the vessel will be traveling at different speeds and difference shear forces would therefore occur. However, this should have result in a greater number of microsphere's exhibiting this roughness when the stir rate was increased to get smaller microspheres. This has not been observed in previous experiments but it was also never directly investigated. If it could be determined how to increase the proportion of microspheres with this rough morphology it could allow for an increased surface area and allow interlocking between microspheres and the surrounding bone tissue.

The internal porosity of the PCL microspheres was the smallest of the 3 polymer emulsions used, when produced under the same conditions. It would have been expected that the least stable polyHIPE would have contained the larger pores due to the material attempting to reduce its surface tension by minimising surface area. This might be due to the difference in fabrication for which the PCL was made using a magnetic stir plate and a magnetic flea instead of an overhead paddle. The pore size could still be tuned by using similar methods to those in chapter 4, although those experiments were not repeated with PCL.

The interconnections between the pores are on a similar scale as those from the EHA/IBOA system and appear to not be a barrier to cell migration. SEM images of microspheres in Figure 6.5 show cells inhabiting a pore with a diameter of 11 μm in size. Lu et al. found that osteoblasts can only pass through interconnections 20 μm or larger, to find cells within pores less than this size is interesting [333]. This

might indicate that osteoblasts can indeed move through and inhabit smaller spaces or that the cell type involved is not an osteoblast cell or that it may be some stage of pre-osteoblastic cell. The histogram in Figure 6.5 indicates that most pores within the material are larger than 11 µm. This means the majority of the materials porosity would be accessible to cell ingrowth. In a direct comparison to the microspheres formed from the EHA/IBOA system the surface porosity appears very similar (Figure 6.6).

The slow degradation of the microspheres ensures that there would be ample time for proliferation, mineralisation and remodelling of the new tissue before the scaffold disintegrated. A simple degradation study was carried out with the PCL material (Figure 6.7). The documented bulk degradation rate for PCL is 3 – 4 years [357]. For a PCL, porous microsphere, the rate is likely to be much faster due to the huge surface area of the material in contact with the solution. The PCL used is also highly crosslinked, making it more amorphous, and therefore prone to faster degradation. As with all tissue engineering utilising degradable scaffolds, the ideal would be for the scaffold to degrade as bone tissue replaces the scaffolds. As long as the scaffold did not degrade too rapidly, it would be suitable for bone regrowth. After 60 days in water the polymer had degraded by 25% and in the accelerating solution which is highlighted by Göpferich's study to increase the degradation rate by a factor of 10 [369] it had degraded by 80%.

Cultures of hES-MP cells were shown to grow successfully on microspheres not coated in pAAc, in contrast to previous materials studied. There is some debate over the suitability of the untreated PCL surface material in the literature for bone tissue engineering with many studies finding inferior cell growth compared to treated surfaces [370, 371]. Many examples exist of treatments that would only improve the biocompatibility further [372]. Previous materials within this thesis required a coating of plasma deposited acrylic acid to increase their biocompatibility sufficiently for stable cell growth. Using PCL would provide the option of removing this step from the methodology and reduce the cost of any potential treatment.

The culture rapidly formed into agglomerations in a similar fashion to those of the thiol-ene and EHA/IBOA polyHIPE microspheres and cells appeared elongated on the surface of the structure. A new method of investigating the agglomeration is in Figure 6.9 where only the cytoskeletons of the cells have been imaged. This gives a much clear indication of how the cells are positioned on the surface of the microspheres and to each other. When growing over a microsphere they appear to spread out into a flatter and more circular morphology but when they are binding the microspheres together the take on a much thinner and aligned morphology (also observable in Figure 6.10). This structure appears similar to that of myofibroblasts or fibroblast cells. This linear formation is likely to reduce later on in culture as cells proliferate and the pressure for the shape is no longer so urgent (holding the

microspheres together). Unless the alignment/morphology of cells below influence the new cells above the morphologies are likely to become more randomly aligned.

The bone cells we are aiming to stimulate typically have a more spherical morphology, this morphology is present within the pores of the microsphere but is not what is observed outside of the microsphere environment. Cell shape plays a very crucial role in cell behaviour and differentiation [373, 374]. Some papers claim that a method of differentiating a cell is supported, if not enabled, by forcing the cell to assume the morphology of the desired cell type [374]. The stretched appearance of the cells is reminiscent of tissue such as muscle or ligaments. It is a possibility these exterior cells could form into fibroblast like cells if left without the additional stimulation of dexamethasone from the media.

Ingrowth of cells into the PCL microspheres can draw many similarities to the cells cultured in the EHA/IBOA system although βGP plays a more significant role in cell ingrowth rates. Culture in growth media still appears to reduce the ingrowth of cells into the microspheres, although to a lesser extent than found in section 6.3.12. For PCL microspheres, only growth media with ascorbate-2-phosphate was significantly different to any of the other media with supplements. The addition of ascorbate-2-phosphate for EHA/IBOA microsphere culture stimulated the lowest level of ingrowth. However, in that experiment there was a significant difference between ascorbate-2-phosphate in growth media compared to growth media, which was not the case for PCL microspheres. It appears that ascorbate-2-phosphate contributes the least, out of all the supplements, in terms of allowing cells in grow into the microspheres. For this experiment, it appears that βGP by itself as a supplement was just as effective as supplemented media, whereas for the EHA/IBOA material they appeared to have a synergistic effect on cell ingrowth. The work within this thesis is insufficient to draw any strong conclusions on the roles of βGP and ascorbate-2-phosphate, which would require more research to determine if the effects are genuine or statistical artefacts.

The penetration depth of cells does not appear to change significantly after the 15th day in culture but the number of cells does increase. Cells reach their deepest penetration depth by day 15 and then cells are rarely found deeper after this time point. The number of cells increases within the microspheres over most of the experiment (until day 25). As it is possible for osteoblasts to differentiate [375] it does not rule out the presence of osteoblasts but it may be that these early cells are a form of pre-osteoblastic cell which proliferates and then differentiates to osteoblasts within the pores.

There are indicators that the cells within the microspheres were at osteoblastic in nature and not chondrocytes. For osteogenic media both calcium and collagen were detected by staining techniques. Interestingly both were strongly detected within the pores of the microsphere, confirming osteoblastic activity within the pores. The appearance of the calcium is very granular which concurs with the findings of the previous chapter and the SEM images in this chapter which show nodules within the

organic material inside the pores. No calcium was easily detected in supplemented media, although day 30 is an early time point and samples from a day 60 time point might have revealed calcium deposits. Collagen deposits are visible on microspheres cultured in supplemented media, indicating some activity, but none was detected within the internal porosity. Proteoglycans were detected within the agglomeration but only at very low levels from within the pores. This indicates that the cells within the PCL microsphere are not chondrocyte cells.

6.5 Conclusion

Degradable materials were investigated in terms of both fabrication and biocompatibility and both polymers were formed into polyHIPE microspheres through the double emulsion technique. The aim was to repeat the experiments from the previous chapter in a degradable material to see if the same results would be found. Initial cell growth was positive on the thiol-ene HIPE but the material was not used further when the fully degradable PCL was evaluated and compared. The thiol-ene microspheres has a more closed surface porosity, with smaller and more sparse pores on the microspheres surface. PCL microspheres were found to be degradable in an accelerated study. PCL was found to not only support cell growth without acrylic acid coatings, which is superior to the EHA/IBOA polymer. The PCL polyHIPE microspheres also allowed ingrowth of cells, cell colonisation within the pores and cell mediated aggregation. Less testing was done on the cells within the material than in chapter 6 but indicators are consistent for osteocyte presence. A decrease in the quantity of proteoglycans was detected when considering the quantity found in the EHA/IBOA polyHIPE.

Chapter 7: Assessment of PolyHIPE microsphere's vascularisation potential using chick chorioallantoic membrane assays

7.1 Chapter aims

1. Measure the vascularisation potential of polyHIPE microspheres within a CAM model
2. Evaluate the differences between porous and non-porous microspheres in terms of vascularisation potential
3. Compare vascularisation potential of EHA/IBOA polymer to PCL polymer microspheres
4. Measure cell survival after undergoing an injection study for delivery

7.2 Introduction

In this chapter, we take the polyHIPE microsphere system to the next stage of testing, having replicated the results of the EHA/IBOA model in PCL microspheres. An injectable tissue engineered solution must be able to vascularise the wound bed it is introduced to, otherwise mass cell death will occur within the scaffold and the new tissue will fail. In this chapter, we investigate the vascularisation response of both PCL microspheres and EHA/IBOA microspheres and compare between the two. The scaffolds were being implanted using the *in-vivo* CAM assay to assess the angiogenic potential of the scaffold. The effect of the length of time of pre-culture of the microspheres with hES-MP cells will be investigated by analysing the angiogenic response, alongside investigating both materials.

7.2.1 Vascularisation of tissue engineered scaffolds

Vascularisation of tissue engineered scaffolds is a major stumbling block in producing full thickness tissues or complete organs [224-226, 238, 376]. Currently only thin scaffolds such as bladder, or avascular tissues such as cartilage or cornea have found success in the clinics. Cells require a fresh supply of both oxygen and nutrients whilst removing waste products such as carbon dioxide and water. The diffusion limit for oxygen in a tissue is 200 μm, the distance at which capillaries are spaced throughout tissue in the body [228]. When a scaffold is designed for tissue engineering any cells beyond this diffusion limit require a blood supply to provide them with the essential nutrients. Without this, cells will be unable to survive and end up undergoing necrosis, releasing many chemicals and enzymes into the local environment. Even a brief lack of vascularisation can cause hypoxia and cause the cells to release hypoxia signalling biomolecules, which may have unintended or unplanned effects [216, 217]. Several techniques exist for vascularising a scaffold which are discussed in more detail in the literature review. The only practical method for vascularising an injectable scaffold is to use in-vivo angiogenesis and to allow room for rapid vessel ingrowth and provide biomolecules to enhance the response.

7.2.2 Injectable microspheres and vascularisation

For injectable bone tissue fillers the method of vascularisation is angiogenesis, that is the stimulation of new blood vessels from existing vasculature [230, 231]. As this scaffold is injectable it is impossible to vascularise in advance and must initiate a rapid response from the local blood supply. This may place a limit on the diameter of a void it can be used on in the body. Current engineered solutions for bone voids usually avoid using cells, to circumvent this problem and allow cells to encroach from the periphery of the implantation site and for the remodelling to begin on the outside and work inwards [27, 377]. This method is far slower than if the scaffold was already pre-seeded with cells.

7.2.3 Chorioallantoic membrane assays as a measure of vascularisation

The CAM assay is a technique to investigate the in-vivo response of a scaffold or treatment on the chorioallantoic membrane of a chicken embryo [378-381]. This is used in tissue engineering as a model to test the vascularisation response of scaffolds in a complicated system. Scaffolds are introduced through an opening in the shell and then the egg is incubated for 7 days, before the egg shell is reopened and the resulting vascularisation can be analysed [381]. The technique less demanding on resources to run high sample numbers due to the easy of acquisition and low cost storage requirements [379]. The CAM assays allows for very complicated responses and analysis of a multitude of cell responses to the implant [380]. However, the animal in question is not mammalian and the vascularisation response of the CAM is far greater than would be found in humans beyond the embryonic stage of development. This technique still provides valuable information on whether further testing in full *in-vivo* studies in mammals can be justified.

7.2.4 Major contributors to the chapter

I would like to acknowledge and thank Giulia Gigliobianco for the work on the implantation and retrieval of the implants in all work using the CAM model in this chapter.

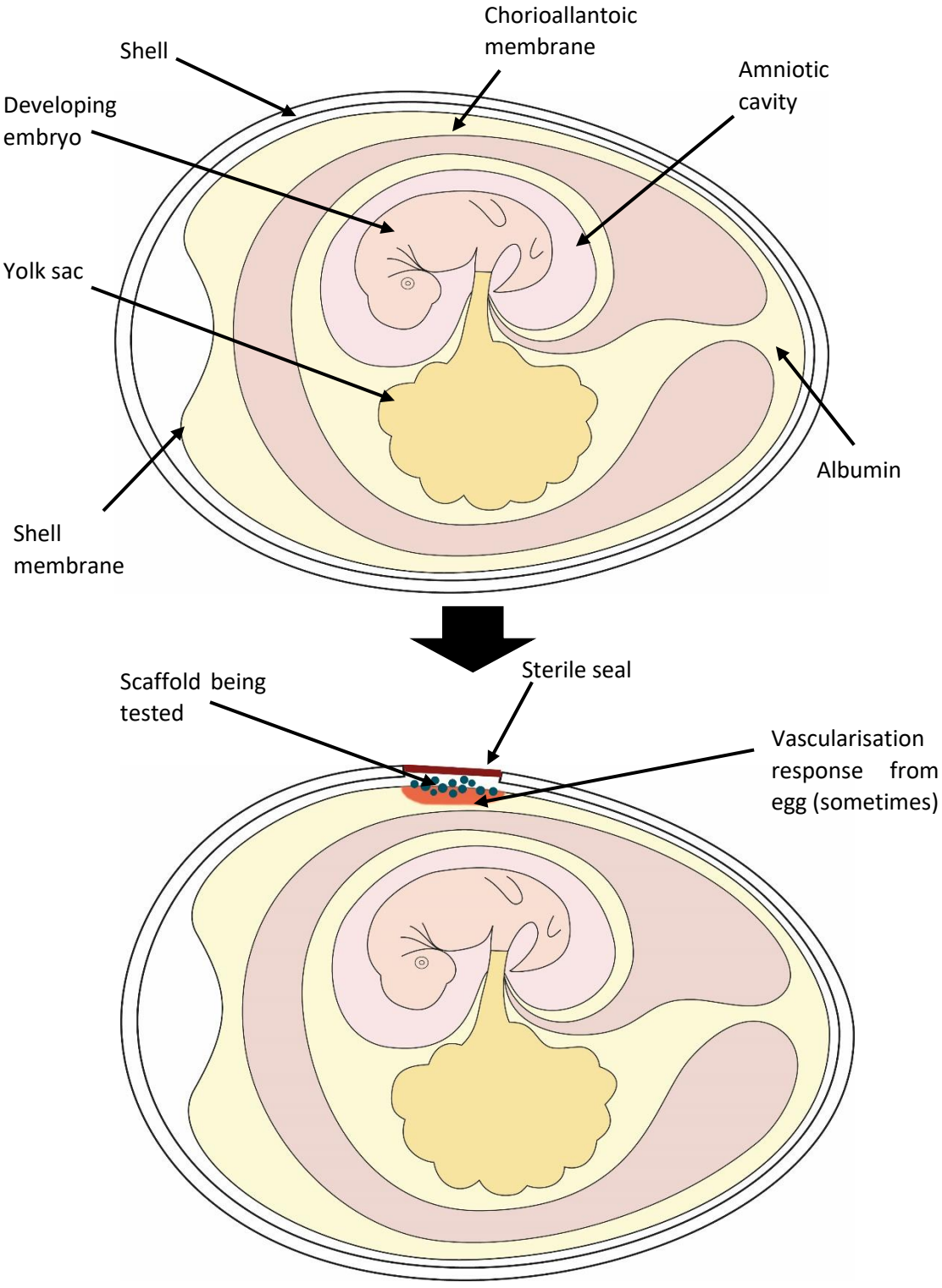

Figure 7.1. Diagram of the CAM assay. Shell is removed and the implant is positioned onto the CAM, after which the shell is re-sealed to prevent infections.

7.3 Results

7.3.1 Vascularisation potential of EHA/IBOA polyHIPE microspheres assessed using a CAM assay

The level of vasculature for microspheres appears far greater than that found in the control samples and microspheres without cells appear to have a significantly less angiogenic effect on the CAM than those pre-cultured for 21 days before implantation (Figure 7.2). After implantation and incubation for 7 days the chicken egg was opened to expose the implantation site and the exposed area was imaged. Microspheres which had been precultured had formed into the agglomerations discussed in previous chapters. Porous microspheres without cells were added to a similar location, although the microspheres often moved during incubation. There are high levels vasculature in the area surrounding the implant (Figure 7.2a).

Seeded microspheres

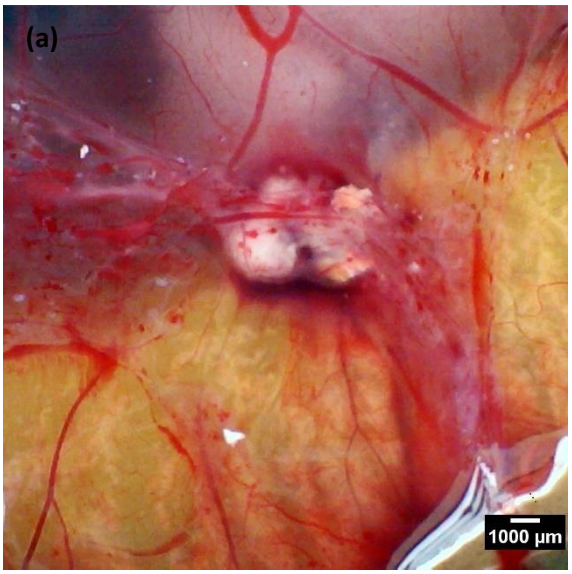

Unseeded microspheres

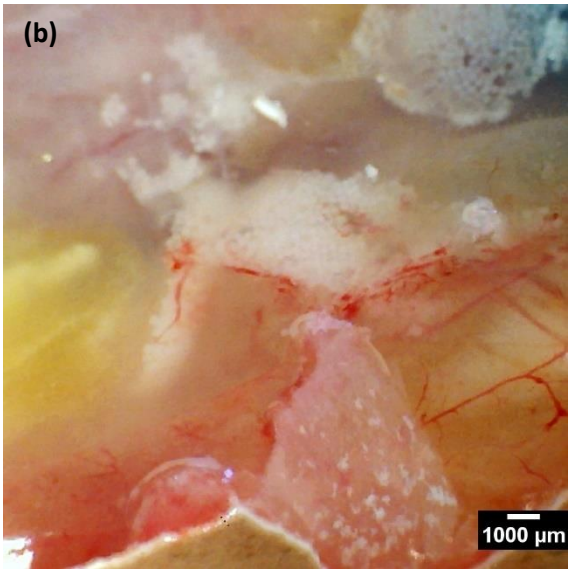

Control

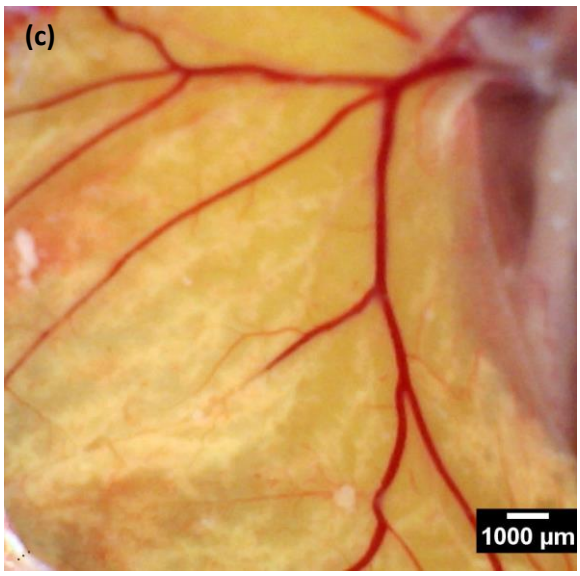

Figure 7.2. Optical images from a handheld USB microscope of the implant site within the CAM models after 7 days incubation. (a) Microspheres were seeded with hES-MP cells for 21 days before implantation into the CAM. (b) Microspheres that were not pre-cultured with any cells. (c) Control from a CAM which had been opened for implantation and then closed.

Pre-seeded microspheres had a significantly higher response vascularisation response than the control or the microspheres devoid of initial cells (Figure 7.3). The number of blood vessels within the implant site were counted along with the number of branches that the blood vessels had. This difference is both for the number of blood vessels present and the branches on each vessel. This confirms the results observed visually in Figure 7.2. There was no statistical difference in the number or bifurcations of the blood vessels between un-seeded microspheres and control CAMs.

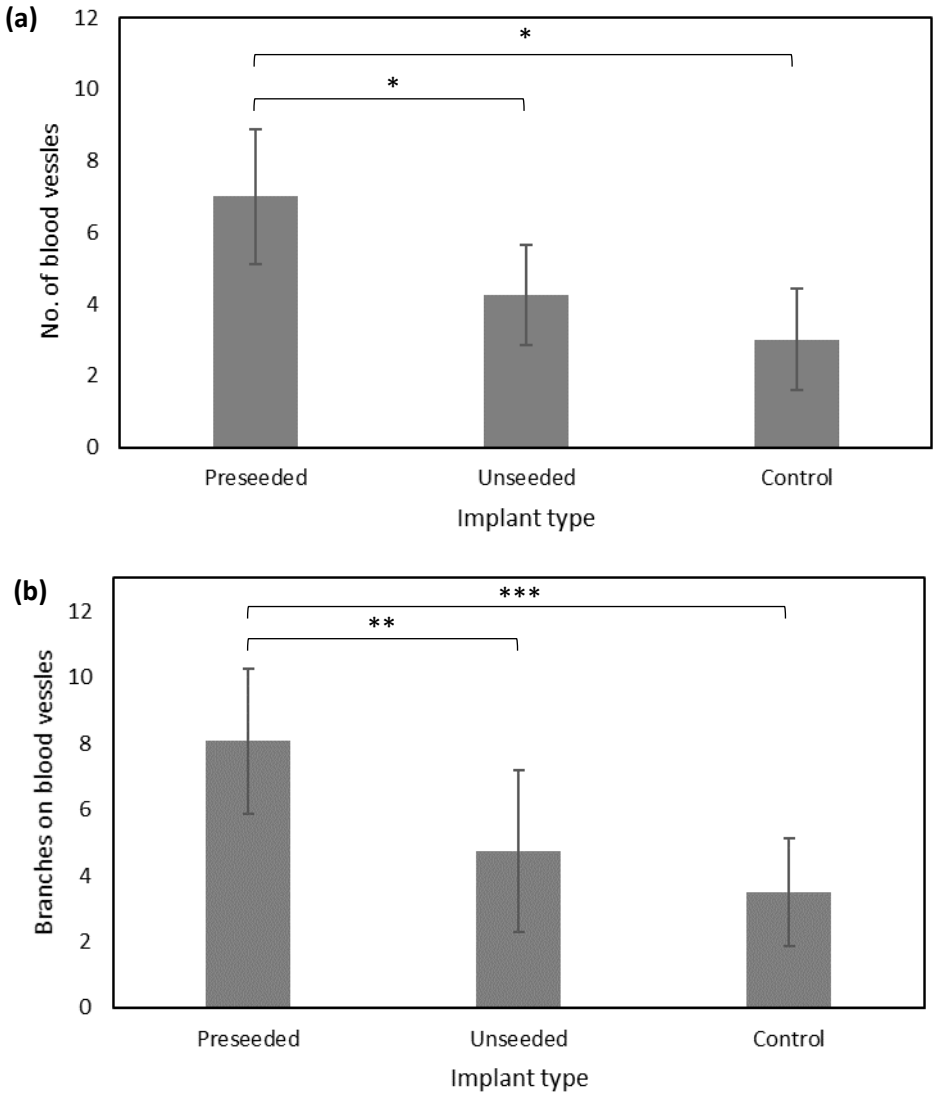

Figure 7.3. (a) Number of blood vessels around the implant were counted over a series of images and displayed on the graph. Significant differences in vessel number was found between the pre-seeded microspheres when compare to the other two implant types (ANOVA). (b) A measure of the number of branches a blood vessel has within a certain area from the implant. Significant differences were found between the pre-seeded microspheres and the other implant types. n = 6 N = 1.

When comparing the cells found within the microspheres a difference in morphology can be observed along with delamination between microsphere agglomerations and the surrounding chick tissue (Figure 7.4). During sectioning, it appears that these tissues have delaminated from one another, suggesting a weak interface or adhesion (Figure 7.4c). For unseeded microspheres, the CAM tissue grows around and incorporates the microspheres (Figure 7.4e). In addition, the cells from the CAM grow into the unseeded microsphere over 7 days. The hES-MP cells in pre-seeded microspheres show the osteocyte like morphology observed in previous chapters (Figure 7.4d), a morphology not observed in cells in unseeded microspheres (Figure 7.4f).

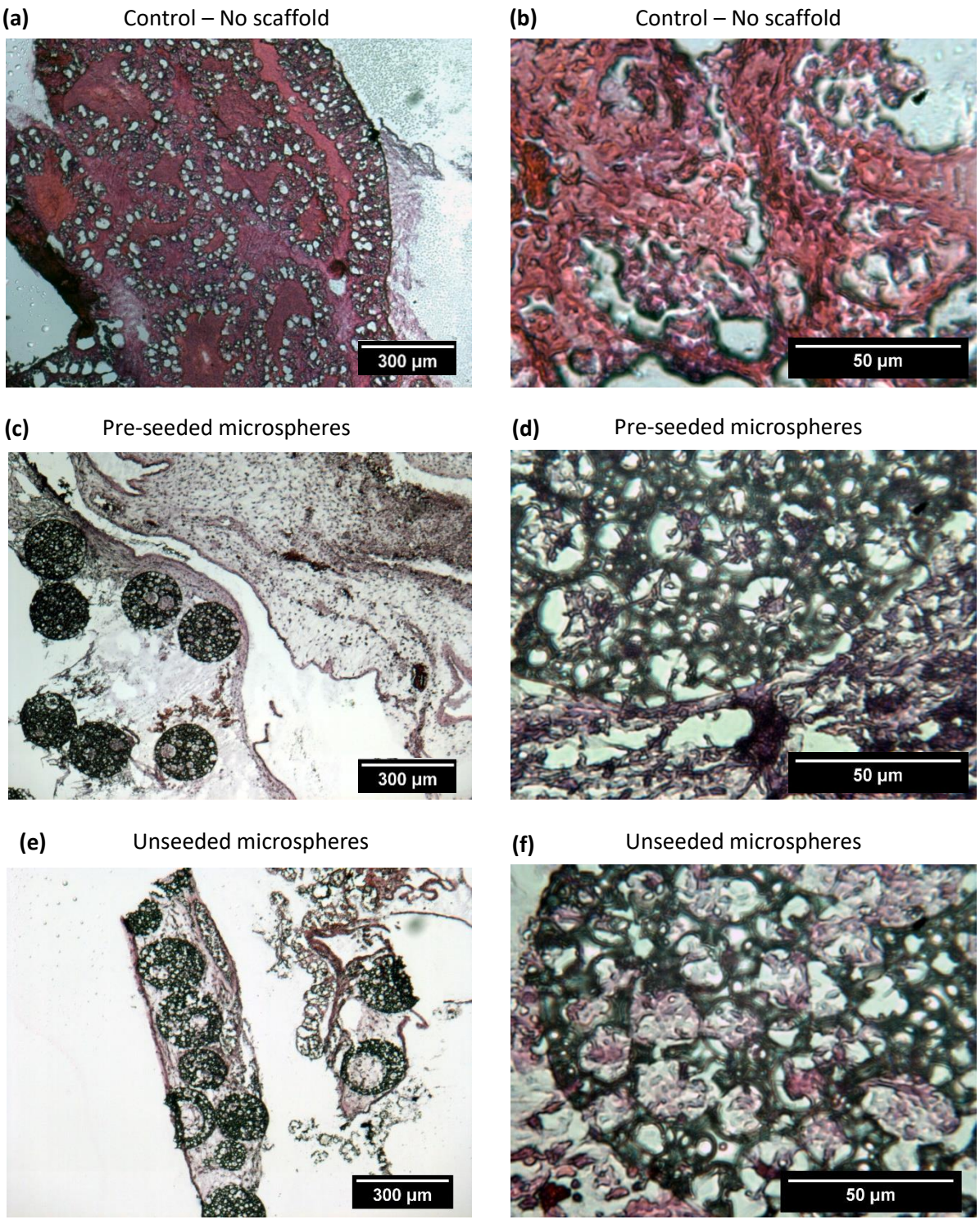

Figure 7.4. H&E staining of 10 µm thick sections of scaffolds and tissue extracted from the implant area. (a & b) Staining of the implant area of the control CAM assay. (c & d) Images from the seeded microspheres, cells can be observed within the pores of (d). (e & f) Images of the unseeded microspheres embedded in CAM tissue. Cells can be seen within the pores of (f) after the 7 days in in-vivo.

For the agglomerate microspheres, the chicken cells can be seen lining up along the interface but with very few penetrating into the tissue (Figure 7.5). Chicken egg blood cells autofluorescence red and their location can be interpreted from the combined presence of actin, indicating a cell, with the red

auto-florescence. For the unseeded microsphere, it can be seen that the chicken cells have surrounded the microspheres and are present within each of the microspheres.

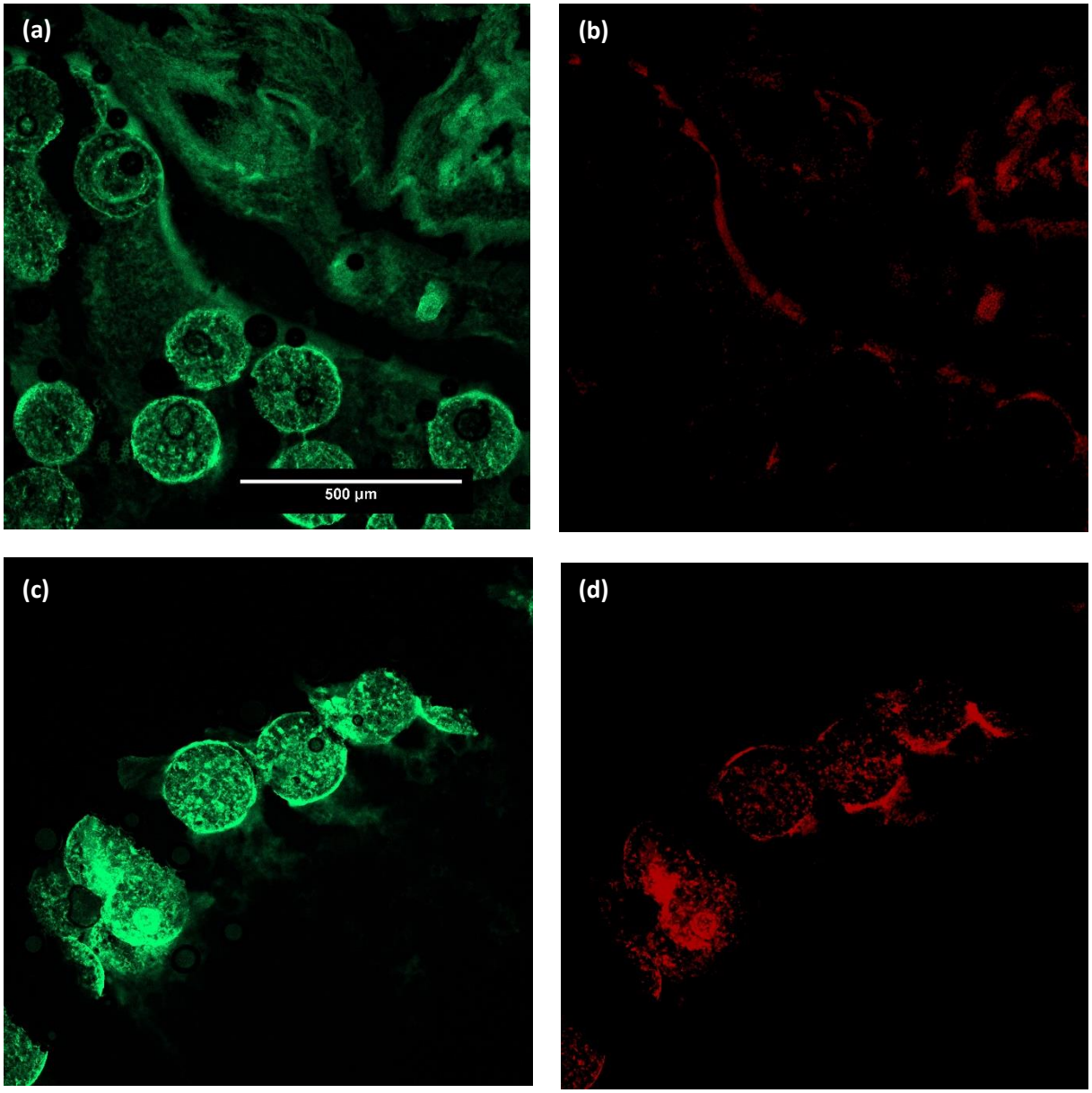

Figure 7.5. (a) FITC-phalloidin stained actin fluorescent image of microspheres from implant site which had been pre-cultured with hES-MP cells for 21 days before implantation. (b) Same sample as (a) but capturing the autofluorescence of the chicken eggs red blood cells. This give an indication to the location of cells from the CAM. (c & d) Same staining method as (a & b) of the implant site when porous EHA/IBOA microspheres were used without the addition of any cells.

These cells were not introduced before the culture but show native CAM cells growing within the pores of the microsphere (figure 7.6). There is a high number of cells within the microspheres, after just 7 days in culture.

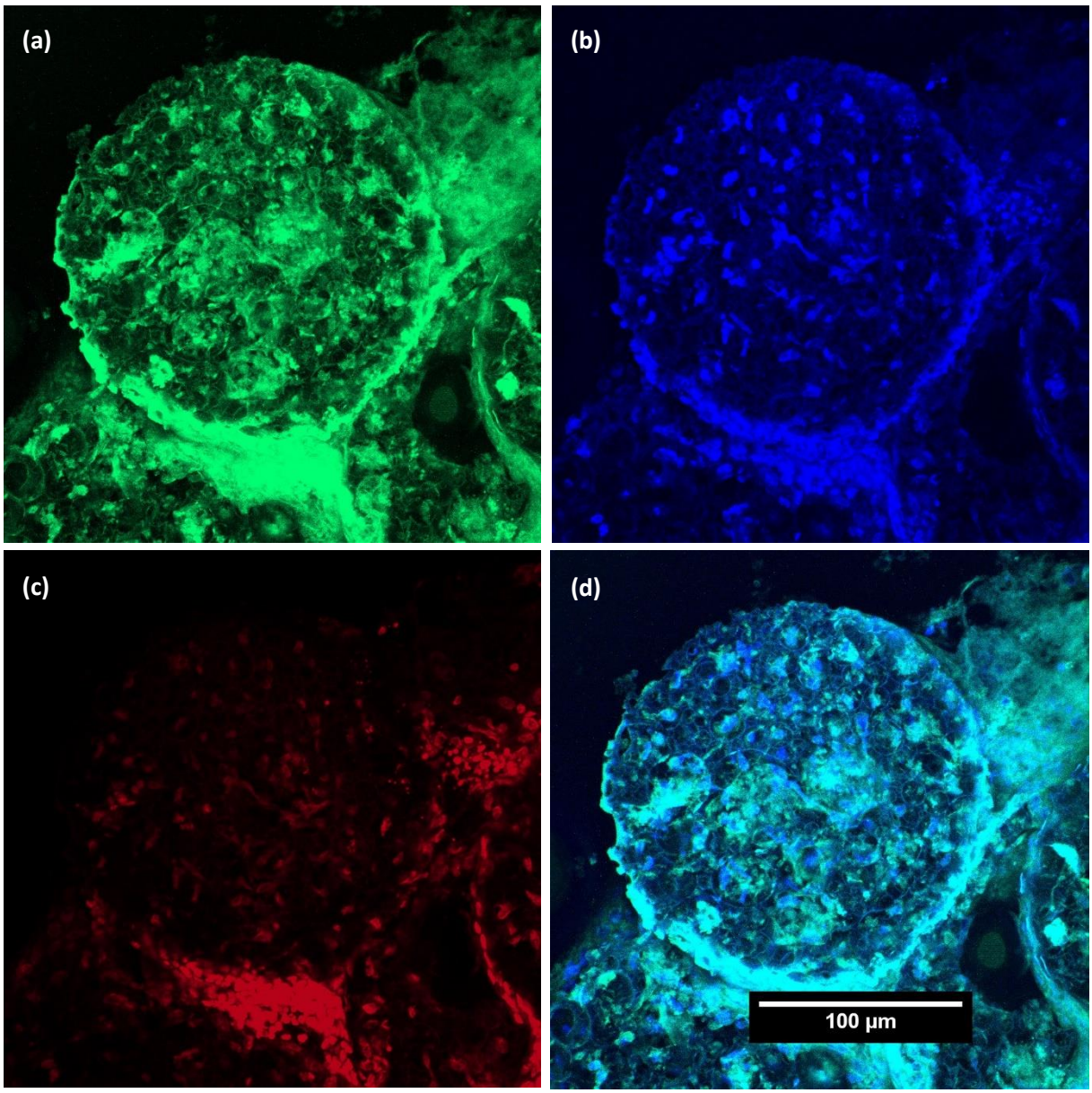

Figure 7.6. Confocal z-stack images of a microsphere from the implant site which had been implanted into the CAM without the addition of any cells. (a) FITC staining of f-actin. (b) DAPI staining of nuclei material. (c) autofluorescence of chicken red blood cells. (d) FITC and DAPI stain combined image.

7.3.2 Survival of cells when injected from a syringe using porous and non-porous carriers

An average of 25 % of cells loaded onto the solid microspheres did not survive the injection process, which is much higher than for porous microspheres (figure 7.7). Loose cells would experience less shear forces due to the relatively large aperture for a cell suspension. The microspheres were much closer in size to the internal diameter of the needle and the surface mounted cells could have experienced much greater forces. An ANOVA was used to determine statistical differences between loose cells, porous microspheres and non-porous microspheres. A statistical difference was observed between non-porous microspheres and all other conditions. There was no statistical difference between porous particles and loose cells.

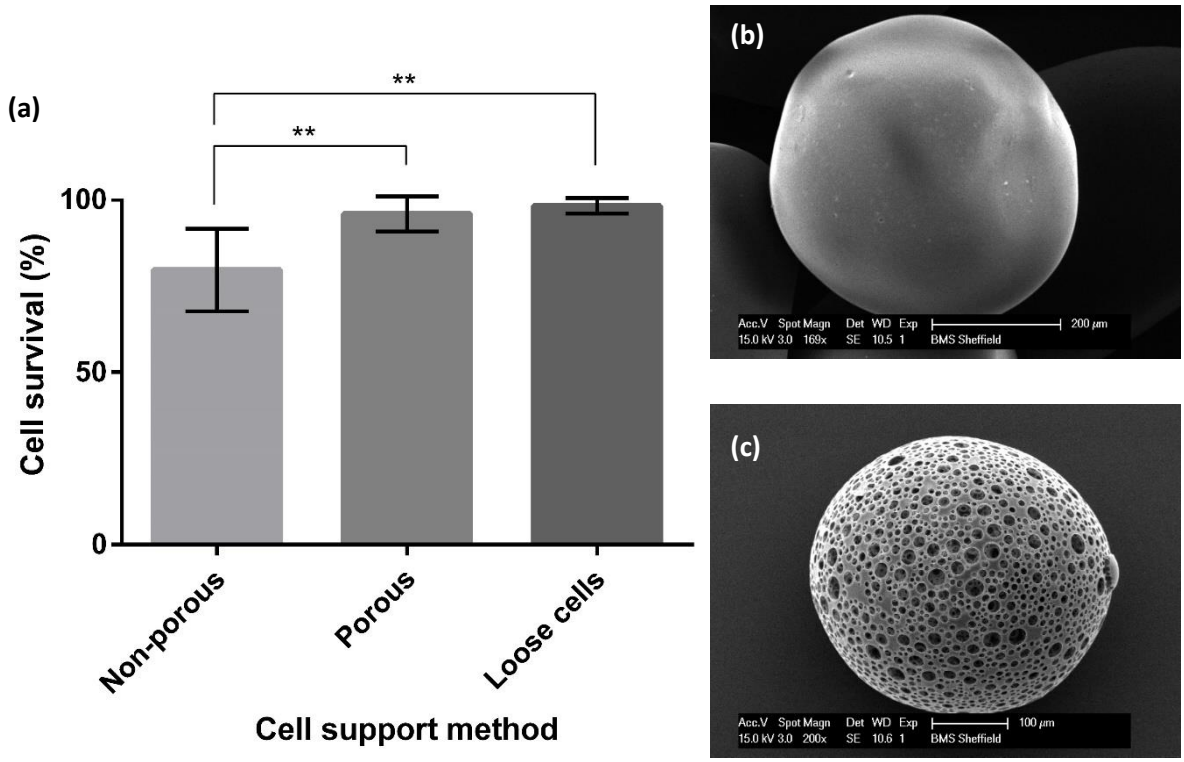

Figure 7.7. Injection study of cell death when culture on porous and non-porous PCL microspheres and injected through a microlance. Cells without a scaffold were used as a control. (a) Graph of cell survival after the injection. (b) SEM micrograph of a non-porous microsphere. (c) SEM micrograph of porous microsphere. ANOVA p = 0.004. n = 5. N = 2 Graph data is mean ± SD.

7.3.3 Analysis of CAM assay after the injection of both porous and non-porous polycaprolactone polymer microspheres with short and long term pre-culture.

Both solid and porous microspheres appeared to induce the growth of vasculature when implanted having been pre-seeded (figure 7.8). Cells cultured for 3 days before implantation were implanted using a microlance dispensing system and were injected onto the CAM. The pre-culture in osteogenic media for 11 days would have caused the cells to begin the differentiation to osteoblasts.

Porous PCL microsphere with an 11-day pre-culture

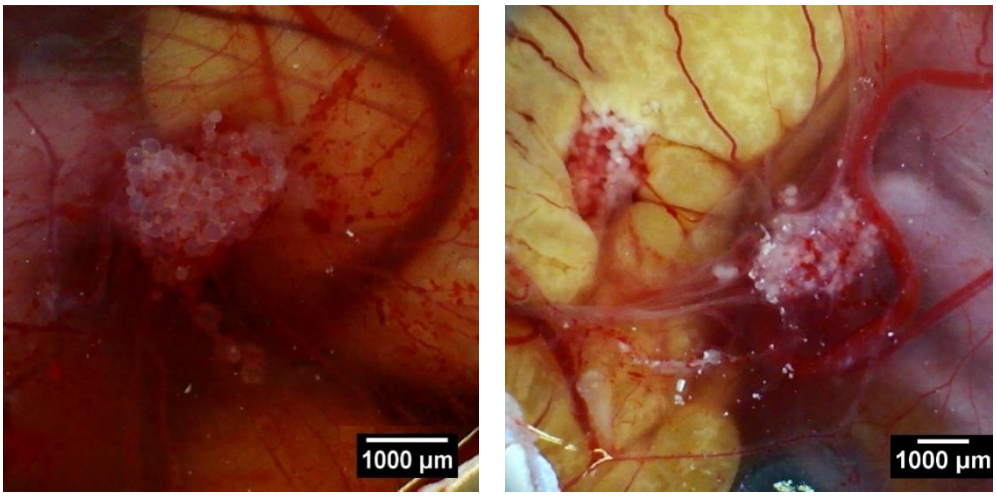

Solid PCL microspheres with 3-day pre-culture with hES-MP cells

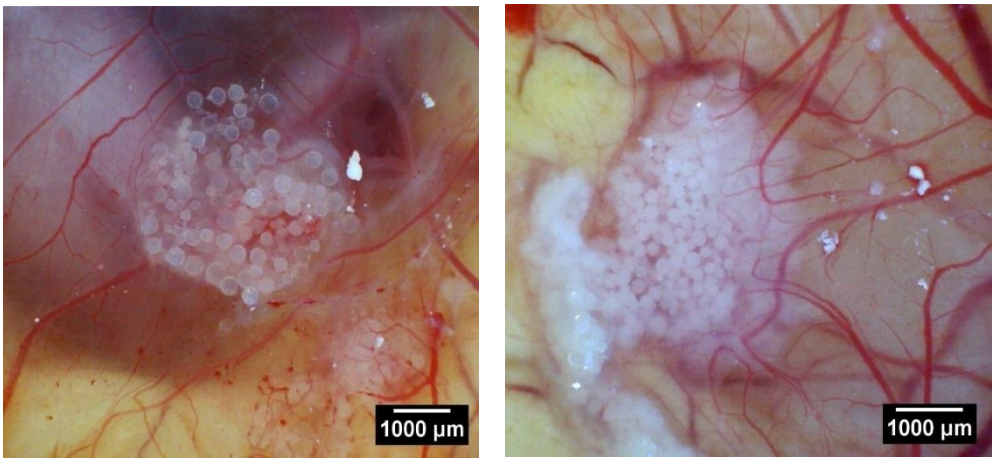

Porous PCL microspheres with 3-day pre-culture with hES-MP cells

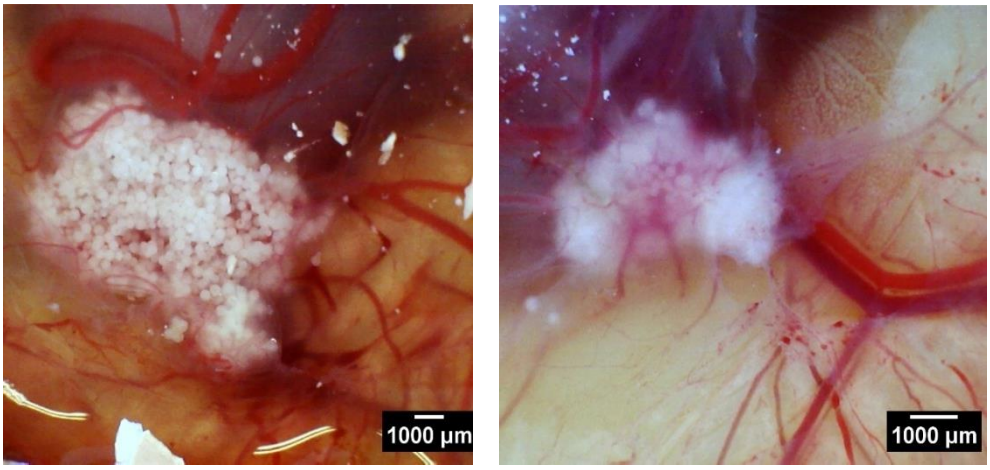

Figure 7.8. Optical images from the CAM implant site after 7 days of culture. Chicken egg shell was removed to view the CAM and the developing embryo. All culture from this figure was performed in osteogenic media.

Statistical differences were found between almost every implant and an hES-MP cell solution control when measuring the number of blood vessels, except for 3 days pre-culture in osteogenic media on porous PCL microspheres (Figure 7.9). For the bifurcation measurements, every implant was

statistically different to the control. The only other difference observed for PCL microspheres was between 3 days in culture with osteogenic media and 11 day pre-culture with the same media. Equally interesting is the lack of difference between porous and non-porous microspheres for both measurements. hES-MP cells cultured in the two different media were also not significantly different to one another.

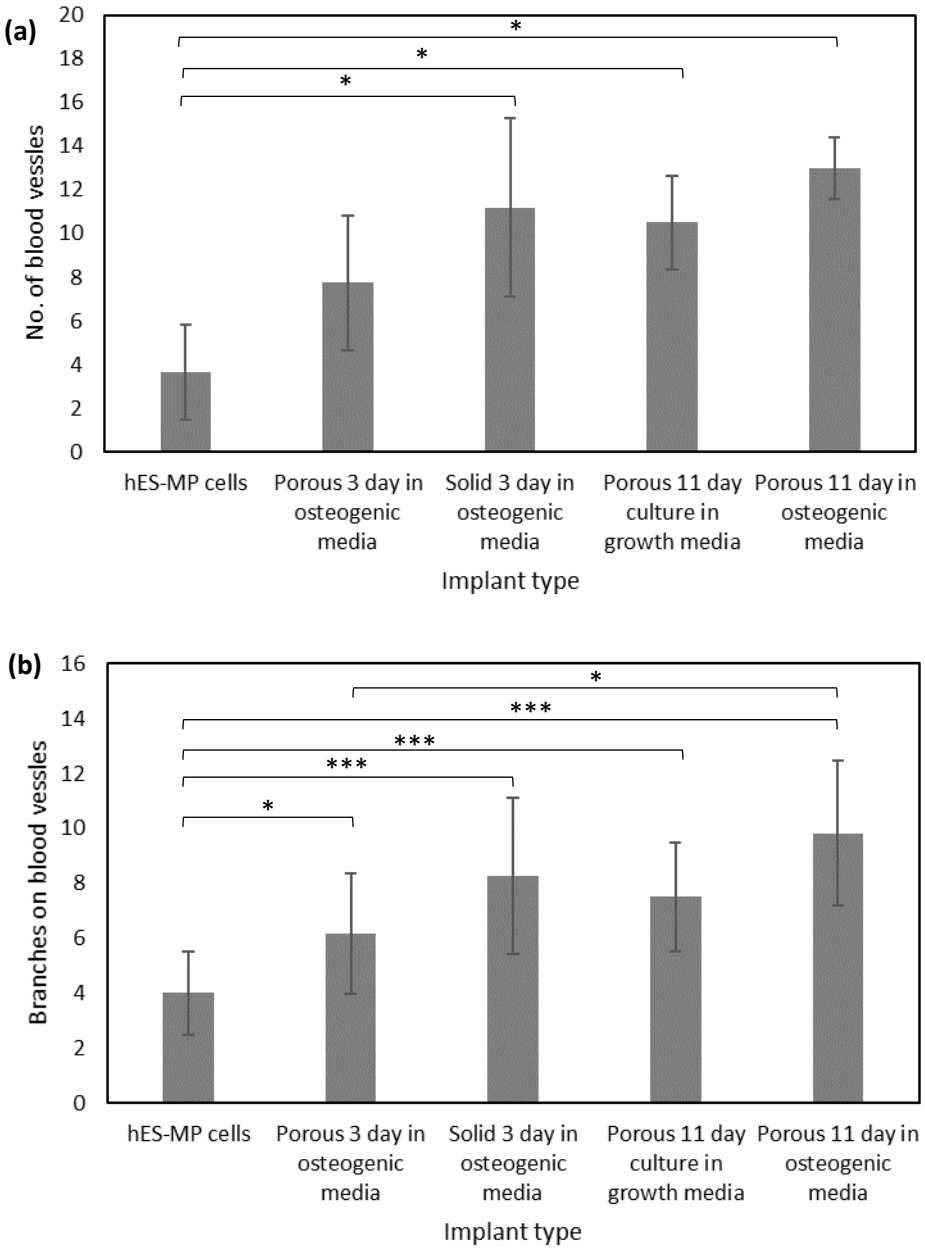

Figure 7.9. (a) Number of blood vessels around the implant were counted over a series of images and displayed on the graph. (b) A measure of the number of branches a blood vessel has within a certain area from the implant. ANOVA p< 0.001. n = 6 N = 1. Graph data is mean ± SD.

Cells can be observed within the pores of each microsphere, although it is impossible to differentiate from these images which species the cells originate from (Figure 7.10). PCL microspheres have all been integrated into the CAM tissue. Several capillary like vessels are visible next to the PCL microsphere in the image Figure 7.11e. An interesting pattern is visible around the solid microspheres in Figure 7.10g & 10h. The seeming empty set of repeating voids is also visible in the control tissue section (Figure 7.4).

Porous PCL microspheres with a 3-day pre-culture of hES-MP cells

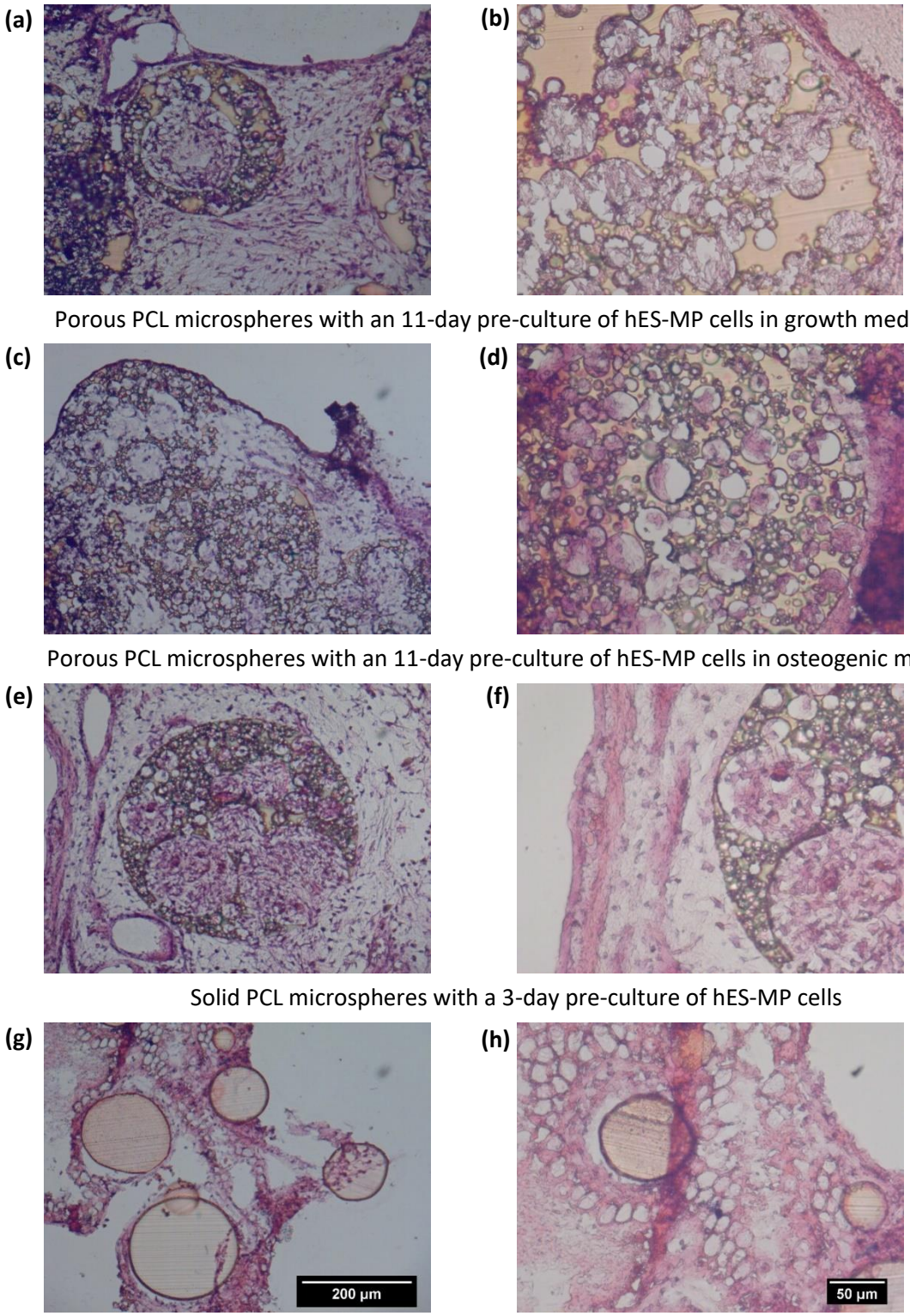

Figure 7.10. H&E stained 10 µm thick sections of tissue taken from within the implant area. PCL microspheres had been implanted to the site and the egg allowed to incubate over 7 days.

7.3.4 Statistical analysis of blood vessels as a method of comparing angiogenic potential of both EHA/IBOA and polycaprolactone microspheres in a CAM model

The PCL microspheres stimulated a superior vascularisation response when compared to the EHA/IBOA material by the majority of the metrics used (Figure 7.11). Blood vessel diameter was not statistically different between the three samples, with the same distributions of diameter present, even if in different quantities. In the measure of vessel bifurcations both EHA/IBOA and PCL microspheres were significantly different to the control but not to one another. For the number of blood vessels present both materials were different to the sample but the PCL microspheres had significantly more local blood vessels than the EHA/IBOA microspheres.

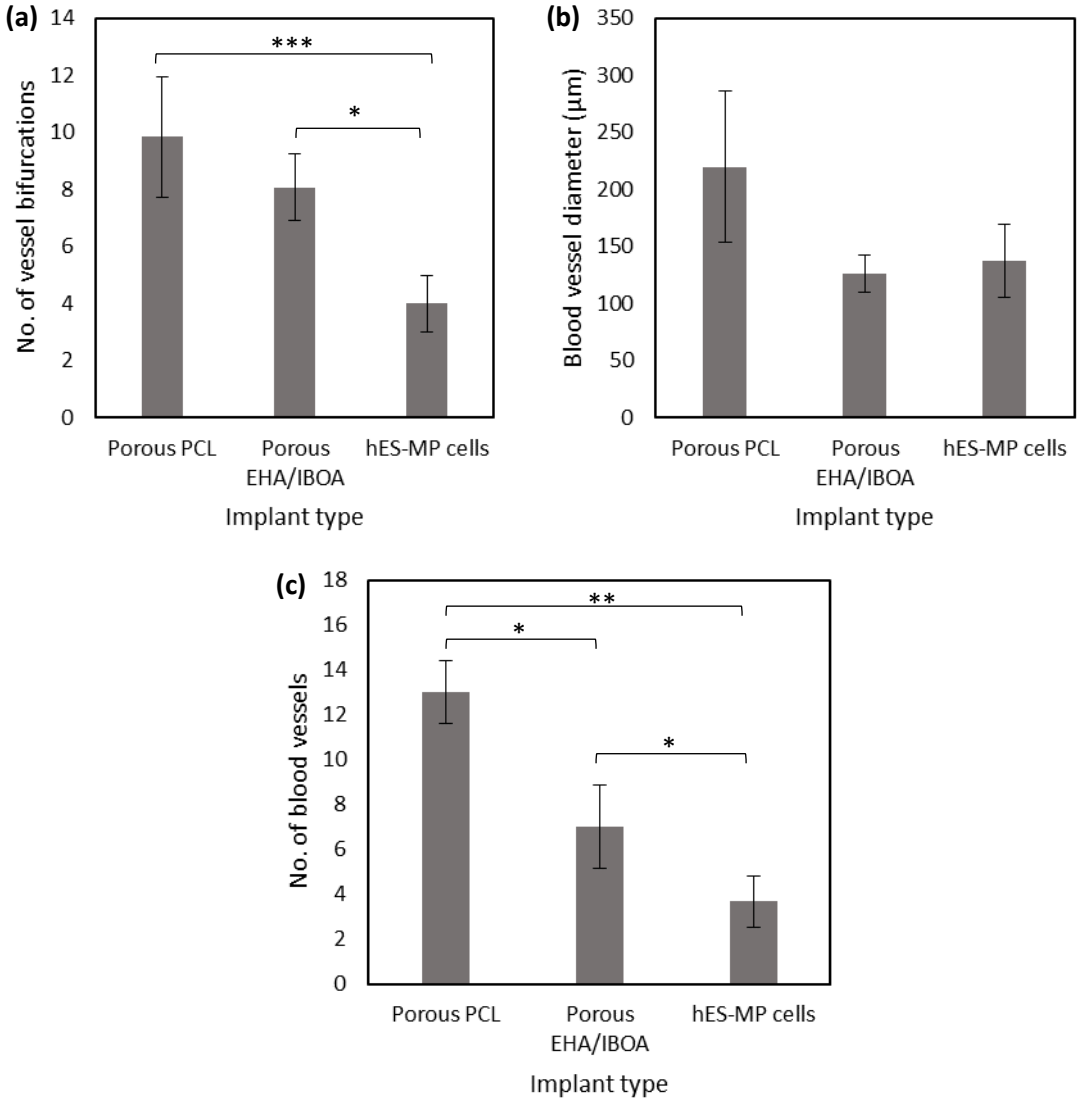

Figure 7.11. Comparison between the two materials as polyHIPE microspheres and their angiogenic response using different metrics. (a) Graph of the number of bifurcations of blood vessels close to the implant. T-test used for individual comparison statistic work. (b) The diameter of the blood vessels near the implant. An ANOVA test found no difference between the 3 implants for blood vessel diameter. (c) Number of blood vessels within to the implant site. ANOVA. n = 6 N = 1. Graph data is mean ± SD.

7.4 Discussion

An increased angiogenic response was observed in a CAM model when EHA/IBOA porous microspheres pre-cultured with hES-MP cells compared to controls. An increased number of both blood vessels and bifurcations were observed when compared to the control. This is supported by both the optical images and the statistical data gathered from analysing the vasculature. Without hES-MP cells the microspheres did not produce an angiogenic response when compared to the control. This is interesting as it also appears that it is not the cells that are responsible for the angiogenic response. This can be seen in Figure 7.9 where a control of hES-MP cells added to the CAM did not perform any better than the no cell control. The synergistic effect of cells bound to the microspheres appears to be the key for angiogenesis. Either the angiogenic response requires the cells to be immobilised in a concentrated location or that the hES-MP cells only survive with a surface to bind to.

We can conclude that while it is not the microspheres themselves which cause the angiogenic response, they are essential for enabling the cells to promote blood vessels formation. The microspheres were added as an agglomeration, within this structure there are many cells within hypoxic environments. These cells will be releasing angiogenic growth factors to encourage the growth of blood vessels as it is the biological response for hypoxic cells [382]. When these hypoxic microenvironments are placed on the CAM the factors that they release would be expected to greatly increase the angiogenic response of the CAM. Early differentiation (days 4 – 14) of MSC cells into osteoblasts is marked by an upregulation of VEGF from the cells [192, 383]. This upregulation may be partially responsible for the increased vascular response, in addition to any potential hypoxic cells.

The agglomerations of microspheres and hES-MP cells appears to prevent the entry of native chicken cells. Evidence of the absence of chicken cell penetration can be found by observing the different morphologies of the cells within the microspheres pores. The cells within the unseeded microspheres have a different morphology to those inside the pre-cultured microspheres. Additionally, the morphology of the cells within the pores of the agglomeration resemble that of differentiated hES-MP cells from the previous two chapters.

The ECM build-up around the microspheres appear form a distinct boundary between the microspheres and the native chicken tissue. This is evidenced by the delamination noted on in Figure 7.4c. When the bond between two structures is weaker than the structures themselves the interface region will fail first under stress, which occurred during the sectioning of the sample. The confocal images reinforce the lack of chicken cells within the microsphere agglomeration. As an injectable material, this could become an issue if the newly growing tissue does not integrate fully with the surrounding wound bed. It is likely the case that with an extended period of time the agglomerations would have fully integrated into the surrounding tissue [67, 384].

Microspheres without the addition of pre-cultured cells were found to recruited the native cell population to grow into the internal porosity of the microspheres. Within 7 days the cells had fully saturated the internal porosity of the microspheres, as opposed to the 30 days we have previously found. Initially we assumed that the microspheres, without the pre-culture of cells, were inert. When looking at the optical images of the CAM assay after sectioning we observed the ingrowth of native cells. In previous chapters we were unsure if only differentiated osteoblast like cells enter the microspheres or if the cells that penetrated the microsphere could have been MSCs. These experiments show that other cell types are able to move within the microspheres and travel between the very small interconnecting porosity. The rate at which this ingress occurred surpassed any of our previous *in-vitro* testing. It appears that this had little angiogenic impact on the CAM assay.

It might be possible to use larger microspheres to recreate the effect of the hypoxia signalling when recruiting native cells by inducing them to grow into hypoxic zones. If a 500 µm wide microsphere was used, then the central 300 µm of the microsphere would be beyond the typical diffusion limit of 100 µm [385]. Any cells which grew into this area would experience hypoxia and would begin to produce hypoxia signals to encourage vessel growth. Although untested this could be a potential future avenue of research if it was desirable to not combine the patient's own cells with the microspheres. Despite the lack of angiogenic response from the CAMs, it might still be possible to utilise microspheres without cells to generate an angiogenic response.

One (fairly crucial) measure of an injectable cell delivery system success to avoid the cell death of the cells being delivered. This study has been performed many times in the literature in various formats to test the ability of a scaffold to protect the cells which are bound to it [386-388]. This is due to its importance for a successful injectable material. Cell death is undesirable not just because it reduces the viably cell number for growth but because the contents of cells released upon cell death. This will induce inflammation have many negative and unpredictable effects on the surrounding cells and may invoke chronic inflammation and prevent wound healing and tissue regeneration [389, 390]. In addition, subjecting cells to forces such as the shear forces can affect the differentiation of the cells and may alter the final expected differentiated cell population.

The increase in survivability of cells on porous scaffolds was significantly higher than that of solid microspheres and controls. The survival rate was the same as cells under no shear forces at all, the 'loose cell' control. This is significant in allowing cells to be delivered undamaged into a patient. The cells are likely to be within the niches of the porous material, and therefore partly shielded from the external forces around the microsphere. Those cultured on solid microspheres are exposed to the surrounding shear forces associated with injection rates. The damage to cells could have been reduced by performing an injection at very low flow rates. At this high rate, the experiment demonstrates the topologies superior nature in aiding cell survival.

Having established that EHA/IBOA microspheres without cells had not increased the angiogenic effect and it was therefore decided to not repeat this condition for PCL microspheres. This allowed experimentation on a larger number of unknown variables and their effect on angiogenesis. Many of the conditions had similar angiogenic effects on the CAM.

Microspheres with cells precultured in different medias (to both induce and not induce osteogenesis) did not produce any significant difference in angiogenesis, suggesting osteoblast cells are not responsible for the angiogenic response. Pre-culture was conducted in two different media to determine the effects of cell differentiation on vascularisation. One implant was cultured with growth media to prevent the formation of osteoblasts and the other was cultured in osteogenic media to promote osteoblast formation. These were cultured for 11 days to allow the cells to begin differentiating. There were no significant differences between the two media on angiogenesis which implies that it is not the osteoblastic nature of the cells that is causing the response. As both cultures formed agglomerations, both would have been producing hypoxia signals from cells deep within the agglomeration. We can conclude that this was the effect of hypoxia signals, or another cell response independent of whether the cells had differentiated.

Both porous and solid PCL microspheres had a similar angiogenic impact on the CAM, suggesting the agglomerations were responsible rather than cells within microspheres. Both had been pre-cultured with hES-MP cells for 3 days and had begun to form small agglomerations. It appears that the hypoxia signalling if mainly arising from cells within the agglomeration but not within the microspheres themselves. This might be because of the large ratio of cells in the agglomeration compared to those within pores or because the cells within the pores are acclimatised to hypoxia conditions and are no longer producing the signals to increase local nutrient and oxygen levels. Cells which might have this response are osteocytes or chondrocytes, cells adapted to survival in environments far from blood supply. The impact this finding would have on the injectable scaffold is that cells would not have to be pre-differentiated before injecting as angiogenesis would occur regardless of the presence of osteocytes or not.

With non-porous microspheres, a specific structure is observed which does not appear in any other implant, a series of circular voids, seemingly too tightly packed together for capillaries. The interesting structure was found surrounding the solid microspheres (see Figure 7.11g &11h. This structure has been observed elsewhere in the study, the control for an untouched CAM assay (Figure 7.4a), suggesting this formation does occur in native tissue. What is unclear is why this structure is surrounding the solid microspheres. This finding might call into question as to the necessity of porosity in microspheres. It is not impossible that this is coincidence that was not observed in other sectioning by chance and is present within all implant systems.

Another result which suggests the agglomeration is important on vascularisation was the increased angiogenic response of scaffolds precultured for a longer before implanting that resulted in larger agglomerations. Once significant difference that was observed in bifurcation formation was that of an 11-day pre-culture of porous microspheres when compared to a 3-day pre-culture under similar conditions. No significance was found between the number of blood vessels when comparing these two conditions. Despite this the time in culture does appear to have some effect on vascularisation. It is unknown if it is the additional number of cells that would be present but it is likely the increased size of the agglomerations. With larger agglomerations, it is possible that the increased hypoxia signals being released by the implant would intensify the angiogenic response. No differences were discovered between 3-day pre-culture in osteogenic and 11-day pre-culture in growth media ($p = 0.094$). While it may have something to do with the differentiation of cells we have evidence to the contrary. This is likely to require future work to fully investigate the cause.

When comparing both PCL and EHA/IBOA several measurements for angiogenesis were similar but a higher number of blood vessels were observed around PCL microspheres, despite a shorter pre-culture time. Measurements such as at the number of bifurcations in vasculature and vessel diameter in the implant area were similar. Differences were observed between the materials when looking at the number of blood vessels within the implant location. A significantly higher number of blood vessels were found around the PCL material than the EHA/IBOA implant. The implants were not identical in pre-culture conditions however. The EHA/IBOA material was cultured for 21 days whereas the PCL material was cultured for 11 days. As we have discovered that increased time in pre-culture increases the angiogenic effect and it may be that the PCL material would receive an even stronger angiogenic effect if cultured for a similar amount of time as the EHA/IBOA. However, we only know that this increase occurs between 3 days and 11 days of pre-culture, there is no evidence that this effect could be extrapolated between later time points. It appears that vessel diameter is a poor measure of angiogenic response (Figure 7.12b). Vessel diameter appears to remain a constant ratio, regardless of the level of vascularisation.

7.5 Conclusion

In this chapter, we have investigated microspheres formed from both materials, EHA/IBOA and PCL, and their angiogenic properties by testing in a CAM assay. For both porous EHA/IBOA and PCL microspheres a significant increase in vasculature was observed when compared to a no scaffold control. Without pre-loading of hES-MP cells onto the microspheres there was no difference in vasculature between this and the control. However, for these 'empty' microspheres sectioning revealed a full infiltration of native chicken cells throughout the scaffold. A simple cell delivery without scaffolds also produced no significant result and it was concluded that both cells and scaffolds were required to stimulate enhanced vasculature formation. Cells cultured for 11 days (and formed into aggregates) were found to produce a greater response than those cultured for a shorter period of time of 3 days (loose microspheres and small aggregates). It was unsure whether increased maturity/aggregation or increased quantity of cells was responsible for this effect. Out of all the comparisons between the materials PCL and EHA/IBOA the only difference detected was in the analysis of then number of vessels within the implant area for which the PCL was statistically significant. In all other areas the scaffolds performed equally. An injection study found cells on porous microspheres suffered greater cell death than those loaded onto porous microspheres.

Chapter 8: Final discussion on an injectable system for bone tissue engineering

8.1 Chapter aims

1. To discuss the previous chapters concentrating on the concept of an injectable bone tissue engineered solution.
2. Discuss the different materials used for microspheres, their merits and disadvantages for this application.
3. Present a summary of all the major results from throughout the thesis.

8.2 Requirements of an injectable scaffold

Sumita Bose et al. postulated 4 key aspects to produce an ideal scaffold [77], these are biocompatibility, mechanical properties, pore size and bioresorbability. To these I will also add manufacturing efficiency, vascularisation response, scaffold deployment and biomolecule release potential as key requirements to discuss the scaffolds used within the thesis.

8.3 Manufacturing efficiency

For a successful scale up to produce products for a commercial replacement product decisions must be made at early stages. As we found in the first results chapter it is possible to use advanced additive manufacturing technology to produce intricately detailed and highly customised micro-particles. As effective as these particles might have been it was not an efficient method of production to form the millions of the particles required for successful upscale. One of the particles produced by the 2-photon direct write system required roughly 4 hours. Methods exist to speed up the production of direct laser write although they are still several orders of magnitude slower than the double emulsion microfluidic method. This technique was chosen because it compromises between a greater speed of production but also contains complex internal structuring. The internal porosity may lack the customisation of the additive manufacturing system but still allows sufficient control to alter the pore sizes and to allow it to be tuned to specific applications. The double emulsion allowed a two-step technique that was as rapid at forming microspheres as other microfluidic methods but allowed the inclusion of internal porosity.

As mentioned before, EHA/IBOA is a very stable emulsion and could remain in storage for many hours before destabilising. The PCL emulsion on the other hand was far less stable, especially at room temperature. When it was first developed, the emulsion would destabilise very quickly if allowed to cool to room temperature and was only suitable to the CSTR method of microsphere manufacture. Later, as the emulsion formulation was improved, it was possible to use the microfluidic method at room temperature for 60 minutes before the emulsion would destabilise. This is still a disadvantage

when compared to EHA/IBOA emulsion but the benefits brought by using PCL far outweighed any disadvantages in increased production time. For additive manufacturing, altering the photocurable material used would not have change the curing time significantly unless there was a decrease in photosensitivity of the new polymer.

8.4 Biocompatibility

A minimum standard for a tissue engineered scaffold is biocompatibility. This is for the material to be compatible with living tissues and cells without causing toxicity and ideally to enhance the growth of cells and tissues. This includes any degradation products that may be formed by the scaffold and the toxicity of any wear debris that may be produced. A scaffold should also be osteogenic, allowing bone cells to attach to the scaffold and to differentiate into bone cells. The scaffold should also stimulate the deposition of new bone formation.

8.4.1 Cell toxicity

Microspheres formed from both materials (EHA/IBOA & PCL) have been shown to support cells and to allow ingrowth into their interconnected porosity. The EHA/IBOA polymer required a plasma deposition of poly acrylic acid before large numbers of cells were able to attach to the scaffold. Activity was measured to be increasing for cells cultured on the microspheres until around day 10, after which the cell activity plateaued. While this cannot be used interchangeable with cell numbers it offers a good indication that the number of cells is remaining static or that cell activity is reduced in the majority of the cells as new cells proliferate. The thiol-ene material did not require a coating for bulk flat disks of the material but when it came to culturing on the microspheres it was found that a coating was required due to the decreased opportunity cells had to attach to the microspheres. For the PCL material there was no need to coat it with pAA as the material supported cells without any additional treatment. Other groups have however shown the PCL can be made to support even greater cell growth or osteogenic properties with coating that increase the hydrophobicity [391], coating with hydroxyapatite [392], coating with collagen [393] among many other techniques [394].

8.4.2 Osteoconductivity/Osteogenesis

Even without the addition of dexamethasone there were still signs of osteoblastic activity in ECM deposits within the agglomeration. The quantity observed was much lower than the quantity found when cells were cultured in media containing dexamethasone. When the EHA/IBOA material was compared to tissue culture plastic it was found that the polyHIPE inhibited or delayed ALP activity. This is more likely to be a material chemical property than a result of the topology. Previous experiments within our lab have shown that the coating of the EHA/IBOA material does have an effect on ALP production which indicates that the response can be altered by changing the material chemistry [395]. Deligianni et.al noted that while the surface roughness affected cell attachment they did not find any

difference in ALP production [396], has have others [397]. However other authors have found the reverse, that of a significant increase in osteoblast differentiation on rougher surfaces [398]. From these reports, it is unclear if ALP should be higher on the rougher surface or that the surface makes no difference. Either way this supports the conclusion that it is the materials surface chemistry which causes the TCP to produce greater amounts ALP per cell than the EHA/IBOA material.

As the inclusion of DEX does cause osteoblast formation then if an initial dose of DEX is administered before injection, enough to begin the formation of osteocytes and osteoblasts then the newly differentiated cells will be able to differentiate remaining MSC cells through the releasing of osteogenic factors [219]. The in-vivo CAM assays demonstrate the ability of microspheres to recruit local cells. When empty microspheres (no pre-cell culture) were added to the CAM it was found that cells were fully infiltrated into the microspheres, even after only 7 days in culture. There is no way of extrapolating this to a bone model of a mammalian species but it does indicate that there is potential.

Osteoblasts

Strong evidence of the formation of osteoblasts was found in both EHA/IBOA and PCL polyHIPE microspheres. Initial evidence from ALP tests showed that cells on flat surfaces begun the transformation to osteoblasts. After 30 days in culture stains for both collagen and calcium returned positive and the stain for calcium after 60 days was stronger than day 30. In addition, mineralised deposits could be seen in the SEM images of inside the microspheres for both systems in pores inhabited by cells.

Osteocytes

Sclerostin positive stains showed that the osteoblast cells had differentiated to osteocytes within the pores of the microsphere for EHA/IBOA polymer. The morphology of cells within the pores of this material were highly similar to those of osteocytes. This is the same morphology as the cells found within the pores of the PCL microspheres exhibited. The expected hypoxia within the system would favour the formation of osteocytes as it is similar to the stimulus experienced by osteoblasts when they encapsulate themselves in bone during bone remodelling as part of the natural method of osteocyte formation [197].

Chondrocytes

It usually requires specialised media to cause MSC to differentiate into chondrocyte cells. When we tested for the presence of proteoglycans it was detected both within the microspheres and inside the agglomeration. This is often taken as a positive indicator for chondrocyte presence. The pores are not only reminiscent of the osteons from bone but also of the lacunae found surrounding chondrocytes in cartilage. Cartilage is also an avascular tissue and the centre of the agglomerations were far beyond the 200 µm diffusion limit of oxygen and nutrients. Within the pores we also found evidence of mineralisation which is usually an indicator of osteoblast activity. Chondrocytes can produce limited

amounts of calcium is they are hypertrophic, meaning they are preparing the surround matrix for transformation into bone. The cell protrusions between the different pores is not observed on standard chondrocyte morphology but only on osteocytes within bone. This is the strongest evidence that the cells observed were not chondrocytes. Less glycoproteins were observed in PCL microspheres, if chondrocytes are present then PCL appears to have a dampening effect on their formation or on their ability to for proteoglycans. An alternative explanation from the GAG staining is that it could be staining the cells glycocalyx, the glycoprotein membrane which surrounds the cell membrane.

8.4.3 Support mineralisation

The microsphere scaffolds were found to promote the deposition of matrix. For calcium, this was mainly observed within the pores of the microspheres with far less observed outside the microspheres in the agglomeration. Collagen was observed both inside the microspheres and within the agglomeration in very high concentrations. The act of binding the microspheres together required to formation of high levels of ECM formation.

8.5 Mechanical properties

The ideal mechanical properties of a bone tissue scaffold are dictated by the size and shape of the implant along with the location of the defect site within the bone [399]. Bone tissue has different material properties with differences caused by type of bone, age of the patient, disease state of the bone and diet of the patient to name but a few. Another important distinction is load bearing scaffolds vs. non-load bearing scaffolds. The utilisation of non-load bearing scaffolds has a significant role in bone tissue engineering, especially if the implantation method allows for injectable delivery. As this application is non-load bearing the bulk mechanical properties are of less importance than the microscale mechanical properties that the cells experience as this helps influence cell differentiation.

8.6 Pore size

Pore size plays a significant role in osteoinduction, with a commonly stated minimum pore size of 100 μm for in-vivo implantation and with a wide range of ideal pore sizes stated in the literature [67, 77, 400]. Pores are also valuable to allow the diffusion of nutrients and oxygen into a scaffold and larger pores are required to allow for blood vessel ingrowth. Pores also contribute a mechanical roughness which is essential for allowing full integration with the surrounding tissue [401, 402]. The pores within the polyHIPE microspheres are limited in size to smaller than the diameter of the microspheres themselves. The ideal size range of 100 μm or larger is impossible to achieve without using very large particles that would greatly reduce the packing density of the implant. In our systems particles were formed up to 1 mm in diameter, although porosity was never observed above 70 μm. Porosity was roughly similar between all the porous polyHIPE materials and the pore size is highly customisable from the processing conditions or from the formulation by altering the level of surfactant. Surprisingly,

osteocyte like cells being found in pores below 20 µm in diameter these experiments were conducted *in-vitro* in which smaller pores are able to support MCS differentiation. In-vivo culture with pores of this magnitude have been reported to produce fibrous tissue formation. Pore size could be increased to compensate but as discussed above this could only be achieved up to a certain size limit.

8.6.1 Control over construction parameters

Being able to control pore size gives the scaffold design greater flexibility to provide suitable niches for cells to reside. It also gives the system flexibility to meet future needs, either through unknown developments in the field or alternative requirements if the system is transferred to treat another disease state. It was found that pores could be altered in diameter by controlling the conditions used to form the initial emulsion. Stir speed and temperature were used as two separate and complimentary systems of altering pore diameter. Interestingly, and of great importance, it was found that processing conditions applied to the double emulsion did not affect the size of the pores in the resulting microspheres. Once formed the initial emulsion did not change further when new conditions were applied to it. This meant that pore size could be chosen irrespective of any processing conditions used to effect microsphere diameter. This flexibility was extensively tested for the EHA/IBOA system but was not repeated for the other systems as it was decided the limited time and resources would be better used to investigate the cell interaction with the material. However, knowing this information allowed us to understand which conditions needed to be controlled to preserve the uniformity in all the microspheres formed.

8.7 Bioresorbability

Controlled degradation of a scaffold is essential for allowing remodelling of the bone or ingrowth from the surrounding areas [403]. The degradation products should not cause direct harm to cells through toxicity, or damage the formation of new bone through decreasing the local pH. The degradation time required for a scaffold is different depending on the type of bone being replaced. Often loading bearing scaffolds must ensure that the material properties of the scaffold does not decrease to rapidly while resorbing and allow the new bone to take up the increased load.

8.7.1 Degradation

Of the three main materials we investigated, two were degradable. EHA/IBOA was used initially due to the highly stable nature of the emulsion and the previous experience within the lab using this polyHIPE. It allowed us to produce the set-ups required to produce the microspheres in a controlled method and to establish methods of cell culture and testing which could then be easily transferred to the new degradable microspheres that were available in a more limited quantity. For the thiol-ene polymer there were reports in the literature which showed that it had been tested for degradation previously. Caldwell *et.al.* found that the material degraded by 20 – 30% over a 7 week time scale [191].

As the PCL polyHIPE formulation had never been published on previously and a degradation test was conducted. The rate of PCL degradation is usually measured over the time scale of years [357], however this is as a bulk structure and not as an extremely high surface area material. The PCL microsphere degraded by around 25% over a 60 day time in distilled water.

This leads to the conclusion that in the 60 day PCL microsphere cultures that the polymers would have become noticeably degraded by the end time point and cells would have been exposed to PCL degradation products. It is reported that in-vivo the degradation is faster than in-vitro experiments [404]. Meredith et.al reported on a comparison of PLGA and PCL degradation products and found that the PCL allowed for superior cell viability and angiogenesis compared to PLGA degradation [404]. They suggested this was due to the acidic conditions produced by the PLGA degradation and the more rapid PLGA degradation releasing an increased volume of degradation products.

This would mean a further difference between the long term cultures, as with the non-degradable EHA/IBOA polymers there would have been no degradation products by day 60. Looking at existing literature after 2 month there is already extensive integration within a bone void [348, 405] so this degradation rate would be highly suitable. For the polymer PCL there is no straightforward method for altering degradation rates, such as changing the blend of the copolymer PLGA system which can alter its degradation between weeks and years [406]. One method would be to change the porosity of the polyHIPE microspheres. Decreasing the porosity would reduce the total available surface area available for degradation. However, this could have serious ramifications for the cell response to this material. Reducing the quantity of crosslinker would produce a less branched polymer that would degrade faster, or the reverse to increase degradation time. Increasing the volume of crosslinker may have effects on cells such as increased toxicity when the polymer degrades.

8.8 Vascularisation response

To ensure a healthy and living bone tissue the scaffold must encourage and become fully vascularised. This is especially important when cells are implanted within a scaffold, as their ability to survive is severely undermined if fresh nutrients and oxygen do not reach them within the first few days. Features can be introduced to increase the vascularisation speed such as adding physical channels into the scaffold for vessel growth, pre-growing vasculature into the scaffold or by releasing factors such as VEGF to increase the speed and quantity of the vascularisation response.

8.8.1 Vascularisation comparison

Microsphere which had been pre-cultured with cells had a greater angiogenic effect than those without cells. We also found that a longer pre-culture time had a greater angiogenic response than those cultured for a shorter period of time. We know from previous chapters that cells formed osteoblasts within the microspheres and an increased period of time would have allowed this

differentiation to have progressed further. This is significant because during initial MSC differentiation VEGF is upregulated by the cells [192], this powerful biomolecule is essential in recruiting blood vessel formation in the surrounding area [407, 408]. An increased number of osteoblast cells is likely to stimulate an increased angiogenic response from the CAM assay. Very few differences were found between PCL and EHA/IBOA materials, possible suggesting the response is more cell based than material based. As cells responded similarly to the two materials, forming osteoblasts on both, it is not surprising that the materials were equal. The only observed difference was that PCL microspheres were found to recruit more blood vessels to the implant area. It therefore appears that the uncoated PCL material had a superior effect although there are many coatings and additives reported in the literature that could further enhance the vascularisation response [409].

8.9 Scaffold deployment

The method of scaffold implantation is dependent on the type of disease state or injury the tissue engineered construct is targeting. For non-invasive scaffold delivery, the size of the particles used is essential as it dictates the bore size of the syringe used to inject them. Cells require additional protection from the severe shear forces present during the injection process. One fantastic example of a deliverable polyHIPE scaffold should be mentioned. Cosgriff-Hernandez *et.al.* [184] have developed a polyHIPE which cures *in-situ* within the human body. This allows the scaffold to have some load bearing properties as while it is deployed through a needle, it forms a bulk scaffold within the wound site.

8.9.1 Injectability

Microspheres were found to be deliverable through a syringe and were deployed in this manner to the in-vivo models. Having a more monodisperse population allowed for a smaller diameter syringe without the risk of having microspheres blocking the needle. It was not easy to deliver the microspheres and this will require more work in the future to increase the efficiency of delivery. When delivering the microspheres in media the liquid would preferentially flow around the microspheres when under pressure instead of propelling the microspheres out of the needle. A needle very closely matched to the diameter of the microspheres would help prevent this problem, as would increasing the viscosity of the solution the microspheres are suspended in. Literature offers many examples of different solutions for dispensing and printing such as alginates and other hydrogels [410].

8.10 Final Conclusions

Within this thesis, a biodegradable, osteogenic, highly porous and injectable microsphere system has been developed. At each stage of development different alternatives were considered and the best compromise was sought. When considering the manufacturing of the central components a rapid and continuous manufacturing system was chosen over an additive manufacturing process. A compromise was found between including controlled microfeatures and speed of manufacture by producing microspheres with internal interconnected porosity using a double emulsion technique. The processing conditions used to form this microsphere were considered and parameters were investigated to give rise to different porosities, microsphere diameters and microsphere size distributions. Two techniques were investigated, controlled stir tank reactor (CSTR) and T-junction microfluidics. CSTR gave rise to a wider range of microsphere size diameters and was a batch process. The microfluidic approach gave rise to populations of near monodisperse size distribution and was eventually set up as a continuous production method.

hES-MP cell was used to investigate the effect of MSC culture. Osteoblasts were found to differentiate into the pores of the microsphere and what appears to be osteocytes were observed at later time points. Cells were found to differentiate throughout the microspheres and by day 60 were present in every pore within the microspheres. The microspheres underwent cell enabled aggregation and formed cell-microsphere agglomerations, bound together by ECM and several 1000 μm in diameter. Having established the system with a non-degradable system (EHA/IBOA) the hES-MP experiments were repeated with two biodegradable polyHIPE systems. Polycaprolactone (PCL) and a thiol-ene material were emulsified and used to manufacture polyHIPE microspheres. Due to poor cell growth experiments and low surface porosity the PCL polyHIPE was chosen over the thiol-ene polyHIPE. PCL microspheres were found to re-create the same results found in the EHA/IBOA microspheres with osteoblast and osteocyte formations within the porosity. The porous microspheres were found to project cells from the shear forces involved in injection and were injected into a CAM model to study the vascularisation response.

Cells precultured on microspheres were found to have a superior angiogenic response to just cells or microspheres alone. Microspheres without a preculture of hES-MP cells were found to be fully infiltrated with the hosts cells after just 7 days. PCL microspheres were found to recruit a greater number of vessels to the implant site than microspheres formed from the EHA/IBOA material. From the experimental work in this thesis, the PCL polyHIPE microspheres would be an ideal candidate for further testing in vivo to assess their effectiveness within a biological system.

8.11 Future work

Having established a suitable injectable biomaterial which satisfies the requirements of an injectable system under its current testing parameters the next step is to explore a full in-vivo model. A rabbit bone defect model has been identified as the most suitable candidate for this experiment to be run over a 3 and 6 month period. From these time points it would be possible to view the beginnings of degradation and to analyse the nature of the replacement tissue and vascularisation.

Further work is also required in pinning down the cell type found within the pores of the polyHIPE after extended periods in culture as it is still not entirely clear that it is not chondrocytes that are present instead of the osteocytes that would indicate an excellent biomaterial for bone.

One final aspect of future work is to explore other tissue systems with this injectable material. As PCL is a relatively soft material it would be possible to investigate neural tissue engineering to replace cell populations found within voids in the brain caused by stroke. Many of the requirements remain the same as for bone such as the need for vascularisation, the requirement to prevent both cell damage upon injection and to prevent cells from leaving the target site. Overall this particle system has great potential for future research and potential use in patients.

Bibliography

1. Priya, S.G., H. Jungvid, and A. Kumar, *Skin tissue engineering for tissue repair and regeneration.* Tissue Engineering Part B: Reviews, 2008. **14**(1): p. 105-118.
2. Crapo, P.M., T.W. Gilbert, and S.F. Badylak, *An overview of tissue and whole organ decellularization processes.* Biomaterials, 2011. **32**(12): p. 3233-3243.
3. Badylak, S.F., et al., *Engineered whole organs and complex tissues.* The Lancet, 2012. **379**(9819): p. 943-952.
4. Nerem, R.M. and A. Sambanis, *Tissue engineering: from biology to biological substitutes.* Tissue Engineering, 1995. **1**(1): p. 3-13.
5. Caplan, A.I., *Adult mesenchymal stem cells for tissue engineering versus regenerative medicine.* Journal of cellular physiology, 2007. **213**(2): p. 341-347.
6. Bianco, P. and P.G. Robey, *Stem cells in tissue engineering.* Nature, 2001. **414**(6859): p. 118-121.
7. Kaviani, A., et al., *The placenta as a cell source in fetal tissue engineering.* Journal of pediatric surgery, 2002. **37**(7): p. 995-999.
8. Körbling, M. and P. Anderlini, *Peripheral blood stem cell versus bone marrow allotransplantation: does the source of hematopoietic stem cells matter?* Blood, 2001. **98**(10): p. 2900-2908.
9. Fraser, J.K., et al., *Fat tissue: an underappreciated source of stem cells for biotechnology.* Trends in Biotechnology, 2006. **24**(4): p. 150-154.
10. Zuk, P.A., et al., *Human adipose tissue is a source of multipotent stem cells.* Molecular biology of the cell, 2002. **13**(12): p. 4279-4295.
11. Kern, S., et al., *Comparative analysis of mesenchymal stem cells from bone marrow, umbilical cord blood, or adipose tissue.* Stem cells, 2006. **24**(5): p. 1294-1301.
12. Scadden, D.T., *The stem-cell niche as an entity of action.* Nature, 2006. **441**(7097): p. 1075-1079.
13. Lutolf, M.P. and H.M. Blau, *Artificial stem cell niches.* Advanced Materials, 2009. **21**(32‐33): p. 3255-3268.
14. Palecek, S.P., et al., *Integrin-ligand binding properties govern cell migration speed through cell-substratum adhesiveness.* Nature, 1997. **385**(6616): p. 537-540.
15. Engler, A., et al., *Extracellular matrix elasticity directs stem cell differentiation.* Journal of Musculoskeletal and Neuronal Interactions, 2007. **7**(4): p. 335.
16. Reilly, G.C. and A.J. Engler, *Intrinsic extracellular matrix properties regulate stem cell differentiation.* Journal of biomechanics, 2010. **43**(1): p. 55-62.
17. Dalby, M.J., et al., *The control of human mesenchymal cell differentiation using nanoscale symmetry and disorder.* Nature Materials, 2007. **6**(12): p. 997-1003.
18. Lim, S.H., et al., *The effect of nanofiber-guided cell alignment on the preferential differentiation of neural stem cells.* Biomaterials, 2010. **31**(34): p. 9031-9039.
19. Xie, J., et al., *The differentiation of embryonic stem cells seeded on electrospun nanofibers into neural lineages.* Biomaterials, 2009. **30**(3): p. 354-362.
20. Engler, A.J., et al., *Matrix elasticity directs stem cell lineage specification.* Cell, 2006. **126**(4): p. 677-689.
21. Discher, D.E., P. Janmey, and Y.-l. Wang, *Tissue cells feel and respond to the stiffness of their substrate.* Science, 2005. **310**(5751): p. 1139-1143.
22. Pek, Y.S., A.C. Wan, and J.Y. Ying, *The effect of matrix stiffness on mesenchymal stem cell differentiation in a 3D thixotropic gel.* Biomaterials, 2010. **31**(3): p. 385-391.
23. Higashi, S., et al., *Polymer-hydroxyapatite composites for biodegradable bone fillers.* Biomaterials, 1986. **7**(3): p. 183-187.
24. Albrektsson, T., et al., *Osseointegrated titanium implants: requirements for ensuring a long-lasting, direct bone-to-implant anchorage in man.* Acta Orthopaedica Scandinavica, 1981. **52**(2): p. 155-170.

25. Murray, D., A. Carr, and C. Bulstrode, *Survival analysis of joint replacements.* Bone & Joint Journal, 1993. **75**(5): p. 697-704.
26. Smith, H.S., *Painful osseous metastases.* Pain physician, 2010. **14**(4): p. E373-403.
27. Weiss, P., et al., *The safety and efficacy of an injectable bone substitute in dental sockets demonstrated in a human clinical trial.* Biomaterials, 2007. **28**(22): p. 3295-3305.
28. Isaac, J., et al., *Effects of strontium-doped bioactive glass on the differentiation of cultured osteogenic cells.* Eur Cell Mater, 2011. **21**: p. 130-43.
29. Wu, C., et al., *Strontium-containing mesoporous bioactive glass scaffolds with improved osteogenic/cementogenic differentiation of periodontal ligament cells for periodontal tissue engineering.* Acta Biomaterialia, 2012. **8**(10): p. 3805-3815.
30. O'Brien, F.J., *Biomaterials & scaffolds for tissue engineering.* Materials Today, 2011. **14**(3): p. 88-95.
31. Johnson, D.W., et al., *Macrostructuring of Emulsion‐templated Porous Polymers by 3D Laser Patterning.* Advanced Materials, 2013. **25**(23): p. 3178-3181.
32. Turunen, T., et al., *Effect of bioactive glass granules and polytetrafluoroethylene membrane on repair of cortical bone defect.* Journal of Materials Science: Materials in Medicine, 1995. **6**(11): p. 639-641.
33. Xiang, Y. and J. Du, *Effect of strontium substitution on the structure of 45S5 bioglasses.* Chemistry of Materials, 2011. **23**(11): p. 2703-2717.
34. Uno, S., W.J. Finger, and U. Fritz, *Long-term mechanical characteristics of resin-modified glass ionomer restorative materials.* Dental Materials, 1996. **12**(1): p. 64-69.
35. McCabe, J.F., *Resin-modified glass-ionomers.* Biomaterials, 1998. **19**(6): p. 521-527.
36. Walsh, W.R., et al., *Spinal fusion using an autologous growth factor gel and a porous resorbable ceramic.* European Spine Journal, 2004. **13**(4): p. 359-366.
37. Santocildes‐Romero, M.E., et al., *The osteogenic response of mesenchymal stromal cells to strontium‐substituted bioactive glasses.* Journal of Tissue Engineering and Regenerative Medicine, 2015. **9**(5): p. 619-631.
38. Sotome, S., et al., *Synthesis and in vivo evaluation of a novel hydroxyapatite/collagen–alginate as a bone filler and a drug delivery carrier of bone morphogenetic protein.* Materials Science and Engineering: C, 2004. **24**(3): p. 341-347.
39. Burg, K.J., S. Porter, and J.F. Kellam, *Biomaterial developments for bone tissue engineering.* Biomaterials, 2000. **21**(23): p. 2347-2359.
40. Freeman, M., G. Bradley, and P. Revell, *Observations upon the interface between bone and polymethylmethacrylate cement.* Bone & Joint Journal, 1982. **64**(4): p. 489-493.
41. Kim, S.B., et al., *The characteristics of a hydroxyapatite–chitosan–PMMA bone cement.* Biomaterials, 2004. **25**(26): p. 5715-5723.
42. Peters, W., et al., *The biological response to zinc polyacrylate cement.* Clinical orthopaedics and related research, 1972. **88**: p. 228-233.
43. Kenny, S. and M. Buggy, *Bone cements and fillers: a review.* Journal of Materials Science: Materials in Medicine, 2003. **14**(11): p. 923-938.
44. Santin, M., et al., *A New Class of Bioactive and Biodegradable Soybean-Based Bone Fillers.* Biomacromolecules, 2007. **8**(9): p. 2706-2711.
45. Drosos, G.I., et al., *Safety and efficacy of commercially available demineralised bone matrix preparations: a critical review of clinical studies.* Injury, 2007. **38**: p. S13-S21.
46. Dimar, J.R., et al., *Two-year fusion and clinical outcomes in 224 patients treated with a single-level instrumented posterolateral fusion with iliac crest bone graft.* The Spine Journal, 2009. **9**(11): p. 880-885.
47. Labet, M. and W. Thielemans, *Synthesis of polycaprolactone: a review.* Chemical Society Reviews, 2009. **38**(12): p. 3484-3504.
48. Azevedo, M., et al., *Development and properties of polycaprolactone/hydroxyapatite composite biomaterials.* Journal of Materials Science: Materials in Medicine, 2003. **14**(2): p. 103-107.

49. Doi, Y., S. Kitamura, and H. Abe, *Microbial synthesis and characterization of poly (3-hydroxybutyrate-co-3-hydroxyhexanoate).* Macromolecules, 1995. **28**(14): p. 4822-4828.
50. Payne, R. and A. Mikos, *Synthesis of synthetic polymers: poly (propylene fumarate).* Methods of tissue engineering. Academic Press, California, 2002: p. 649-652.
51. Nichol, J.W. and A. Khademhosseini, *Modular tissue engineering: engineering biological tissues from the bottom up.* Soft Matter, 2009. **5**(7): p. 1312-1319.
52. Elbert, D.L., *Bottom-up tissue engineering.* Current Opinion in Biotechnology, 2011. **22**(5): p. 674-680.
53. Khademhosseini, A. and R. Langer, *Microengineered hydrogels for tissue engineering.* Biomaterials, 2007. **28**(34): p. 5087-5092.
54. Wang, H.A., et al., *The Use of Micro- and Nanospheres as Functional Components for Bone Tissue Regeneration.* Tissue Engineering Part B-Reviews, 2012. **18**(1): p. 24-39.
55. Hori, Y., A.M. Winans, and D.J. Irvine, *Modular injectable matrices based on alginate solution/microsphere mixtures that gel in situ and co-deliver immunomodulatory factors.* Acta Biomaterialia, 2009. **5**(4): p. 969-982.
56. Oliveira, S.M., et al., *Injectability of a bone filler system based on hydroxyapatite microspheres and a vehicle with in situ gel‐forming ability.* Journal of Biomedical Materials Research Part B: Applied Biomaterials, 2008. **87**(1): p. 49-58.
57. Duvvuri, S., K.G. Janoria, and A.K. Mitra, *Development of a novel formulation containing poly (d, l-lactide-co-glycolide) microspheres dispersed in PLGA–PEG–PLGA gel for sustained delivery of ganciclovir.* Journal of Controlled Release, 2005. **108**(2): p. 282-293.
58. Hammond, P.T., *Recent explorations in electrostatic multilayer thin film assembly.* Current Opinion in Colloid & Interface Science, 1999. **4**(6): p. 430-442.
59. Bowden, N., et al., *Self-assembly of mesoscale objects into ordered two-dimensional arrays.* Science, 1997. **276**(5310): p. 233-235.
60. Melchels, F.P.W., et al., *Additive manufacturing of tissues and organs.* Progress in Polymer Science, 2012. **37**(8): p. 1079-1104.
61. Jiang, T., W.I. Abdel-Fattah, and C.T. Laurencin, *In vitro evaluation of chitosan/poly(lactic acid-glycolic acid) sintered microsphere scaffolds for bone tissue engineering.* Biomaterials, 2006. **27**(28): p. 4894-4903.
62. Dean, D., K.-J. Min, and A. Bond, *Computer aided design of large-format prefabricated cranial plates.* Journal of Craniofacial Surgery, 2003. **14**(6): p. 819-832.
63. Bible, E., et al., *The support of neural stem cells transplanted into stroke-induced brain cavities by PLGA particles.* Biomaterials, 2009. **30**(16): p. 2985-2994.
64. Hofmann, M., et al., *Monitoring of bone marrow cell homing into the infarcted human myocardium.* Circulation, 2005. **111**(17): p. 2198-2202.
65. Choi, S.-W., et al., *Biodegradable porous beads and their potential applications in regenerative medicine.* Journal of Materials Chemistry, 2012. **22**(23): p. 11442-11451.
66. Xu, H. and M. Weir, *Injectable, load-bearing cell/microbead/calcium phosphate bone paste for bone tissue engineering*, 2013, Google Patents.
67. Hollister, S.J., *Porous scaffold design for tissue engineering.* Nature Materials, 2005. **4**(7): p. 518-524.
68. Yanagawa, F., et al., *Directed assembly of cell-laden microgels for building porous three-dimensional tissue constructs.* Journal of Biomedical Materials Research Part A, 2011. **97A**(1): p. 93-102.
69. Oliveira, M.B. and J.F. Mano, *Polymer-Based Microparticles in Tissue Engineering and Regenerative Medicine.* Biotechnology Progress, 2011. **27**(4): p. 897-912.
70. van Wezel, A.L., J.A. van Herwaarden, and E.W. van de Heuvel-de Rijk, *Large-scale concentration and purification of virus suspension from microcarrier culture for the preparation of inactivated virus vaccines.* Dev Biol Stand, 1979. **42**: p. 65-9.
71. Davies, P.F., *Flow-mediated endothelial mechanotransduction.* Physiological reviews, 1995. **75**(3): p. 519-560.

72. Kang, S.-W., et al., *Porous poly (lactic-co-glycolic acid) microsphere as cell culture substrate and cell transplantation vehicle for adipose tissue engineering.* Tissue Engineering Part C: Methods, 2008. **14**(1): p. 25-34.
73. Kretlow, J.D., L. Klouda, and A.G. Mikos, *Injectable matrices and scaffolds for drug delivery in tissue engineering.* Advanced Drug Delivery Reviews, 2007. **59**(4): p. 263-273.
74. Brown, J.L., L.S. Nair, and C.T. Laurencin, *Solvent/non‐solvent sintering: A novel route to create porous microsphere scaffolds for tissue regeneration.* Journal of Biomedical Materials Research Part B: Applied Biomaterials, 2008. **86**(2): p. 396-406.
75. Pereira, I.H., et al., *Photopolymerizable and injectable polyurethanes for biomedical applications: synthesis and biocompatibility.* Acta Biomaterialia, 2010. **6**(8): p. 3056-3066.
76. Salem, A.K., et al., *Porous polymer and cell composites that self‐assemble in situ.* Advanced Materials, 2003. **15**(3): p. 210-213.
77. Bose, S., M. Roy, and A. Bandyopadhyay, *Recent advances in bone tissue engineering scaffolds.* Trends in Biotechnology, 2012. **30**(10): p. 546-554.
78. Xu, C. and C. Di, *The BMP signaling and in vivo bone formation.* Gene, 2005. **357**(1): p. 1-8.
79. Garcia, P., et al., *Temporal and Spatial Vascularization Patterns of Unions and Nonunions: Role of Vascular Endothelial Growth Factor and Bone Morphogenetic Proteins.* Journal of Bone and Joint Surgery-American Volume, 2012. **94A**(1): p. 49-58.
80. Beenken, A. and M. Mohammadi, *The FGF family: biology, pathophysiology and therapy.* Nature Reviews Drug Discovery, 2009. **8**(3): p. 235-253.
81. Li, R., et al., *Effect of Cell-Based VEGF Gene Therapy on Healing of a Segmental Bone Defect.* Journal of Orthopaedic Research, 2009. **27**(1): p. 8-14.
82. Levengood, S.K.L., et al., *The effect of BMP-2 on micro- and macroscale osteointegration of biphasic calcium phosphate scaffolds with multiscale porosity.* Acta Biomaterialia, 2010. **6**(8): p. 3283-3291.
83. Bessa, P.C., M. Casal, and R.L. Reis, *Bone morphogenetic proteins in tissue engineering: the road from laboratory to clinic, part II (BMP delivery).* Journal of Tissue Engineering and Regenerative Medicine, 2008. **2**(2-3): p. 81-96.
84. Kempen, D.H.R., et al., *Effect of local sequential VEGF and BMP-2 delivery on ectopic and orthotopic bone regeneration.* Biomaterials, 2009. **30**(14): p. 2816-2825.
85. Bose, S. and S. Tarafder, *Calcium phosphate ceramic systems in growth factor and drug delivery for bone tissue engineering: A review.* Acta Biomaterialia, 2012. **8**(4): p. 1401-1421.
86. Dang, J.M. and K.W. Leong, *Natural polymers for gene delivery and tissue engineering.* Advanced Drug Delivery Reviews, 2006. **58**(4): p. 487-499.
87. Kimelman-Bleich, N., et al., *Targeted Gene-and-host Progenitor Cell Therapy for Nonunion Bone Fracture Repair.* Molecular Therapy, 2011. **19**(1): p. 53-59.
88. Keeney, M., et al., *The ability of a collagen/calcium phosphate scaffold to act as its own vector for gene delivery and to promote bone formation via transfection with VEGF(165).* Biomaterials, 2010. **31**(10): p. 2893-2902.
89. Bružauskaitė, I., et al., *Scaffolds and cells for tissue regeneration: different scaffold pore sizes—different cell effects.* Cytotechnology, 2016. **68**(3): p. 355-369.
90. Smith, I.O., et al., *Nanostructured polymer scaffolds for tissue engineering and regenerative medicine.* Wiley Interdisciplinary Reviews: Nanomedicine and Nanobiotechnology, 2009. **1**(2): p. 226-236.
91. Liu, X. and P.X. Ma, *Polymeric scaffolds for bone tissue engineering.* Annals of biomedical engineering, 2004. **32**(3): p. 477-486.
92. Hatano, K., et al., *Effect of surface roughness on proliferation and alkaline phosphatase expression of rat calvarial cells cultured on polystyrene.* Bone, 1999. **25**(4): p. 439-445.
93. Karageorgiou, V. and D. Kaplan, *Porosity of 3D biomaterial scaffolds and osteogenesis.* Biomaterials, 2005. **26**(27): p. 5474-5491.
94. Lee, S.J., et al., *Response of MG63 osteoblast-like cells onto polycarbonate membrane surfaces with different micropore sizes.* Biomaterials, 2004. **25**(19): p. 4699-4707.

95. Woodard, J.R., et al., *The mechanical properties and osteoconductivity of hydroxyapatite bone scaffolds with multi-scale porosity.* Biomaterials, 2007. **28**(1): p. 45-54.
96. Scaglione, S., et al., *Order versus Disorder: in vivo bone formation within osteoconductive scaffolds.* Scientific Reports, 2012. **2**.
97. Hulbert, S., et al., *Potential of ceramic materials as permanently implantable skeletal prostheses.* Journal of biomedical materials research, 1970. **4**(3): p. 433-456.
98. Chang, H.-I. and Y. Wang, *Cell responses to surface and architecture of tissue engineering scaffolds*. 2011: INTECH Open Access Publisher.
99. Saunders, K.B. and P.A. D'Amore, *An in vitro model for cell-cell interactions.* In Vitro Cellular & Developmental Biology - Animal, 1992. **28**(7): p. 521-528.
100. Kim, S., et al., *A novel culture technique for human embryonic stem cells using porous membranes.* Stem cells, 2007. **25**(10): p. 2601-2609.
101. Li, D., et al., *Growth and migration of umbilical cord mesenchymal stem cells on polycarbonate membrane with different pore sizes.* Zhonghua yi xue za zhi, 2011. **91**(10): p. 699-702.
102. Peyton, S.R., et al., *Marrow-Derived stem cell motility in 3D synthetic scaffold is governed by geometry along with adhesivity and stiffness.* Biotechnology and Bioengineering, 2011. **108**(5): p. 1181-1193.
103. Akino, K., et al., *Human mesenchymal stem cells may be involved in keloid pathogenesis.* International journal of dermatology, 2008. **47**(11): p. 1112-1117.
104. Akram, K.M., et al., *Mesenchymal stem cells promote alveolar epithelial cell wound repair in vitro through distinct migratory and paracrine mechanisms.* Respiratory research, 2013. **14**(1): p. 1.
105. Wolf, K., et al., *Physical limits of cell migration: control by ECM space and nuclear deformation and tuning by proteolysis and traction force.* The Journal of cell biology, 2013. **201**(7): p. 1069-1084.
106. Nichol, J.W., et al., *Cell-laden microengineered gelatin methacrylate hydrogels.* Biomaterials, 2010. **31**(21): p. 5536-5544.
107. Wang, C.M., R.R. Varshney, and D.A. Wang, *Therapeutic cell delivery and fate control in hydrogels and hydrogel hybrids.* Advanced Drug Delivery Reviews, 2010. **62**(7-8): p. 699-710.
108. Therriault, D., S.R. White, and J.A. Lewis, *Chaotic mixing in three-dimensional microvascular networks fabricated by direct-write assembly.* Nature Materials, 2003. **2**(4): p. 265-271.
109. Takahashi, H., et al., *Acetaminophen particle design using chitosan and a spray-drying technique.* Chemical & Pharmaceutical Bulletin, 2005. **53**(1): p. 37-41.
110. Elversson, J. and A. Millqvist-Fureby, *Particle size and density in spray drying - Effects of carbohydrate properties.* Journal of Pharmaceutical Sciences, 2005. **94**(9): p. 2049-2060.
111. da Silva-Junior, A.A., et al., *Thermal behavior and stability of biodegradable spray-dried microparticles containing triamcinolone.* International Journal of Pharmaceutics, 2009. **368**(1-2): p. 45-55.
112. Sinchaipanid, N., V. Junyaprasert, and A. Mitrevej, *Application of hot-melt coating for controlled release of propranolol hydrochloride pellets.* Powder Technology, 2004. **141**(3): p. 203-209.
113. Jannin, V. and Y. Cuppok, *Hot-melt coating with lipid excipients.* International Journal of Pharmaceutics, 2013. **457**(2): p. 480-487.
114. Pham, L. and J.M. Christensen, *Preparation of acetaminophen capsules containing beads prepared by hot-melt direct blend coating.* Pharmaceutical Development and Technology, 2014. **19**(1): p. 91-102.
115. Becker, K., S. Salar-Behzadi, and A. Zimmer, *Solvent-Free Melting Techniques for the Preparation of Lipid-Based Solid Oral Formulations.* Pharmaceutical Research, 2015. **32**(5): p. 1519-1545.
116. Shi, J., N.M. Alves, and J.F. Mano, *Chitosan coated alginate beads containing poly(N-isopropylacrylamide) for dual-stimuli-responsive drug release.* Journal of Biomedical Materials Research Part B-Applied Biomaterials, 2008. **84B**(2): p. 595-603.

117. Yang, C.H., et al., *Core-shell structure microcapsules with dual pH-responsive drug release function.* Electrophoresis, 2014. **35**(18): p. 2673-2680.
118. Costa, N.L., P. Sher, and J.F. Mano, *Liquefied Capsules Coated with Multilayered Polyelectrolyte Films for Cell Immobilization.* Advanced Engineering Materials, 2011. **13**(6): p. B218-B224.
119. Moshaverinia, A., et al., *Regulation of the Stem Cell-Host Immune System Interplay Using Hydrogel Coencapsulation System with an Anti-Inflammatory Drug.* Advanced Functional Materials, 2015. **25**(15): p. 2296-2307.
120. Elkharraz, K., A. Dashevsky, and R. Bodmeier, *Microparticles prepared by grinding of polymeric films.* Journal of Microencapsulation, 2003. **20**(5): p. 661-673.
121. Wolff, M.F.H., et al., *Attritor-milling of poly(amide imide) suspensions.* Particuology, 2014. **17**: p. 92-96.
122. Xu, Y.L., et al., *Dissolution improvement of poorly water-soluble drug by cogrinding method using jar mill.* Pakistan Journal of Pharmaceutical Sciences, 2013. **26**(3): p. 495-502.
123. Tapia-Hernandez, J.A., et al., *Micro- and Nanoparticles by Electrospray: Advances and Applications in Foods.* Journal of Agricultural and Food Chemistry, 2015. **63**(19): p. 4699-4707.
124. Lee, Y.-H., et al., *Release profile characteristics of biodegradable-polymer-coated drug particles fabricated by dual-capillary electrospray.* Journal of Controlled Release, 2010. **145**(1): p. 58-65.
125. Cooper, A.I., *Porous Materials and Supercritical Fluids.* Advanced Materials, 2003. **15**(13): p. 1049-1059.
126. Koushik, K. and U. Kompella, *Preparation of Large Porous Deslorelin-PLGA Microparticles with Reduced Residual Solvent and Cellular Uptake Using a Supercritical Carbon Dioxide Process.* Pharmaceutical Research, 2004. **21**(3): p. 524-535.
127. Jung, J. and M. Perrut, *Particle design using supercritical fluids: Literature and patent survey.* The Journal of Supercritical Fluids, 2001. **20**(3): p. 179-219.
128. Go, D.P., et al., *Porous PLGA microspheres tailored for dual delivery of biomolecules via layer-by-layer assembly.* Journal of Biomedical Materials Research Part A, 2014: p. n/a-n/a.
129. Maeng, Y.-J., et al., *Culture of human mesenchymal stem cells using electrosprayed porous chitosan microbeads.* Journal of Biomedical Materials Research Part A, 2010. **92A**(3): p. 869-876.
130. Zhang, T., et al., *The controllable preparation of porous PLGA microspheres by the oil/water emulsion method and its application in 3D culture of ovarian cancer cells.* Colloids and Surfaces A: Physicochemical and Engineering Aspects, 2014. **452**(0): p. 115-124.
131. Lim, S.M., et al., *Novel Fabrication of PCL Porous Beads for Use as an Injectable Cell Carrier System.* Journal of Biomedical Materials Research Part B-Applied Biomaterials, 2009. **90B**(2): p. 521-530.
132. Choi, S.W., et al., *Uniform Beads with Controllable Pore Sizes for Biomedical Applications.* Small, 2010. **6**(14): p. 1492-1498.
133. Lu, Y., et al., *A digital micro-mirror device-based system for the microfabrication of complex, spatially patterned tissue engineering scaffolds.* Journal of Biomedical Materials Research Part A, 2006. **77A**(2): p. 396-405.
134. Han, L.H., et al., *Fabrication of three-dimensional scaffolds for heterogeneous tissue engineering.* Biomedical Microdevices, 2010. **12**(4): p. 721-725.
135. Choi, J.W., et al., *Fabrication of 3D biocompatible/biodegradable micro-scaffolds using dynamic mask projection microstereolithography.* Journal of Materials Processing Technology, 2009. **209**(15-16): p. 5494-5503.
136. Dendukuri, D., et al., *Continuous-flow lithography for high-throughput microparticle synthesis.* Nature Materials, 2006. **5**(5): p. 365-369.
137. Dendukuri, D., et al., *Controlled synthesis of nonspherical microparticles using microfluidics.* Langmuir, 2005. **21**(6): p. 2113-2116.
138. Helgeson, M.E., S.C. Chapin, and P.S. Doyle, *Hydrogel microparticles from lithographic processes: Novel materials for fundamental and applied colloid science.* Current Opinion in Colloid & Interface Science, 2011. **16**(2): p. 106-117.

139. Shim, T.S., S.H. Kim, and S.M. Yang, *Elaborate Design Strategies Toward Novel Microcarriers for Controlled Encapsulation and Release.* Particle & Particle Systems Characterization, 2013. **30**(1): p. 9-45.
140. Waldbaur, A., et al., *Let there be chip-towards rapid prototyping of microfluidic devices: one-step manufacturing processes.* Analytical Methods, 2011. **3**(12): p. 2681-2716.
141. Hwang, D.K., et al., *Stop-Flow Lithography for the Production of Shape-Evolving Degradable Microgel Particles.* Journal of the American Chemical Society, 2009. **131**(12): p. 4499-4504.
142. Baah, D., et al., *Microfluidic synthesis and post processing of non-spherical polymeric microparticles.* Microfluidics and Nanofluidics, 2012. **12**(1-4): p. 657-662.
143. Chung, S.E., et al., *Optofluidic maskless lithography system for real-time synthesis of photopolymerized microstructures in microfluidic channels.* Applied Physics Letters, 2007. **91**(4).
144. Chung, S.E., Y. Jung, and S. Kwon, *Three-Dimensional Fluidic Self-Assembly by Axis Translation of Two-Dimensionally Fabricated Microcomponents in Railed Microfluidics.* Small, 2011. **7**(6): p. 796-803.
145. Laza, S.C., et al., *Two-Photon Continuous Flow Lithography.* Advanced Materials, 2012. **24**(10): p. 1304-1308.
146. Laza, S.C., et al., *Two‐Photon Continuous Flow Lithography.* Advanced Materials, 2012.
147. Wang, J.T., J. Wang, and J.J. Han, *Fabrication of Advanced Particles and Particle-Based Materials Assisted by Droplet-Based Microfluidics.* Small, 2011. **7**(13): p. 1728-1754.
148. Shepherd, R.F., et al., *Microfluidic assembly of homogeneous and janus colloid-filled hydrogel granules.* Langmuir, 2006. **22**(21): p. 8618-8622.
149. Chung, B.G., et al., *Microfluidic fabrication of microengineered hydrogels and their application in tissue engineering.* Lab on a Chip, 2012. **12**(1): p. 45-59.
150. Cameron, N.R., *High internal phase emulsion templating as a route to well-defined porous polymers.* Polymer, 2005. **46**(5): p. 1439-1449.
151. Barbetta, A. and N.R. Cameron, *Morphology and surface area of emulsion-derived (PolyHIPE) solid foams prepared with oil-phase soluble porogenic solvents: Span 80 as surfactant.* Macromolecules, 2004. **37**(9): p. 3188-3201.
152. Pierre, S.J., et al., *Covalent enzyme immobilization onto photopolymerized highly porous monoliths.* Advanced Materials, 2006. **18**(14): p. 1822-1826.
153. Walstra, P., *Principles of emulsion formation.* Chemical Engineering Science, 1993. **48**(2): p. 333-349.
154. Li, Z., et al., *The facile synthesis of PMMA polyHIPEs with highly interconnected porous microstructures.* Journal of Materials Science, 2016. **51**(19): p. 9005-9018.
155. Pakeyangkoon, P., et al. *Effect of soxhlet extraction and surfactant system on morphology and properties of poly (DVB) polyHIPE*. in *Macromolecular symposia*. 2008. Wiley Online Library.
156. Evans, N.D., et al., *Substrate stiffness affects early differentiation events in embryonic stem cells.* Eur Cell Mater, 2009. **18**(1): p. e13.
157. Engh, C., J. Bobyn, and A.H. Glassman, *Porous-coated hip replacement. The factors governing bone ingrowth, stress shielding, and clinical results.* Bone & Joint Journal, 1987. **69**(1): p. 45-55.
158. Huiskes, R., H. Weinans, and B. Van Rietbergen, *The relationship between stress shielding and bone resorption around total hip stems and the effects of flexible materials.* Clinical orthopaedics and related research, 1992. **274**: p. 124-134.
159. Ikem, V.O., A. Menner, and A. Bismarck, *High-porosity macroporous polymers sythesized from titania-particle-stabilized medium and high internal phase emulsions.* Langmuir, 2010. **26**(11): p. 8836-8841.
160. Lovelady, E., et al., *Preparation of emulsion-templated porous polymers using thiol–ene and thiol–yne chemistry.* Polymer Chemistry, 2011. **2**(3): p. 559-562.
161. Gurevitch, I. and M.S. Silverstein, *Nanoparticle-based and organic-phase-based AGET ATRP polyHIPE synthesis within pickering HIPEs and surfactant-stabilized HIPEs.* Macromolecules, 2011. **44**(9): p. 3398-3409.

162. Kovačič, S., P. Krajnc, and C. Slugovc, *Inherently reactive polyHIPE material from dicyclopentadiene.* Chemical Communications, 2010. **46**(40): p. 7504-7506.
163. Deleuze, H., R. Faivre, and V. Herroguez, *Preparation and functionalisation of emulsion-derived microcellular polymeric foams (polyHIPEs) by ring-opening metathesis polymerisation (ROMP).* Chemical Communications, 2002(23): p. 2822-2823.
164. Audouin, F., et al., *Synthesis of porous materials by 2‐nitroresorcinol/cyanuric chloride thermal polycondensation in emulsions.* Journal of applied polymer science, 2008. **108**(5): p. 2808-2813.
165. Cameron, N., et al., *Study of the formation of the open-cellular morphology of poly (styrene/divinylbenzene) polyHIPE materials by cryo-SEM.* Colloid and Polymer Science, 1996. **274**(6): p. 592-595.
166. Menner, A. and A. Bismarck. *New evidence for the mechanism of the pore formation in polymerising high internal phase emulsions or why polyHIPEs have an interconnected pore network structure*. in *Macromolecular symposia*. 2006. Wiley Online Library.
167. Tadros, T., et al., *Formation and stability of nano-emulsions.* Advances in colloid and interface science, 2004. **108**: p. 303-318.
168. Kabalnov, A.S. and E.D. Shchukin, *Ostwald ripening theory: applications to fluorocarbon emulsion stability.* Advances in colloid and interface science, 1992. **38**: p. 69-97.
169. Taylor, P., *Ostwald ripening in emulsions.* Advances in colloid and interface science, 1998. **75**(2): p. 107-163.
170. Rubino, J., *The influence of charged lipids on the flocculation and coalescence of oil-in-water emulsions. I: Kinetic assessment of emulsion stability.* Journal of parenteral science and technology: a publication of the Parenteral Drug Association, 1989. **44**(4): p. 210-215.
171. Howe, A.M., A.R. Mackie, and M.M. Robins, *Technique to measure emulsion creaming by velocity of ultrasound.* JOURNAL OF DISPERSION SCIENCE ANDTECHNOLOGY, 1986. **7**(2): p. 231-243.
172. Dickinson, E., M. Golding, and M.J. Povey, *Creaming and flocculation of oil-in-water emulsions containing sodium caseinate.* Journal of Colloid and Interface Science, 1997. **185**(2): p. 515-529.
173. Binks, B.P. and R. Murakami, *Phase inversion of particle-stabilized materials from foams to dry water.* Nature Materials, 2006. **5**(11): p. 865-869.
174. Throckmorton, P.E., et al., *Biodegradable surfactants derived from corn starch.* Journal of the American Oil Chemists Society, 1974. **51**(11): p. 486-494.
175. Capron, I. and B. Cathala, *Surfactant-free high internal phase emulsions stabilized by cellulose nanocrystals.* Biomacromolecules, 2013. **14**(2): p. 291-296.
176. Gurevitch, I. and M.S. Silverstein, *Polymerized pickering HIPEs: Effects of synthesis parameters on porous structure.* Journal of Polymer Science Part A: Polymer Chemistry, 2010. **48**(7): p. 1516-1525.
177. Menner, A., et al., *High internal phase emulsion templates solely stabilised by functionalised titania nanoparticles.* Chemical Communications, 2007(41): p. 4274-4276.
178. Niu, X., et al., *Porous nano-HA/collagen/PLLA scaffold containing chitosan microspheres for controlled delivery of synthetic peptide derived from BMP-2.* Journal of Controlled Release, 2009. **134**(2): p. 111-117.
179. Liao, S., et al., *Hierarchically biomimetic bone scaffold materials: nano‐HA/collagen/PLA composite.* Journal of Biomedical Materials Research Part B: Applied Biomaterials, 2004. **69**(2): p. 158-165.
180. Lei, L., et al., *High internal phase emulsion with double emulsion morphology and their templated porous polymer systems.* Journal of Colloid and Interface Science, 2016.
181. Vladisavljević, G.T., et al., *Shirasu Porous Glass membrane emulsification: Characterisation of membrane structure by high-resolution X-ray microtomography and microscopic observation of droplet formation in real time.* Journal of Membrane Science, 2007. **302**(1): p. 243-253.
182. Yanagishita, T., et al., *Fabrication of monodisperse polymer nanoparticles by membrane emulsification using ordered anodic porous alumina.* Langmuir, 2009. **26**(3): p. 1516-1519.

183. Gokmen, M.T., et al., *Fabrication of porous "clickable" polymer beads and rods through generation of high internal phase emulsion (HIPE) droplets in a simple microfluidic device.* Macromolecules, 2009. **42**(23): p. 9289-9294.
184. Moglia, R.S., et al., *Injectable PolyHIPEs as High-Porosity Bone Grafts.* Biomacromolecules, 2011. **12**(10): p. 3621-3628.
185. Akay, G., M.A. Birch, and M.A. Bokhari, *Microcellular polyHIPE polymer supports osteoblast growth and bone formation in vitro.* Biomaterials, 2004. **25**(18): p. 3991-4000.
186. Busby, W., N.R. Cameron, and C.A. Jahoda, *Emulsion-derived foams (PolyHIPEs) containing poly (ε-caprolactone) as matrixes for tissue engineering.* Biomacromolecules, 2001. **2**(1): p. 154-164.
187. Hayman, M.W., et al., *Growth of human stem cell-derived neurons on solid three-dimensional polymers.* Journal of Biochemical and Biophysical Methods, 2005. **62**(3): p. 231-240.
188. Moglia, R., et al., *Solvent‐Free Fabrication of polyHIPE Microspheres for Controlled Release of Growth Factors.* Macromolecular rapid communications, 2014. **35**(14): p. 1301-1305.
189. Wang, M., et al., *Preparation of polycaprolactone microspheres-aggregated scaffold with ultra big pores and fuzzy sphere surface by a one-step phase separation method.* Journal of Biomedical Materials Research Part A, 2013. **101**(11): p. 3219-3227.
190. Kircher, L., P. Theato, and N.R. Cameron, *Reactive thiol-ene emulsion-templated porous polymers incorporating pentafluorophenyl acrylate.* Polymer, 2013. **54**(7): p. 1755-1761.
191. Caldwell, S., et al., *Degradable emulsion-templated scaffolds for tissue engineering from thiol–ene photopolymerisation.* Soft Matter, 2012. **8**(40): p. 10344-10351.
192. Huang, Z.N., et al., *The sequential expression profiles of growth factors from osteroprogenitors to osteoblasts In vitro.* Tissue Engineering, 2007. **13**(9): p. 2311-2320.
193. Chamberlain, G., et al., *Concise review: mesenchymal stem cells: their phenotype, differentiation capacity, immunological features, and potential for homing.* Stem cells, 2007. **25**(11): p. 2739-2749.
194. Pittenger, M.F., et al., *Multilineage potential of adult human mesenchymal stem cells.* Science, 1999. **284**(5411): p. 143-147.
195. Tatsumi, S., et al., *Targeted ablation of Osteocytes induces osteoporosis with defective mechanotransduction.* Cell Metabolism, 2007. **5**(6): p. 464-475.
196. Bonewald, L.F., *Osteocytes as dynamic multifunctional cells*, in *Skeletal Biology and Medicine, Pt A: Aspects of Bone Morphogenesis and Remodeling*, M. Zaidi, Editor. 2007. p. 281-290.
197. Bonewald, L.F., *The Amazing Osteocyte.* Journal of Bone and Mineral Research, 2011. **26**(2): p. 229-238.
198. Matsuo, K. and N. Nango, *Osteocytic osteolysis : measurements of the volume of osteocytic lacunae.* Clin Calcium, 2012. **22**(5): p. 677-83.
199. Boyle, W.J., W.S. Simonet, and D.L. Lacey, *Osteoclast differentiation and activation.* Nature, 2003. **423**(6937): p. 337-342.
200. Miller, S.C., et al., *Bone lining cells: structure and function.* Scanning microscopy, 1989. **3**(3): p. 953-60; discussion 960-1.
201. Mackie, E., et al., *Endochondral ossification: how cartilage is converted into bone in the developing skeleton.* The international journal of biochemistry & cell biology, 2008. **40**(1): p. 46-62.
202. Crisan, M., et al., *A perivascular origin for mesenchymal stem cells in multiple human organs.* Cell stem cell, 2008. **3**(3): p. 301-313.
203. Lincks, J., et al., *Response of MG63 osteoblast-like cells to titanium and titanium alloy is dependent on surface roughness and composition.* Biomaterials, 1998. **19**(23): p. 2219-2232.
204. Kato, Y., et al., *Establishment of an osteocyte‐like cell line, MLO‐Y4.* Journal of Bone and Mineral Research, 1997. **12**(12): p. 2014-2023.
205. Bonewald, L.F. and Y. Kato, *Osteocyte cell lines*, 2002, Google Patents.
206. Thomson, J.A., et al., *Embryonic stem cell lines derived from human blastocysts.* Science, 1998. **282**(5391): p. 1145-1147.
207. Karlsson, C., et al., *Human embryonic stem cell-derived mesenchymal progenitors-Potential in regenerative medicine.* Stem Cell Research, 2009. **3**(1): p. 39-50.

208. Moon, S., et al., *Development of a Novel Two-dimensional Directed Differentiation System for Generation of Cardiomyocytes From Human ES Cells and iPS Cells.* Circulation, 2009. **120**(18): p. S765-S765.
209. Kehat, I., et al., *Development of cardiomyocytes from human ES cells*, in *Differentiation of Embryonic Stem Cells*, P.M. Wassarman and G.M. Keller, Editors. 2003. p. 461-+.
210. Sottile, V., A. Thomson, and J. McWhir, *In vitro osteogenic differentiation of human ES cells.* Cloning and Stem Cells, 2003. **5**(2): p. 149-155.
211. D'Amour, K.A., et al., *Production of pancreatic hormone-expressing endocrine cells from human embryonic stem cells.* Nature Biotechnology, 2006. **24**(11): p. 1392-1401.
212. Lavon, N., O. Yanuka, and N. Benvenisty, *Differentiation and isolation of hepatic-like cells from human embryonic stem cells.* Differentiation, 2004. **72**(5): p. 230-238.
213. Carpenter, M.K., et al., *Enrichment of neurons and neural precursors from human embryonic stem cells.* Experimental Neurology, 2001. **172**(2): p. 383-397.
214. Coelho, M. and M. Fernandes, *Human bone cell cultures in biocompatibility testing. Part II: effect of ascorbic acid, β-glycerophosphate and dexamethasone on osteoblastic differentiation.* Biomaterials, 2000. **21**(11): p. 1095-1102.
215. Hirao, M., et al., *Oxygen tension is an important mediator of the transformation of osteoblasts to osteocytes.* Journal of bone and mineral metabolism, 2007. **25**(5): p. 266-276.
216. Utting, J., et al., *Hypoxia inhibits the growth, differentiation and bone-forming capacity of rat osteoblasts.* Experimental Cell Research, 2006. **312**(10): p. 1693-1702.
217. Arnett, T.R., et al., *Hypoxia is a major stimulator of osteoclast formation and bone resorption.* Journal of cellular physiology, 2003. **196**(1): p. 2-8.
218. Hinoi, E., et al., *Positive regulation of osteoclastic differentiation by growth differentiation factor 15 upregulated in osteocytic cells under hypoxia.* Journal of Bone and Mineral Research, 2012. **27**(4): p. 938-949.
219. Birmingham, E., et al., *Osteogenic differentiation of mesenchymal stem cells is regulated by osteocyte and osteoblast cells in a simplified bone niche.* European Cells & Materials, 2012. **23**: p. 13-27.
220. Ilmer, M., et al., *Human Osteoblast-Derived Factors Induce Early Osteogenic Markers in Human Mesenchymal Stem Cells.* Tissue Engineering Part A, 2009. **15**(9): p. 2397-2409.
221. Lu, Z.F., et al., *Osteoblasts on Rod Shaped Hydroxyapatite Nanoparticles Incorporated PCL Film Provide an Optimal Osteogenic Niche for Stem Cell Differentiation.* Tissue Engineering Part A, 2011. **17**(11-12): p. 1651-1661.
222. Hoey, D.A., D.J. Kelly, and C.R. Jacobs, *A role for the primary cilium in paracrine signaling between mechanically stimulated osteocytes and mesenchymal stem cells.* Biochemical and Biophysical Research Communications, 2011. **412**(1): p. 182-187.
223. Heino, T.J., T.A. Hentunen, and H.K. Vaananen, *Conditioned medium from osteocytes stimulates the proliferation of bone marrow mesenchymal stem cells and their differentiation into ostcoblasts.* Experimental Cell Research, 2004. **294**(2): p. 458-468.
224. Rouwkema, J., N.C. Rivron, and C.A. van Blitterswijk, *Vascularization in tissue engineering.* Trends in Biotechnology, 2008. **26**(8): p. 434-441.
225. Novosel, E.C., C. Kleinhans, and P.J. Kluger, *Vascularization is the key challenge in tissue engineering.* Advanced Drug Delivery Reviews, 2011. **63**(4-5): p. 300-311.
226. Bramfeldt, H., et al., *Scaffold Vascularization: A Challenge for Three-Dimensional Tissue Engineering.* Current Medicinal Chemistry, 2010. **17**(33): p. 3944-3967.
227. Jain, R.K., et al., *Engineering vascularized tissue.* Nature Biotechnology, 2005. **23**(7): p. 821-823.
228. Malda, J., et al., *Oxygen gradients in tissue-engineered PEGT/PBT cartilaginous constructs: Measurement and modeling.* Biotechnology and Bioengineering, 2004. **86**(1): p. 9-18.
229. Griffith, L.G. and G. Naughton, *Tissue Engineering--Current Challenges and Expanding Opportunities.* Science, 2002. **295**(5557): p. 1009-1014.
230. Risau, W., *Mechanisms of angiogenesis.* Nature, 1997. **386**(6626): p. 671-674.

231. Karamysheva, A., *Mechanisms of angiogenesis.* Biochemistry (Moscow), 2008. **73**(7): p. 751-762.
232. Risau, W. and I. Flamme, *Vasculogenesis.* Annual review of cell and developmental biology, 1995. **11**(1): p. 73-91.
233. Carmeliet, P., *Angiogenesis in life, disease and medicine.* Nature, 2005. **438**(7070): p. 932-936.
234. Baldwin, J., et al., *In vitro pre-vascularisation of tissue-engineered constructs A co-culture perspective.* Vascular cell, 2014. **6**(1): p. 1.
235. Duffy, G.P., et al., *Towards in vitro vascularisation of collagen-GAG scaffolds.* Eur Cell Mater, 2011. **21**(15): p. e30.
236. Kaully, T., et al., *Vascularization—the conduit to viable engineered tissues.* Tissue Engineering Part B: Reviews, 2009. **15**(2): p. 159-169.
237. Wang, Z., et al., *Rapid vascularization of tissue-engineered vascular grafts in vivo by endothelial cells in co-culture with smooth muscle cells.* Journal of Materials Science: Materials in Medicine, 2012. **23**(4): p. 1109-1117.
238. Koob, S., et al., *Bone Formation and Neovascularization Mediated by Mesenchymal Stem Cells and Endothelial Cells in Critical-Sized Calvarial Defects.* Tissue Engineering Part A, 2011. **17**(3-4): p. 311-321.
239. Gorustovich, A.A., J.A. Roether, and A.R. Boccaccini, *Effect of bioactive glasses on angiogenesis: a review of in vitro and in vivo evidences.* Tissue Engineering Part B: Reviews, 2009. **16**(2): p. 199-207.
240. Auerbach, R., et al., *Angiogenesis assays: a critical overview.* Clinical chemistry, 2003. **49**(1): p. 32-40.
241. Ortega, I., et al., *Fabrication of biodegradable synthetic perfusable vascular networks via a combination of electrospinning and robocasting.* Biomaterials science, 2015. **3**(4): p. 592-596.
242. Nicosia, R.F. and A. Ottinetti, *Growth of microvessels in serum-free matrix culture of rat aorta. A quantitative assay of angiogenesis in vitro.* Laboratory investigation; a journal of technical methods and pathology, 1990. **63**(1): p. 115-122.
243. Moses, M.A., *Chorioallantoic Membrane (CAM) Assay.* Encyclopedia of Systems Biology, 2013: p. 400-401.
244. Schlatter, P., et al., *Quantitative study of intussusceptive capillary growth in the chorioallantoic membrane (CAM) of the chicken embryo.* Microvascular research, 1997. **54**(1): p. 65-73.
245. Akhtar, N., E.B. Dickerson, and R. Auerbach, *The sponge/Matrigel angiogenesis assay.* Angiogenesis, 2002. **5**(1-2): p. 75-80.
246. Li, M., et al., *The In Ovo Chick Chorioallantoic Membrane (CAM) Assay as an Efficient Xenograft Model of Hepatocellular Carcinoma.* JoVE (Journal of Visualized Experiments), 2015(104): p. e52411-e52411.
247. Hayward, A.S., et al., *Acrylic-Acid-Functionalized PolyHIPE Scaffolds for Use in 3D Cell Culture.* Macromolecular rapid communications, 2013. **34**(23-24): p. 1844-1849.
248. Filova, E., et al., *Regionally-Selective Cell Colonization of Micropatterned Surfaces Prepared by Plasma Polymerization of Acrylic Acid and 1,7-Octadiene.* Physiological Research, 2009. **58**(5): p. 669-684.
249. Curran, J.M., et al., *The osteogenic response of mesenchymal stem cells to an injectable PLGA bone regeneration system.* Biomaterials, 2013. **34**(37): p. 9352-9364.
250. Alexander, M.R. and T.M. Duc, *The chemistry of deposits formed from acrylic acid plasmas.* Journal of Materials Chemistry, 1998. **8**(4): p. 937-943.
251. Gregory, C.A., et al., *An Alizarin red-based assay of mineralization by adherent cells in culture: comparison with cetylpyridinium chloride extraction.* Analytical biochemistry, 2004. **329**(1): p. 77-84.
252. Gigliobianco, G., C.K. Chong, and S. MacNeil, *Simple surface coating of electrospun poly-L-lactic acid scaffolds to induce angiogenesis.* Journal of biomaterials applications, 2015. **30**(1): p. 50-60.

253. Kasten, P., et al., *Porosity and pore size of β-tricalcium phosphate scaffold can influence protein production and osteogenic differentiation of human mesenchymal stem cells: An in vitro and in vivo study.* Acta Biomaterialia, 2008. **4**(6): p. 1904-1915.
254. Sun, H.-B. and S. Kawata, *Two-Photon Laser Precision Microfabrication and Its Applications to Micro-Nano Devices and Systems.* Journal of Lightwave Technology, 2003. **21**(3): p. 624.
255. Cooke, M.N., et al., *Use of stereolithography to manufacture critical-sized 3D biodegradable scaffolds for bone ingrowth.* Journal of Biomedical Materials Research Part B: Applied Biomaterials, 2003. **64B**(2): p. 65-69.
256. Carter, P.W. *Advances in rapid prototyping and rapid manufacturing*. in *Electrical Insulation Conference and Electrical Manufacturing & Coil Winding Conference, 2001. Proceedings*. 2001.
257. Zhang, Y.-L., et al., *Designable 3D nanofabrication by femtosecond laser direct writing.* Nano Today, 2010. **5**(5): p. 435-448.
258. Wu, S., J. Serbin, and M. Gu, *Two-photon polymerisation for three-dimensional micro-fabrication.* Journal of Photochemistry and Photobiology A: Chemistry, 2006. **181**(1): p. 1-11.
259. Ovsianikov, A., et al., *Ultra-Low Shrinkage Hybrid Photosensitive Material for Two-Photon Polymerization Microfabrication.* ACS Nano, 2008. **2**(11): p. 2257-2262.
260. Raimondi, M.T., et al., *Two-photon laser polymerization: from fundamentals to biomedical application in tissue engineering and regenerative medicine.* Journal of Applied Biomaterials & Functional Materials, 2012. **10**(1): p. 55-65.
261. Eijkel, J.C.T. and A. van den Berg, *Nanotechnology for membranes, filters and sieves.* Lab on a Chip, 2006. **6**(1): p. 19-23.
262. Lévesque, S.G., R.M. Lim, and M.S. Shoichet, *Macroporous interconnected dextran scaffolds of controlled porosity for tissue-engineering applications.* Biomaterials, 2005. **26**(35): p. 7436-7446.
263. Hwang, S.J., et al., *Production of uniform emulsion droplets using a simple fluidic device with a peristaltic pump.* Macromolecular Research, 2014. **22**(5): p. 557-561.
264. Moon, S.K., I.W. Cheong, and S.W. Choi, *Effect of flow rates of the continuous phase on droplet size in dripping and jetting regimes in a simple fluidic device for coaxial flow.* Colloids and Surfaces a-Physicochemical and Engineering Aspects, 2014. **454**: p. 84-88.
265. Zhang, T.Z., et al., *The controllable preparation of porous PLGA microspheres by the oil/water emulsion method and its application in 3D culture of ovarian cancer cells.* Colloids and Surfaces a-Physicochemical and Engineering Aspects, 2014. **452**: p. 115-124.
266. Bacakova, L., et al., *Cell adhesion on artificial materials for tissue engineering.* Physiological Research, 2004. **53**: p. S35-S45.
267. Kim, P., et al., *Fabrication of non-biofouling polyethylene glycol micro- and nanochannels by ultraviolet-assisted irreversible sealing.* Lab on a Chip, 2006. **6**(11): p. 1432-1437.
268. Suh, K.Y., et al., *A simple soft lithographic route to fabrication of poly(ethylene glycol) microstructures for protein and cell patterning.* Biomaterials, 2004. **25**(3): p. 557-563.
269. Sawhney, A.S., C.P. Pathak, and J.A. Hubbell, *Bioerodible hydrogels based on photopolymerized poly(ethylene glycol)-co-poly(.alpha.-hydroxy acid) diacrylate macromers.* Macromolecules, 1993. **26**(4): p. 581-587.
270. McKoy, V.B. and A. Gupta, *Photocurable acrylic composition, and U.V. curing with development of U.V. absorber*, 1992, Google Patents.
271. Lu, Y., et al., *A digital micro-mirror device-based system for the microfabrication of complex, spatially patterned tissue engineering scaffolds.* Journal of Biomedical Materials Research Part A, 2006. **77A**(2): p. 396-405.
272. Gokmen, M.T., et al., *Complexity from Simplicity: Unique Polymer Capsules, Rods, Monoliths, and Liquid Marbles Prepared via HIPE in Microfluidics.* Particle & Particle Systems Characterization, 2013. **30**(5): p. 438-444.
273. Gokmen, M.T. and F.E. Du Prez, *Porous polymer particles-A comprehensive guide to synthesis, characterization, functionalization and applications.* Progress in Polymer Science, 2012. **37**(3): p. 365-405.

274. Menner, A. and A. Bismarck, *New Evidence for the Mechanism of the Pore Formation in Polymerising High Internal Phase Emulsions or Why polyHIPEs Have an Interconnected Pore Network Structure.* Macromolecular Symposia, 2006. **242**(1): p. 19-24.
275. Bhuva, R.L., et al., *Data loading circuit for digital micro-mirror device*, 1997, Google Patents.
276. Pateman, C.J., et al., *Nerve guides manufactured from photocurable polymers to aid peripheral nerve repair.* Biomaterials, 2015. **49**: p. 77-89.
277. Hsiao, C., et al., *Effects of 3-D microwell culture on initial fate specification in human embryonic stem cells.* Aiche Journal, 2014. **60**(4): p. 1225-1235.
278. Sun, C., et al., *Projection micro-stereolithography using digital micro-mirror dynamic mask.* Sensors and Actuators A: Physical, 2005. **121**(1): p. 113-120.
279. Martínez, E., et al., *Effects of artificial micro- and nano-structured surfaces on cell behaviour.* Annals of Anatomy - Anatomischer Anzeiger, 2009. **191**(1): p. 126-135.
280. Yeong, W.Y., et al., *Multiscale Topological Guidance for Cell Alignment via Direct Laser Writing on Biodegradable Polymer.* Tissue Engineering Part C-Methods, 2010. **16**(5): p. 1011-1021.
281. Lee, K.-S., et al., *Advances in 3D nano/microfabrication using two-photon initiated polymerization.* Progress in Polymer Science, 2008. **33**(6): p. 631-681.
282. Seet, K.K., et al., *Three‐Dimensional Spiral‐Architecture Photonic Crystals Obtained By Direct Laser Writing.* Advanced Materials, 2005. **17**(5): p. 541-545.
283. Kang, S.W., O. Jeon, and B.S. Kim, *Poly(lactic-co-glycolic acid) microspheres as an injectable scaffold for cartilage tissue engineering.* Tissue Engineering, 2005. **11**(3-4): p. 438-447.
284. Dendukuri, D., et al., *Stop-flow lithography in a microfluidic device.* Lab on a Chip, 2007. **7**(7): p. 818-828.
285. Peng, S., et al., *Evaluation of a mPEG-polyester-based hydrogel as cell carrier for chondrocytes.* Journal of Biomedical Materials Research Part A, 2013: p. n/a-n/a.
286. del Burgo, L.S., et al., *Microencapsulation of therapeutic bispecific antibodies producing cells: immunotherapeutic organoids for cancer management.* Journal of Drug Targeting, 2015. **23**(2): p. 170-179.
287. Shepherd, J.N.H., et al., *3D Microperiodic Hydrogel Scaffolds for Robust Neuronal Cultures.* Advanced Functional Materials, 2011. **21**(1): p. 47-54.
288. Oliveira, M.B., et al., *Development of an injectable system based on elastin-like recombinamer particles for tissue engineering applications.* Soft Matter, 2011. **7**(14): p. 6426-6434.
289. Scott, B., et al., *Soft lithography and microfabrication.* Physics World, 1998. **11**(5): p. 31.
290. Workman, V.L., et al., *Microfluidic chip-based synthesis of alginate microspheres for encapsulation of immortalized human cells.* Biomicrofluidics, 2007. **1**(1): p. 014105.
291. Shin-Hyun, K., et al., *Microfluidic fabrication of microparticles with structural complexity using photocurable emulsion droplets.* New Journal of Physics, 2009. **11**(7): p. 075014.
292. Dang, T.D., et al., *Preparation of monodisperse PEG hydrogel microparticles using a microfluidic flow-focusing device.* Journal of Industrial and Engineering Chemistry, 2012. **18**(4): p. 1308-1313.
293. Coupland, J.N. and D. Julian McClements, *Droplet size determination in food emulsions: comparison of ultrasonic and light scattering methods.* Journal of Food Engineering, 2001. **50**(2): p. 117-120.
294. Mengual, O., et al., *TURBISCAN MA 2000: multiple light scattering measurement for concentrated emulsion and suspension instability analysis.* Talanta, 1999. **50**(2): p. 445-456.
295. Carmelo, J.G., et al., *A xeno-free microcarrier-based stirred culture system for the scalable expansion of human mesenchymal stem/stromal cells isolated from bone marrow and adipose tissue.* Biotechnology journal, 2015. **10**(8): p. 1235-47.
296. Oh, S.K.W., et al., *Long-term microcarrier suspension cultures of human embryonic stem cells.* Stem Cell Research, 2009. **2**(3): p. 219-230.
297. Jain, R., et al., *The use of native chemical functional groups presented by wound beds for the covalent attachment of polymeric microcarriers of bioactive factors.* Biomaterials, 2013. **34**(2): p. 340-352.

298. Declercq, H.A., et al., *Bone grafts engineered from human adipose-derived stem cells in dynamic 3D-environments.* Biomaterials, 2013. **34**(4): p. 1004-1017.
299. Custodio, C.A., et al., *Cell selective chitosan microparticles as injectable cell carriers for tissue regeneration.* Biomaterials, 2015. **43**: p. 23-31.
300. Haycock, J.W., *3D Cell Culture: A Review of Current Approaches and Techniques*, in *3d Cell Culture: Methods and Protocols*, J.W. Haycock, Editor. 2011, Humana Press Inc: Totowa. p. 1-15.
301. Moglia, R., et al., *Solvent-Free Fabrication of polyHIPE Microspheres for Controlled Release of Growth Factors.* Macromolecular rapid communications, 2014. **35**(14): p. 1301-1305.
302. Silverstein, M.S., *PolyHIPEs: Recent advances in emulsion-templated porous polymers.* Progress in Polymer Science, 2014. **39**(1): p. 199-234.
303. Cameron, N.R., et al., *Study of the formation of the open cellular morphology of poly(styrene/divinylbenzene) polyHIPE materials by cryo-SEM.* Colloid and Polymer Science, 1996. **274**(6): p. 592-595.
304. Owen R, S.C., Paterson T, Green NH, Reilly GC, Claeyssens F, *Emulsion Templated Scaffolds with Tunable Mechanical Properties for Bone Tissue Engineering.* J Mech Behav Biomed Mater., 2015. **54**: p. 159-172.
305. Johnson, D.W., et al., *Macrostructuring of Emulsion-templated Porous Polymers by 3D Laser Patterning.* Advanced Materials, 2013. **25**(23): p. 3178-3181.
306. Zhou, H.O., T.J. Shi, and X. Zhou, *Aqueous Core Polystyrene Microspheres Fabricated via Suspension Polymerization Basing on a Multiple Pickering Emulsion.* Journal of Applied Polymer Science, 2014. **131**(2).
307. Bou, R., S. Cofrades, and F. Jimenez-Colmenero, *Influence of high pressure and heating treatments on physical parameters of water-in-oil-in-water emulsions.* Innovative Food Science & Emerging Technologies, 2014. **23**: p. 1-9.
308. Brugarolas, T., F. Tu, and D. Lee, *Directed Assembly of Particles Using Microfluidic Droplets and Bubbles.* Soft Matter, 2013.
309. Kansal, A.R., S. Torquato, and F.H. Stillinger, *Computer generation of dense polydisperse sphere packings.* Journal of Chemical Physics, 2002. **117**(18): p. 8212-8218.
310. Viswanathan, P., et al., *3D surface topology guides stem cell adhesion and differentiation.* Biomaterials, 2015. **52**: p. 140-147.
311. Brunner, C.A., et al., *Cell migration through small gaps.* European Biophysics Journal with Biophysics Letters, 2006. **35**(8): p. 713-719.
312. Brunner, C.A., et al., *Cell migration through small gaps.* European Biophysics Journal, 2006. **35**(8): p. 713-719.
313. Carnachan, R.J., et al., *Tailoring the morphology of emulsion-templated porous polymers.* Soft Matter, 2006. **2**(7): p. 608-616.
314. Choi, S.-W., et al., *Uniform Beads with Controllable Pore Sizes for Biomedical Applications.* Small, 2010. **6**(14): p. 1492-1498.
315. Degner, B.M., et al., *Factors Influencing the Freeze-Thaw Stability of Emulsion-Based Foods.* Comprehensive Reviews in Food Science and Food Safety, 2014. **13**(2): p. 98-113.
316. Farr, R.S. and R.D. Groot, *Close packing density of polydisperse hard spheres.* Journal of Chemical Physics, 2009. **131**(24).
317. de Peppo, G.M., et al., *Osteogenic Potential of Human Mesenchymal Stem Cells and Human Embryonic Stem Cell-Derived Mesodermal Progenitors: A Tissue Engineering Perspective.* Tissue Engineering Part A, 2010. **16**(11): p. 3413-3426.
318. Drissi, H., et al., *Derivation and Chondrogenic Commitment of Human Embryonic Stem Cell-Derived Mesenchymal Progenitors*, in *Cartilage Tissue Engineering: Methods and Protocols*, P.M. Doran, Editor. 2015, Humana Press Inc: Totowa. p. 65-78.
319. M. Pr ideaux, L.F.B., *The osteocyte: doing the hard work backstage.* Medicographia, 2012. **34**: p. 228-235.
320. Arboleya, L. and S. Castaneda, *Osteoimmunology: the study of the relationship between the immune system and bone tissue.* Reumatologia clinica, 2013. **9**(5): p. 303-15.

321. Beck, G.R., *Inorganic phosphate as a signaling molecule in osteoblast differentiation.* Journal of Cellular Biochemistry, 2003. **90**(2): p. 234-243.
322. Krawetz, R.J., et al., *Collagen I Scaffolds Cross-Linked with Beta-Glycerol Phosphate Induce Osteogenic Differentiation of Embryonic Stem Cells In Vitro and Regulate Their Tumorigenic Potential In Vivo.* Tissue Engineering Part A, 2012. **18**(9-10): p. 1014-1024.
323. Franceschi, R.T., B.S. Iyer, and Y. Cui, *Effects of ascorbic acid on collagen matrix formation and osteoblast differentiation in murine MC3T3-E1 cells.* Journal of Bone and Mineral Research, 1994. **9**(6): p. 843-854.
324. Langenbach, F. and J. Handschel, *Effects of dexamethasone, ascorbic acid and beta-glycerophosphate on the osteogenic differentiation of stem cells in vitro.* Stem Cell Research & Therapy, 2013. **4**.
325. Tenenbaum, H.C. and J.N.M. Heersche, *Dexamethasone stimulates osteogenesis in chick periosteum in vitro.* Endocrinology, 1985. **117**(5): p. 2211-2217.
326. Villanueva, M.A., M. Schindler, and J.L. Wang, *The nucleocytoplasmic microfilament network in protoplasts from cultured soybean cells is a plastic entity that pervades the cytoplasm except the central vacuole.* Cell biology international, 2005. **29**(11): p. 936-942.
327. Braet, F., R. deZanger, and E. Wisse, *Drying cells for SEM, AFM and TEM by hexamethyldisilazane: A study on hepatic endothelial cells.* Journal of Microscopy-Oxford, 1997. **186**: p. 84-87.
328. Malayeri, A., et al., *Osteosarcoma growth on trabecular bone mimicking structures manufactured via laser direct write.* 2016, 2016. **2**(2).
329. Barry, J.J.A., et al., *Using Plasma Deposits to Promote Cell Population of the Porous Interior of Three-Dimensional Poly(D,L-Lactic Acid) Tissue-Engineering Scaffolds.* Advanced Functional Materials, 2005. **15**(7): p. 1134-1140.
330. Lassen, B. and M. Malmsten, *Competitive protein adsorption at plasma polymer surfaces.* Journal of Colloid and Interface Science, 1997. **186**(1): p. 9-16.
331. Mano, J.F., *Antibody Coated Microparticles to Fabricate Functional 3D Constructs in Combination with Cells*. ESB. 2014, Liverpool.
332. Kuboki, Y., Q. Jin, and H. Takita, *Geometry of carriers controlling phenotypic expression in BMP-induced osteogenesis and chondrogenesis.* J Bone Joint Surg Am, 2001. **83**(1 suppl 2): p. S105-S115.
333. Lu, J., et al., *Role of interconnections in porous bioceramics on bone recolonization in vitro and in vivo.* Journal of Materials Science: Materials in Medicine, 1999. **10**(2): p. 111-120.
334. Huri, P.Y., et al., *Scaffold pore size modulates in vitro osteogenesis of human adipose-derived stem/stromal cells.* Biomedical materials (Bristol, England), 2014. **9**(4): p. 045003.
335. Moglia, R.S., et al., *Injectable Polymerized High Internal Phase Emulsions with Rapid in Situ Curing.* Biomacromolecules, 2014. **15**(8): p. 2870-2878.
336. Akay, G., M. Birch, and M. Bokhari, *Microcellular polyHIPE polymer supports osteoblast growth and bone formation in vitro.* Biomaterials, 2004. **25**(18): p. 3991-4000.
337. Lind, M., et al., *Chemotaxis of human osteoblasts.* Apmis, 1995. **103**(1-6): p. 140-146.
338. Fukuyama, R., et al., *Statins inhibit osteoblast migration by inhibiting Rac-Akt signaling.* Biochemical and Biophysical Research Communications, 2004. **315**(3): p. 636-642.
339. Choi, K.M., et al., *Effect of ascorbic acid on bone marrow-derived mesenchymal stem cell proliferation and differentiation.* Journal of Bioscience and Bioengineering, 2008. **105**(6): p. 586-594.
340. Tenenbaum, H.C., *Levamisole and inorganic pyrophosphate inhibit beta-glycerophosphate induced mineralization of bone formed in vitro.* Bone and mineral, 1987. **3**(1): p. 13-26.
341. Chung, C.H., et al., *Mechanism of action of beta-glycerophosphate on bone cell mineralization.* Calcified tissue international, 1992. **51**(4): p. 305-311.
342. Tang, Y., et al., *TGF-β1–induced migration of bone mesenchymal stem cells couples bone resorption with formation.* Nature medicine, 2009. **15**(7): p. 757-765.
343. Nakayama, H., et al., *Dexamethasone Enhancement of Betaglycan (TGF-β Type III Receptor) Gene Expression in Osteoblast-like Cells.* Experimental Cell Research, 1994. **211**(2): p. 301-306.

344. Dodd, J., J. Raleigh, and T. Gross, *Osteocyte hypoxia: a novel mechanotransduction pathway.* American Journal of Physiology-Cell Physiology, 1999. **277**(3): p. C598-C602.
345. Kanichai, M., et al., *Hypoxia promotes chondrogenesis in rat mesenchymal stem cells: A role for AKT and hypoxia-inducible factor (HIF)-1α.* Journal of cellular physiology, 2008. **216**(3): p. 708-715.
346. Robins, J.C., et al., *Hypoxia induces chondrocyte-specific gene expression in mesenchymal cells in association with transcriptional activation of Sox9.* Bone, 2005. **37**(3): p. 313-322.
347. Schipani, E., et al., *Hypoxia in cartilage: HIF-1α is essential for chondrocyte growth arrest and survival.* Genes & development, 2001. **15**(21): p. 2865-2876.
348. Roosa, S.M.M., et al., *The pore size of polycaprolactone scaffolds has limited influence on bone regeneration in an in vivo model.* Journal of Biomedical Materials Research Part A, 2010. **92**(1): p. 359-368.
349. Dahlin, R.L., et al., *Hypoxia and flow perfusion modulate proliferation and gene expression of articular chondrocytes on porous scaffolds.* AIChE Journal, 2013. **59**(9): p. 3158-3166.
350. Holmbeck, K., et al., *The metalloproteinase MT1-MMP is required for normal development and maintenance of osteocyte processes in bone.* Journal of Cell Science, 2005. **118**(1): p. 147-156.
351. Okada, S., et al., *The canalicular structure of compact bone in the rat at different ages.* Microscopy and Microanalysis, 2002. **8**(2): p. 104-115.
352. Bianco, P., et al., *Bone formation via cartilage models: the "borderline" chondrocyte.* Matrix biology, 1998. **17**(3): p. 185-192.
353. Schmid, T.M., R.G. Popp, and T.F. Linsenmayer, *Hypertrophic cartilage matrix.* Annals of the New York Academy of Sciences, 1990. **580**(1): p. 64-73.
354. Winkler, D.G., et al., *Osteocyte control of bone formation via sclerostin, a novel BMP antagonist.* The EMBO journal, 2003. **22**(23): p. 6267-6276.
355. Poole, K.E., et al., *Sclerostin is a delayed secreted product of osteocytes that inhibits bone formation.* The FASEB journal, 2005. **19**(13): p. 1842-1844.
356. Zhang, N., H. Yan, and X. Wen, *Tissue-engineering approaches for axonal guidance.* Brain Research Reviews, 2005. **49**(1): p. 48-64.
357. Woodruff, M.A. and D.W. Hutmacher, *The return of a forgotten polymer—polycaprolactone in the 21st century.* Progress in Polymer Science, 2010. **35**(10): p. 1217-1256.
358. Kweon, H., et al., *A novel degradable polycaprolactone networks for tissue engineering.* Biomaterials, 2003. **24**(5): p. 801-808.
359. Yang, S., et al., *The design of scaffolds for use in tissue engineering. Part I. Traditional factors.* Tissue engineering, 2001. **7**(6): p. 679-689.
360. Lumelsky, Y., et al., *A degradable, porous, emulsion-templated polyacrylate.* Journal of Polymer Science Part A: Polymer Chemistry, 2009. **47**(24): p. 7043-7053.
361. Gong, X., W. Wen, and P. Sheng, *Microfluidic fabrication of porous polymer microspheres: dual reactions in single droplets.* Langmuir, 2009. **25**(12): p. 7072-7077.
362. Schuster, M., et al. *Development of biodegradable photopolymers for bone tissue engineering*. in *RadTech Europe*. 2005.
363. Kim, S.H. and C.C. Chu, *Fabrication of a biodegradable polysaccharide hydrogel with riboflavin, vitamin B2, as a photo-initiator and L-arginine as coinitiator upon UV irradiation.* Journal of Biomedical Materials Research Part B: Applied Biomaterials, 2009. **91**(1): p. 390-400.
364. Bowers, K.T., et al., *Optimization of surface micromorphology for enhanced osteoblast responses in vitro.* International Journal of Oral & Maxillofacial Implants, 1992. **7**(3).
365. Shellenberger, K. and B.E. Logan, *Effect of molecular scale roughness of glass beads on colloidal and bacterial deposition.* Environmental science & technology, 2002. **36**(2): p. 184-189.
366. Haycock, J.W., *3D Cell Culture: A Review of Current Approaches and Techniques*, in *3D Cell Culture: Methods and Protocols*, W.J. Haycock, Editor. 2011, Humana Press: Totowa, NJ. p. 1-15.
367. Lamson, M., et al., *Synthesis of degradable polyHIPEs by AGET ATRP.* Polymer, 2013. **54**(17): p. 4480-4485.

368. Christenson, E.M., et al., *Biodegradable Fumarate-Based PolyHIPEs as Tissue Engineering Scaffolds.* Biomacromolecules, 2007. **8**(12): p. 3806-3814.
369. Göpferich, A., *Polymer Scaffolding and Hard Tissue EngineeringMechanisms of polymer degradation and erosion.* Biomaterials, 1996. **17**(2): p. 103-114.
370. Li, X., et al., *Coating electrospun poly (ε-caprolactone) fibers with gelatin and calcium phosphate and their use as biomimetic scaffolds for bone tissue engineering.* Langmuir, 2008. **24**(24): p. 14145-14150.
371. Yeo, M.G. and G.H. Kim, *Preparation and characterization of 3D composite scaffolds based on rapid-prototyped PCL/β-TCP struts and electrospun PCL coated with collagen and HA for bone regeneration.* Chemistry of Materials, 2011. **24**(5): p. 903-913.
372. Elbert, D.L. and J.A. Hubbell, *Surface treatments of polymers for biocompatibility.* Annual Review of Materials Science, 1996. **26**(1): p. 365-394.
373. McBeath, R., et al., *Cell shape, cytoskeletal tension, and RhoA regulate stem cell lineage commitment.* Developmental cell, 2004. **6**(4): p. 483-495.
374. Mathieu, P.S. and E.G. Loboa, *Cytoskeletal and focal adhesion influences on mesenchymal stem cell shape, mechanical properties, and differentiation down osteogenic, adipogenic, and chondrogenic pathways.* Tissue Engineering Part B: Reviews, 2012. **18**(6): p. 436-444.
375. Chau, J., W.F. Leong, and B. Li, *Signaling pathways governing osteoblast proliferation, differentiation and function.* Histology and histopathology, 2009. **24**(12): p. 1593-1606.
376. Lynn, D.M. and R. Langer, *Degradable poly (β-amino esters): synthesis, characterization, and self-assembly with plasmid DNA.* Journal of the American Chemical Society, 2000. **122**(44): p. 10761-10768.
377. Low, K.L., et al., *Calcium phosphate -based composites as injectable bone substitute materials.* Journal of Biomedical Materials Research Part B: Applied Biomaterials, 2010. **94**(1): p. 273-286.
378. Crissman, A., F. Traganos, and J. Steinkamp, *Angiogenesis induced by degradation products of hyaluronic acid.* 1985.
379. Lokman, N.A., et al., *Chick chorioallantoic membrane (CAM) assay as an in vivo model to study the effect of newly identified molecules on ovarian cancer invasion and metastasis.* International journal of molecular sciences, 2012. **13**(8): p. 9959-9970.
380. Wilting, J., B. Christ, and M. Bokeloh, *A modified chorioallantoic membrane (CAM) assay for qualitative and quantitative study of growth factors.* Anatomy and embryology, 1991. **183**(3): p. 259-271.
381. Dohle, D.S., et al., *Chick ex ovo culture and ex ovo CAM assay: how it really works.* JoVE (Journal of Visualized Experiments), 2009(33): p. e1620-e1620.
382. Pugh, C.W. and P.J. Ratcliffe, *Regulation of angiogenesis by hypoxia: role of the HIF system.* Nature medicine, 2003. **9**(6): p. 677-684.
383. Puwanun, S., *Developing a tissue engineering strategy for cleft palate repair*, 2014, University of Sheffield.
384. Hutmacher, D.W., *Scaffolds in tissue engineering bone and cartilage.* Biomaterials, 2000. **21**(24): p. 2529-2543.
385. Carmeliet, P. and R.K. Jain, *Angiogenesis in cancer and other diseases.* Nature, 2000. **407**(6801): p. 249-257.
386. Chang, R., J. Nam, and W. Sun, *Effects of dispensing pressure and nozzle diameter on cell survival from solid freeform fabrication-based direct cell writing.* Tissue Engineering Part A, 2008. **14**(1): p. 41-48.
387. Yao, R., et al., *Alginate and alginate/gelatin microspheres for human adipose-derived stem cell encapsulation and differentiation.* Biofabrication, 2012. **4**(2): p. 025007.
388. Cheng, H.-W., et al., *Decellularization of chondrocyte-encapsulated collagen microspheres: a three-dimensional model to study the effects of acellular matrix on stem cell fate.* Tissue Engineering Part C: Methods, 2009. **15**(4): p. 697-706.
389. Menke, N.B., et al., *Impaired wound healing.* Clinics in dermatology, 2007. **25**(1): p. 19-25.
390. Gurtner, G.C., et al., *Wound repair and regeneration.* Nature, 2008. **453**(7193): p. 314-321.

391. Jiang, X., et al., *Selective enhancement of human stem cell proliferation by mussel inspired surface coating.* Rsc Advances, 2016. **6**(65): p. 60206-60214.
392. Siddiqi, S., et al., *Mesenchymal stem cell (MSC) viability on PVA and PCL polymer coated hydroxyapatite scaffolds derived from cuttlefish.* Rsc Advances, 2016. **6**(39): p. 32897-32904.
393. Xin, Q., et al., *Three-dimensional poly (ε -caprolactone)/hydroxyapatite/collagen scaffolds incorporating bone marrow mesenchymal stem cells for the repair of bone defects.* Biomedical Materials, 2016. **11**(2): p. 025005.
394. Ma, Z., Z. Mao, and C. Gao, *Surface modification and property analysis of biomedical polymers used for tissue engineering.* Colloids and Surfaces B: Biointerfaces, 2007. **60**(2): p. 137-157.
395. Owen, R., et al., *Emulsion templated scaffolds with tunable mechanical properties for bone tissue engineering.* Journal of the Mechanical Behavior of Biomedical Materials, 2016. **54**: p. 159-172.
396. Deligianni, D.D., et al., *Effect of surface roughness of the titanium alloy Ti–6Al–4V on human bone marrow cell response and on protein adsorption.* Biomaterials, 2001. **22**(11): p. 1241-1251.
397. Postiglione, L., et al., *Behavior of SaOS-2 cells cultured on different titanium surfaces.* Journal of dental research, 2003. **82**(9): p. 692-696.
398. Rosa, A.L. and M.M. Beloti, *Rat bone marrow cell response to titanium and titanium alloy with different surface roughness.* Clinical Oral Implants Research, 2003. **14**(1): p. 43-48.
399. Olszta, M.J., et al., *Bone structure and formation: A new perspective.* Materials Science & Engineering R-Reports, 2007. **58**(3-5): p. 77-116.
400. Murphy, C.M., M.G. Haugh, and F.J. O'Brien, *The effect of mean pore size on cell attachment, proliferation and migration in collagen-glycosaminoglycan scaffolds for bone tissue engineering.* Biomaterials, 2010. **31**(3): p. 461-466.
401. Grizon, F., et al., *Enhanced bone integration of implants with increased surface roughness: a long term study in the sheep.* Journal of dentistry, 2002. **30**(5): p. 195-203.
402. Buser, D., et al., *Influence of surface characteristics on bone integration of titanium implants. A histomorphometric study in miniature pigs.* Journal of biomedical materials research, 1991. **25**(7): p. 889-902.
403. Williams, D.F., *On the mechanisms of biocompatibility.* Biomaterials, 2008. **29**(20): p. 2941-2953.
404. Sung, H.-J., et al., *The effect of scaffold degradation rate on three-dimensional cell growth and angiogenesis.* Biomaterials, 2004. **25**(26): p. 5735-5742.
405. Yamada, Y., et al., *Bone regeneration following injection of mesenchymal stem cells and fibrin glue with a biodegradable scaffold.* Journal of Cranio-Maxillofacial Surgery, 2003. **31**(1): p. 27-33.
406. Blackwood, K.A., et al., *Development of biodegradable electrospun scaffolds for dermal replacement.* Biomaterials, 2008. **29**(21): p. 3091-3104.
407. Ferrara, N., H.-P. Gerber, and J. LeCouter, *The biology of VEGF and its receptors.* Nature medicine, 2003. **9**(6): p. 669-676.
408. Geiger, F., et al., *VEGF producing bone marrow stromal cells (BMSC) enhance vascularization and resorption of a natural coral bone substitute.* Bone, 2007. **41**(4): p. 516-522.
409. Lindhorst, D., et al., *Effects of VEGF loading on scaffold–confined vascularization.* Journal of Biomedical Materials Research Part A, 2010. **95**(3): p. 783-792.
410. Murphy, S.V. and A. Atala, *3D bioprinting of tissues and organs.* Nature biotechnology, 2014. **32**(8): p. 773-785.